

Fall 2019

Study of Transition State Stabilization Using Molecular Rotors

Erik Carl Vik

Follow this and additional works at: <https://scholarcommons.sc.edu/etd>



Part of the [Chemistry Commons](#)

Recommended Citation

Vik, E. C.(2019). *Study of Transition State Stabilization Using Molecular Rotors*. (Doctoral dissertation). Retrieved from <https://scholarcommons.sc.edu/etd/5540>

This Open Access Dissertation is brought to you by Scholar Commons. It has been accepted for inclusion in Theses and Dissertations by an authorized administrator of Scholar Commons. For more information, please contact dillarda@mailbox.sc.edu.

STUDY OF TRANSITION STATE STABILIZATION USING MOLECULAR ROTORS

by

Erik Carl Vik

Bachelor of Science
State University of New York at Oswego, 2014

Submitted in Partial Fulfillment of the Requirements

For the Degree of Doctor of Philosophy in

Chemistry

College of Arts and Sciences

University of South Carolina

2019

Accepted by:

Ken D. Shimizu, Major Professor

Linda S. Shimizu, Committee Member

Dmitry V. Peryshkov, Committee Member

Bo Cai, Committee Member

Cheryl L. Addy, Vice Provost and Dean of the Graduate School

© Copyright by Erik Carl Vik, 2019
All Rights Reserved.

DEDICATION

To Cassie.

ACKNOWLEDGEMENTS

There have been many people who have helped me get to where I am today, and it would be impossible to list them all here. Let it be known that I appreciate every single person that I have known thus far, for every experience guides my current decision making. I hope that we all have great fulfilling lives.

To my advisor, Dr. Ken D. Shimizu, I would like to thank you for your guidance during my studies, your openness to my seeking research directions, and your patience during our many hour-long conversations. Thank you for purchasing the most powerful workstations I have ever used, and your openness to my requests of purchasing new computational software programs. I can only hope that any bosses I may have in the future will have your stature and goodwill.

ABSTRACT

Molecular devices that function as rotors and measurement devices are the main topic of this dissertation. Each study contains a device based on an N-phenylimide framework, which has restricted rotation about the N-C (imide-phenyl) single bond due to a steric clash from the imide carbonyl and the phenyl rings *ortho* substituent. In general, two ground states are observed by ^1H NMR, which are separated by a single transition state (TS). Incorporation of non-covalent interactions into the TS led to measurable changes in the rate for rotation. While the molecules in this dissertation revealed details that could not have been predicted, the most important advances were the new methods and strategies that were developed to study and interrogate NCIs. The studies highlighted in this dissertation include three kinetic studies of TS stabilized molecular rotors, a series of analyses of steric interactions, and one study of DFT benchmarks of rotational barriers.

TABLE OF CONTENTS

DEDICATION	iii
ACKNOWLEDGEMENTS.....	iv
ABSTRACT	v
LIST OF TABLES	viii
LIST OF FIGURES	xiii
LIST OF SCHEMES.....	xxiii
LIST OF ABBREVIATIONS.....	xxiv
CHAPTER 1 UTILIZING EMPIRICAL PARAMETERS AND COMPUTATIONAL CALCULATIONS TO STUDY NON-COVALENT INTERACTIONS	1
1.1 ABSTRACT.....	2
1.2 NON-COVALENT INTERACTIONS	2
1.3 EMPIRICAL AND CALCULATED PARAMETERS	5
1.4 COMPUTATIONAL CALCULATIONS	7
1.5 QUANTITATIVE ANALYSIS.....	14
CHAPTER 2 TRANSITION STATE STABILIZATION BY $n \rightarrow \pi^*$ INTERACTIONS MEASURED USING MOLECULAR ROTORS	19
2.1 ABSTRACT.....	20
2.2 MAIN TEXT	20
2.3 CONCLUSION	29
2.4 SUPPLEMENTAL INFORMATION.....	29

CHAPTER 3 ORIGINS OF A LARGE TRANSITION STATE STABILIZATION BY A WEAK HYDROGEN BOND	103
3.1 ABSTRACT.....	104
3.2 MAIN TEXT	104
3.3 CONCLUSION.....	118
3.4 SUPPLEMENTAL INFORMATION.....	119
CHAPTER 4 $n \cdots \pi_{(AR)}$ INTERACTIONS ARE BEST DESCRIBED AS ELECTROSTATIC INTERACTIONS	187
4.1 ABSTRACT.....	188
4.2 MAIN TEXT	188
4.3 CONCLUSION.....	196
4.3 SUPPLEMENTAL INFORMATION.....	197
CHAPTER 5 FUTURE WORK	221
5.1 OUTLOOK	222
5.2 LONE PAIR – LONE PAIR REPULSION.....	222
5.3 ACCURACY IN CALCULATING ROTATIONAL BARRIERS	223
5.4 EMPIRICAL MODEL OF ROTATIONAL BARRIERS	224
REFERENCES	230
APPENDIX A EMPIRICAL PARAMETERS	238
APPENDIX B COPYRIGHT CLEARANCE.....	241

LIST OF TABLES

TABLE 2.1 EXPERIMENTAL ROTATIONAL BARRIERS FOR 1 (R) VIA EXSY NMR	52
TABLE 2.2 CALCULATED ($\Delta G^{\ddagger}_{\text{CALC.}}$, KCAL/MOL) _A AND EXPERIMENTAL ($\Delta G^{\ddagger}_{\text{EXP.}}$, KCAL/MOL) _B ROTATIONAL BARRIER ENERGIES FOR ROTORS 1 AND 2 , AND THE ERROR (KCAL/MOL) _C REPORTED AS THE DIFFERENCE BETWEEN THE CALCULATED AND EXPERIMENTAL VALUES.	62
TABLE 2.3 XYZ COORDINATES OF THE GS AND TS STRUCTURES OF 1 (BR)	63
TABLE 2.4 XYZ COORDINATES OF THE GS AND TS STRUCTURES OF 1 (C(CH ₂)CH ₃).....	64
TABLE 2.5 XYZ COORDINATES OF THE GS AND TS STRUCTURES OF 1 (CCH).....	65
TABLE 2.6 XYZ COORDINATES OF THE GS AND TS STRUCTURES OF 1 (CF ₃).....	66
TABLE 2.7 XYZ COORDINATES OF THE GS AND TS STRUCTURES OF 1 (CHO)	67
TABLE 2.8 XYZ COORDINATES OF THE GS AND TS STRUCTURES OF 1 (CL)	68
TABLE 2.9 XYZ COORDINATES OF THE GS AND TS STRUCTURES OF 1 (CN)	69
TABLE 2.10 XYZ COORDINATES OF THE GS AND TS STRUCTURES OF 1 (COCH ₃).....	70
TABLE 2.11 XYZ COORDINATES OF THE GS AND TS STRUCTURES OF 1 (C(CH ₂)CH ₃).....	71
TABLE 2.12 XYZ COORDINATES OF THE GS AND TS STRUCTURES OF 1 (CH ₂ CH ₃)	72
TABLE 2.13 XYZ COORDINATES OF THE GS AND TS STRUCTURES OF 1 (I)	73
TABLE 2.14 XYZ COORDINATES OF THE GS AND TS STRUCTURES OF 1 (<i>I</i> -Pr)	74
TABLE 2.15 XYZ COORDINATES OF THE GS AND TS STRUCTURES OF 1 (CH ₃).....	75
TABLE 2.16 XYZ COORDINATES OF THE GS AND TS STRUCTURES OF 1 (OCH ₃)	76
TABLE 2.17 XYZ COORDINATES OF THE GS AND TS STRUCTURES OF 1 (Ph)	77
TABLE 2.18 XYZ COORDINATES OF THE GS AND TS STRUCTURES OF 1 (SCH ₃).....	78

TABLE 2.19 XYZ COORDINATES OF THE GS AND TS STRUCTURES OF 2(Br) ^A	79
TABLE 2.20 XYZ COORDINATES OF THE GS AND TS STRUCTURES OF 2(CCH)	80
TABLE 2.21 XYZ COORDINATES OF THE GS AND TS STRUCTURES OF 2(CF₃)	81
TABLE 2.22 XYZ COORDINATES OF THE GS AND TS STRUCTURES OF 2(CH₃) ^A	82
TABLE 2.23 XYZ COORDINATES OF THE GS AND TS STRUCTURES OF 2(CHO)	83
TABLE 2.24 XYZ COORDINATES OF THE GS AND TS STRUCTURES OF 2(CL) ^A	84
TABLE 2.25 XYZ COORDINATES OF THE GS AND TS STRUCTURES OF 2(CN)	85
TABLE 2.26 XYZ COORDINATES OF THE GS AND TS STRUCTURES OF 2(COCH₃) ^A	86
TABLE 2.27 XYZ COORDINATES OF THE GS AND TS STRUCTURES OF 2(CH₂CH₃) ^A	87
TABLE 2.28 XYZ COORDINATES OF THE GS AND TS STRUCTURES OF 2(<i>I</i>-Pr) ^A	88
TABLE 2.29 XYZ COORDINATES OF THE GS AND TS STRUCTURES OF 2(I) ^A	89
TABLE 2.30 XYZ COORDINATES OF THE GS AND TS STRUCTURES OF 2(OCH₃)	90
TABLE 2.31 XYZ COORDINATES OF THE GS AND TS STRUCTURES OF 2(Ph)	91
TABLE 2.32 XYZ COORDINATES OF THE GS AND TS STRUCTURES OF 2(SCH₃)	92
TABLE 2.33 EXPERIMENTAL ($\Delta G^{\ddagger}_{\text{EXP}}$) AND CALCULATED ($\Delta G^{\ddagger}_{\text{CALC.}}$) BARRIERS FOR PARA-SUBSTITUTED 1(CH₃) AND 3(CH₃)	94
TABLE 2.34 XYZ COORDINATES OF THE GS AND TS STRUCTURES OF 1(CH₃) WITH PARA-NO ₂	97
TABLE 2.35 XYZ COORDINATES OF THE GS AND TS STRUCTURES OF 1(CH₃) WITH PARA-CHO	98
TABLE 2.36 XYZ COORDINATES OF THE GS AND TS STRUCTURES OF 1(CH₃) WITH PARA-CN	99
TABLE 2.37 XYZ COORDINATES OF THE TSII OF 1(SCH₃) AND TWO THIOETHER CONFORMERS.	100
TABLE 2.38 EXPERIMENTALLY MEASURED ($\Delta G^{\ddagger}_{\text{EXP.}}$, KCAL/MOL) AND CALCULATED ($\Delta G^{\ddagger}_{\text{CALC.}}$, KCAL/MOL) ROTATIONAL BARRIERS FOR ROTOR 1 WITH VARIOUS R-GROUPS AT 25 °C, EXPERIMENTALLY QUANTIFIED TS STABILIZATION	

($\Delta\Delta G^{\ddagger}_{\text{EXP.}}$, KCAL/MOL) ^C , CALCULATED TS NBO ENERGIES (E_{NBO} , KCAL/MOL) BETWEEN THE IMIDE CARBONYL OXYGENS AND R-GROUPS, AND NATURAL BOND ORBITAL ATOMIC CHARGES (NBO CHARGE, A.U.) FOR THE ACCEPTING CARBON ATOMS AS A PHENYL SUBSTITUENT.....	101
TABLE 3.1 EXPERIMENTAL ROTATIONAL BARRIER (ΔG^{\ddagger} , KCAL/MOL) FOR ROTORS 1 AND 2 VIA COALESCENCE TEMPERATURE AND EXCHANGE LINE-SHAPE ANALYSES.	146
TABLE 3.2 GIBBS FREE ASSOCIATION ENERGY (ΔG_{KA} , KCAL/MOL) ^A FOR THE HYDROGEN BONDED HOST-GUEST COMPLEXES OF <i>N</i> -METHYL PYRROLIDONE AND (SUBSTITUTED) PHENOLS IN DICHLOROMETHANE-D ₂	152
TABLE 3.3 CRYSTAL DATA AND STRUCTURE REFINEMENT FOR 1 (X = H).....	163
TABLE 3.4 CRYSTAL DATA AND STRUCTURE REFINEMENT FOR 1 (X = <i>p</i> -CL).....	164
TABLE 3.5 CRYSTAL DATA AND STRUCTURE REFINEMENT FOR 1 (X = <i>m</i> -CL).	165
TABLE 3.6 CRYSTAL DATA AND STRUCTURE REFINEMENT FOR 2 (X = <i>p</i> -NO ₂).	166
TABLE 3.7 CRYSTAL DATA AND STRUCTURE REFINEMENT FOR 2 (X = <i>p</i> -CL).....	167
TABLE 3.8 CRYSTAL DATA AND STRUCTURE REFINEMENT FOR 2 (X = <i>p</i> -CN).....	168
TABLE 3.9 CALCULATED (ΔG^{\ddagger} CALC., KCAL/MOL) _A AND EXPERIMENTAL (ΔG^{\ddagger} EXP., KCAL/MOL) _B ROTATIONAL BARRIER ENERGIES FOR ROTORS 1 AND 2 AS WELL AS THE ERROR (KCAL/MOL) _C FOR THE CALCULATIONS REPORTED AS THE DIFFERENCE BETWEEN THE CALCULATED AND EXPERIMENTAL VALUES.....	170
TABLE 3.10 STATISTICAL VALUES FOR THE ERROR OF THE CALCULATED (B2GP-PLYP-D3(BJ)/DEF2-TZVP) ROTATIONAL BARRIERS FOR THE PHENOL AND ANISOLE ROTORS.....	173
TABLE 3.11 SAPT TOTAL (E_{TOTAL} , KCAL/MOL) AND COMPONENT ENERGIES (E_{ELST} , E_{EXCH} , E_{IND} , AND E_{DISP} , KCAL/MOL) FOR THE NMP-PHENOL COMPLEX IN TWO CONFIGURATIONS (FIGURE 3.61) AT 11 DIFFERENT O-TO-O DISTANCES (D) AS WELL AS THE DIFFERENCES IN ENERGY ($\Delta E = E^{\text{HB}} - E^{\text{NHB}}$) BETWEEN THE TWO CONFIGURATIONS.....	175
TABLE 3.12 SAPT TOTAL (E_{TOTAL} , KCAL/MOL) AND COMPONENT ENERGIES (E_{ELST} , E_{EXCH} , E_{IND} , AND E_{DISP} , KCAL/MOL) FOR THE NMP-PHENOL COMPLEX IN TWO CONFIGURATIONS (FIGURE 3.61) AT 2.5 Å AS WELL AS THE DIFFERENCES IN ENERGY ($E^{\text{A}} = E^{\text{HB}} - E^{\text{NHB}}$) BETWEEN THE TWO CONFIGURATIONS.....	178

TABLE 3.13 XYZ COORDINATES FOR THE GS AND TS STRUCTURES OF ANISOLE ROTOR 2	180
TABLE 3.14 XYZ COORDINATES FOR THE GS AND TS STRUCTURE OF PHENOL ROTOR 1 WITH HYDROGEN BOND.....	181
TABLE 3.15 XYZ COORDINATES FOR THE GS AND TS STRUCTURE OF PHENOL ROTOR 1 WITHOUT HYDROGEN BOND	182
TABLE 3.16 XYZ COORDINATES FOR NMP-PHENOL COMPLEX WITH A HYDROGEN BOND AT D = 2.0 Å (LEFT), D = 2.1 Å (MIDDLE) AND D = 2.2 (RIGHT)	183
TABLE 3.17 XYZ COORDINATES FOR NMP-PHENOL COMPLEX WITH A HYDROGEN BOND AT D = 2.3 Å (LEFT), D = 2.4 Å (MIDDLE) AND D = 2.5 (RIGHT)	183
TABLE 3.18 XYZ COORDINATES FOR NMP-PHENOL COMPLEX WITH A HYDROGEN BOND AT D = 2.6 Å (LEFT), D = 2.7 Å (MIDDLE) AND D = 2.8 (RIGHT)	184
TABLE 3.19 XYZ COORDINATES FOR NMP-PHENOL COMPLEX WITH A HYDROGEN BOND AT D = 2.9 Å (LEFT) AND D = 3.0 (RIGHT)	184
TABLE 3.20 XYZ COORDINATES FOR NMP-PHENOL COMPLEX WITHOUT A HYDROGEN BOND AT D = 2.0 Å (LEFT), D = 2.1 Å (MIDDLE) AND D = 2.2 (RIGHT)	185
TABLE 3.21 XYZ COORDINATES FOR NMP-PHENOL COMPLEX WITHOUT A HYDROGEN BOND AT D = 2.3 Å (LEFT), D = 2.4 Å (MIDDLE) AND D = 2.5 (RIGHT)	185
TABLE 3.22 XYZ COORDINATES FOR NMP-PHENOL COMPLEX WITHOUT A HYDROGEN BOND AT D = 2.6 Å (LEFT), D = 2.7 Å (MIDDLE) AND D = 2.8 (RIGHT)	186
TABLE 3.23 XYZ COORDINATES FOR NMP-PHENOL COMPLEX WITHOUT A HYDROGEN BOND AT D = 2.9 Å (LEFT) AND D = 3.0 (RIGHT)	186
TABLE 4.1 PROPERTIES OF THE $n \bullet \bullet \bullet \pi_{(AR)}$ ROTORS.	191
TABLE 4.2 EXPERIMENTAL ROTATIONAL BARRIERS FOR THE ROTORS IN CHAPTER 4 VIA EXSY NMR.....	209
TABLE 4.3 XYZ COORDINATES OF THE GS AND TS STRUCTURES OF PH-F ₁	212
TABLE 4.4 XYZ COORDINATES OF THE GS AND TS STRUCTURES OF PH-F ₃	213
TABLE 4.5 XYZ COORDINATES OF THE GS AND TS STRUCTURES OF PH-F ₅	214

TABLE 4.6 XYZ COORDINATES OF THE GS AND TS STRUCTURES OF PH-NO ₂	215
TABLE 4.7 XYZ COORDINATES OF THE GS AND TS STRUCTURES OF PH-(NO ₂) ₂	216
TABLE 4.8 ESP PARAMETERS CALCULATED AT THE B3LYP-D3/6-311G* LEVEL OF THEORY	218
TABLE 4.9 NBO ENERGY FROM THE n→π* ORBITAL-ORBITAL INTERACTION	220
TABLE 5.1 STATISTICAL ANALYSIS FOR THE CALCULATED ROTATIONAL BARRIERS IN THIS DISSERTATION.	226
TABLE 5.2 EFFECTIVE RADII OF THE SUBSTITUENTS	228
TABLE A.1 EMPIRICAL PARAMETERS USED TO MODEL STERIC HINDRANCE FOR COMMON SUBSTITUENTS.	239
TABLE A.2 EMPIRICAL PARAMETERS USED TO MODEL ELECTROSTATICS FOR COMMON SUBSTITUENTS.	240

LIST OF FIGURES

FIGURE 1.1 PHYSICAL PROPERTIES OF MATERIAL ARE GOVERNED BY NCIs, AND NCIs ARE GOVERNED BY FUNDAMENTAL INTERACTIONS.....	4
FIGURE 1.2 COMMON EMPIRICAL PARAMETERS	6
FIGURE 1.3 SUGGESTED GENERAL COMBINATION OF LEVEL OF THEORY AND COMPUTATIONAL METHODS	14
FIGURE 1.4 NON-COVALENT INTERACTIONS ARE BEST INTERPRETED BY UTILIZING EXPERIMENTAL AND COMPUTATIONAL MEASUREMENTS.....	17
FIGURE 1.5 MOLECULAR ROTOR BOND ROTATION REACTION COORDINATE DIAGRAM FOR ROTORS WITH AND WITHOUT STABILIZING TS NCIs.	17
FIGURE 1.6 GENERAL WORKFLOW USED IN THIS DISSERTATION. THE PROCESS STARTS OUT EXPERIMENTALLY (GREEN), AND LATER UTILIZES COMPUTATION (RED) FOR ANALYSIS.	18
FIGURE 2.1 CORRELATION PLOT OF THE EXPERIMENTALLY MEASURED ROTATIONAL BARRIERS FOR ROTOR 1 (R) VERSUS THE STERIC B-VALUES OF THE R GROUPS. THE STERIC TRENDLINE IS DRAWN THROUGH THE ROTORS THAT HAVE ORTHO R GROUPS WITHOUT A π^* ORBITAL (BLACK CIRCLES) AND THUS LACK $n \rightarrow \pi^*$ INTERACTIONS. THE BLUE CIRCLES CORRESPOND TO THE ROTORS THAT CAN FORM $n \rightarrow \pi^*$ INTERACTIONS	25
FIGURE 2.2 OVERLAP OF n AND π^* ORBITALS IN THE CALCULATED TS (B3LYP-D3/6-311G*) OF 1 (COCH ₃) IN THE THREE DIMENSIONAL ORBITAL RENDERING AND THE CHEMDRAW PRESENTATION OF TS HIGHLIGHTING THE INTRAMOLECULAR $n \rightarrow \pi^*$ INTERACTION (BLUE ARROW).....	26
FIGURE 2.3 DEFINITIONS OF THE PARAMETER Θ MEASURING THE PYRAMIDALIZATION OF SP ² AND BENDING OF SP ¹ ACCEPTOR CARBONS IN $n \rightarrow \pi^*$ INTERACTIONS AND THE DISTANCE PARAMETER D MEASURING THE O...C DISTANCE.....	27
FIGURE 2.4 (A) CORRELATION PLOT OF THE MEASURED TS STABILIZATION ($\Delta\Delta G^\ddagger_{\text{EXP}}$) AND THE CALCULATED NATURAL BOND ORDER (NBO) ENERGIES FOR THE TS $n \rightarrow \pi^*$ INTERACTION IN 1 (R). (B) CORRELATION PLOT OF THE	

MEASURED TS STABILIZATION ($\Delta\Delta G_{\ddagger}^{\text{EXP}}$) AND THE CALCULATED DONOR-TO-ACCEPTOR DISTANCE (D) IN THE TS OF 1 (R).....	28
FIGURE 2.5 SYNTHESIS OF ROTOR 1 (SCH ₃).....	31
FIGURE 2.6 SYNTHESIS OF ROTOR 1 (PH)	32
FIGURE 2.7 SYNTHESIS OF ROTOR 1 (CF ₃)	33
FIGURE 2.8 SYNTHESIS OF ROTOR 1 (CHO)	34
FIGURE 2.9 SYNTHESIS OF ROTOR 1 (COCH ₃)	35
FIGURE 2.10 SYNTHESIS OF ROTOR 1 (COPH).....	36
FIGURE 2.11 SYNTHESIS OF ROTOR 1 (C(CH ₂)CH ₃).....	37
FIGURE 2.12 SYNTHESIS OF ROTOR 1 (CCH)	38
FIGURE 2.13 SYNTHESIS OF ROTOR 1 (CN)	39
FIGURE 2.14 ¹ H NMR SPECTRA OF ROTOR 1 (SCH ₃) (400 MHz, CHLOROFORM-D).....	40
FIGURE 2.15 ¹³ C NMR SPECTRA OF ROTOR 1 (SCH ₃) (100 MHz, CHLOROFORM-D)	40
FIGURE 2.16 ¹ H NMR SPECTRA OF ROTOR 1 (PH) (400 MHz, CHLOROFORM-D).....	41
FIGURE 2.17 ¹³ C NMR SPECTRA OF ROTOR 1 (PH) (100 MHz, CHLOROFORM-D).....	41
FIGURE 2.18 ¹ H NMR SPECTRA OF ROTOR 1 (CF ₃) (400 MHz, CHLOROFORM-D)	42
FIGURE 2.19 ¹³ C NMR SPECTRA OF ROTOR 1 (CF ₃) (100 MHz, CHLOROFORM-D)	42
FIGURE 2.20 ¹ H NMR SPECTRA OF ROTOR 1 (CHO) (400 MHz, CHLOROFORM-D).....	43
FIGURE 2.21 ¹³ C NMR SPECTRA OF ROTOR 1 (CHO) (100 MHz, CHLOROFORM-D).....	43
FIGURE 2.22 ¹ H NMR SPECTRA OF ROTOR 1 (COCH ₃) (400 MHz, CHLOROFORM-D)	44
FIGURE 2.23 ¹³ C NMR SPECTRA OF ROTOR 1 (COCH ₃) (100 MHz, CHLOROFORM-D)	44
FIGURE 2.24 ¹ H NMR SPECTRA OF ROTOR 1 (COPH) (400 MHz, CHLOROFORM-D)	45
FIGURE 2.25 ¹³ C NMR SPECTRA OF ROTOR 1 (COPH) (100 MHz, CHLOROFORM-D)	45

FIGURE 2.26 ^1H NMR SPECTRA OF ROTOR 1 (C(CH ₂)CH ₃) (400 MHz, CHLOROFORM-D).....	46
FIGURE 2.27 ^{13}C NMR SPECTRA OF ROTOR 1 (C(CH ₂)CH ₃) (100 MHz, CHLOROFORM-D).....	46
FIGURE 2.28 ^1H NMR SPECTRA OF ROTOR 1 (CCH) (400 MHz, CHLOROFORM-D)	47
FIGURE 2.29 ^{13}C NMR SPECTRA OF ROTOR 1 (CCH) (100 MHz, CHLOROFORM-D)	47
FIGURE 2.30 ^1H NMR SPECTRA OF ROTOR 1 (CN) (400 MHz, CHLOROFORM-D).....	48
FIGURE 2.31 ^{13}C NMR SPECTRA OF ROTOR 1 (CN) (100 MHz, CHLOROFORM-D).....	48
FIGURE 2.32 EYRING PLOT FOR 1 (CHO)	50
FIGURE 2.33 ^1H NMR OF 1 (CHO) AT VARIOUS TEMPERATURES (-35, -30, -25, -20, -15, 0, AND 25 °C), HIGHLIGHTING THE PEAKS FOR THE ORTHO-HYDROGEN ON THE <i>N</i> -PHENYL ROTOR TO SHOW A CLEAR DECOALESCENCE.	51
FIGURE 2.34 NOESY/EXSY SPECTRA OF ROTOR 1 (CHO) AT -15 °C (400 MHz, DICHLOROMETHANE-D ²)	53
FIGURE 2.35 NOESY/EXSY SPECTRA OF ROTOR 1 (CHO) AT -20 °C (400 MHz, DICHLOROMETHANE-D ²)	53
FIGURE 2.36 NOESY/EXSY SPECTRA OF ROTOR 1 (CHO) AT -25 °C (400 MHz, DICHLOROMETHANE-D ²)	54
FIGURE 2.37 NOESY/EXSY SPECTRA OF ROTOR 1 (CHO) AT -30 °C (400 MHz, DICHLOROMETHANE-D ²)	54
FIGURE 2.38 NOESY/EXSY SPECTRA OF ROTOR 1 (CHO) AT -35 °C (400 MHz, DICHLOROMETHANE-D ²)	55
FIGURE 2.39 NOESY/EXSY SPECTRA OF ROTOR 1 (COCH ₃) AT -40 °C (400 MHz, DICHLOROMETHANE-D ²)	55
FIGURE 2.40 NOESY/EXSY SPECTRA OF ROTOR 1 (COCH ₃) AT -45 °C (400 MHz, DICHLOROMETHANE-D ²)	56
FIGURE 2.41 NOESY/EXSY SPECTRA OF ROTOR 1 (COCH ₃) AT -50 °C (400 MHz, DICHLOROMETHANE-D ²)	56
FIGURE 2.42 NOESY/EXSY SPECTRA OF ROTOR 1 (COCH ₃) AT -55 °C (400 MHz, DICHLOROMETHANE-D ²)	57

FIGURE 2.43 NOESY/EXSY SPECTRA OF ROTOR 1 (COCH ₃) AT -60 °C (400 MHZ, DICHLOROMETHANE-D ²)	57
FIGURE 2.44 NOESY/EXSY SPECTRA OF ROTOR 1 (COPh) AT -20 °C (400 MHZ, DICHLOROMETHANE-D ²)	58
FIGURE 2.45 NOESY/EXSY SPECTRA OF ROTOR 1 (COPh) AT -30 °C (400 MHZ, DICHLOROMETHANE-D ²)	58
FIGURE 2.46 NOESY/EXSY SPECTRA OF ROTOR 1 (COPh) AT -25 °C (400 MHZ, DICHLOROMETHANE-D ²)	59
FIGURE 2.47 NOESY/EXSY SPECTRA OF ROTOR 1 (COPh) AT -35 °C (400 MHZ, DICHLOROMETHANE-D ²)	59
FIGURE 2.48 NOESY/EXSY SPECTRA OF ROTOR 1 (COPh) AT -40 °C (400 MHZ, DICHLOROMETHANE-D ²)	60
FIGURE 2.49 CORRELATION PLOT BETWEEN GROUND STATE POPULATION RATIOS AND ROTATIONAL BARRIER ENERGIES (KCAL/MOL).....	60
FIGURE 2.50 CORRELATION OF THE CALCULATED ($\Delta G_{\text{CALC}}^{\ddagger}$) AND EXPERIMENTAL ($\Delta G_{\text{EXP}}^{\ddagger}$) ROTATIONAL BARRIERS FOR 1 (R). STRUCTURES WERE CALCULATED AT THE B3LYP-D3(0)/6-311G* LEVEL OF THEORY WITH THERMODYNAMIC CORRECTIONS.	61
FIGURE 2.51 STRUCTURES OF THE PARA-SUBSTITUTED <i>N</i> -(O-TOLYL)IMIDE ROTORS 1 (CH ₃) AND 3 (CH ₃).....	94
FIGURE 2.52 THE TWO CALCULATED TS GEOMETRIES (TS _I AND TS _{II} , B3LYP-D3/6-311G*) FOR 1 (SCH ₃) AND THE CORRESPONDING CONFORMATIONS OF THE THIOETHER MOTIF (CAPPED WITH HYDROGEN). THE CALCULATED N→Σ* STABILIZATION (E(N→Σ*), ΩB97M-V/6-311G*) ASSOCIATED WITH TS _I AND TS _{II} AS WELL AS THE SINGLE POINT ENERGIES (E, B3LYP-D3/6-311G*) FOR THE CORRESPONDING HYDROGEN-CAPPED THIOETHERS.....	96
FIGURE 2.53 CORRELATION PLOT OF THE MEASURED TS STABILIZATION ($\Delta\Delta G_{\text{EXP}}^{\ddagger}$) AND THE CALCULATED NBO ATOMIC CHARGES (B3LYP-D3/6-311G*) OF THE FIRST CARBON ATOM OF THE <i>ORTHO</i> R-GROUPS.	102
FIGURE 3.1 (A) THE <i>SYN-ANTI</i> CONFORMATIONAL EQUILIBRIUM OF MOLECULAR ROTORS 1 , 2 , AND 3 DESIGNED TO ISOLATE AND MEASURE THE TS STABILIZATION OF THE INTRAMOLECULAR HYDROGEN BOND VIA CHANGES IN THE RATE OF ROTATION. (B) REPRESENTATIONS OF THE TS GEOMETRIES AND THE NON-COVALENT AND STERIC INTERACTIONS FORMED IN THE TS	106

FIGURE 3.2 ¹ H NMR MEASURED ROTATIONAL BARRIERS (ΔG^\ddagger) OF SUBSTITUTED ROTORS 1 , 2 (LEFT TO RIGHT, X = <i>P</i> -NO ₂ , <i>M</i> -NO ₂ , <i>P</i> -CN, <i>M</i> -CL, <i>P</i> - <i>T</i> -AMYL, <i>P</i> -CL, AND H) PLOTTED AGAINST THE MEASURED ASSOCIATION ENERGIES OF THE ANALOGOUSLY SUBSTITUTED PHENOL•NMP COMPLEXES IN CD ₂ CL ₂ . THE DIFFERENCE IN THE ROTATIONAL BARRIER BETWEEN 1 AND 2 CORRESPONDS TO THE TS STABILIZATION OF THE HYDROGEN BOND.....	109
FIGURE 3.3 THE BIMOLECULAR COMPLEXES BETWEEN <i>N</i> -METHYL PYRROLIDONE (NMP) AND SUBSTITUTED PHENOLS USED TO INDEPENDENTLY MEASURE THE PHENOL-CARBONYL HYDROGEN BOND STRENGTHS.	111
FIGURE 3.4 HAMMETT PLOT CORRELATING THE INTERMOLECULAR HYDROGEN BOND STRENGTH	111
FIGURE 3.5 THE OPTIMIZED TS STRUCTURES (B3LYP-D3(BJ)/DEF2-TZVP) AND ENERGIES (B2GP-PLYP-D3(BJ)/DEF2-TZVP) FOR ROTORS 1 AND 2 AND ROTOR 1 CONSTRAINED WITH THE PHENOL HYDROGEN FIXED IN A NON-HYDROGEN BONDING GEOMETRY.	113
FIGURE 3.6 (A) HYDROGEN BONDING AND NON-HYDROGEN BONDING BIMOLECULAR COMPLEXES USED IN THE SAPT ANALYSES WITH THE OVERLAPPING VDW RADII OF THE OXYGEN ATOMS HIGHLIGHTED IN RED. (B) SAPT ENERGIES ($E_{\text{EL.ST.}}$ = ELECTROSTATIC, $E_{\text{EXCH.}}$ = EXCHANGE, $E_{\text{IND.}}$ = INDUCTION, $E_{\text{DISP.}}$ = DISPERSION, E_{TOTAL} = SUM OF ALL COMPONENT ENERGIES) CALCULATED (CCSD/CC-PVTZ) FOR THE PHENOL•NMP COMPLEX (X = H) IN THE HYDROGEN BONDING AND NON-HYDROGEN BONDING GEOMETRIES, AND THE DIFFERENCE ENERGIES: ΔE = (HYDROGEN BONDING E) - (NON-HYDROGEN BONDING E).	115
FIGURE 3.7 STATE EQUATIONS FOR CALCULATING THE THERMODYNAMIC (EQ. 1) AND TS NCI (EQ. 2) INTERACTION ENERGIES. THE ENERGIES ARE CALCULATED FROM THE DIFFERENCE BETWEEN THE NCI STRUCTURES (RIGHT) AND NON-NCI CONTROL STRUCTURES (LEFT).....	117
FIGURE 3.8 SYNTHESIS OF ROTOR 1 (X = H)	120
FIGURE 3.9 SYNTHESIS OF ROTOR 1 (X = <i>P</i> -NO ₂).....	121
FIGURE 3.10 SYNTHESIS OF ROTOR 1 (X = <i>M</i> -NO ₂).....	121
FIGURE 3.11 SYNTHESIS OF ROTOR 1 (X = <i>P</i> -CL)	122
FIGURE 3.12 SYNTHESIS OF ROTOR 1 (X = <i>M</i> -CL)	123
FIGURE 3.13 SYNTHESIS OF ROTOR 1 (X = <i>P</i> -CN)	124

FIGURE 3.14 SYNTHESIS OF ROTOR 1 (X = <i>P-T</i> -AMYL)	124
FIGURE 3.15 SYNTHESIS OF ROTOR 2 (X = H)	125
FIGURE 3.16 SYNTHESIS OF ROTOR 2 (X = <i>P</i> -NO ₂).....	126
FIGURE 3.17 SYNTHESIS OF ROTOR 2 (X = <i>M</i> -NO ₂).....	127
FIGURE 3.18 SYNTHESIS OF ROTOR 2 (X = <i>P</i> -CL)	128
FIGURE 3.19 SYNTHESIS OF ROTOR 2 (X = <i>M</i> -CL)	129
FIGURE 3.20 SYNTHESIS OF ROTOR 2 (X = <i>P</i> -CN)	130
FIGURE 3.21 SYNTHESIS OF ROTOR 2 (X = <i>P-T</i> -AMYL)	131
FIGURE 3.22 ¹ H NMR SPECTRA OF ROTOR 1 (X = H) (400 MHz, DICHLOROMETHANE-D ₂).....	132
FIGURE 3.23 ¹³ C NMR SPECTRA OF ROTOR 1 (X = H) (100 MHz, DICHLOROMETHANE-D ₂).....	132
FIGURE 3.24 ¹ H NMR SPECTRA OF ROTOR 1 (X = <i>P</i> -NO ₂) (400 MHz, ACETONE-D ₆)	133
FIGURE 3.25 ¹³ C NMR SPECTRA OF ROTOR 1 (X = <i>P</i> -NO ₂) (100 MHz, ACETONE-D ₆)	133
FIGURE 3.26 ¹ H NMR SPECTRA OF ROTOR 1 (X = <i>M</i> -NO ₂) (400 MHz, ACETONE-D ₆).....	134
FIGURE 3.27 ¹³ C NMR SPECTRA OF ROTOR 1 (X = <i>M</i> -NO ₂) (100 MHz, ACETONE-D ₆).....	134
FIGURE 3.28 ¹ H NMR SPECTRA OF ROTOR 1 (X = <i>P</i> -CL) (400 MHz, ACETONE-D ₆)	135
FIGURE 3.29 ¹³ C NMR SPECTRA OF ROTOR 1 (X = <i>P</i> -CL) (100 MHz, ACETONE-D ₆).....	135
FIGURE 3.30 ¹ H NMR SPECTRA OF ROTOR 1 (X = <i>M</i> -CL) (400 MHz, ACETONE-D ₆)	136
FIGURE 3.31 ¹³ C NMR SPECTRA OF ROTOR 1 (X = <i>M</i> -CL) (100 MHz, ACETONE-D ₆).....	136
FIGURE 3.32 ¹ H NMR SPECTRA OF ROTOR 1 (X = <i>P</i> -CN) (400 MHz, ACETONE-D ₆)	137
FIGURE 3.33 ¹³ C NMR SPECTRA OF ROTOR 1 (X = <i>P</i> -CN) (100 MHz, ACETONE-D ₆)	137
FIGURE 3.34 ¹ H NMR SPECTRA OF ROTOR 1 (X = <i>P-T</i> -AMYL) (400 MHz, CHLOROFORM-D ₁)	138

FIGURE 3.35 ^{13}C NMR SPECTRA OF ROTOR 1 ($\text{X} = P\text{-T-AMYL}$) (100 MHz, CHLOROFORM- D_1)	138
FIGURE 3.36 ^1H NMR SPECTRA OF ROTOR 2 ($\text{X} = P\text{-NO}_2$) (400 MHz, TETRACHLOROETHANE- D_4)	139
FIGURE 3.37 ^{13}C NMR SPECTRA OF ROTOR 2 ($\text{X} = P\text{-NO}_2$) (400 MHz, TETRACHLOROETHANE- D_4)	139
FIGURE 3.38 ^1H NMR SPECTRA OF ROTOR 2 ($\text{X} = M\text{-NO}_2$) (400 MHz, CHLOROFORM- D_1).....	140
FIGURE 3.39 ^{13}C NMR SPECTRA OF ROTOR 2 ($\text{X} = M\text{-NO}_2$) (100 MHz, CHLOROFORM- D_1)	140
FIGURE 3.40 ^1H NMR SPECTRA OF ROTOR 2 ($\text{X} = P\text{-CL}$) (100 MHz, ACETONE- D_6).....	141
FIGURE 3.41 ^{13}C NMR SPECTRA OF ROTOR 2 ($\text{X} = P\text{-CL}$) (100 MHz, ACETONE- D_6).....	141
FIGURE 3.42 ^1H NMR SPECTRA OF ROTOR 2 ($\text{X} = M\text{-CL}$) (400 MHz, ACETONE- D_6)	142
FIGURE 3.43 ^{13}C NMR SPECTRA OF ROTOR 2 ($\text{X} = M\text{-CL}$) (100 MHz, ACETONE- D_6).....	142
FIGURE 3.44 ^1H NMR SPECTRA OF ROTOR 2 ($\text{X} = P\text{-CN}$) (400 MHz, ACETONE- D_6).....	143
FIGURE 3.45 ^{13}C NMR SPECTRA OF ROTOR 2 ($\text{X} = P\text{-CN}$) (100 MHz, ACETONE- D_6).....	143
FIGURE 3.46 ^1H NMR SPECTRA OF ROTOR 2 ($\text{X} = P\text{-T-AMYL}$) (400 MHz, ACETONE- D_6).....	144
FIGURE 3.47 ^{13}C NMR SPECTRA OF ROTOR 2 ($\text{X} = P\text{-T-AMYL}$) (100 MHz, ACETONE- D_6).....	144
FIGURE 3.48 SPECTRAL REGIONS OF ROTOR 1 (A) AND ROTOR 2 (B AND C) IN VT NMR EXPERIMENT: A) ETHENE PROTONS ON ROTOR 1 COALESCED AT $-55\text{ }^\circ\text{C}$ (DICHLOROMETHANE- D_2); B) ETHENE PROTONS ON ROTOR 2 DID NOT REACH COALESCENCE UP TO $117\text{ }^\circ\text{C}$; C) METHOXY PROTONS ON ROTOR 2 COALESCED AT $113\text{ }^\circ\text{C}$ (TETRACHLOROETHANE- D_2).....	147
FIGURE 3.49 ^1H NMR EXCHANGE LINE-SHAPE ANALYSIS FOR UNSUBSTITUTED PHENOL ROTOR 1 IN DICHLOROMETHANE- D_2 SHOWING THE OVERLAID EXPERIMENTAL (BLUE LINES) AND SIMULATED (GREEN LINES) TRACES	148
FIGURE 3.50 EYRING PLOTS FOR ROTORS 1 AND 2	149

FIGURE 3.51 INTERMOLECULAR HYDROGEN BOND BETWEEN <i>N</i> -METHYLPYRROLIDONE (NMP) AND SUBSTITUTED PHENOLS.	150
FIGURE 3.52 EXPERIMENTALLY MEASURED AND FITTED ISOTHERMS (IN DICHLOROMETHANE-D ₂) OF NMP (GUEST) BINDING OF <i>m</i> -NITROPHENOL (HOST) BASED ON CHEMICAL SHIFT CHANGE ($\Delta\Delta$) OF THE PHENOLIC PROTON AS NMP GUEST WAS GRADUALLY ADDED.	151
FIGURE 3.53 CRYSTAL STRUCTURE OF ROTOR 1 (X = H)	153
FIGURE 3.54 CRYSTAL STRUCTURE OF ROTOR 1 (X = <i>p</i> -Cl)	155
FIGURE 3.55 CRYSTAL STRUCTURE OF ROTOR 1 (X = <i>m</i> -Cl).....	156
FIGURE 3.56 CRYSTAL STRUCTURE OF ROTOR 2 (X = <i>p</i> -NO ₂).....	158
FIGURE 3.57 CRYSTAL STRUCTURE OF ROTOR 2 (X = <i>m</i> -Cl).....	160
FIGURE 3.58 CRYSTAL STRUCTURE OF ROTOR 2 (X = <i>p</i> -CN)	162
FIGURE 3.59 CORRELATION OF THE CALCULATED ($\Delta G^{\ddagger}_{\text{CALC.}}$) AND EXPERIMENTAL ($\Delta G^{\ddagger}_{\text{EXP.}}$) ROTATIONAL BARRIERS FOR THE PHENOL (LEFT) AND ANISOLE (RIGHT) ROTORS. STRUCTURES WERE CALCULATED AT THE B2GP-PLYP-D3(BJ)/DEF2-TZVP LEVEL OF THEORY WITH THERMODYNAMIC CORRECTIONS.....	171
FIGURE 3.60 CALCULATED ROTATIONAL BARRIERS FOR THE UNSUBSTITUTED PHENOL 1 AND ANISOLE 2 ROTORS WITH (ΔG^{\ddagger}) AND WITHOUT (ΔE^{\ddagger}) THERMODYNAMIC CORRECTIONS.	172
FIGURE 3.61 TWO CONFIGURATIONS OF THE BIMOLECULAR COMPLEX OF NMP AND PHENOL (X=H) USED FOR SAPT ANALYSIS: HYDROGEN BONDING (HB, LEFT) AND NON-HYDROGEN BONDING (NHB, RIGHT).	173
FIGURE 3.62 SAPT ENERGIES FOR THE NMP-PHENOL COMPLEX BETWEEN 2.0 AND 3.0 Å IN THE CONFIGURATIONS WITH (A) AND WITHOUT (B) HYDROGEN BOND AS WELL AS THE CORRESPONDING ENERGY DIFFERENCE (C).	176
FIGURE 3.63 CORRELATIONS OF THE CALCULATED HYDROGEN BOND ACE TOTAL (ΔE_{TOTAL} , KCAL/MOL) AND COMPONENT ENERGY TERMS (ΔE_{ELST} , ΔE_{EXCH} , ΔE_{IND} , AND ΔE_{DISP} KCAL/MOL) WITH THE EXPERIMENTALLY MEASURED ASSOCIATION ENERGIES (ΔG_{KA} , KCAL/MOL) IN THE BIMOLECULAR COMPLEXES OF NMP AND SUBSTITUTED PHENOLS. THE CALCULATED TOTAL AND COMPONENT TERMS WERE TABULATED IN TABLE 3.12, AND THE EXPERIMENTALLY MEASURED ASSOCIATION ENERGIES WERE TABULATED IN TABLE 3.2.	179

FIGURE 4.1 CORRELATION PLOT OF THE EXPERIMENTALLY MEASURED ROTATIONAL BARRIERS FOR $n \rightarrow \pi^*$ ROTORS AND $n \cdots \pi_{(AR)}$ ROTORS VERSUS THE STERIC B-VALUES OF THE R GROUPS. THE STERIC TRENDLINE IS DRAWN THROUGH THE ROTORS THAT HAVE ORTHO R GROUPS WITHOUT A π^* ORBITAL (BLACK CIRCLES) AND THUS LACK $n \rightarrow \pi^*$ INTERACTIONS. THE BLUE CIRCLES CORRESPOND TO THE ROTORS THAT FORM $n \rightarrow \pi^*$ INTERACTIONS AND THE GREEN CIRCLES CORRESPOND TO THE ROTORS THAT FORM $n \cdots \pi_{(AR)}$ INTERACTIONS.	191
FIGURE 4.2 CORRELATION PLOT OF THE MEASURED TS STABILIZATION ($\Delta\Delta G^\ddagger_{EXP}$) AND THE CALCULATED ESP PARAMETERS (ESP) FOR THE $n \cdots \pi_{(AR)}$ AND $n \rightarrow \pi^*$ ROTORS. (B) CORRELATION PLOT OF THE MEASURED TS STABILIZATION ($\Delta\Delta G^\ddagger_{EXP}$) AND THE CALCULATED NBO ENERGY FOR THE $n \cdots \pi_{(AR)}$ AND $n \rightarrow \pi^*$ ROTORS.	193
FIGURE 4.3 LINEAR FREE ENERGY PLOT FOR THE $n \cdots \pi_{(AR)}$ AND $n \rightarrow \pi^*$ ROTORS.	195
FIGURE 4.4 GENERAL ROUTE FOR THE SYNTHESIS OF THE ORTHO-PHENYL SUBSTITUTED ANILINES.	197
FIGURE 4.5 SYNTHESIS OF ROTOR (PH-F).....	198
FIGURE 4.6 SYNTHESIS OF ROTOR (PH-F ₃)	199
FIGURE 4.7 SYNTHESIS OF ROTOR (PH-F ₅)	199
FIGURE 4.8 SYNTHESIS OF ROTOR (PH-NO ₂).....	200
FIGURE 4.9 SYNTHESIS OF ROTOR (PH-(NO ₂) ₂).....	201
FIGURE 4.10 ¹ H NMR SPECTRA OF ROTOR 13 (400 MHZ, CHLOROFORM-D)	202
FIGURE 4.11 ¹³ C NMR SPECTRA OF ROTOR (PH-H) (400 MHZ, CHLOROFORM-D).....	202
FIGURE 4.12 ¹⁹ F NMR SPECTRA OF ROTOR (PH-H) (400 MHZ, CHLOROFORM-D)	203
FIGURE 4.13 ¹ H NMR SPECTRA OF ROTOR (PH-P-F) (400 MHZ, CHLOROFORM-D)	203
FIGURE 4.14 ¹³ C NMR SPECTRA OF ROTOR (PH-P-F) (400 MHZ, CHLOROFORM-D).....	204
FIGURE 4.15 ¹⁹ F NMR SPECTRA OF ROTOR (PH-M,M,P-F ₃) (400 MHZ, CHLOROFORM-D).....	204
FIGURE 4.16 ¹ H NMR SPECTRA OF ROTOR (PH-M,M,P-F ₃) (400 MHZ, CHLOROFORM-D).....	205

FIGURE 4.17 ^{13}C NMR SPECTRA OF ROTOR (PH-F ₅) (400 MHZ, CHLOROFORM-D).....	205
FIGURE 4.18 ^{19}F NMR SPECTRA OF ROTOR (PH-F ₅) (400 MHZ, CHLOROFORM-D)	206
FIGURE 4.19 ^1H NMR SPECTRA OF ROTOR (PH-P-NO ₂) (400 MHZ, CHLOROFORM-D)	206
FIGURE 4.20 ^{13}C NMR SPECTRA OF ROTOR (PH-P-NO ₂) (400 MHZ, CHLOROFORM-D).....	207
FIGURE 4.21 ^1H NMR SPECTRA OF ROTOR (PH-M,M-(NO ₂) ₂) (400 MHZ, CHLOROFORM-D).....	207
FIGURE 4.22 ^{13}C NMR SPECTRA OF ROTOR (PH-M,M-(NO ₂) ₂) (400 MHZ, CHLOROFORM-D).....	208
FIGURE 4.23 EYRING PLOT FOR THE PH-F ₅ ROTOR	210
FIGURE 4.24 CORRELATION OF THE CALCULATED ($\Delta G^\ddagger_{\text{CALC}}$) AND EXPERIMENTAL ($\Delta G^\ddagger_{\text{EXP}}$) ROTATIONAL BARRIERS USED IN THIS DISSERTATION. STRUCTURES WERE CALCULATED AT THE B3LYP-D3(0)/6-311G* LEVEL OF THEORY WITH THERMODYNAMIC CORRECTIONS.	211
FIGURE 4.25 ESP MAPS FOR THE R-GROUPS USED IN THIS STUDY.	219
FIGURE 5.1 STERIC CORRELATION PLOT.....	226
FIGURE 5.2 FOUR DIFFERENT MOLECULAR ROTORS USED TO STUDY SUBSTITUENTS EFFECTIVE RADII. ^{15-21,94}	227
FIGURE 5.3 (LEFT) CORRELATION PLOT OF THE INDIVIDUAL ROTORS TO THE PREDICTED ROTATIONAL BARRIER WITH SOME OUTLIERS. (RIGHT) COMBINATION OF THE INDIVIDUAL ROTORS CORRELATED TO THE PREDICTED ROTATIONAL BARRIER.....	229

LIST OF SCHEMES

SCHEME 2.1 (A) CONFORMATIONAL <i>SYN-ANTI</i> EQUILIBRIUM OF MOLECULAR ROTOR 1 (R) ARISING FROM ROTATION OF THE <i>N</i> -PHENYL RING, AND ITS PLANAR TS, AND (B) CONFORMATIONAL S_A-R_A EQUILIBRIUM OF BIPHENYL ROTOR 2 (R) USED TO MEASURE MAZZANTI'S STERIC PARAMETER B -VALUE OF THE R GROUPS, AND ITS PLANAR TS.....	21
SCHEME 2.2 GENERAL ROUTE FOR SYNTHESIZING MOLECULAR ROTORS.....	30
SCHEME 3.1 GENERAL ROUTE FOR SYNTHESIZING MOLECULAR ROTORS.....	119
SCHEME 4.1 ISOMERIZATION PROCESS FOR THE MOLECULAR ROTORS USED IN THIS STUDY.....	190
SCHEME 4.2 GENERAL ROUTE FOR SYNTHESIZING MOLECULAR ROTORS.....	197
SCHEME 5.1 ROTATIONAL BARRIER FOR THE STERIC SUBSTITUENTS	227

LIST OF ABBREVIATIONS

ΔG^\ddagger	Difference in Gibb's free energy between GS and TS energy
ΔH^\ddagger	Difference in enthalpy between GS and TS energy
ΔS^\ddagger	Difference in entropy between GS and TS energy
$\Delta \nu$	Difference in peak frequency in the slow exchange regime
$\Delta \delta_{HG}$	Maximum change in peak frequency upon host-guest binding
DFT	Density Functional Theory
GS	Ground State
$[H]_{free}$	Free host concentration after the i th guest addition
$[H]_i$	Total host concentration after the i th guest addition
$[H]_0$	Initial host concentration
k_B	Boltzmann's constant
k_c	Exchange rate at T_c
k_{ex}	Exchange rate
K_a	Association constant
NBO	Natural Bond Order
R	Gas Constant
SAPT	Symmetry Adapted Perturbation Theory
T	Temperature
T_c	Coalescence Temperature
TS	Transition State

V_0 Initial Volume
 V_i Volume after the i th guest addition
 $[G]_i$ Total guest concentration after the i th guest addition
 $[G]_0$ Guest concentration in the stock solution

CHAPTER 1 UTILIZING EMPIRICAL PARAMETERS AND COMPUTATIONAL
CALCULATIONS TO STUDY NON-COVALENT INTERACTIONS

1.1 ABSTRACT

The first chapter of this dissertation introduces the application of empirical parameters and computational calculations to study non-covalent interactions. Non-covalent interactions are present throughout our world and are important for the utility of everyday items from materials to drugs. By combining empirical parameters and computational calculations, non-covalent interactions can be predicted and understood with a high degree of precision and accuracy. Empirical parameters are experimentally measured values collected for a series of structures or subunits, which can be utilized to explain non-covalent interactions and predict properties through extrapolation. Computational calculations utilize molecular mechanics (empirical parameters), quantum mechanics (*ab initio*), or a combination of the two (semi-empirical) to reproduce experimental measurements. Calculations can also decompose interaction energies into physically meaningful components like electrostatics, exchange, induction, dispersion, and charge-transfer.

1.2 NON-COVALENT INTERACTIONS

Non-covalent interactions (NCIs) impact our everyday life by governing many aspects of the world we live in from the water that we drink to the air that we breathe. NCIs are widely studied because of the important role they play in many physical phenomena. Comprehensive reviews of NCIs can be found in recently published books and articles.¹⁻⁷ Herein, several key questions relating to NCIs will be addressed because they provide the background and framework for the research presented in this dissertation. The questions are: Why should NCIs be studied? How are NCIs analyzed? How close are we to constructing a universal model that accurately explains all interactions and their energies?

One reason why NCIs should be studied is to construct a model that can predict interaction energies and trends with high accuracy. If we could predict NCI strengths accurately, then we would be able to rationally construct better materials and pharmaceuticals. In addition, properties of materials could be predicted eliminating the need for resource intensive optimization processes. Determination of better designed drugs for a binding site on a protein could be made with higher confidence. Another reason is the development of new and improved catalysts.⁸ Many catalysts utilize NCIs such as hydrogen bonding, cation-pi, and aromatic stacking to stabilize TSs, and control reaction selectivity.⁹ However, the measurement of NCIs in a TS is much more challenging than in stable structures and complexes.¹⁰

NCIs can be broken down into 5 different fundamental interactions (Figure 1.1): **electrostatic interactions** involving the attraction or repulsion between charges or multipoles (e.g. charge-charge, charge-multipole, multipole-multipole), **exchange repulsion** involving repulsion due to the Pauli exclusion principle from electron cloud overlap, **charge-transfer** involving stabilization due to the direct transfer of electron density from one orbital to another (e.g. a lone pair donating into an antibonding orbital), **induction interactions** involving the attraction from charges or multipoles on one molecule/group inducing polarization onto a separate molecule/group (e.g. charge-induced multipole, multipole-induced multipole), **dispersion interactions** involving the attraction of spontaneously induced multipoles (e.g. induced multipole-induced multipole).^{2,11} NCIs are normally governed by one or two of the fundamental interactions while the other fundamental interactions have a negligible impact on the total interaction energy. However, fundamental interactions are often interdependent and difficult to experimentally isolate.

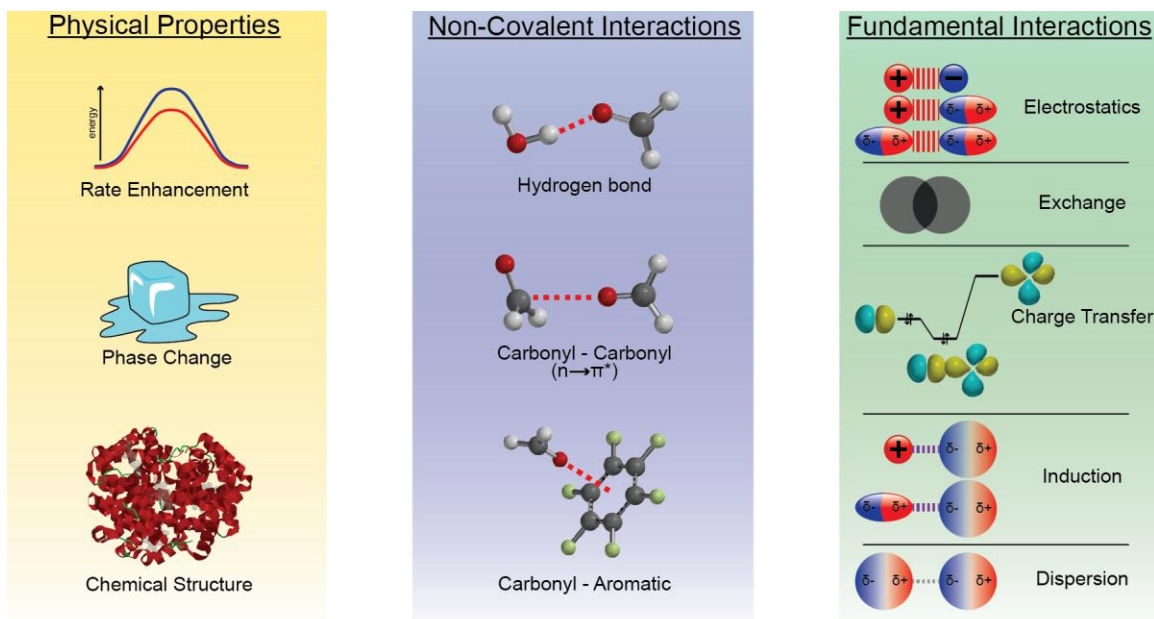


Figure 1.1 Physical properties of material are governed by NCIs, and NCIs are governed by fundamental interactions

NCIs can be clustered into groups that act similarly based on which fundamental interaction is providing the greatest contribution to the overall interaction energy. For NCIs where charge-transfer is dominant, the stabilization of the interactions increases when the electron donor and acceptor have similarly matched orbital energies or are closer in space.¹² For NCIs that are governed by electrostatic interactions, the stabilization depends on the environment (solvent and adjacent atoms) and the difference in charge between the groups (which can approach ionic bonding).¹³ There are also NCIs where the interactions are destabilizing and are governed by exchange repulsion (steric hindrance). In these cases, the energy depends on the size and overlap of the interacting groups.

Empirical and computational parameters have been used to identify similar trends and the governing fundamental interactions. Currently, most predictive models of NCI energies are limited in scope or require too much computing power. There are many studies that attempt to predict specific interactions like hydrogen bonds via empirical models, however, environmental effects (e.g. solvent and adjacent atoms) complicate the predictive

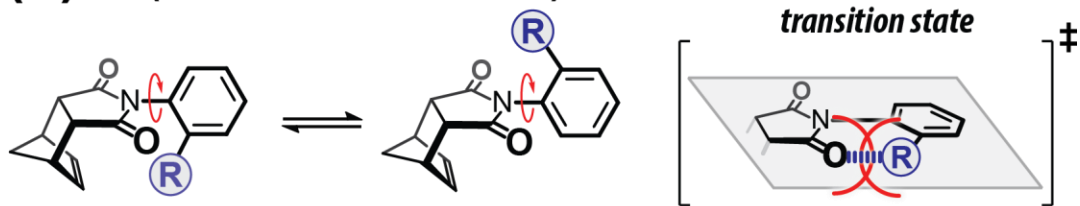
accuracy and are useful only in similar situations such as intermolecular vs. intramolecular. Some of the most accurate energy predictions come from *ab initio* calculations, but their errors can often be greater than the overall NCI interaction energy.¹⁴

1.3 EMPIRICAL AND CALCULATED PARAMETERS

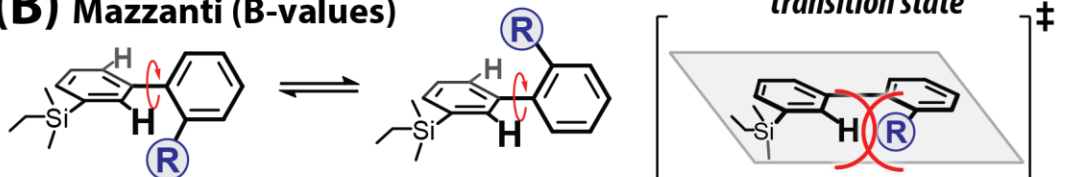
Empirical and computational parameters have been used to identify trends and the governing fundamental interactions. Empirical parameters are experimentally measured values or derived from measured values. Examples include interaction strengths, equilibrium ratios, barrier heights, reaction rates, atom radii, bond distances, bond angles, or any other experimental observable. Computational parameters are calculated properties from the molecules or subunits being studied. Examples include atomic or surface charges, surface areas, volume, distances, bond angles, or any other calculated property. The utilization of empirical and calculated parameters extends from catalyst design to drug development. Predictive models can be designed by combining useful parameters into linear free energy relationships (LFER) which have been used to estimate quantitative values for new or theoretical molecules. From a LFER, the importance for each parameter can be determined, which can assist in identifying the governing fundamental interaction. A major limitation of LFER models is the system dependence as a LFER model for one system or interaction is will not necessarily be applicable to a different system.

There are many empirical and computational parameters in the literature. An exhausting list of these parameters would be impractical for the purposes of this chapter. Instead a list of selected structural parameters found generally useful and utilized in this dissertation can be found in Appendix A. These parameters are split into three different types: steric hindrance, electrostatics, and polarizability.

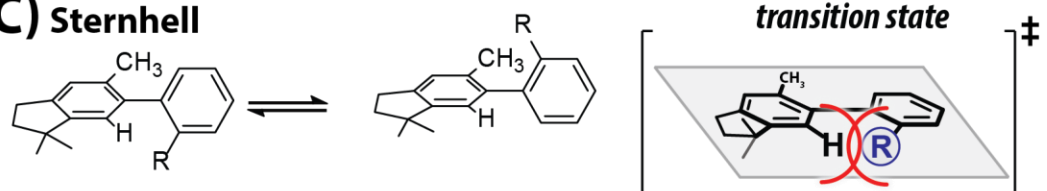
(A) Vik (imide rotational barrier)



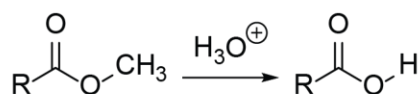
(B) Mazzanti (B-values)



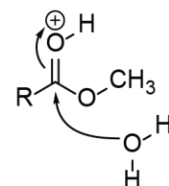
(C) Sternhell



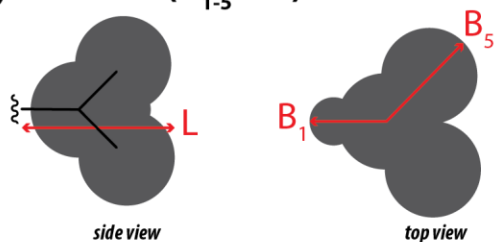
(D) Taft/Charton (E_s/v)



rate determining step



(E) Sterimol (B_{1-5} & L)



(F) Winstein-Holness (A-Values)

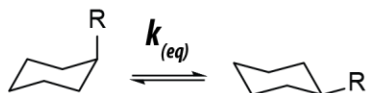


Figure 1.2 Common empirical parameters

Empirical parameters which correlate well to steric hindrance can be found in Figure 1.2. These parameters are best applied to similar processes. For example, a bond rotation process should correlate better to a bond rotation parameter, rather than to a nucleophilic addition to a carbonyl parameter. Parameters A-C in Figure 1.1 are all rotational barriers, which have their barrier energy dependent on the size of the R-group.¹⁵⁻²¹ Large R-groups (I, *i*-Pr, and CF₃) have larger barriers while small R-groups (F and OH) have small barriers. Parameter A in Figure 1.2 also has a significant contribution from electrostatics due to the partial negative charge on the imide carbonyl. Taft and Charton parameters are based on the rate of nucleophilic addition to an ester carbonyl.²²⁻²⁷ These parameters were measured under both acidic and basic conditions, which alter the barrier for certain substituents. Sterimol parameters are based on Corey-Pauling-Koltun (CPK) molecular models,²⁸ which are space filling models based on atomic radii.²⁹ There are different Sterimol parameters for each principle axis of a substituent. For example, the B₁ value is the minimum distance perpendicular to the primary axis, B₅ is the maximum distance perpendicular to the primary axis, and L is distance parallel to primary axis. Finally, A-values represent the conformation energy difference for an R-group in the axial vs. equatorial position on a cyclohexane.³⁰⁻³³

1.4 COMPUTATIONAL CALCULATIONS

Computational chemistry can be helpful in modeling and predicting physical properties. This section describes computational methods used in the dissertation. While there is a significant learning curve to effectively utilize computational chemistry, I firmly believe learning these techniques are worth the time and effort. Calculations can be used to quickly make predictions for experimental measurements.

A common aphorism in statistics from George E. P. Box is “All models are wrong, but some are useful.” This advise should be kept in mind while performing computational calculations. All computational results should be evaluated by statistical analysis to assess their accuracy. The accuracy of all methods should be questioned, unless previously established by benchmarking. For example, the commonly used B3LYP functional has a root mean square deviation of ± 5.96 kcal/mol for calculating reaction barrier heights, but the wB97M-V functional is more accurate with a root mean square deviation of ± 1.68 kcal/mol.¹⁴ However, the fact that the wB97M-V is more accurate than B3LYP in predicting barrier heights does not mean wB97M-V will be accurate in predicting the pKa of acidic protons. A new benchmark needs to be created in order quantify the accuracy of the functional for each specific task or system.

1.4.1 TECHNIQUES

Computational chemistry spans a broad range of techniques which are applicable in specific and general applications. The techniques discussed in this section will be limited to the ones utilized for the research in this dissertation. This section will include discussions of: (1) conformer distribution, (2) energy profile, (3) GS & TS geometry optimization, (4) density and electrostatic potential maps, and (5) perturbation theory. In general, these calculations should be performed in this order to ensure the accuracy of the GS & TS geometries.

1.4.1.1 CONFORMER DISTRIBUTION

A conformer distribution search should be the first calculation performed on a molecule or complex and will give an array of local ground states (minima) which hopefully includes the global ground state. The conformer distribution is calculated by

altering degrees of freedom in either a systematic or random (Monte-Carlo) search. Degrees of freedom are automatically identified in Spartan, but the torsions can also be manually selected. Low cost techniques such as molecular mechanics should be used for conformer distributions unless a small number of conformers are expected to exist.

1.4.1.2 ENERGY PROFILE

The energy profile calculation optimizes the molecular structure while systematically altering 1 or 2 degrees of freedom over a predetermined number of steps. If the conformer distribution does not select a conformer you expect to be present or if a transition state structure is needed, an energy profile calculation can be used. For example, the molecule biphenyl can have an energy profile calculated based on conformers generated from the rotation about the C-C single bond connecting the two aromatic rings. In this calculation, only 10 – 30 individual structures are optimized and calculated. Therefore, a low-level DFT method and basis set can be used, such as B3LYP/6-31G**.

1.4.1.3 GROUND AND TRANSITION STATE GEOMETRY OPTIMIZATION

Geometry and transition state geometry optimization are then performed on selected ground and transition state structures identified from the conformer distribution and energy profile searches. The geometries are calculated using self-consistent field theory at a higher level of theory than the conformational search calculations. The optimized GS can be verified by zero imaginary frequencies in the IR spectrum, and the TS can be verified by the presence of a single imaginary frequency.

1.4.1.4 DENSITY AND ELECTROSTATIC POTENTIAL MAP

Once a geometry (GS, TS or otherwise) is calculated using DFT, a density and/or electrostatic potential (ESP) map can be calculated. A density map can be calculated by

estimating the probability of locating an electron around the molecule with a specific density (the density map size can be altered by altering the density of electrons). This density map can be utilized for its surface area, solvent accessible surface area, and volume parameters. Alternatively, an ESP map can be calculated which uses the same electron probability to create the density map but also rotates a negative point charge around the density map to calculate the attractive/repulsive electrostatic interactions. Density and ESP maps can be useful in predicting dispersive and electrostatic interactions of a molecule. ESP maps have also been used to identify electron deficient regions on a molecule where charge-transfer can occur.

1.4.1.5 PERTURBATION THEORY

When computing interaction energies, the energy of two molecules infinitely separated and in contact can be computed and subtracted from each other. Alternatively, a perturbative expression for the interaction can be used instead. The terms in the perturbative expression are physically meaningful and can be used to describe the interaction energy. Two commonly used perturbation theory calculations are symmetry adapted perturbation theory (SAPT) and natural bond orbital (NBO). A more in depth description of the theory and applications of SAPT^{34,35} and NBO³⁶ analysis can be found in recent review articles. SAPT decomposes the total interaction energy of intermolecular complexes into fundamental electrostatics, exchange, induction, dispersion, and charge-transfer (using SAPT/cDFT) interactions. NBO can be used for inter- or intramolecular interactions and can be used to calculate charge-transfer interactions. SAPT calculations are highly dependent on the by basis set size, therefore larger basis sets are suggested.

1.4.2 METHODS

While performing calculations, the method should gradually increase in accuracy from molecular mechanics with a conformer distribution to coupled-cluster singles, doubles, and triples with SAPT and NBO calculations. The methods discussed in this section are listed in order of increasing accuracy: molecular mechanics, semi-empirical, Hartree-Fock, density functional theory, and correlated wavefunction. The two most commonly used methods are molecular mechanics and density functional theory. For example, a general approximation of geometry and energy can be made with molecular mechanics, and then density functional theory can improve those approximations.

1.4.2.1 MOLECULAR MECHANICS

Molecular mechanics (MM) are force fields optimized using experimental and calculated data. Their use should be limited to systems closely related to those that were used to develop and optimize the force field. Some commonly used molecular mechanic methods include AMBER, MMFF, and MMX. MM force fields are currently being optimized for drug discovery and substrate binding to proteins.³⁷

1.4.2.2 SEMI-EMPIRICAL

Semi-empirical (SE) methods are essentially a combination of *ab initio* and empirical parameters. By adding empirical corrections and coefficients to the HF method a more useful method can be created. Some SE methods can reproduce interaction energies similar to more costly methods.³⁸ In general, SE methods are used for specific cases in order to cut down computational cost for repeated calculations. Utilizing MM methods for geometry optimization and later re-optimizing using DFT methods leads to accurate geometries with reasonable computational cost.

1.4.2.3 HARTREE-FOCK

The Hartree-Fock (HF) method (also known as self-consistent field (SCF) theory) has added significant value to the computational chemistry field. HF is the first *ab initio* method which attempts to approximate the Schrodinger equation.³⁹ HF is guided by a Slater determinant which is a simple model but is inaccurate if more than one electron is present in the system.⁴⁰ Density functional theory and correlated wavefunctions were able to improve upon HF theory and create significantly more accurate approximations of the Schrodinger equation. HF calculations can take an order of magnitude longer than density functional theory and are usually less accurate.

1.4.2.4 DENSITY FUNCTIONAL THEORY

Density functional theory (DFT) is an *ab initio* method that approximates the Schrodinger equation using SCF theory to optimize geometries and orbitals. DFT is usually faster and more accurate than HF. DFT has an accuracy advantage over HF due to the added electron correlation and a reduction in CPU time by cutting out long-range electron exchange. Due to the versatility of functionals like B3LYP, DFT has been the generally accepted method for most types of calculations. In general, the accuracy of DFT calculations is ± 1 kcal/mol. Therefore, DFT has difficulty with weak interactions that are usually on the order of 1 kcal/mol or less.

1.4.2.5 CORRELATED WAVEFUNCTION

Correlated wavefunction (CW) methods are the most accurate computational methods. CW methods improve upon HF theory by including an estimate of electron-electron correlation. Common CW methods include MP2, MP3, MP4, CCSD, CCSD(T), CISD, and CISDT. In general, coupled-cluster (CC) methods are assumed to be more

accurate than configurational interaction (CI) methods, but full CI is assumed to be more accurate than full CC.

Hartree-fock, density functional theory, and correlation wavefunction methods need to be coupled with a basis set. A basis set is a series of functions that calculate the orbitals for each atom. The choice of type and number of basis sets can be daunting, but with assessment of some key features, the selection process can be made much easier. There are many different types of basis sets that were developed by different groups (Pople, Ahlrich, Jorge, Sapporo, Roos, Dunning, Peterson, and Jenson).⁴¹ In general, these basis sets are classified by the number of functions that calculate the valence orbitals, referred to as SZ (single zeta), DZ (double zeta), TZ (triple zeta), ... NZ (n-zeta) which have 1, 2, 3, ... n-functions for the valence orbitals respectively. For example, a single zeta basis set has only a single s-function for hydrogen and helium (1s), but second-row elements have 2 s-functions (1s & 2s) and 1 set of p-functions (2p_z, 2p_y, and 2p_x). While a double zeta basis set has 2 s-functions for hydrogen and helium (1s and 1s'), but second-row elements have 4 s-functions (1s, 1s', 2s and 2s') and 2 sets of p-functions (2p and 2p'). Theoretically, more functions should lead to more accurate energies and geometries. However, there are cases that deviate from these expectations. For example, the triple zeta Pople basis set (6-311++G(2d,p)) has been shown to be superior to a quadruple zeta dunning basis set (aug-cc-pVQZ).⁴² An organized table of the types of orbitals such as single, double, triple, quadruple, and pentuple zeta basis sets can be found here.⁴¹ The most important requirement when deciding which basis set to use is whether the elements can be used, which can be determined in the basis set exchange.⁴³

The balance between accuracy and computational cost should be considered when performing a calculation (Figure 1.3). If a conformer distribution needs to be performed, then MM should be used due to its low cost. Once the conformer distribution is completed, a select group of lowest energy conformers can be optimized using a higher level of theory, like DFT (B3LYP/6-31G*).⁴⁴ If a perturbative calculation is performed, then a CW method should be used (like CCSD(T)/aug-cc-pVQZ) because no further geometry optimization is needed.

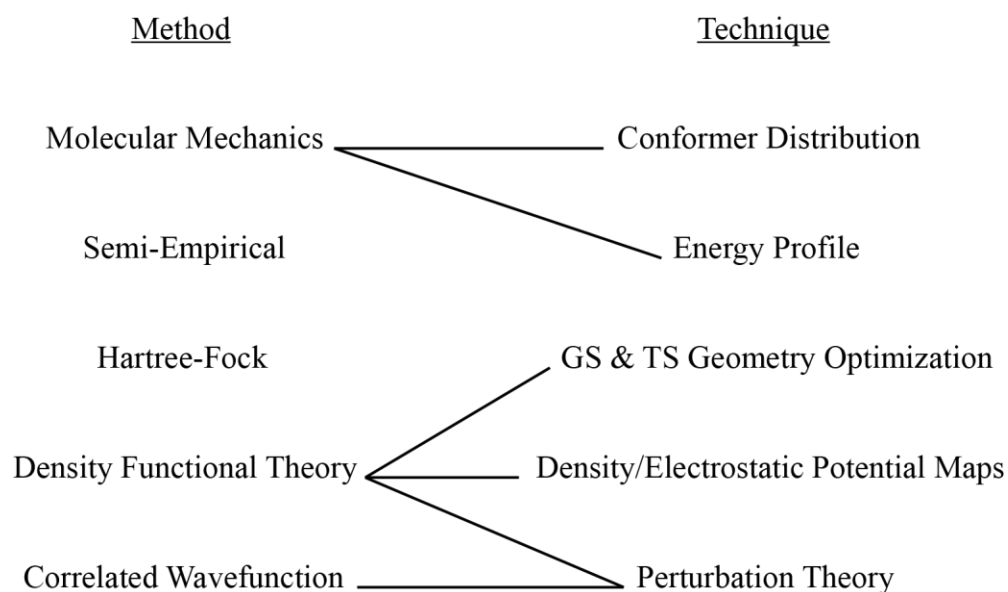


Figure 1.3 Suggested general combination of level of theory and computational methods

1.5 QUANTITATIVE ANALYSIS

The goal of this section is to tie together the preceding three sections by explaining how to apply empirical parameters and computational methods to study NCIs (Figure 1.4). One goal of our studies is to construct a predictive model, which can accurately predict the NCI energy of new molecules. The predictive model can then be analyzed, and a conclusion can be made based on which parameters are most important in the model.

The formation of TS NCIs in the bond rotation process of molecular rotors will be used as an example of how experimental and computational measurements can be used to solve problems. Similar molecular rotors will also be studied in Chapters 2 – 4; therefore, this section serves the additional purpose of providing a general introduction to molecular rotors. These molecular rotors have two GSs (*syn*- and *anti*-) separated by a single TS, where the R-group on the phenyl rotor comes in close contact to the imide carbonyl oxygen (Figure 1.5). The steric interactions between the R-group and the imide carbonyl oxygen governs the magnitude of the repulsive interaction in the TS. Thus, the intramolecular TS interaction between the R-group and the carbonyl oxygen determines the height of the rotational barrier. The magnitude of the stabilizing non-covalent interactions effects in the TS are assessed based on the difference in the barriers between a control rotor which only forms steric TS interactions versus a rotor which forms both steric and stabilizing non-covalent TS interactions. The rotational barriers for the *N*-phenylimide molecular rotor range from 10.9 kcal/mol where the R-group is a hydroxyl group to 25.6 kcal/mol where the R-group is a trifluoromethyl group.

The workflow for the study of the bond rotation process and the stabilizing TS interactions is shown in Figure 1.6. Calculation of the rotational barriers before synthesis and experimental measurements helps assess their potential utility in testing hypotheses and trends. Once a key rotor is identified based on its calculated barrier, synthesis and experimental measurements can be performed. After a series of experimental barriers are collected, two types of analysis can be applied. First, the experimentally measured barriers are correlated with individual empirical parameters to identify the major components of the TS interaction. Second, a benchmark analysis should be conducted using multiple

methods to assess the accuracy of the calculated rotational barrier energies, GS geometries, and TS geometries. If a good linear correlation ($R^2 > 0.8$) is found for an empirical parameter, and a high level of accuracy (root mean square deviation < 1.5 kcal/mol) is observed in the computational benchmark analysis, then the TS structures can be analyzed to assess whether TS NCIs are formed, and perturbative calculations conducted to estimate the contributing interactions. The choice of perturbative calculation to be performed depends on which empirical parameters were well correlated with the experimental values. For example, if a steric, electrostatic, dispersion, or induction empirical parameter was found to correlate to the experimental values then a perturbative calculation which outputs exchange or electrostatics should be used like SAPT, SAPT/cDFT, or ALMO. However, if charge-transfer is thought to be the governing interaction then, a perturbative calculation like NBO or SAPT/cDFT should be used.

The application of this workflow will be demonstrated in Chapters 2-4 of this dissertation. Utilizing this workflow, four different types of R-groups will be identified, allowing for an empirical approximation of the stabilization from the TS interactions. With adequate DFT benchmarking the calculated geometries and energies can be utilized for the independent interactions. Perturbative calculations can be conducted on the optimized geometries to quantify the fundamental interactions. Future studies should follow the workflow described in this section to conduct quantitative analysis of the TS stabilization.

Computational
 conformational analysis
 barrier height
 energy decomposition
 natural bond orbital
 symmetry adapted perturbation theory

Experimental
 crystal structure
 characterization
 equilibrium constant
 exchange rate

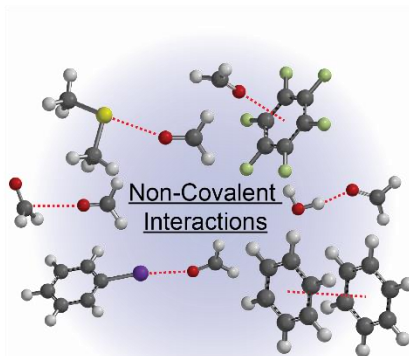


Figure 1.4 Non-covalent interactions are best interpreted by utilizing experimental and computational measurements.

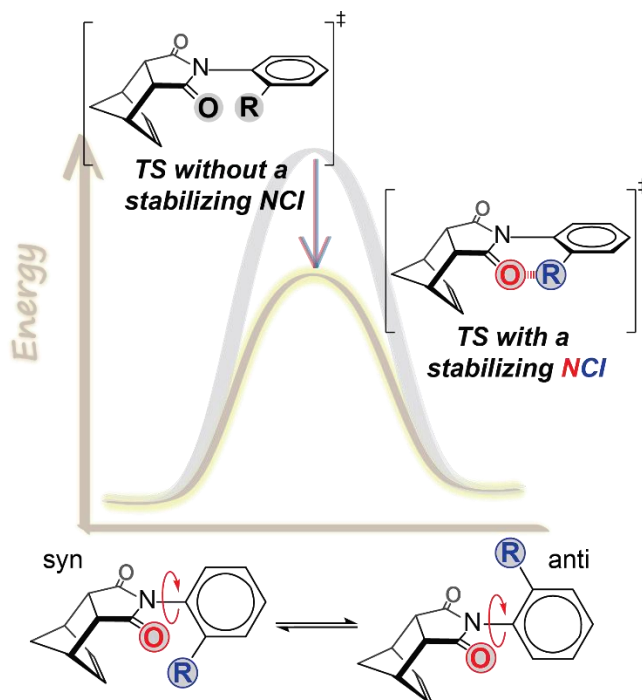


Figure 1.5 Molecular rotor bond rotation reaction coordinate diagram for rotors with and without stabilizing TS NCIs.

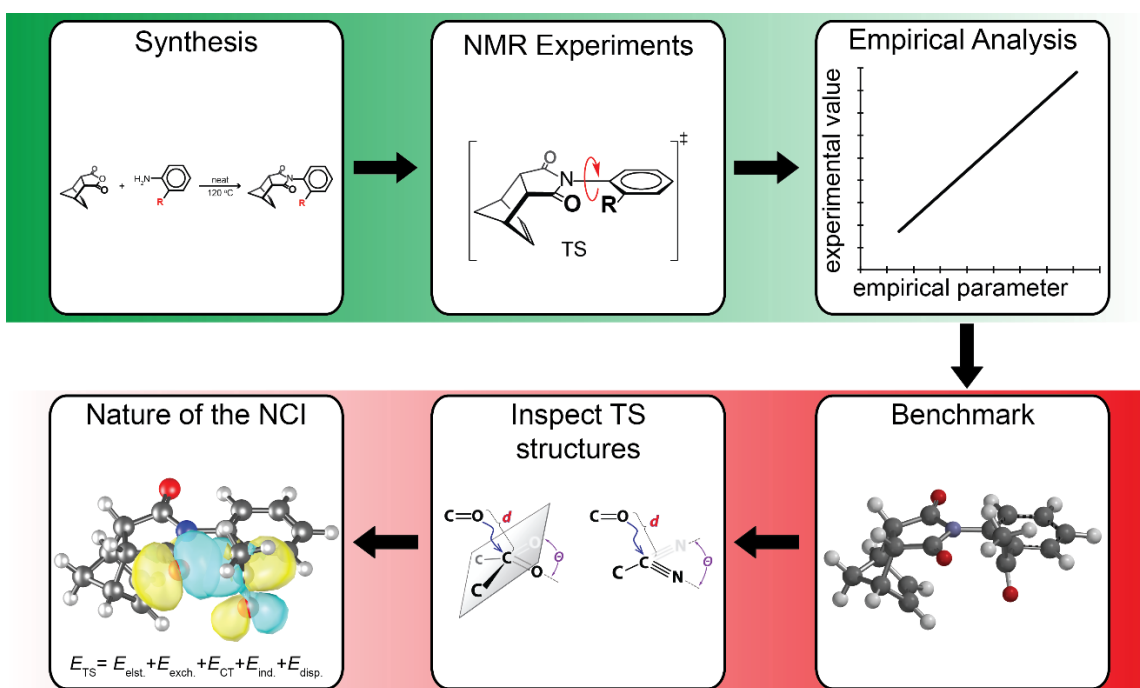


Figure 1.6 General workflow used in this dissertation. The process starts out experimentally (green), and later utilizes computation (red) for analysis.

CHAPTER 2 TRANSITION STATE STABILIZATION BY $n \rightarrow \pi^*$ INTERACTIONS
MEASURED USING MOLECULAR ROTORS

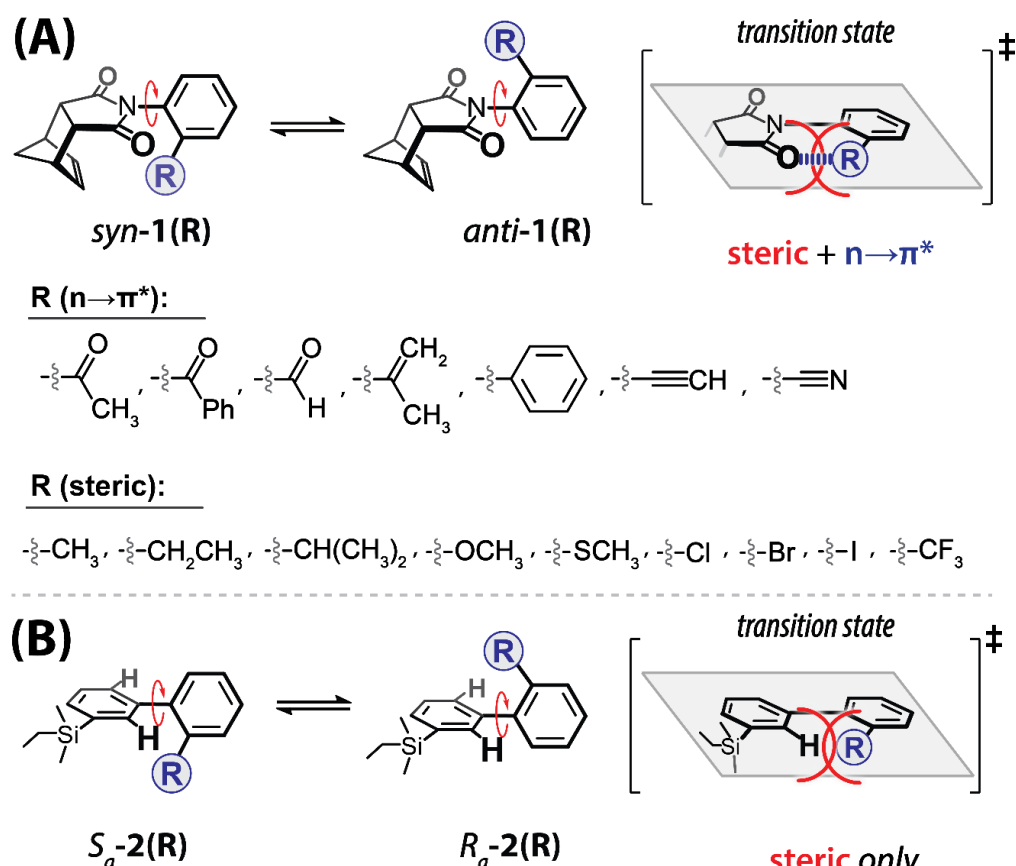
Reprinted with permission from Vik, E. C.; Li, P.; Pellechia, P. J.; Shimizu, K. D. Transition-State Stabilization by $n \rightarrow \pi^*$ Interactions Measured Using Molecular Rotors. *J. Am. Chem. Soc.* **2019**, *141* (42), 16579–16583. Copyright 2019 American Chemical Society.

2.1 ABSTRACT

A series of 16 molecular rotors were synthesized to investigate the ability of $n \rightarrow \pi^*$ interactions to stabilize transition states (TSs) of bond rotation. Steric contributions to the rotational barrier were isolated using control rotors, which could not form $n \rightarrow \pi^*$ interactions. Rotors with strong acceptor π^* orbitals, such as ketones and aldehydes, had greatly increased rates of rotation. The TS stabilization of up to ~ 10 kcal/mol was consistent with the formation of a strong $n \rightarrow \pi^*$ stabilization between the imide carbonyl oxygens and the ortho R group in the planar TS. Computational studies effectively modeled the TS stabilization and geometry, and NBO analysis confirmed the role of $n \rightarrow \pi^*$ interactions in stabilizing the TS.

2.2 MAIN TEXT

The $n \rightarrow \pi^*$ interactions^{12,45-47} have been cited as playing a role in determining protein structures,^{6,12,48,49} molecular^{50,51} and polymer conformations,⁵² and fluorescent properties.^{53,54} However, studies of $n \rightarrow \pi^*$ interactions have primarily focused on thermodynamic measurements in the context of proteins and peptides.^{12,50,51,55-60} Despite their potential in catalysis, few researchers have examined their kinetic effects in reaction selectivity⁶¹⁻⁶³ or enzymatic processes.⁶⁴ Thus, in this study, we systematically examined the ability of $n \rightarrow \pi^*$ interactions to increase the rate of rotation using rotor **1(R)** (Scheme 1). Intramolecular $n \rightarrow \pi^*$ interactions in the planar transition state (TS) between the ortho R groups of the *N*-phenyl ring and the imide carbonyl oxygens dramatically lowered the barrier to rotation by up to ~ 10 kcal/mol. These results suggest that $n \rightarrow \pi^*$ interactions could be used to design new catalysts and could play a significant role in enzyme catalysis.^{61,62,64,65}



Scheme 2.1 (A) Conformational *syn-anti* equilibrium of molecular rotor **1**(R) arising from rotation of the *N*-phenyl ring, and its planar TS, and (B) Conformational *S_a-R_a* equilibrium of biphenyl rotor **2**(R) used to measure Mazzanti's steric parameter B-value of the R groups, and its planar TS

Studies of non-covalent interactions have been primarily measured in stable molecules and complexes.^{3,13,66,67} Few studies have quantified the effects of non-covalent interactions in unstable TSs and/or intermediates,^{7,68,69} despite the frequently cited role of these forces in catalysis and selectivity.^{11,70} The challenge lies in the isolation and measurement of noncovalent interactions within these high-energy and crowded structures.^{10,71} We were particularly interested in whether the strength and stability trend of $n \rightarrow \pi^*$ interactions in the TS were similar to those previously observed in ground-state (GS) systems. *N*-Phenylimide molecular rotors provide a simple model system to address these questions, as they have been successfully applied to measure the kinetic effects of

noncovalent interactions such as intermolecular⁷² and intramolecular hydrogen bonding^{73–76} and metal coordination.⁷⁷

Rotor **1**(R) adopts distinct *syn*- and *anti*-conformers, which slowly interconvert via rotation around the C_{aryl}–N_{imide} single bond (Scheme 1A). The ortho R groups are held near the imide carbonyl oxygens in the planar TS, usually within the vdW radii. R groups that have an acceptor π^* orbital on an sp² or sp¹ carbon, such as ketones (COCH₃, CPh), nitrile (CN), alkenes (C(CH₂)CH₃, Ph), and alkynes (CCH), have the potential to form stabilizing intramolecular n $\rightarrow\pi^*$ interactions with the lone-pair on the imide oxygen. On the other hand, rotors with ortho R groups that do not have an acceptor π^* orbital, such as CH₃, CH₂CH₃, CH(CH₃)₂, OCH₃, SCH₃, Cl, Br, I, and CF₃, cannot form n $\rightarrow\pi^*$ interactions and serve as controls for isolating the steric component in the TS interactions (*vide infra*). The rotational barriers were measured using ¹H NMR exchange spectroscopy (EXSY).⁷⁸ All rotors were studied in the slow exchange regime (–60 to 130 °C) where the *syn*- and *anti*-conformers gave distinct sets of peaks.⁷⁹ Eyring plots provided the enthalpy and entropy of the rotational barriers, and the free energies (ΔG^\ddagger exp) of rotation were recalculated for 25 °C. The ΔG^\ddagger exp values ranged widely from 12.9 (R = CPh) to 24.0 kcal/mol (R = CF₃).

The ability of n $\rightarrow\pi^*$ interactions to stabilize the TS was initially assessed by comparing the rotational barriers (ΔG^\ddagger exp) of rotors **1**(R) with similarly sized R groups. This set of rotors had in their R group an sp² carbon as the first atom carrying an acceptor π^* orbital: **1**(COCH₃), **1**(CPh), **1**(CHO), **1**(C(CH₂)CH₃), and **1**(Ph). The steric sizes of these R groups are very similar as the atom type and hybridization of the first atom is the primary determinant for the steric term of the rotational barrier (*vide infra*).^{16,21} Yet, the barriers varied widely from 12.9 to 21.5 kcal/mol, suggesting the presence of additional

important interactions in the TS. The variations correlated with the ability of the R groups to form $n \rightarrow \pi^*$ interactions.^{51,58} For example, rotors **1**(COPh), **1**(COCH₃), and **1**(CHO) contain polar carbonyl groups that are strong acceptors and had the lowest barriers (12.9, 13.9, and 15.2 kcal/mol). The through-bond (mesomeric) effects of these groups are relatively small and thus cannot explain the large reductions in rotational barriers.⁸⁰ By comparison, rotors **1**(C(CH₂)CH₃), and **1**(Ph) with nonpolar sp² carbons had high rotational barriers (19.5 and 21.5 kcal/mol) presumably due to weaker $n \rightarrow \pi^*$ interactions. Similar trends were observed for rotors **1**(CN) and **1**(CCH) with sp¹ carbons as the first atom. Again, the rotor **1**(CN) with the stronger acceptor *ortho*-cyano group had a lower barrier (15.4 kcal/mol) than the rotor **1**(CCH) with the weaker acceptor alkynyl group (18.8 kcal/mol).

Quantification of the TS $n \rightarrow \pi^*$ stabilizations required separating the steric and $n \rightarrow \pi^*$ components of the rotational barriers.⁵⁸ The steric component is the major determinant of the rotational barrier, which is evident by the observed barriers tracking the steric trend of the R groups. The steric component of the barriers in rotors **1**(R) was assessed using Mazzanti's steric B-value parameter.¹⁶⁻²⁰ B-values are well-suited to this study because they are measured from the rotational barriers of biphenyl rotors **2**(R) with varying *ortho*-R groups (Scheme 1B). The B-values for the C(CH₂)CH₃ and COPh groups were calculated (B3LYP-D3/6-311G*) from the rotational barriers of **2**(C(CH₂)CH₃) and **2**(COPh). The R groups in rotor **2**(R) cannot form $n \rightarrow \pi^*$ interactions due to the absence of lone-pair donors on the hydrogens on the opposing phenyl ring.

The rotors were divided into two groups based on whether their R groups contained acceptor orbitals. The first group of rotors had R groups without acceptor π^* orbitals (R =

CH₃, CH₂CH₃, CH(CH₃)₂, OCH₃, SCH₃, Cl, Br, I, CF₃) and thus cannot form n→π* interactions. Hence, their barriers are primarily due to steric interactions as evidenced by the correlation (R² = 0.87) of ΔG[‡] exp with the B-values of the R groups (Figure 2.1, black circles). The stabilizing n_(O)→σ*_(S) interaction in the TS of **1**(SCH₃) was likely negated by the unfavorable steric strains associated with aligning the thioether group (see section 2.4.7. of this dissertation) This steric trendline also provided an estimate of the steric component in the rotational barriers for the rotors that formed n→π* interactions.

Rotors with acceptor orbitals that could form n→π* interactions (R = CPh, COCH₃, CHO, CN, C(CH₂)CH₃, CCH, Ph) generally deviated from the steric trendline (Figure 2.1, blue circles). Most n→π* rotors had barriers noticeably below the steric trendline, suggesting that the additional TS interactions were stabilizing. Thus, a measure of the n→π* interaction is provided by the deviation of the barrier from the steric trendline on the y-axis. The magnitude of the n→π* stabilizations varied widely from -0.3 kcal/mol for **1**(Ph) to -9.7 kcal/mol for **1**(COPh). The R groups with strong acceptor abilities (COPh, COCH₃, and CHO), due to the presence of electronegative oxygens, had the strongest n→π* stabilizations of -8.4 to -9.7 kcal/mol. The R group with moderate acceptor ability (CN) was moderately stabilizing (-5.2 kcal/mol). Finally, R groups with weak acceptor abilities (C(CH₂)CH₃, Ph, and CCH) due to the lack of electronegative atoms yielded the least stabilizing n→π* stabilizations of -0.3 to -2.7 kcal/mol. Interestingly, the acceptor abilities of these *ortho*-R groups appeared to follow the NBO atomic charges of their first atoms (Figure 2.53).⁸¹

Computational modeling was conducted to establish the role of n→π* interactions in stabilizing the TS of **1**(R). DFT calculations of rotors **1**(R) and **2**(R) with the 16 R groups

(B3LYP-D3/6-311G*) were able to reproduce the experimental barriers ($\Delta G^\ddagger_{\text{exp}}$) with an accuracy of ± 1.2 kcal/mol (Figure 2.50). The calculated TS and GS geometries were thus deemed accurate and adopted for further analysis on TS $n \rightarrow \pi^*$ stabilization.

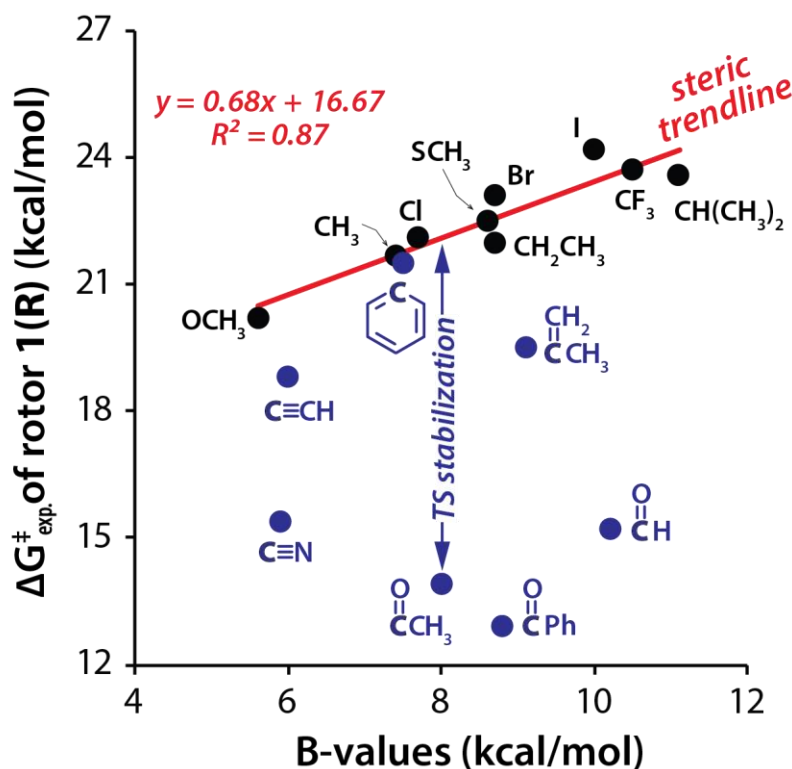


Figure 2.1 Correlation plot of the experimentally measured rotational barriers for rotor **1(R)** versus the steric B-values of the R groups. The steric trendline is drawn through the rotors that have ortho R groups without a π^* orbital (black circles) and thus lack $n \rightarrow \pi^*$ interactions. The blue circles correspond to the rotors that can form $n \rightarrow \pi^*$ interactions

Pyramidalization or bending of the acceptor atoms of the R groups provided the structural evidence for the formation of TS $n \rightarrow \pi^*$ interactions.^{12,51,82} The $n \rightarrow \pi^*$ orbital-orbital interaction is known to alter the geometry of the acceptor atom.⁵¹ Trigonal planar sp^2 acceptor atoms become pyramidalized and linear sp^1 acceptor atoms become bent when forming $n \rightarrow \pi^*$ interactions. The geometry change is quantified by the parameter Θ (Figure 2.3), which measures the angle of deviation from planarity or linearity. R groups

with good acceptors displayed significant TS pyramidalization or bending. For example, the sp^2 acceptor carbons of the ketone (**1**(COCH₃) and **1**(COPh)) and aldehyde (**1**(CHO)) rotors displayed the highest degree of pyramidalization ($\Theta = 13.0^\circ$, 11.3° , and 11.0° respectively). These Θ values are significantly larger than the $n \rightarrow \pi^*$ interactions in protein and peptide crystal structures ($\sim 2^\circ - 7^\circ$) and are consistent with the observed stronger TS $n \rightarrow \pi^*$ interactions.⁸³ Similarly, the sp^1 -hybridized cyano group of **1**(CN) displayed significant bending ($\Theta = 15.4^\circ$) in the TS. Interestingly, this is also one of the few examples of an $n \rightarrow \pi^*$ interaction involving an sp^1 -hybridized acceptor.

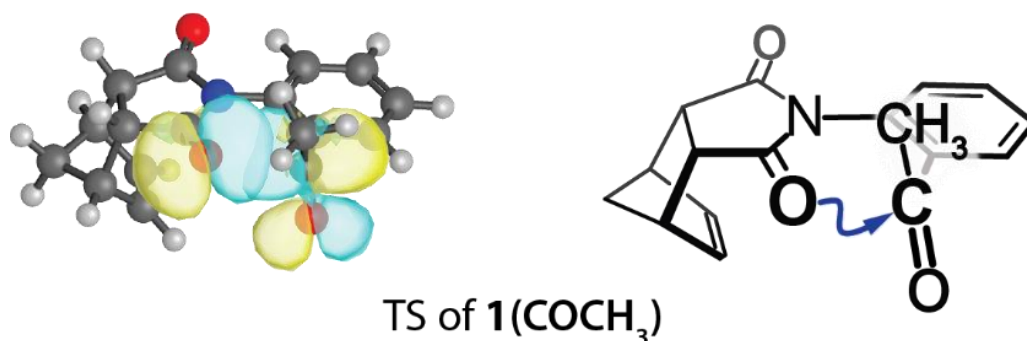


Figure 2.2 Overlap of n and π^* orbitals in the calculated TS (B3LYP-D3/6-311G*) of **1**(COCH₃) in the three dimensional orbital rendering and the ChemDraw presentation of TS highlighting the intramolecular $n \rightarrow \pi^*$ interaction (blue arrow).

The orbital-orbital interaction energies were estimated via a natural bond order (NBO) analysis of the TS geometries of rotors **1**(R). NBO calculations can estimate the stabilization from the mixing of two non-bonding orbitals. NBO calculations (ω B97M-V/6-311G*) were performed on the calculated TS geometries of rotors **1**(R) (Tables 2.3 - 2.32).^{36,84} The orbital-orbital interaction energies (E_{NBO}) between the imide oxygen (n) and the R group acceptor carbon (π^*) showed an excellent linear correlation ($R^2 = 0.94$) with

the measured TS stabilizations ($\Delta\Delta G^+$ exp) (Figure 2.4.B). The strong correlation and similar magnitudes suggest that most of the TS stabilization can be attributed to the orbital-orbital $n \rightarrow \pi^*$ interaction. Note that the NBO analysis systematically overestimated the strength of $n \rightarrow \pi^*$ interaction as the slope of the correlation plot is 0.55, presumably due to discounting the effects of solvent on experimental models.

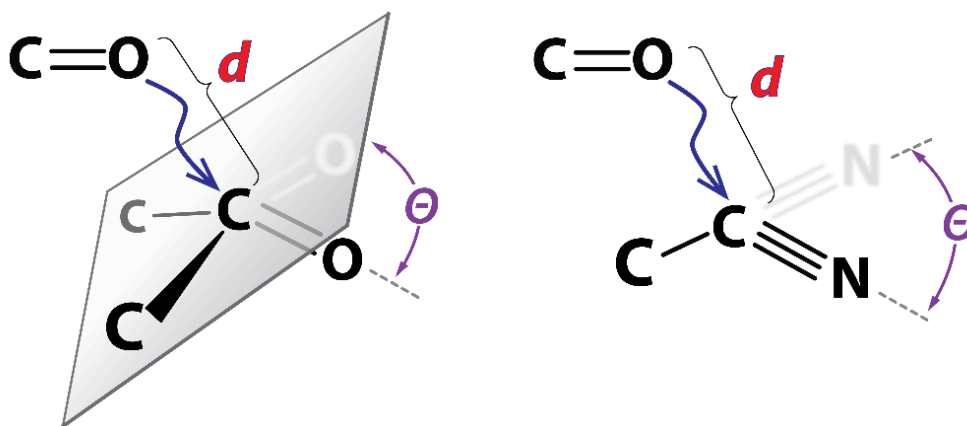


Figure 2.3 Definitions of the parameter Θ measuring the pyramidalization of sp^2 and bending of sp^1 acceptor carbons in $n \rightarrow \pi^*$ interactions and the distance parameter d measuring the $O \cdots C$ distance.

Finally, the origins of the strong TS stabilizing $n \rightarrow \pi^*$ effects (5.3–9.7 kcal/mol) were investigated especially in comparison with the much weaker GS $n \rightarrow \pi^*$ interactions in peptides and proteins (~ 0.3 – 0.7 kcal/mol).¹² The discrepancy cannot be attributed to the donor and acceptor properties of the interacting groups in rotors **1(R)**, as they are very similar to those of the amide oxygen and amide carbon of peptide and protein systems.^{57,64,85} A portion of the difference can be attributed to the choice of the control rotors that selectively removed the repulsive component of the compactly positioned atoms in the TS interactions. However, the attractive component of the interactions appeared to be significantly enhanced by the compact nature of the TS. The $O \cdots C$ distances (d , Figure

2.3) in the TSs of **1**(COCH₃), **1**(COPh), and **1**(CHO) were all significantly shorter (2.35, 2.37, and 2.37 Å) than the sum of the vdW radii (3.22 Å). By comparison, proline-containing α -helices have some of the shortest $n \rightarrow \pi^*$ O \cdots C distances which are only slightly shorter than the vdW radii (2.89 ± 0.10 Å).⁴⁸ Confirmation of the short, strong $n \rightarrow \pi^*$ interactions in **1**(R) was provided by an analysis of the measured TS stabilization energies ($\Delta\Delta G^\ddagger_{\text{exp}}$) versus the calculated TS O \cdots C distances (Figure 2.4).¹² For R groups that can form $n \rightarrow \pi^*$ interactions, a strong linear correlation ($R^2 = 0.91$) was observed with shorter atom distances corresponding to stronger interactions.^{51,86} The trend-line had a steep slope showing that the magnitude of the TS stabilization increased rapidly as the O \cdots C distance decreased.

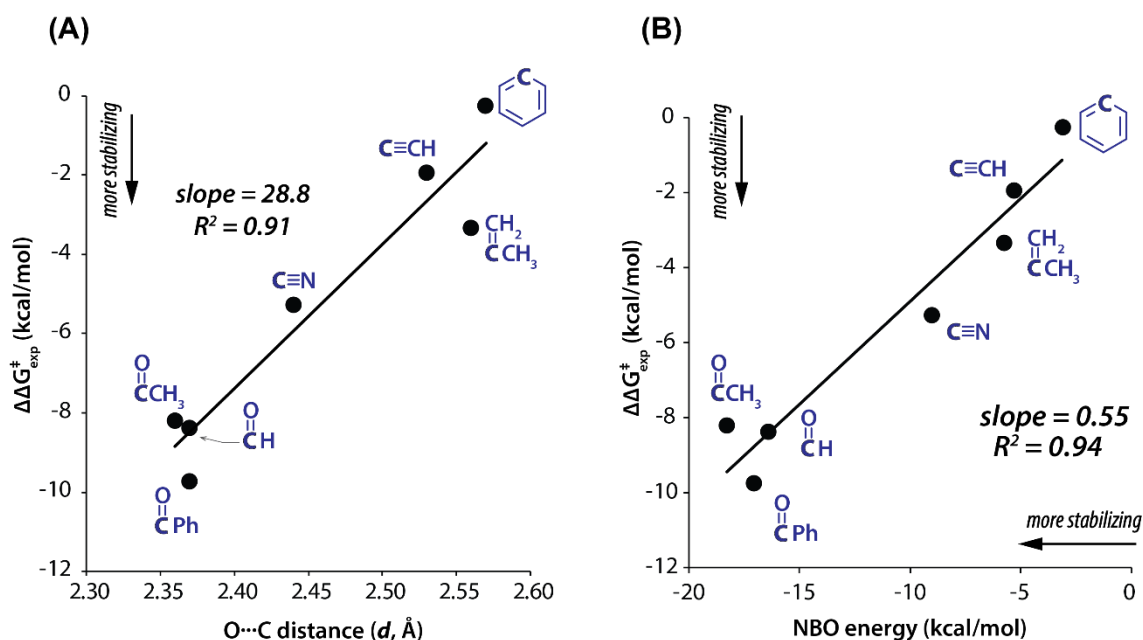


Figure 2.4 (A) Correlation plot of the measured TS stabilization ($\Delta\Delta G^\ddagger_{\text{exp}}$) and the calculated natural bond order (NBO) energies for the TS $n \rightarrow \pi^*$ interaction in **1**(R). (B) Correlation plot of the measured TS stabilization ($\Delta\Delta G^\ddagger_{\text{exp}}$) and the calculated donor-to-acceptor distance (d) in the TS of **1**(R).

2.3 CONCLUSION

Molecular rotor **1** was successfully employed to measure the kinetic and TS stabilizing effects of $n \rightarrow \pi^*$ interactions. Rotors that form an intramolecular $n \rightarrow \pi^*$ interaction in the TS between the imide oxygen and the ortho R group had significantly lower rotational barriers. The $n \rightarrow \pi^*$ interactions stabilized the TS of rotors 1(R) by up to 9.7 kcal/mol, significantly exceeding the stabilizations (~ 0.3 – 0.7 kcal/mol) imparted by the similar $n \rightarrow \pi^*$ interactions in peptides and proteins. The steric component of the rotational barriers was measured using the steric parameter B-value, allowing the isolation of the attractive component, and thus the stabilizing effect, of the $n \rightarrow \pi^*$ interactions. The presence of $n \rightarrow \pi^*$ interactions was confirmed by the pyramidalization or bending of the acceptor carbon and the strong correlation between the experimentally quantified TS stabilizations and the calculated NBO energies. The large TS stabilizing effects of $n \rightarrow \pi^*$ interactions were found to be closely associated with the short donor-to-acceptor ($O \cdots C$) distance in the compact TS. The results of this work provide support for the potential applications of $n \rightarrow \pi^*$ interactions in reaction kinetics and chemical catalysis.

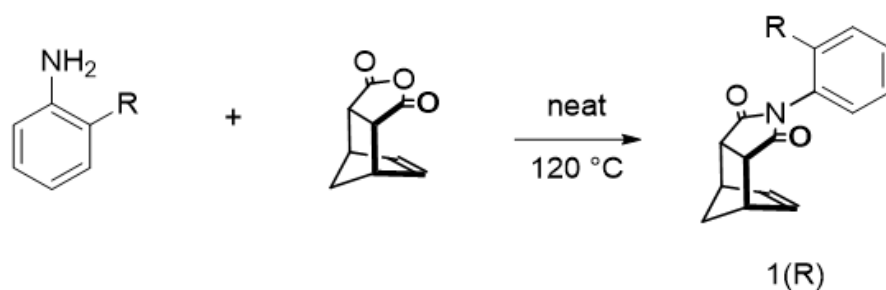
2.4 SUPPLEMENTAL INFORMATION

2.4.1 GENERAL EXPERIMENTAL INFORMATION

NMR spectra were recorded on a Bruker 400 MHz spectrometer. Chemical shifts are reported in ppm (δ) referenced to solvent residue. All spectra given for characterization purposes were taken at room temperature. All chemicals and solvents were purchased from commercial suppliers and used as received. Flash chromatography was performed using silica gel from Sorbent Technologies (60 Å, 200 – 400 mesh).

2.4.2 SYNTHESIS

Rotors **1(R)** were all prepared via a thermal condensation between an *ortho*-substituted aniline and a bicyclic anhydride (Figure 2.2).⁸⁷ Rotors **1(OCH₃)**, **1(Cl)**, **1(Br)**, **1(I)**, **1(CH₃)**, **1(CH₂CH₃)** and **1(CH(CH₃)₂)** have been reported previously, and their synthesis and characterization are not detailed here. The rest of the rotors are newly reported compounds and fully characterized.



Rotor	"R" Substituent	Rotor	"R" Substituent
1(COCH₃)		1(SCH₃)	
1(COPh)		1(Cl)	
1(CHO)		1(Br)	
1(C(CH₂)CH₃)		1(I)	
1(Ph)		1(CF₃)	
1(CCH)		1(CH₃)	
1(CN)		1(CH₂CH₃)	
1(OCH₃)		1(CH(CH₃)₂)	

Scheme 2.2 General route for synthesizing molecular rotors

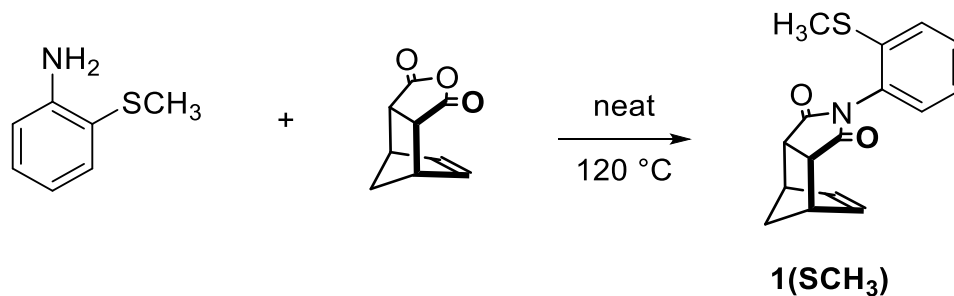


Figure 2.5 Synthesis of rotor **1(SCH₃)**

(3*aR*,4*S*,7*R*,7*aS*)-2-(2-(methylthio)phenyl)-3*a*,4,7,7*a*-tetrahydro-1*H*-4,7-methanoisindole-1,3(2*H*)-dione. **1(SCH₃)**: *cis*-5-Norbornene-*endo*-2,3-dicarboxylic anhydride (100 mg, 0.61 mmol) and 2-(methylthio)aniline (93 mg, 0.67 mmol) were added to a 20-dram vial with a magnetic stir bar. The vial was then capped and heated to 120 °C in a silicon oil bath for 12 hours while stirring. After letting the vial cool to room temperature, the crude material was purified by column chromatography (ethyl acetate/hexanes = 1:5, v/v) to give **1(SCH₃)** as a white powder (156 mg, 90%). ¹H NMR (400 MHz, chloroform-*d*) δ 7.43-7.31 (m, 2H *syn* and *anti*), 7.23 (ddd, *J* = 7.8, 7.2, 1.8 Hz, 1H *syn* and *anti*), 7.01 (dd, *J* = 7.8, 1.2 Hz, 1H *syn*), 6.92 (dd, *J* = 7.8, 1.2 Hz, *anti*), 6.40 (t, *J* = 1.5 Hz, 2H *syn*), 6.33-6.31 (m, 2H *anti*), 3.52-3.47 (m, 4H *syn* and *anti*), 2.43 (s, 1H *syn* and *anti*), 1.81 (d, *J* = 8.7 Hz, 1H *syn* and *anti*), 1.64 (d, *J* = 8.7 Hz, 1H *syn* and *anti*). ¹³C NMR (100 MHz, chloroform-*d*) δ 176.55, 176.24, 137.65, 137.37, 135.41, 134.69, 130.47, 130.16, 130.04, 129.89, 129.13, 128.62, 127.56, 126.93, 126.02, 125.77, 52.50, 52.39, 47.08, 45.97, 45.38, 45.32, 15.98, 15.82. HRMS (EI) *m/z* calculated for [C₁₆H₁₅NO₂S]⁺ (M⁺): calculated 285.0824; observed 285.0828.

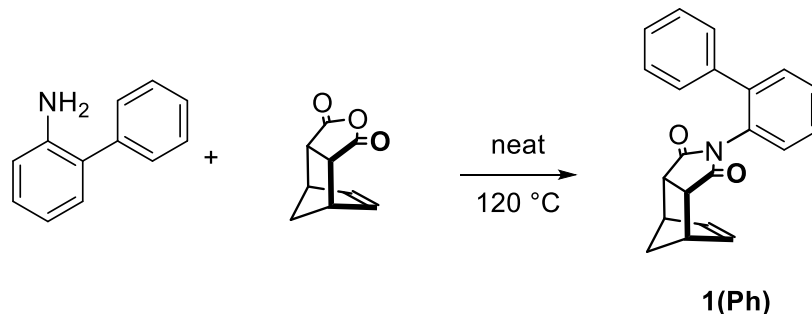


Figure 2.6 Synthesis of rotor **1(Ph)**

(3*aR*,4*S*,7*R*,7*aS*)-2-([1,1'-biphenyl]-2-yl)-3*a*,4,7,7*a*-tetrahydro-1*H*-4,7-methanoisindole-1,3(2*H*)-dione **1(Ph)**: *cis*-5-Norbornene-*endo*-2,3-dicarboxylic anhydride (100 mg, 0.61 mmol) and [1,1'-biphenyl]-2-amine (113 mg, 0.67 mmol) were added to a 20-dram vial with a magnetic stir bar. The vial was then capped and heated to 120 °C in a silicon oil bath for 12 hours while stirring. After letting the vial cool to room temperature, the crude material was purified by column chromatography (ethyl acetate/hexanes = 1:5, v/v) to give **1(Ph)** as a white powder (183 mg, 95%). ¹H NMR (400 MHz, chloroform-*d*) δ 7.51-7.02 (m, 9H *syn* and *anti*), 6.30 (t, *J* = 1.7 Hz, 2H *anti*), 5.31 (t, *J* = 1.7 Hz, 2H *syn*), 3.42-3.16 (m, 4H *syn* and *anti*), 1.75 (d, *J* = 8.9 Hz, 1H *anti*), 1.60 (d, *J* = 8.9 Hz, 1H *syn*), 1.52 (d, *J* = 8.9 Hz, 1H *anti*), 1.47 (d, *J* = 8.9 Hz, 1H *syn*). ¹³C NMR (100 MHz, chloroform-*d*) δ 177.01, 176.78, 141.94, 141.10, 138.87, 138.55, 134.64, 134.40, 131.33, 130.74, 130.34, 129.96, 129.62, 129.38, 129.13, 128.69, 128.66, 128.47, 128.46, 128.31, 128.24, 127.78, 127.68, 127.63, 52.51, 52.29, 46.67, 45.65, 45.22, 44.72. HRMS (EI) *m/z* calculated for [C₂₁H₁₇NO₂]⁺ (M⁺): calculated 315.1259; observed 315.1258.

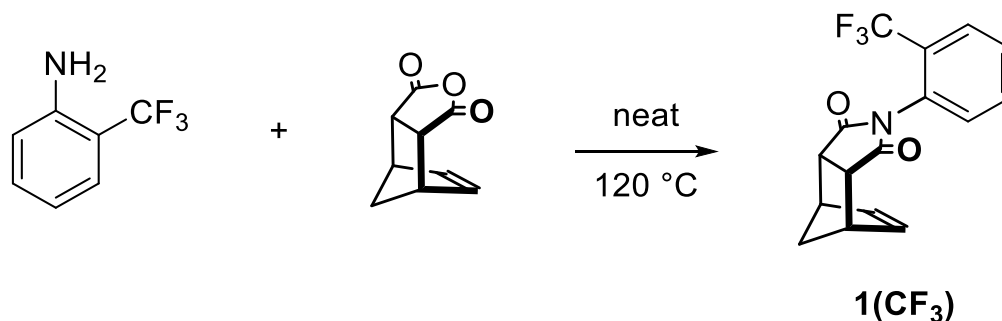


Figure 2.7 Synthesis of rotor **1(CF₃)**

(3*aR*,4*S*,7*R*,7*aS*)-2-(2-(trifluoromethyl)phenyl)-3*a*,4,7,7*a*-tetrahydro-1*H*-4,7-methanoisindole-1,3(2*H*)-dione **1(CF₃)**: *cis*-5-Norbornene-*endo*-2,3-dicarboxylic anhydride (100 mg, 0.61 mmol) and 2-(trifluoromethyl)aniline (108 mg, 0.67 mmol) were added to a 20-dram vial with a magnetic stir bar. The vial was then capped and heated to 120 °C in a silicon oil bath for 12 hours while stirring. After letting the vial cool to room temperature, the crude material was purified by column chromatography (ethyl acetate/hexanes = 1:5, v/v) to give **1(CF₃)** as a white powder (161 mg, 86%). ¹H NMR (400 MHz, chloroform-*d*) δ 7.78 (d, *J* = 7.8 Hz, 1H *syn* and *anti*), 7.67-7.55 (m, 2H *syn* and *anti*), 7.13 (d, *J* = 7.8 Hz, 1H *syn*), 7.04 (d, *J* = 7.8 Hz, 1H *anti*), 6.35 (s, 2H *anti*), 6.28 (s, 2H *syn*), 3.53-3.48 (m, 4H *syn* and *anti*), 1.83 (d, *J* = 8.9 Hz, 1H *syn* and *anti*), 1.65 (d, *J* = 8.9 Hz, 1H *syn* and *anti*). ¹³C NMR (100 MHz, chloroform-*d*) δ 176.61, 176.46, 134.82, 134.75, 133.29, 133.14, 131.25, 130.67, 130.48, 130.46, 129.92, 129.85, 129.29, 129.14, 128.98, 128.83, 128.67, 128.36, 127.48, 127.43, 127.39, 127.34, 127.30, 127.25, 126.92, 124.20, 123.86, 121.48, 121.14, 53.03, 52.42, 47.06, 46.08, 45.27, 45.24. HRMS (EI) *m/z* calculated for [C₁₆H₁₂F₃NO₂]⁺ (M⁺): calculated 307.0824; observed 307.0821.

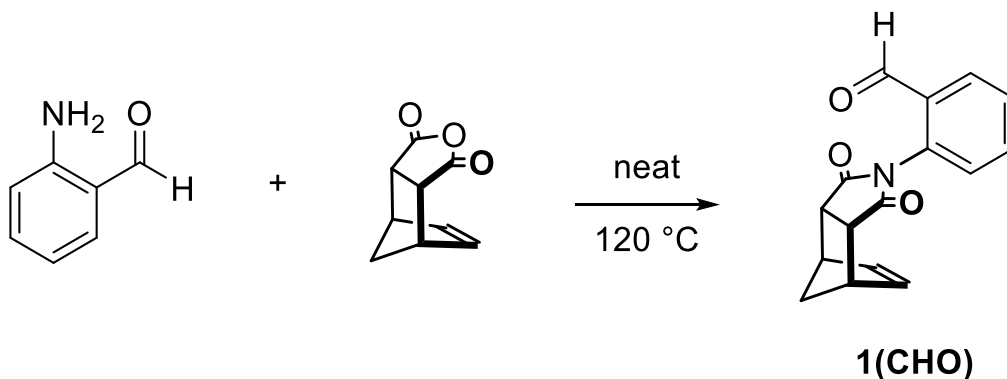


Figure 2.8 Synthesis of rotor **1(CHO)**

2-((3aR,4S,7R,7aS)-1,3-dioxo-1,3,3a,4,7,7a-hexahydro-2H-4,7-methanoisindol-2-yl)benzaldehyde **1(CHO)**: *cis*-5-Norbornene-*endo*-2,3-dicarboxylic anhydride (100 mg, 0.61 mmol) and 2-aminobenzaldehyde (81 mg, 0.67 mmol) were added to a 20-dram vial with a magnetic stir bar. The vial was then capped and heated to 120 °C in a silicon oil bath for 12 hours while stirring. After letting the vial cool to room temperature, the crude material was purified by column chromatography (ethyl acetate/hexanes = 1:5, v/v) to give **1(CHO)** as a white powder (117 mg, 72%). ¹H NMR (400 MHz, chloroform-d) δ 9.80-9.74 (m, 1H *syn* and *anti*), 7.92-7.84 (m, 1H *syn* and *anti*), 7.60 (dd, *J* = 7.6, 1.0 Hz, *syn* and *anti*), 7.53-7.50 (m, 1H *syn* and *anti*), 7.10-7.01 (m, 1H *syn* and *anti*), 6.24 (s, 2H *syn* and *anti*), 3.47-3.45 (m, 4H *syn* and *anti*), 1.75-1.73 (m, 1H *syn* and *anti*), 1.58 (d, *J* = 8.6 Hz, *syn* and *anti*). ¹³C NMR (100 MHz, chloroform-d) δ 189.41, 188.42, 176.83, 135.50, 134.76, 134.64, 132.94, 131.99, 131.72, 129.71, 129.37, 53.04, 52.51, 46.94, 46.22, 45.39. HRMS (EI) *m/z* calculated for [C₁₆H₁₃NO₃]⁺ (M⁺): calculated 267.0895; observed 267.0885.

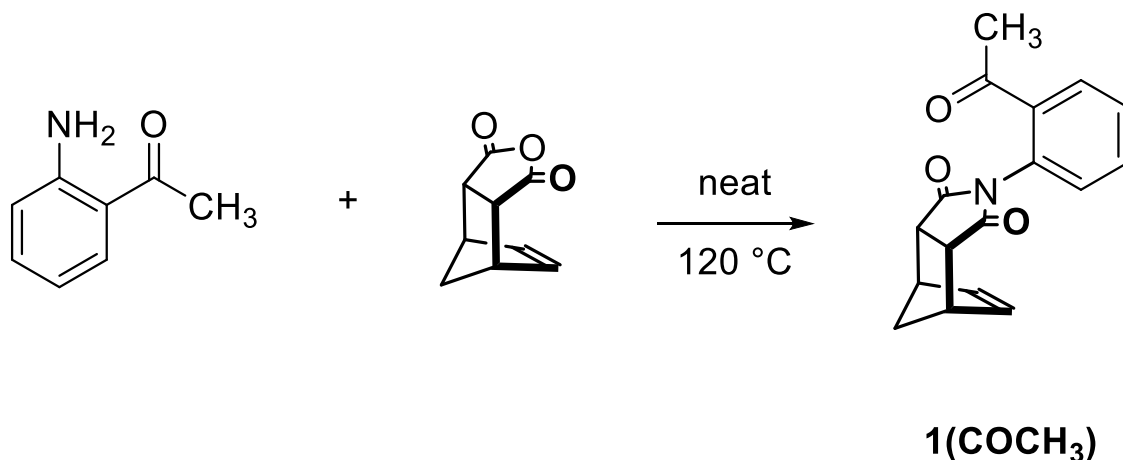


Figure 2.9 Synthesis of rotor **1(COCH₃)**

(3*aR*,4*S*,7*R*,7*aS*)-2-(2-acetylphenyl)-3*a*,4,7,7*a*-tetrahydro-1*H*-4,7-methanoisindole-1,3(2*H*)-dione **1(COCH₃)**: *cis*-5-Norbornene-*endo*-2,3-dicarboxylic anhydride (100 mg, 0.61 mmol) and 1-(2-aminophenyl)ethan-1-one (91 mg, 0.67 mmol) were added to a 20-dram vial with a magnetic stir bar. The vial was then capped and heated to 120 °C in a silicon oil bath for 12 hours while stirring. After letting the vial cool to room temperature, the crude material was purified by column chromatography (ethyl acetate/hexanes = 1:5, v/v) to give **1(COCH₃)** as a white powder (144 mg, 84%). ¹H NMR (400 MHz, chloroform-*d*) δ 7.82-7.80 (m, 1H), 7.57 (td, *J* = 7.7, 1.4 Hz), 7.51-7.47 (m 1H), 7.08 (d, *J* = 7.7 Hz, 1H), 6.29 (s, 2H), 3.50-3.47 (m, 4H), 2.55 (s, 3H), 1.79 (d, *J* = 8.8 Hz, 1H), 1.62 (d, *J* = 8.8 Hz, 1H). ¹³C NMR (100 MHz, chloroform-*d*) δ 198.54, 176.90, 135.19, 134.67, 132.54, 129.65, 129.45, 129.09, 52.51, 46.25, 45.28, 28.50. HRMS (EI) *m/z* calculated for [C₁₇H₁₅NO₃]⁺ (M⁺): calculated 281.1052; observed 281.1059.

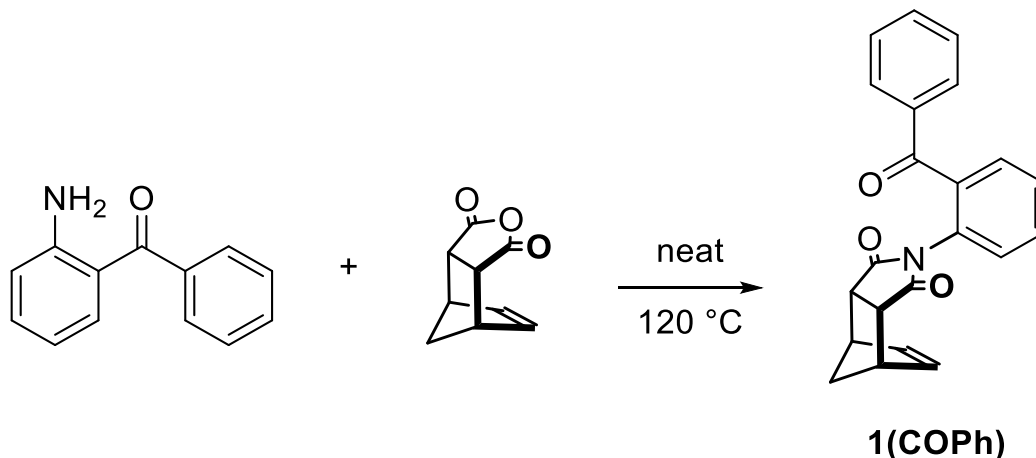


Figure 2.10 Synthesis of rotor **1(COPh)**

(3*aR*,4*S*,7*R*,7*aS*)-2-(2-benzoylphenyl)-3*a*,4,7,7*a*-tetrahydro-1*H*-4,7-methanoisindole-1,3(2*H*)-dione **1(COPh)**: *cis*-5-Norbornene-*endo*-2,3-dicarboxylic anhydride (100 mg, 0.61 mmol) and (2-aminophenyl)(phenyl)methanone (132 mg, 0.67 mmol) were added to a 20-dram vial with a magnetic stir bar. The vial was then capped and heated to 120 °C in a silicon oil bath for 12 hours while stirring. After letting the vial cool to room temperature, the crude material was purified by column chromatography (ethyl acetate/hexanes = 1:5, v/v) to give **1(COPh)** as a white powder (180 mg, 86%). ¹H NMR (400 MHz, chloroform-*d*) δ 7.77-7.75 (m, 2H), 7.63-7.57 (m, 3H), 7.51-7.44 (m, 3H), 7.18 (d, *J* = 7.8 Hz, 1H), 6.21 (br, 2H), 3.40 (s, 2H), 3.14 (br, 2H), 1.72 (d, *J* = 8.8 Hz, 1H), 1.52 (d, *J* = 8.8 Hz, 1H). ¹³C NMR (100 MHz, chloroform-*d*) δ 194.74, 176.47, 137.07, 135.80, 134.57, 133.01, 131.77, 130.54, 129.93, 128.47, 128.31, 52.34, 45.89, 45.26. HRMS (EI) *m/z* calculated for [C₂₂H₁₇NO₃]⁺ (M⁺): calculated 343.1208; observed 343.1215.

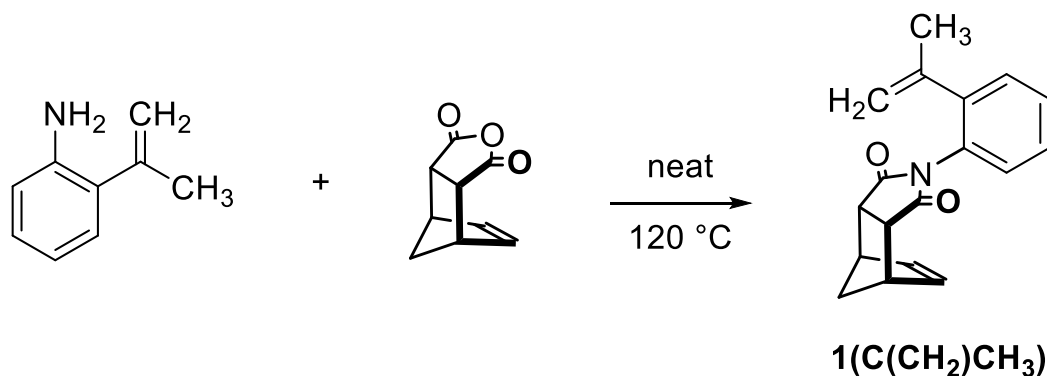


Figure 2.11 Synthesis of rotor **1(C(CH₂)CH₃)**

(3*aR*,4*S*,7*R*,7*aS*)-2-(2-(prop-1-en-2-yl)phenyl)-3*a*,4,7,7*a*-tetrahydro-1*H*-4,7-methanoisindole-1,3(2*H*)-dione **1(C(CH₂)CH₃)**: *cis*-5-Norbornene-*endo*-2,3-dicarboxylic anhydride (100 mg, 0.61 mmol) and 2-(prop-1-en-2-yl)aniline (157 mg, 0.67 mmol) were added to a 20-dram vial with a magnetic stir bar. The vial was then capped and heated to 120 °C in a silicon oil bath for 12 hours while stirring. After letting the vial cool to room temperature, the crude material was purified by column chromatography (ethyl acetate/hexanes = 1:5, v/v) to give **1(C(CH₂)CH₃)** as a white powder (157 mg, 92%). ¹H NMR (400 MHz, chloroform-*d*) δ 7.32-7.17 (m, 3H *syn* and *anti*), 6.91-6.82 (m, 1H *syn* and *anti*), 6.22 (t, *J* = 1.8 Hz, 2H *anti*), 6.08 (t, *J* = 1.8 Hz, 2H *syn*), 5.00-4.98 (m, 1H *syn* and *anti*), 4.68-4.65 (m, 1H *syn* and *anti*), 3.42-3.30 (m, 4H *syn* and *anti*), 1.93-1.89 (m, 3H *syn* and *anti*), 1.72-1.69 (m, 1H *syn* and *anti*), 1.53-1.51 (m, 1H *syn* and *anti*). ¹³C NMR (100 MHz, chloroform-*d*) δ 177.15, 176.93, 143.17, 142.36, 142.14, 141.35, 135.01, 134.59, 129.45, 129.16, 129.11, 128.99, 128.73, 128.61, 128.35, 127.92, 127.79, 116.17, 114.86, 52.83, 52.32, 46.83, 45.80, 45.29, 45.07, 24.47, 23.62. HRMS (EI) *m/z* calculated for [C₁₈H₁₇NO₂]⁺ (M⁺): calculated 279.1259; observed 279.1261.

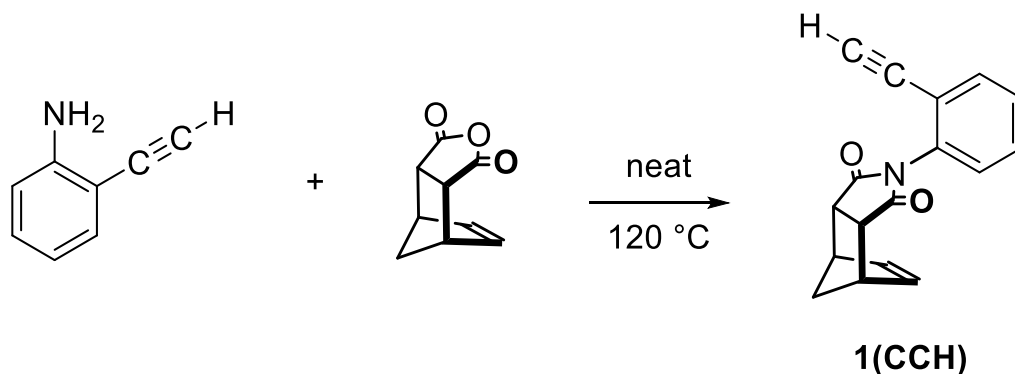


Figure 2.12 Synthesis of rotor **1(CCH)**

(3*aR*,4*S*,7*R*,7*aS*)-2-(2-ethynylphenyl)-3*a*,4,7,7*a*-tetrahydro-1*H*-4,7-methanoisindole-1,3(2*H*)-dione **1(CCH)**: *cis*-5-Norbornene-*endo*-2,3-dicarboxylic anhydride (100 mg, 0.61 mmol) and 2-ethynylaniline (78 mg, 0.67 mmol) were added to a 20-dram vial with a magnetic stir bar. The vial was then capped and heated to 120 °C in a silicon oil bath for 12 hours while stirring. After letting the vial cool to room temperature, the crude material was purified by column chromatography (ethyl acetate/hexanes = 1:5, v/v) to give **1(CCH)** as a white powder (133 mg, 83%). ¹H NMR (400 MHz, chloroform-*d*) δ 7.64-7.62 (m, 1H *syn* and *anti*), 7.47-7.36 (m, 2H *syn* and *anti*), 7.10 (dd, *J* = 7.8, 1.1 Hz, *syn*), 7.01 (dd, *J* = 7.8, 1.1 Hz, *anti*), 6.32-6.31 (m, 2H *syn* and *anti*), 3.53-3.49 (m, 4H *syn* and *anti*), 3.22 (s, 1H *syn*), 3.19 (s, 1H *anti*), 1.84-1.80 (m, 1H *syn* and *anti*), 1.66-1.63 (m, 1H *syn* and *anti*). ¹³C NMR (100 MHz, chloroform-*d*) δ 176.43, 176.19, 135.32, 134.77, 134.69, 134.17, 133.97, 133.77, 129.92, 129.88, 129.37, 129.22, 128.97, 128.43, 121.57, 121.38, 82.96, 82.62, 80.47, 79.38, 52.71, 52.56, 46.95, 46.16, 45.49, 45.39. HRMS (EI) *m/z* calculated for [C₁₇H₁₃NO₂]⁺ (M⁺): calculated 263.0946; observed 263.0936.

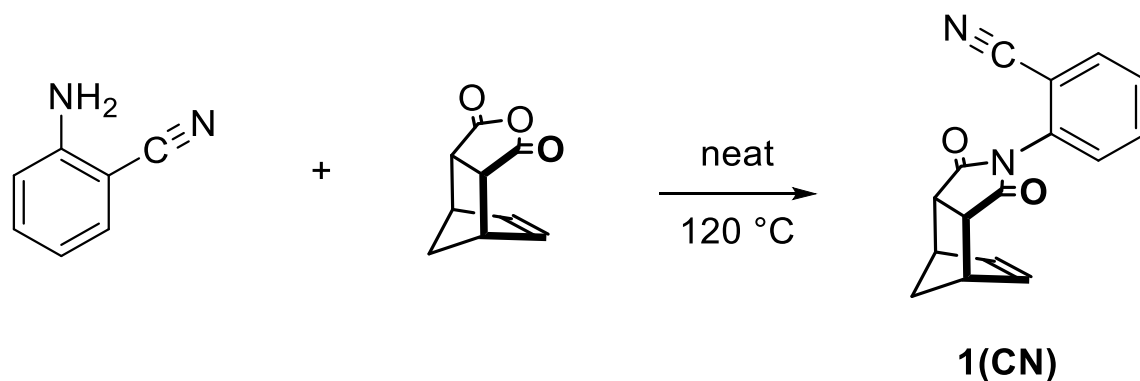


Figure 2.13 Synthesis of rotor **1(CN)**

2-((3aR,4S,7R,7aS)-1,3-dioxo-1,3,3a,4,7,7a-hexahydro-2H-4,7-methanoisindol-2-yl)benzonitrile **1(CN)**: *cis*-5-Norbornene-*endo*-2,3-dicarboxylic anhydride (100 mg, 0.61 mmol) and 2-aminobenzonitrile (79 mg, 0.67 mmol) were added to a 20-dram vial with a magnetic stir bar. The vial was then capped and heated to 120 °C in a silicon oil bath for 12 hours while stirring. After letting the vial cool to room temperature, the crude material was purified by column chromatography (ethyl acetate/hexanes = 1:5, v/v) to give **1(CN)** as a white powder (130 mg, 81%). ¹H NMR (400 MHz, chloroform-d) δ 7.77 (dd, *J* = 7.8, 1.3 Hz, 1H *syn* and *anti*), 7.68 (td, *J* = 7.8, 1.5 Hz, 1H *syn* and *anti*), 7.51 (t, *J* = 7.7 Hz, 1H *syn* and *anti*), 7.26-7.17 (m, 1H *syn* and *anti*), 6.44-6.31 (m, 2H *syn* and *anti*), 3.57-3.54 (m, 4H *syn* and *anti*), 1.83 (d, *J* = 8.8 Hz, 1H *syn* and *anti*), 1.66-1.64 (m, 1H *syn* and *anti*). ¹³C NMR (100 MHz, chloroform-d) δ 175.67, 135.26, 134.80, 134.35, 134.04, 133.61, 129.33, 128.89, 116.03, 115.72, 112.44, 112.04, 52.48, 46.72, 46.18, 45.50. HRMS (EI) *m/z* calculated for [C₁₆H₁₂N₂O₂]⁺ (M⁺): calculated 264.0899; observed 264.0898.

2.4.3 ^1H AND ^{13}C NMR SPECTRA

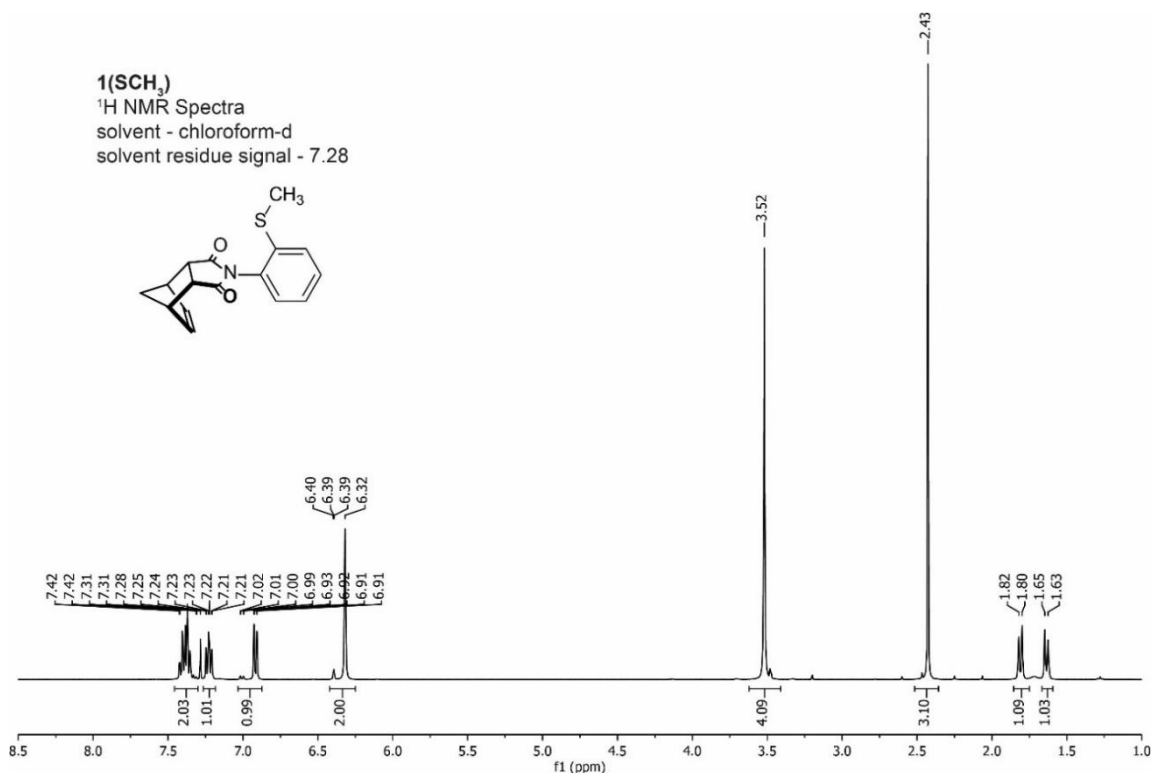


Figure 2.14 ^1H NMR spectra of rotor 1(SCH₃) (400 MHz, chloroform-d)

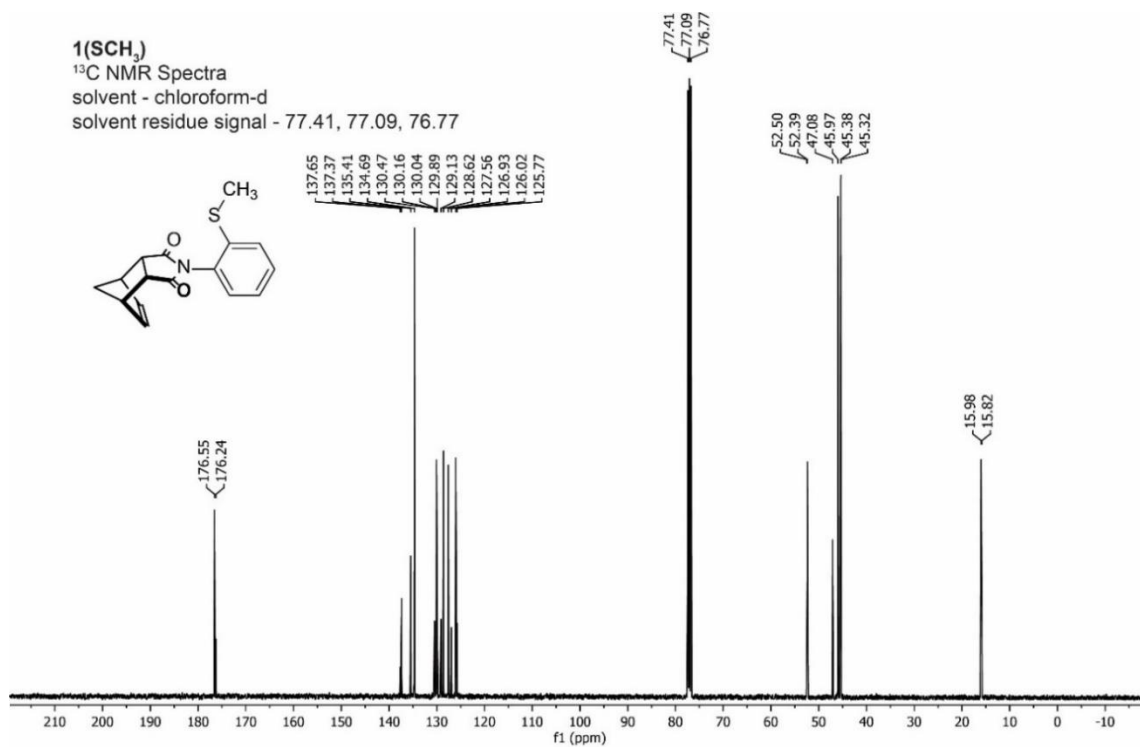


Figure 2.15 ^{13}C NMR spectra of rotor 1(SCH₃) (100 MHz, chloroform-d)

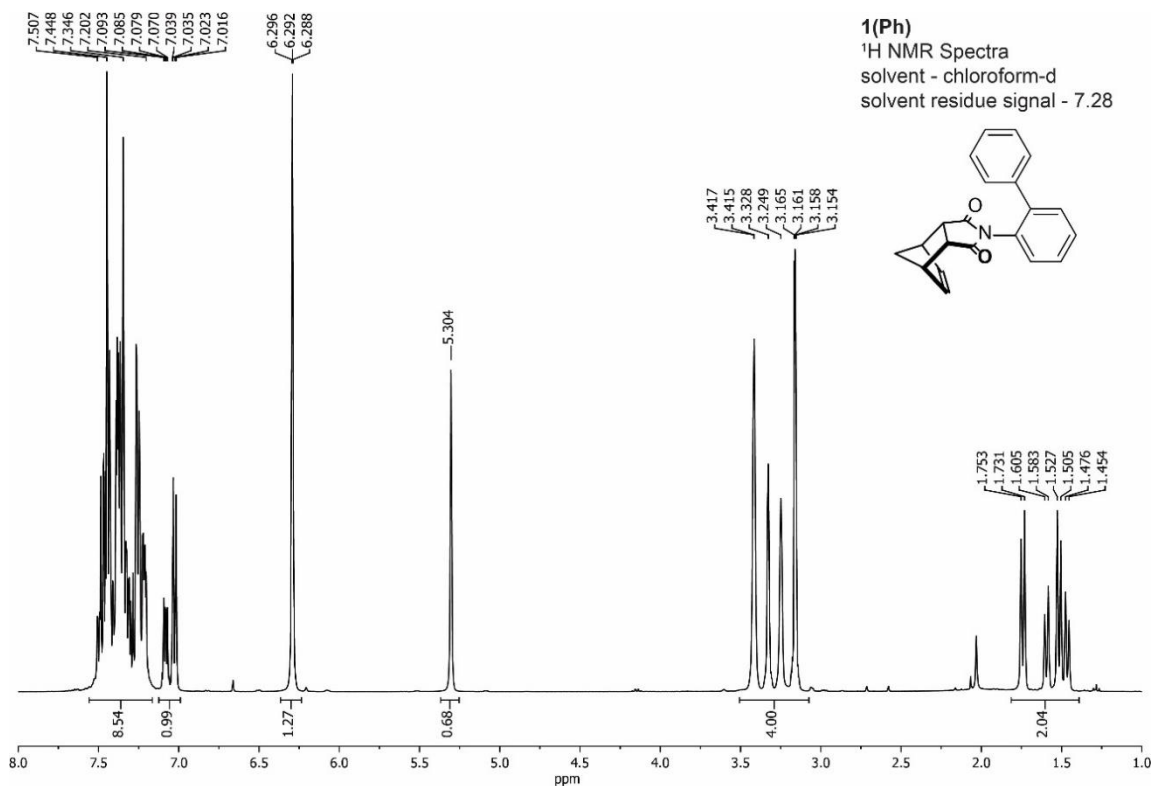


Figure 2.16 ¹H NMR spectra of rotor **1(Ph)** (400 MHz, chloroform-d)

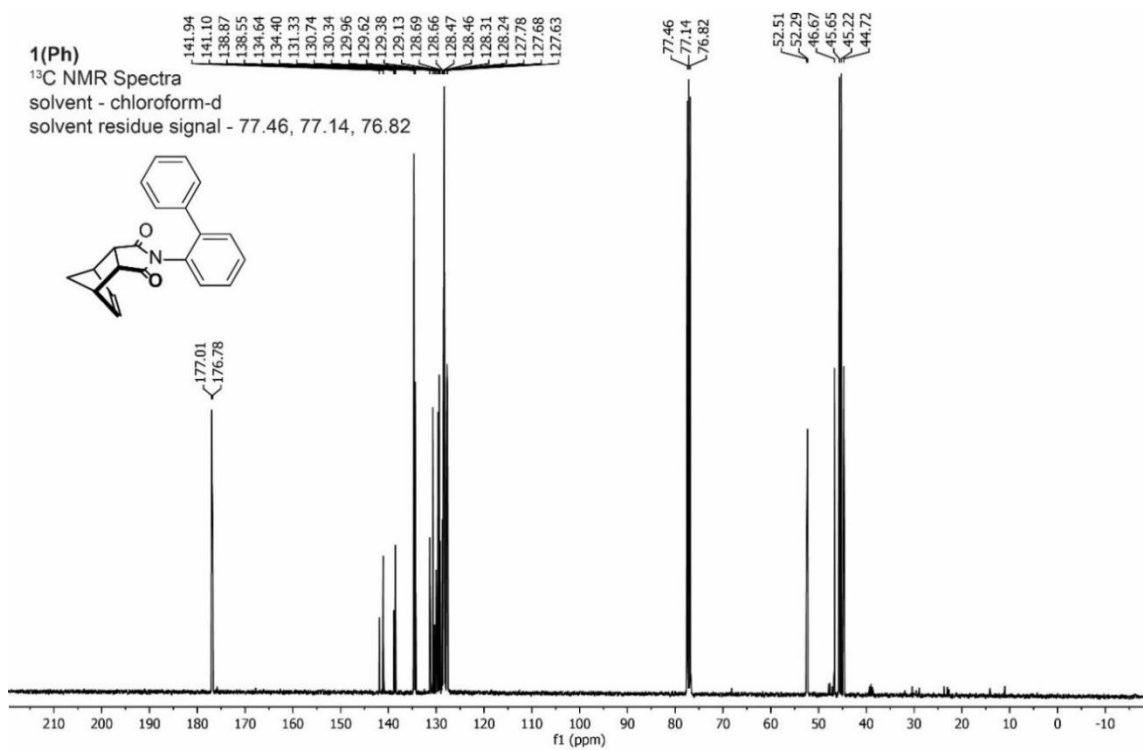


Figure 2.17 ¹³C NMR spectra of rotor **1(Ph)** (100 MHz, chloroform-d)

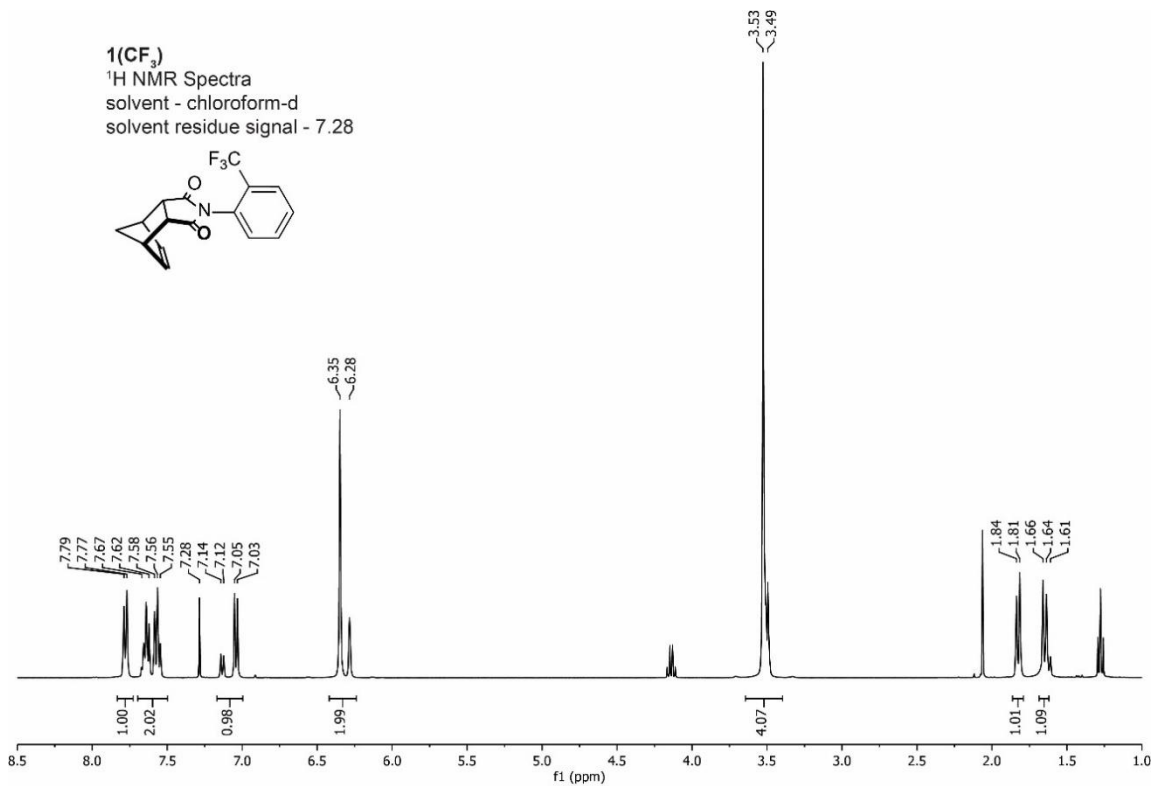


Figure 2.18 ¹H NMR spectra of rotor **1(CF₃)** (400 MHz, chloroform-d)

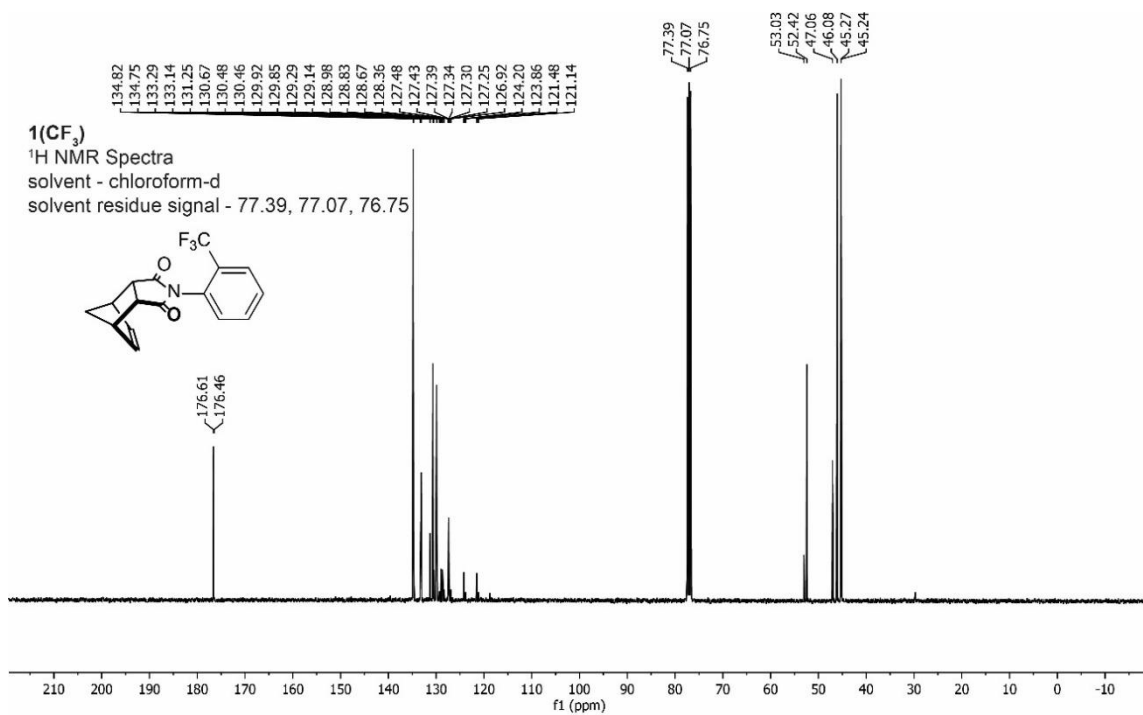


Figure 2.19 ¹³C NMR spectra of rotor **1(CF₃)** (100 MHz, chloroform-d)

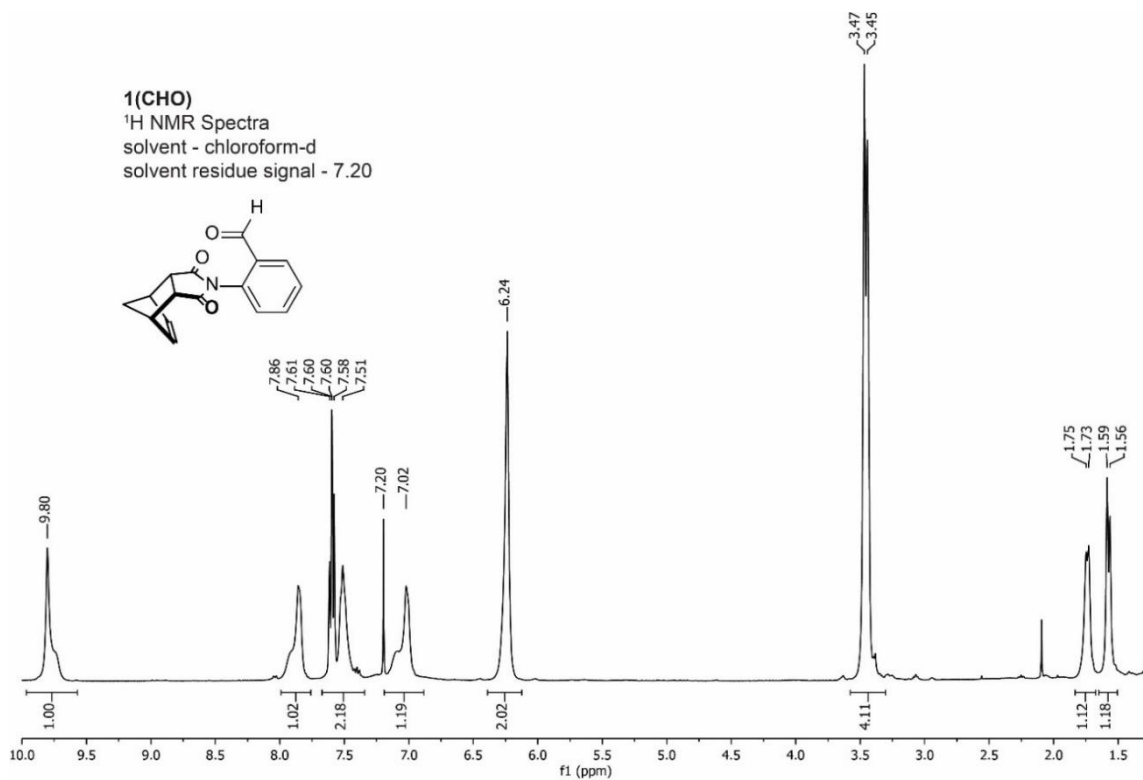


Figure 2.20 ¹H NMR spectra of rotor **1(CHO)** (400 MHz, chloroform-d)

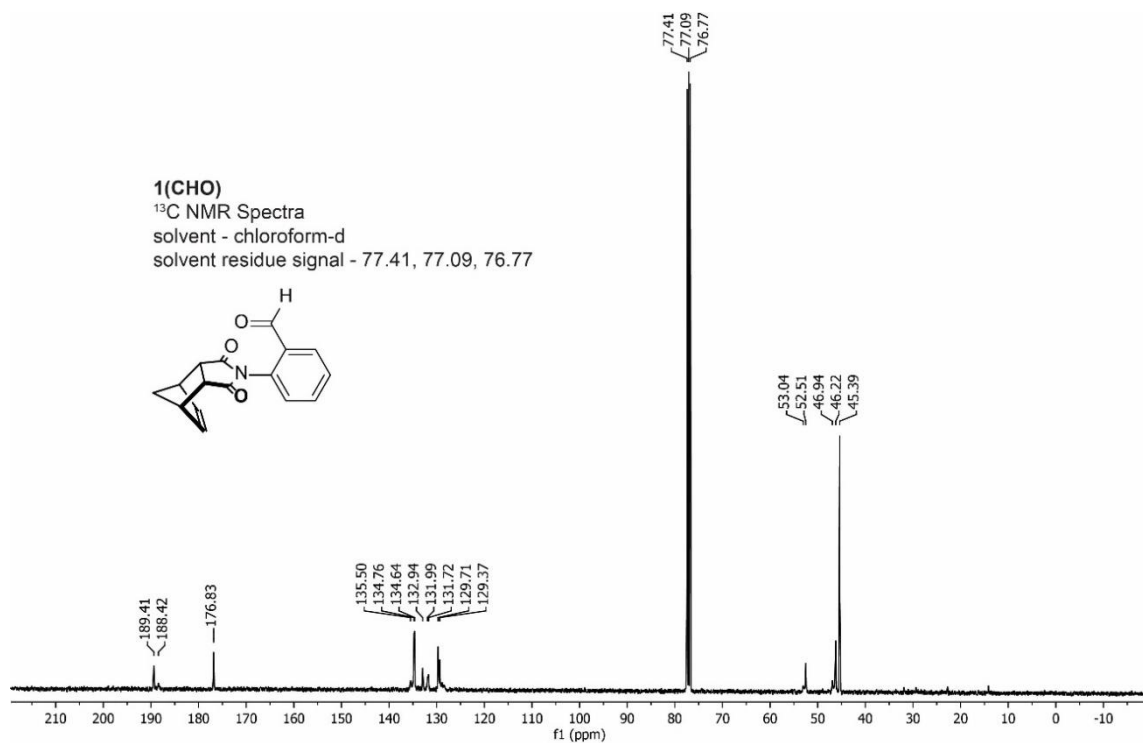


Figure 2.21 ¹³C NMR spectra of rotor **1(CHO)** (100 MHz, chloroform-d)

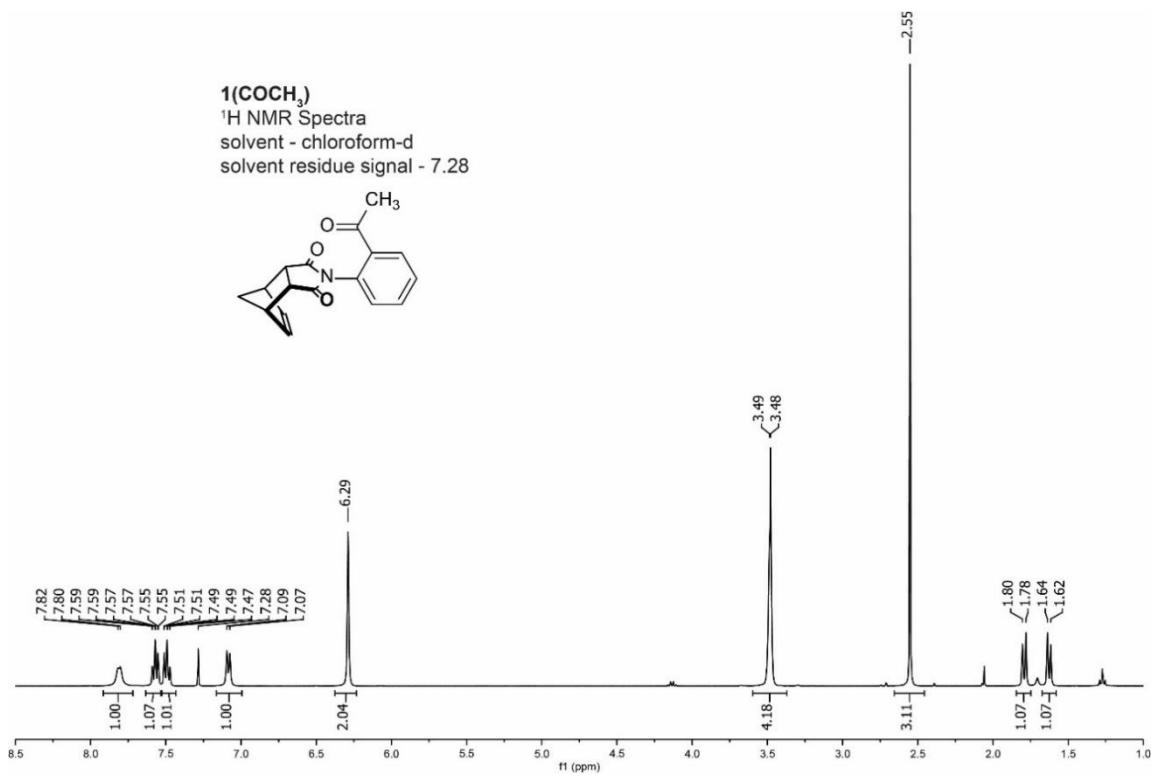


Figure 2.22 ¹H NMR spectra of rotor 1(COCH₃) (400 MHz, chloroform-d)

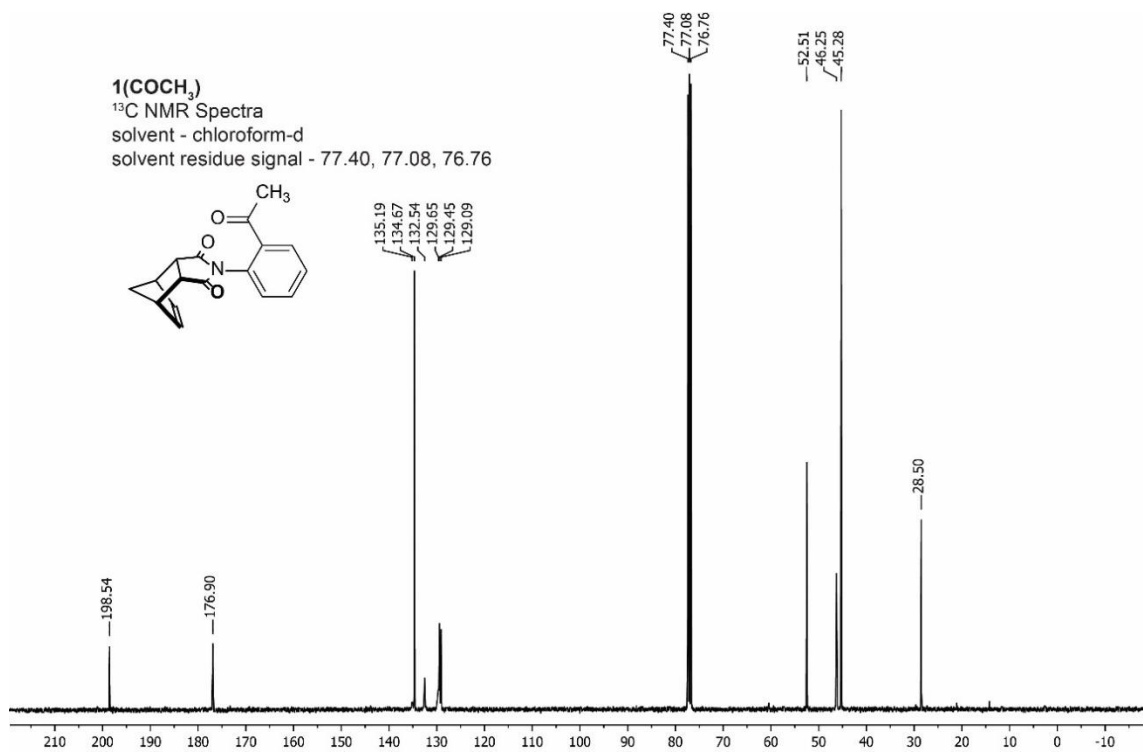


Figure 2.23 ¹³C NMR spectra of rotor 1(COCH₃) (100 MHz, chloroform-d)

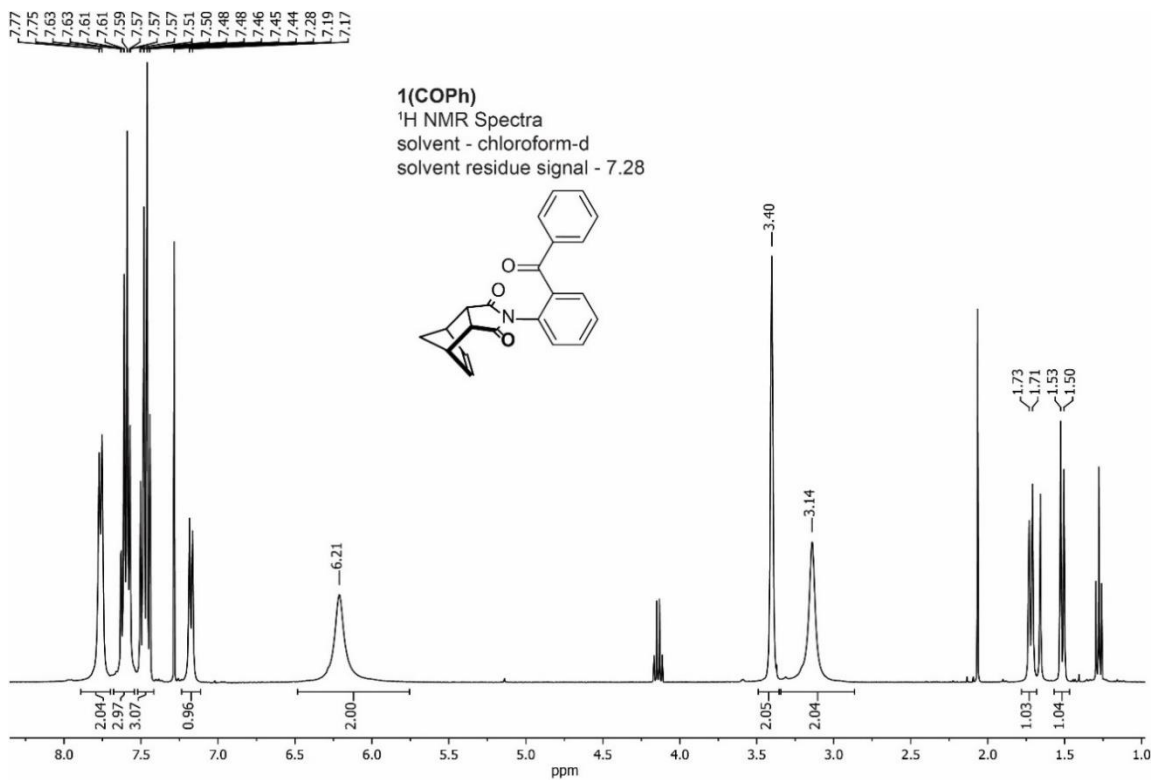


Figure 2.24 ¹H NMR spectra of rotor **1(COPh)** (400 MHz, chloroform-d)

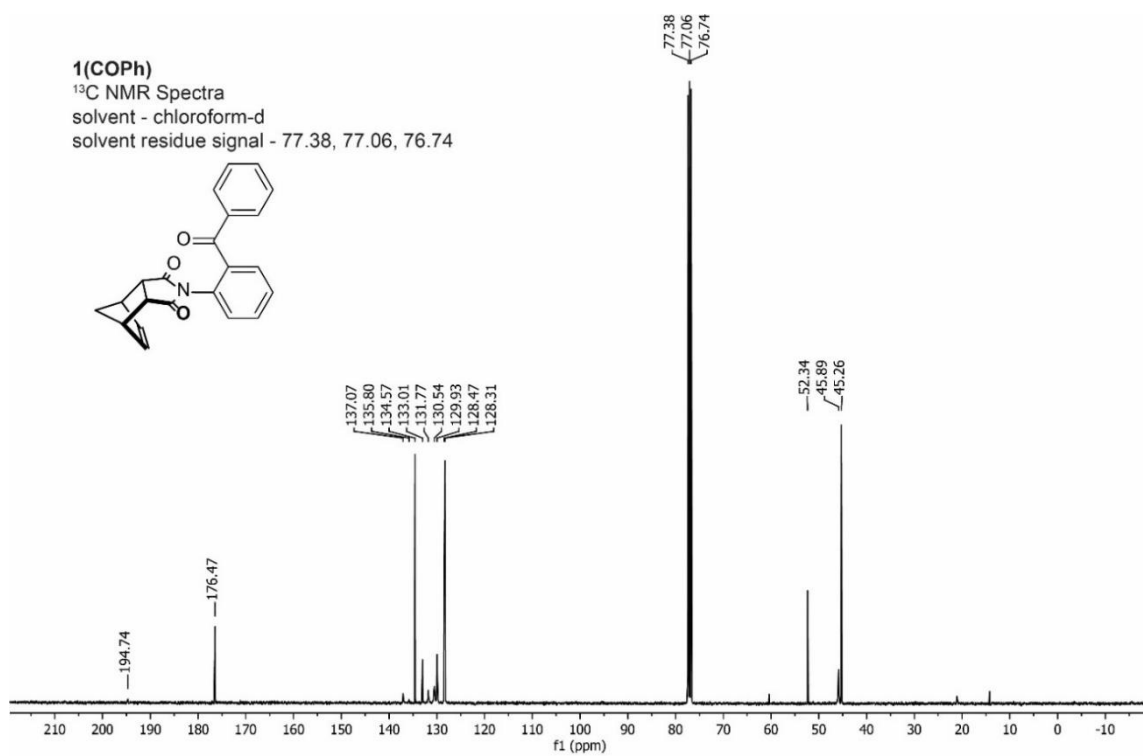


Figure 2.25 ¹³C NMR spectra of rotor **1(COPh)** (100 MHz, chloroform-d)

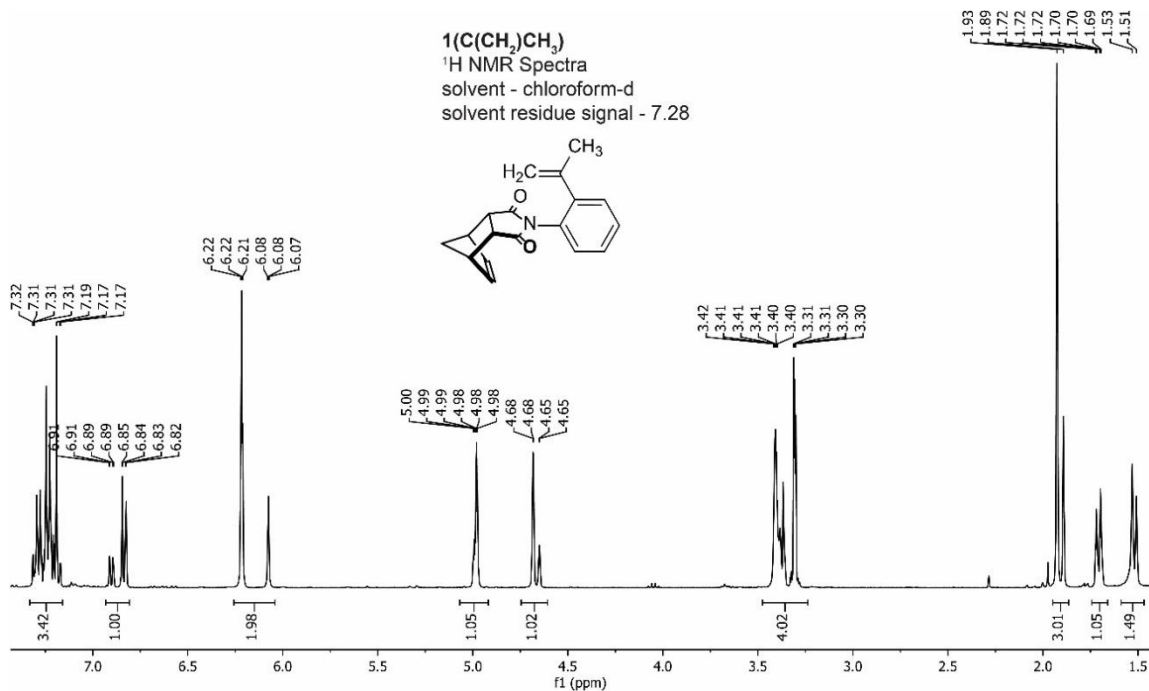


Figure 2.26 ¹H NMR spectra of rotor **1(C(CH₂)CH₃)** (400 MHz, chloroform-d)

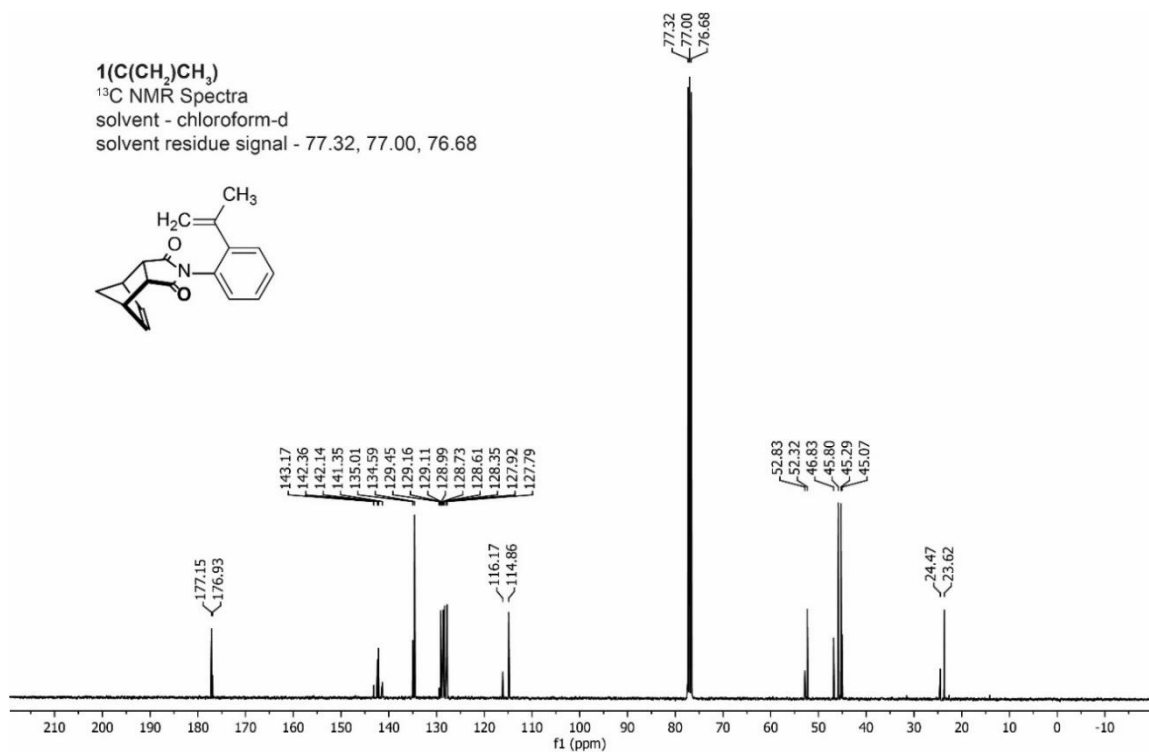


Figure 2.27 ¹³C NMR spectra of rotor **1(C(CH₂)CH₃)** (100 MHz, chloroform-d)

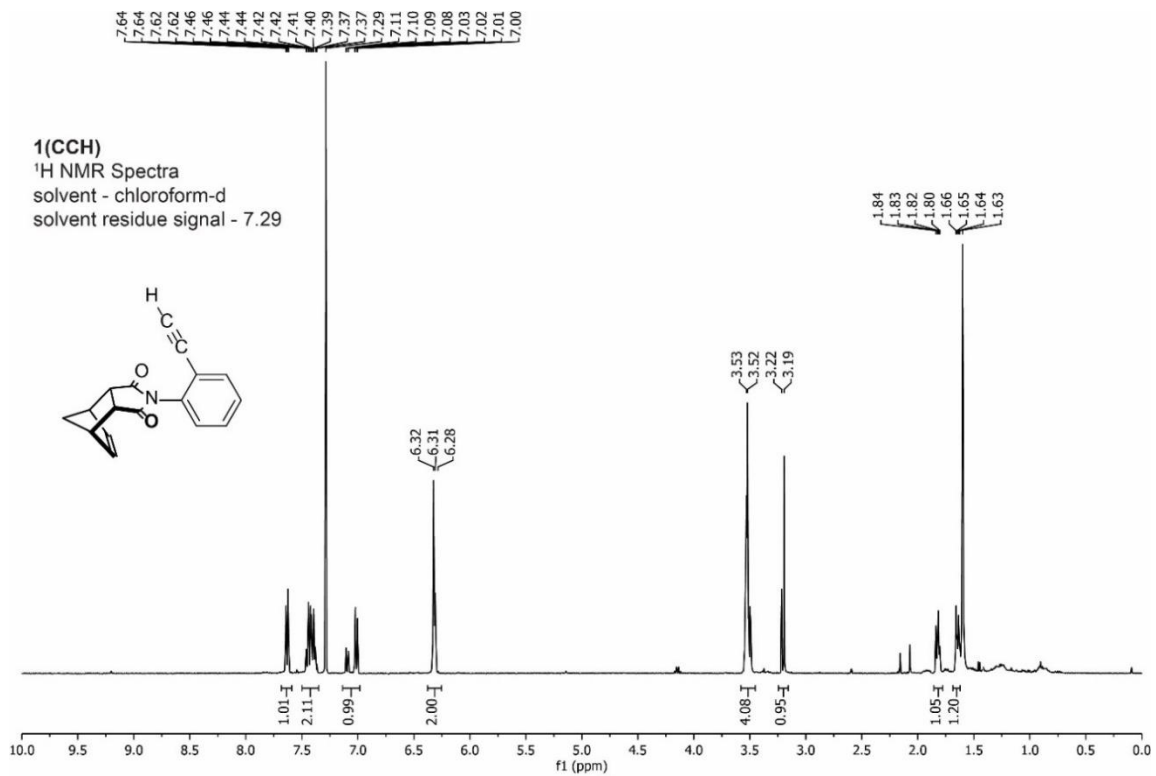


Figure 2.28 ¹H NMR spectra of rotor **1(CCH)** (400 MHz, chloroform-d)

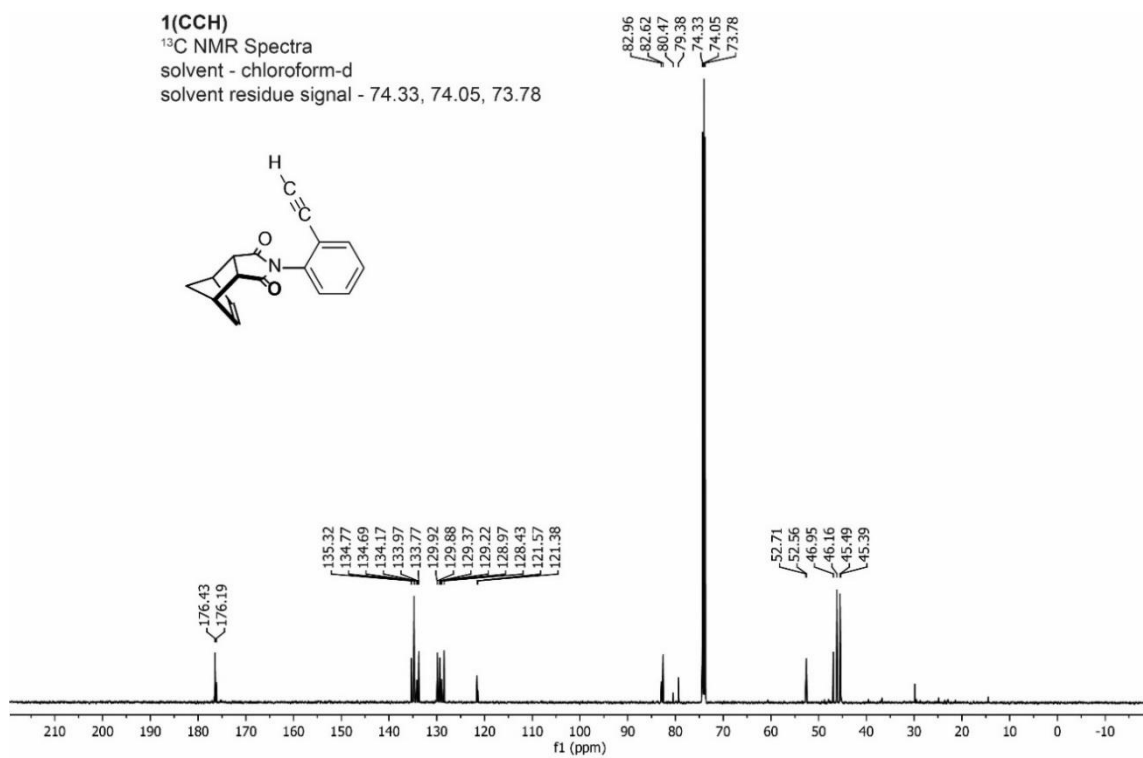


Figure 2.29 ¹³C NMR spectra of rotor **1(CCH)** (100 MHz, chloroform-d)

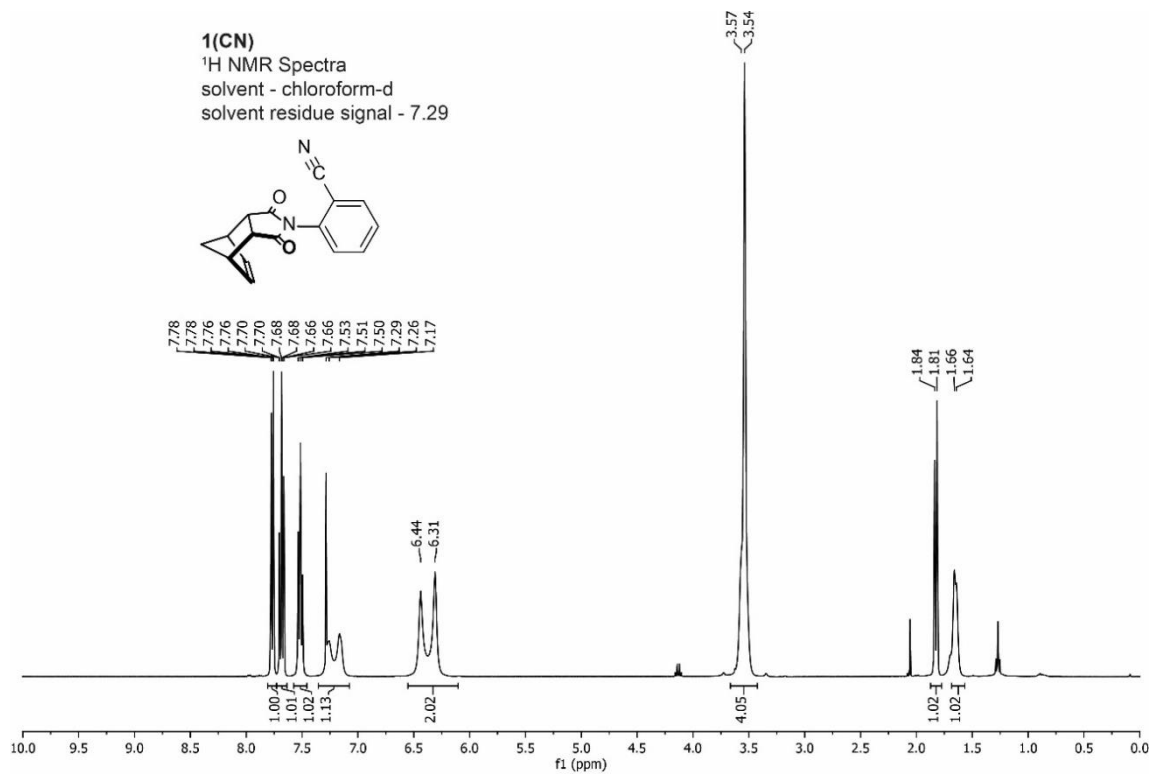


Figure 2.30 ¹H NMR spectra of rotor **1(CN)** (400 MHz, chloroform-d)

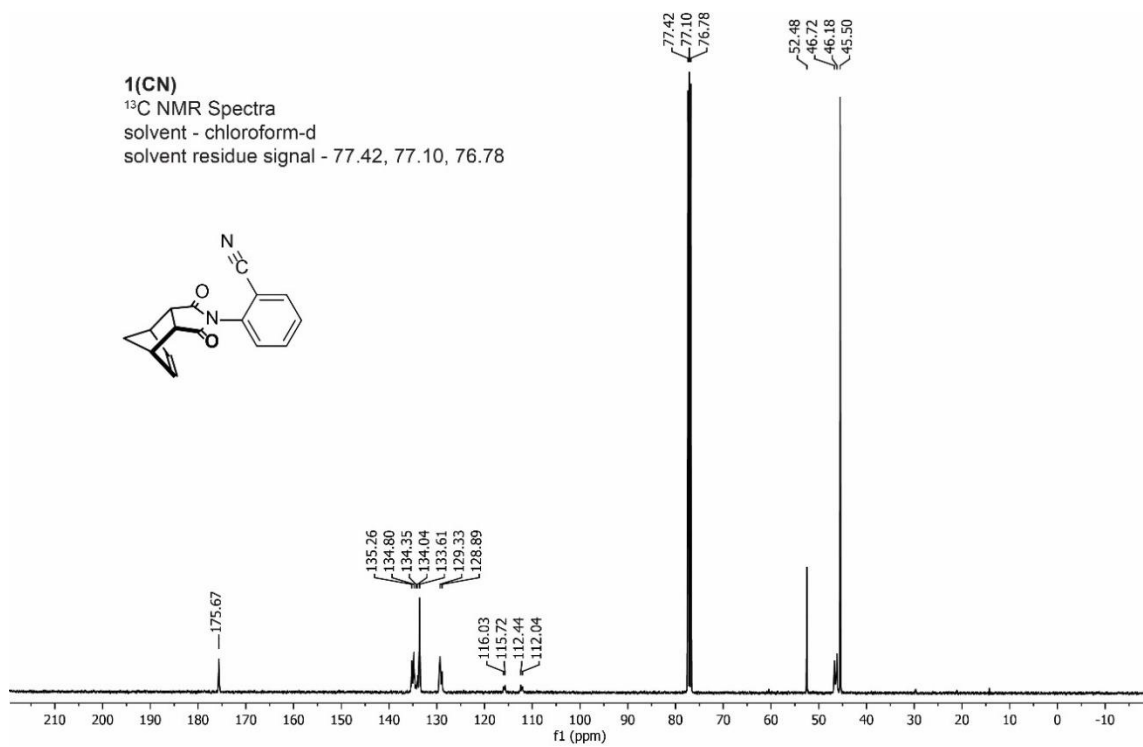


Figure 2.31 ¹³C NMR spectra of rotor **1(CN)** (100 MHz, chloroform-d)

2.4.4 EXPERIMENTAL DETERMINATION OF ROTATIONAL BARRIERS

The rotational barriers of **1(R)** (Table 2.1) were determined via exchange spectroscopy (EXSY) NMR experiments. EXSY NMR is observable by running nuclear Overhauser effect spectroscopy (NOESY) NMR experiments. In the spectra obtained from the NOESY experiments, out-of-phase signals off the diagonal of the 2D spectra originate from the nuclear Overhauser effect, while in-phase signals off the diagonal originate from exchange dynamics.⁷⁸ Integration of the signals were performed using Topspin software, and rate constants were obtained using the EXSYCalc software.

The rotational barrier for each rotor were extrapolated to the room temperature for consistency. The TS enthalpy (ΔH^\ddagger) and TS entropy (ΔS^\ddagger) were obtained from the Eyring plots (Figure 2.32) following Equation 2.1. The rotation barriers were determined by plugging the TS enthalpy and entropy along with a temperature into Equation 2.2.

$$\ln\left(\frac{k_{ex}}{T}\right) = \frac{-\Delta H^\ddagger}{R} \times \frac{1}{T} + \ln\left(\frac{k_B}{h}\right) + \frac{-\Delta S^\ddagger}{R} \dots\dots\dots \text{Equation 2.1}$$

$$\Delta G^\ddagger = \Delta H^\ddagger - T\Delta S^\ddagger \dots\dots\dots \text{Equation 2.2}$$

Due to the wide temperature range needed for rotational barrier determination *two* solvents (dichloromethane and tetrachloroethane) with similar chemical properties but different melting/boiling temperatures were chosen. Dichloromethane-d₂ (melting point = -95 °C, boiling point = 40 °C) is an appropriate choice for the rotors that requires a temperature range below 25 °C. Meanwhile, tetrachloroethane-d₂ (melting point = -45 °C, boiling point = 145 °C) was an appropriate choice for the rotors that requires a temperature range above 25 °C.

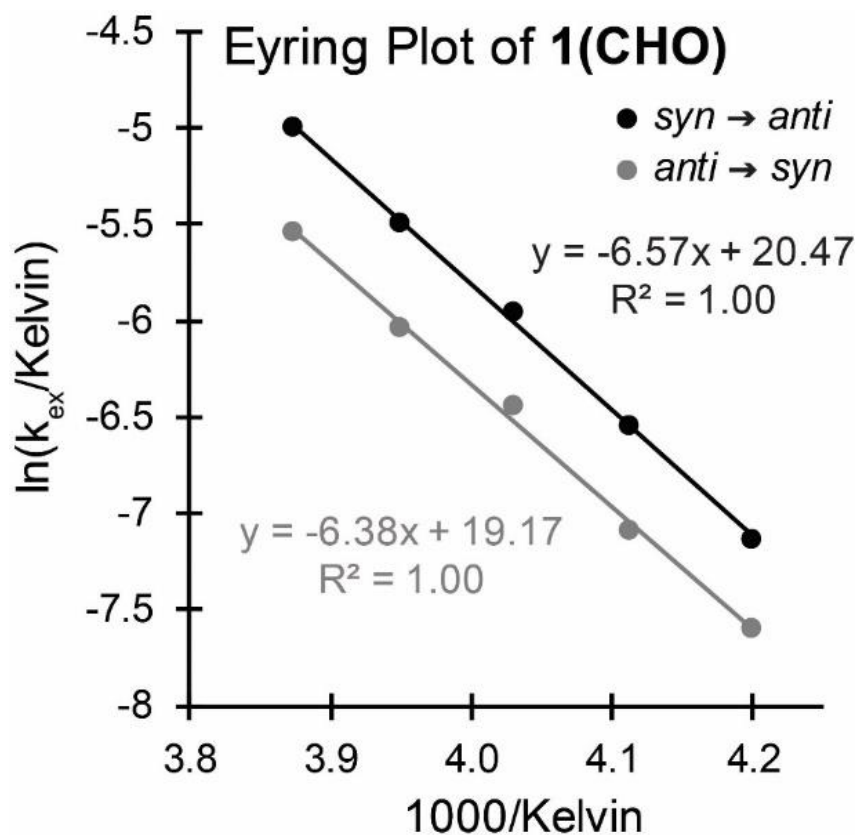


Figure 2.32 Eyring plot for 1(CHO)

The *syn*- and *anti*-conformers were identified at the temperatures in which the NOESY experiments were operable. The doublet of doublet (dd) signals for the *ortho*-hydrogen of *N*-phenyl ring are clearly indicative of the presence of the *syn*- and *anti*-conformer (Figure 2.33). The upfield-shifted dd peak corresponds to the *anti*-conformer in every case consisting with previous reports of the same molecular model.⁸⁸ No further decoalescence of the ¹H signals was observed at temperatures lower than -60 °C for either rotors in this study. The NOESY experiments were carried out on either the ethene protons or the *ortho*-hydrogen on the *N*-phenyl ring depending on which had better decoalescence and separation from neighboring signals.

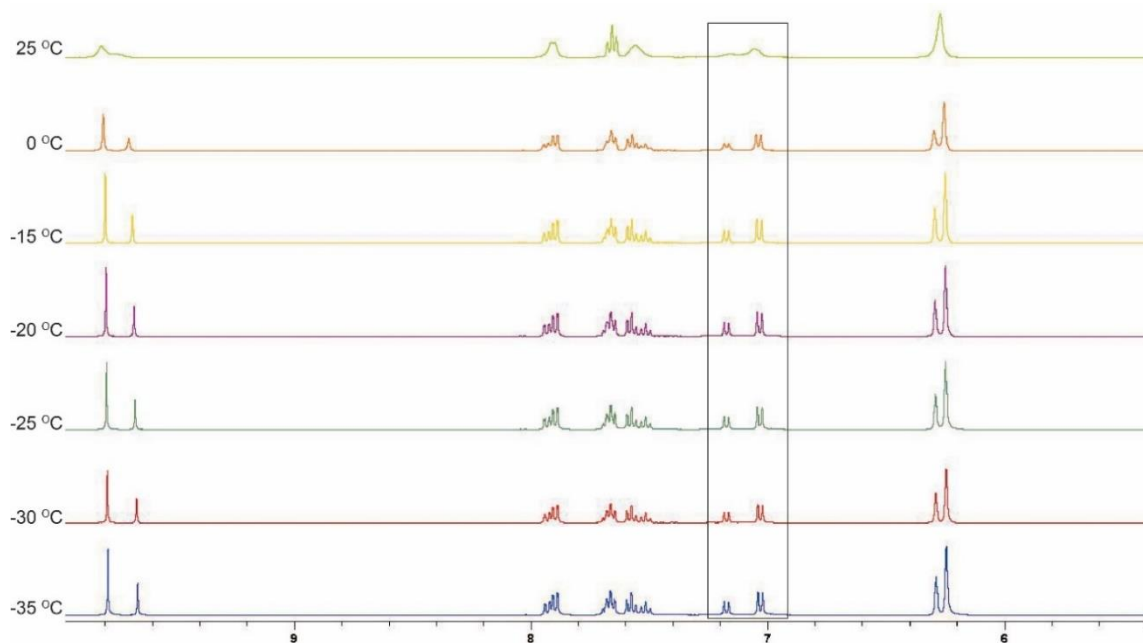


Figure 2.33 ^1H NMR of **1**(CHO) at various temperatures (-35, -30, -25, -20, -15, 0, and 25 $^\circ\text{C}$), highlighting the peaks for the ortho-hydrogen on the *N*-phenyl rotor to show a clear decoalescence.

Table 2.1 Experimental rotational barriers for **1**(R) via EXSY NMR

Rotor		rotational barrier (kcal/mol)						average $\Delta G^{\ddagger a}$
		<i>syn</i> \rightarrow <i>anti</i>			<i>anti</i> \rightarrow <i>syn</i>			
name	R	$\Delta G^{\ddagger a}$	ΔH^{\ddagger}	$T\Delta S^{\ddagger a}$	$\Delta G^{\ddagger a}$	ΔH^{\ddagger}	$T\Delta S^{\ddagger a}$	
1 (COCH ₃)		13.61	10.67	-2.93	14.20	13.36	-0.84	13.90
1 (COPh)		12.46	19.05	6.59	13.28	11.27	-2.01	12.87
1 (CHO)		14.95	13.26	-1.69	15.35	12.77	-2.59	15.15
1 (C(CH ₂)CH ₃)		19.13	17.77	-1.36	19.94	18.39	-1.55	19.54
1 (Ph)		21.25	22.84	1.57	21.70	23.18	1.47	21.48
1 (CCH)		18.58	16.05	-2.42	18.97	16.41	-2.45	18.78
1 (CN)		15.43	12.47	-2.96	15.45	12.73	-2.72	15.44
1 (OCH ₃)		20.26	20.22	-0.04	20.14	20.16	0.017	20.20
1 (SCH ₃)		22.71	20.11	-2.60	22.37	20.96	-1.42	22.54
1 (Cl)		21.79	19.67	-2.13	22.45	21.62	-0.83	22.12
1 (Br)		22.96	21.62	-1.33	23.25	20.87	-2.38	23.11
1 (I)		23.60	23.09	-0.51	24.87	24.48	-0.09	24.24
1 (CF ₃)		23.50	22.51	-0.99	23.93	21.21	-2.72	23.72
1 (CH ₃)		21.70	21.24	-0.46	21.72	20.88	-0.84	21.71
1 (CH ₂ CH ₃)		21.91	22.01	0.10	22.01	21.16	-0.85	21.96
1 (CH(CH ₃) ₂)		23.31	20.86	-2.44	23.82	22.69	-1.14	23.56

^a at 298.15 K.

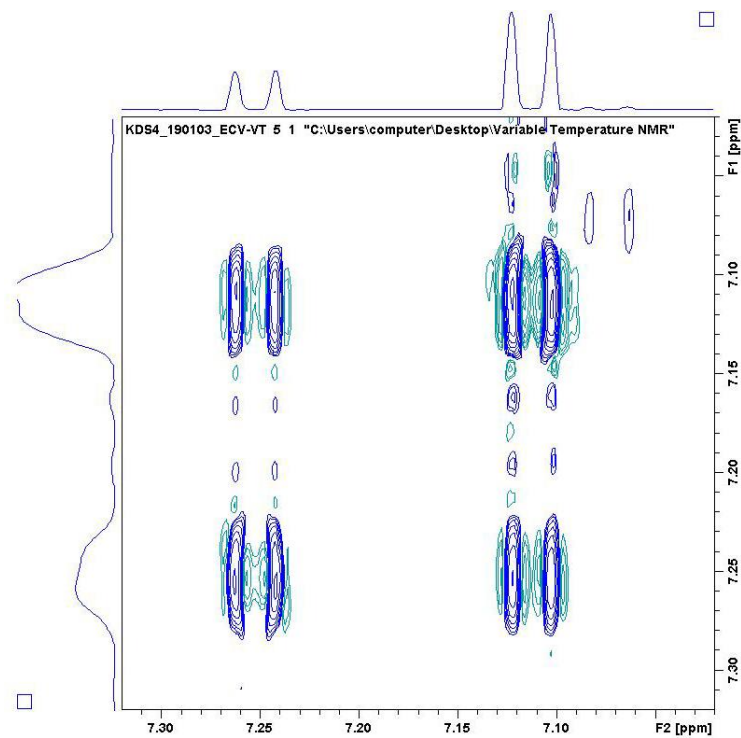


Figure 2.34 NOESY/EXSY spectra of rotor **1**(CHO) at -15 °C (400 MHz, dichloromethane-d²)

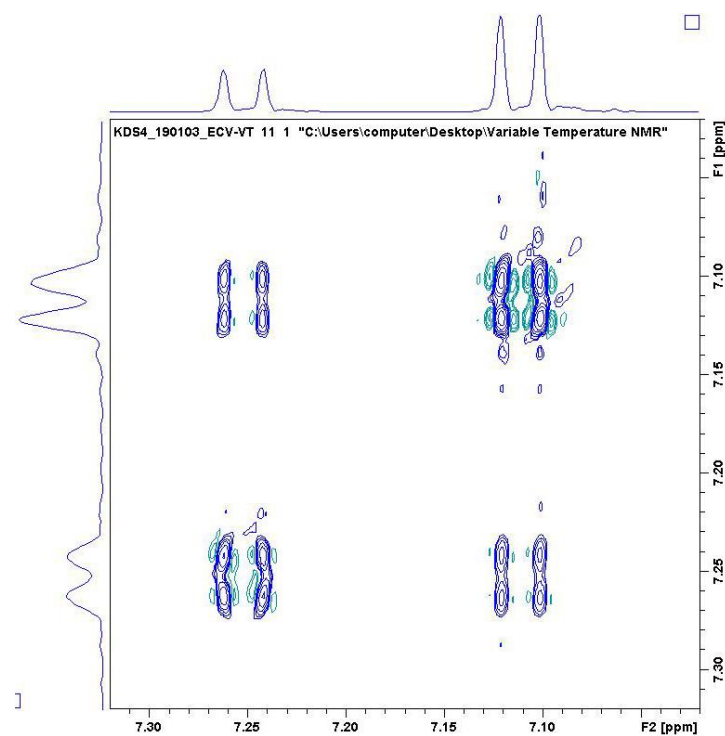


Figure 2.35 NOESY/EXSY spectra of rotor **1**(CHO) at -20 °C (400 MHz, dichloromethane-d²)

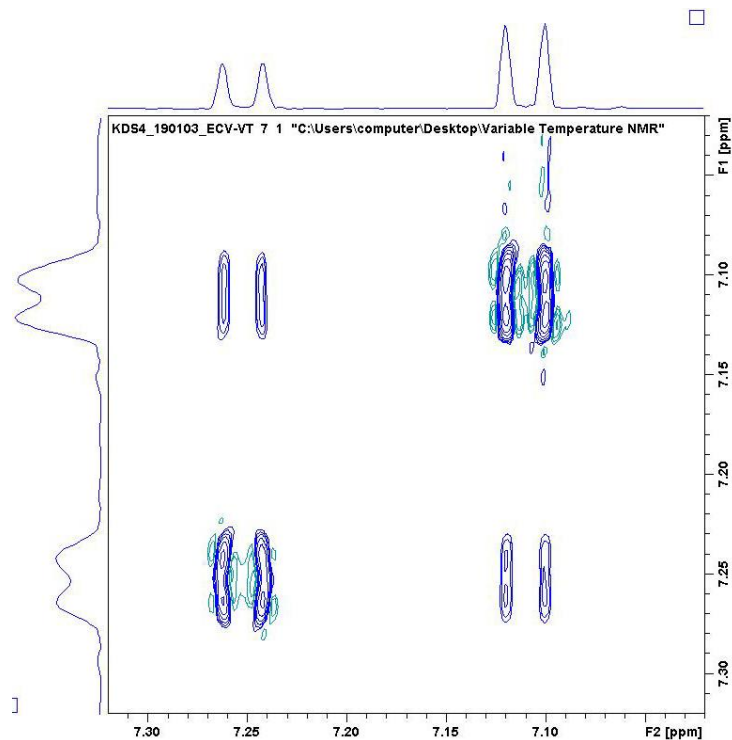


Figure 2.36 NOESY/EXSY spectra of rotor **1**(CHO) at $-25\text{ }^{\circ}\text{C}$ (400 MHz, dichloromethane- d^2)

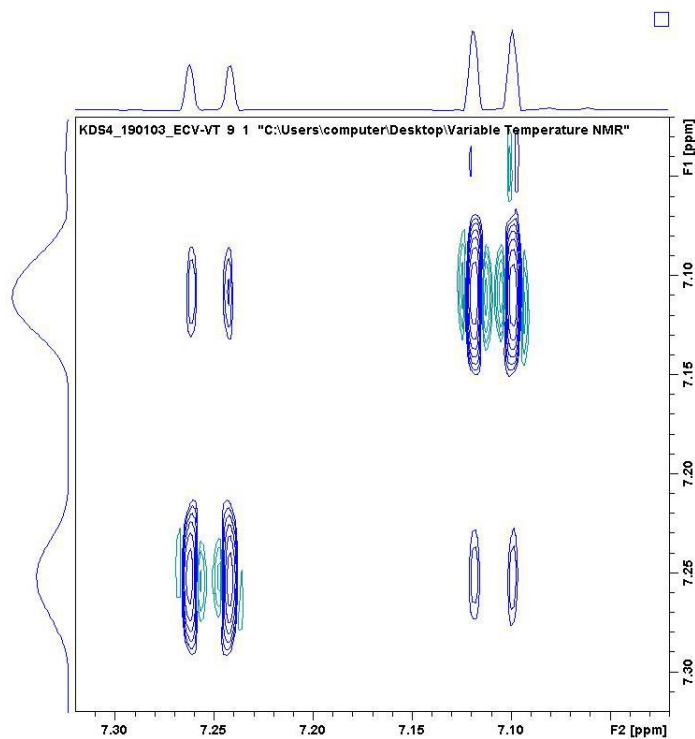


Figure 2.37 NOESY/EXSY spectra of rotor **1**(CHO) at $-30\text{ }^{\circ}\text{C}$ (400 MHz, dichloromethane- d^2)

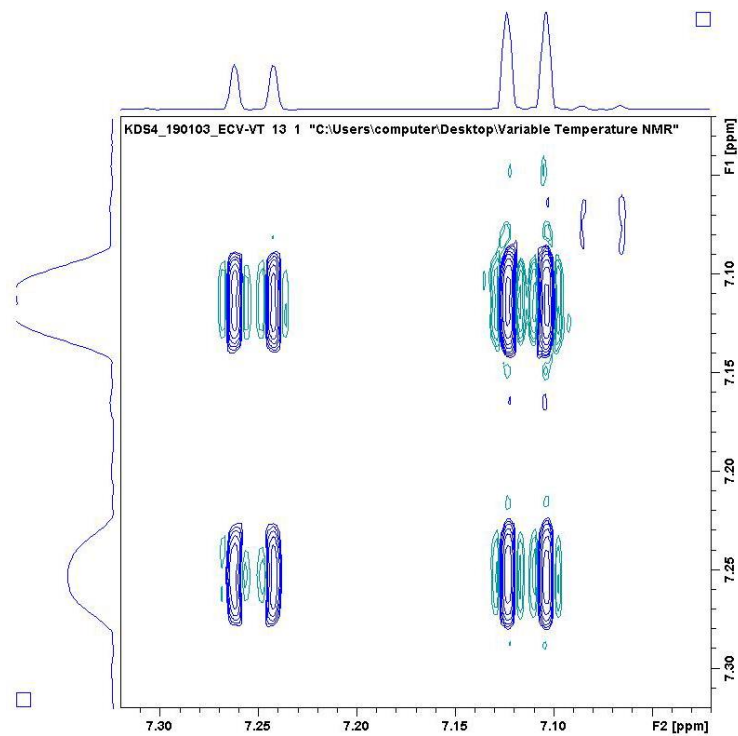


Figure 2.38 NOESY/EXSY spectra of rotor **1(CHO)** at $-35\text{ }^{\circ}\text{C}$ (400 MHz, dichloromethane- d_2)

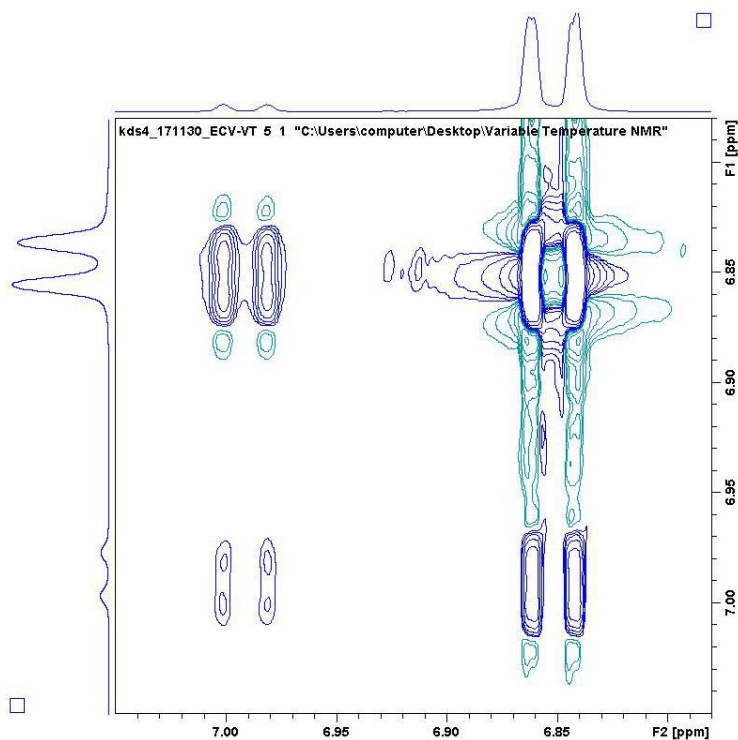


Figure 2.39 NOESY/EXSY spectra of rotor **1(COCH3)** at $-40\text{ }^{\circ}\text{C}$ (400 MHz, dichloromethane- d_2)

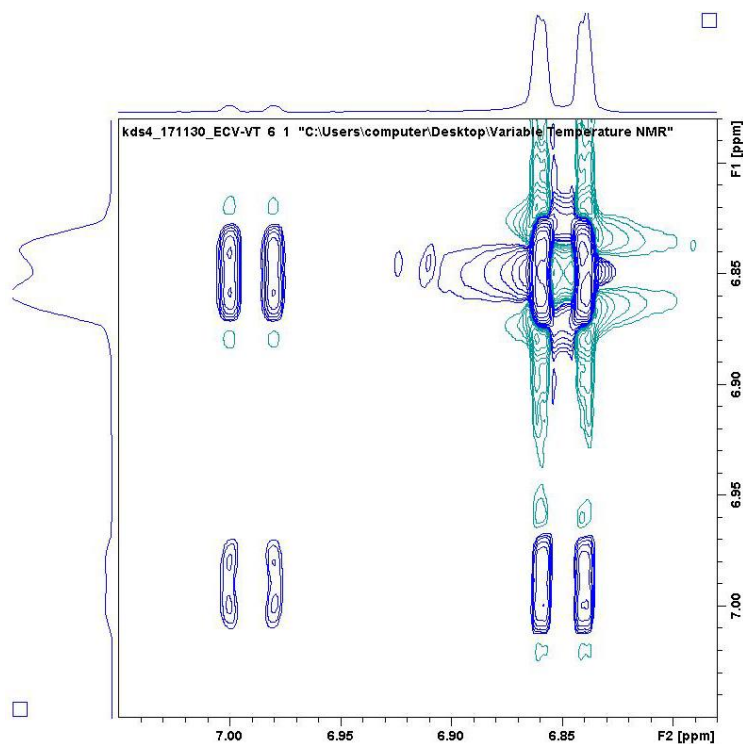


Figure 2.40 NOESY/EXSY spectra of rotor **1**(COCH₃) at -45 °C (400 MHz, dichloromethane-d₂)

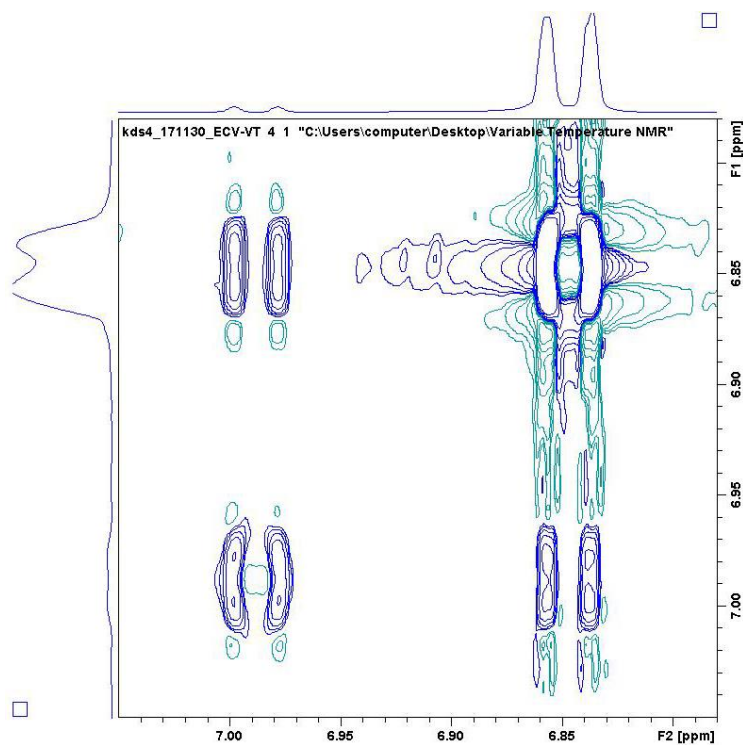


Figure 2.41 NOESY/EXSY spectra of rotor **1**(COCH₃) at -50 °C (400 MHz, dichloromethane-d₂)

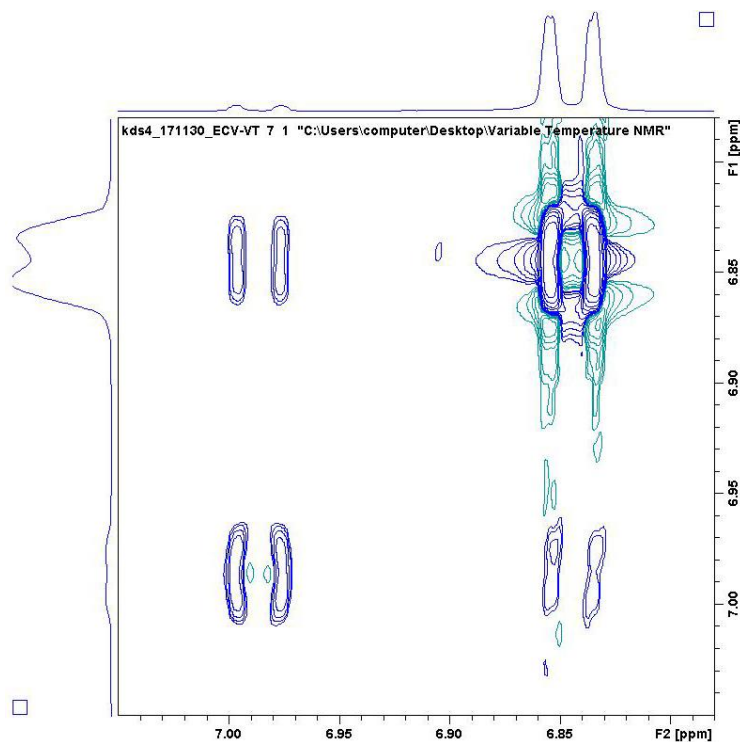


Figure 2.42 NOESY/EXSY spectra of rotor **1**(COCH₃) at -55 °C (400 MHz, dichloromethane-d₂)

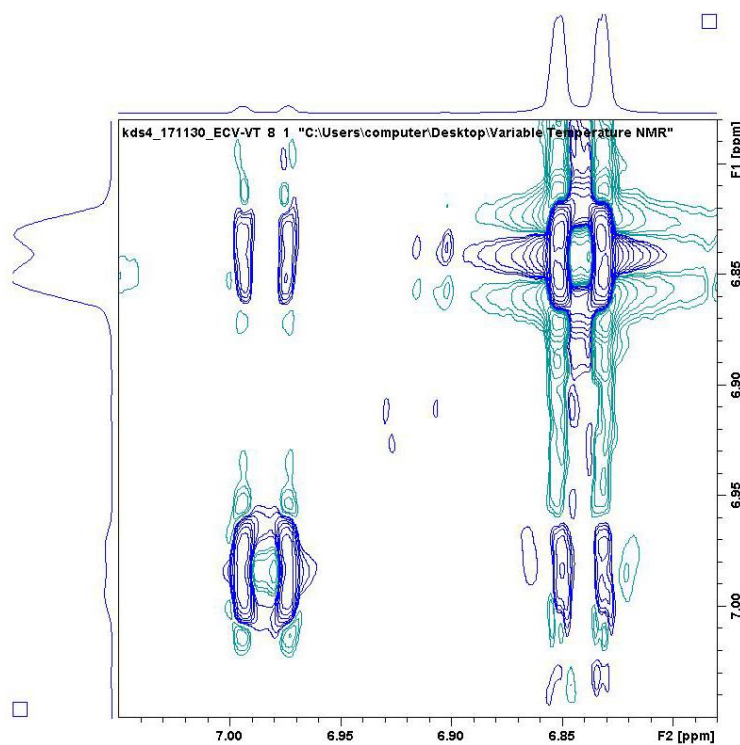


Figure 2.43 NOESY/EXSY spectra of rotor **1**(COCH₃) at -60 °C (400 MHz, dichloromethane-d₂)

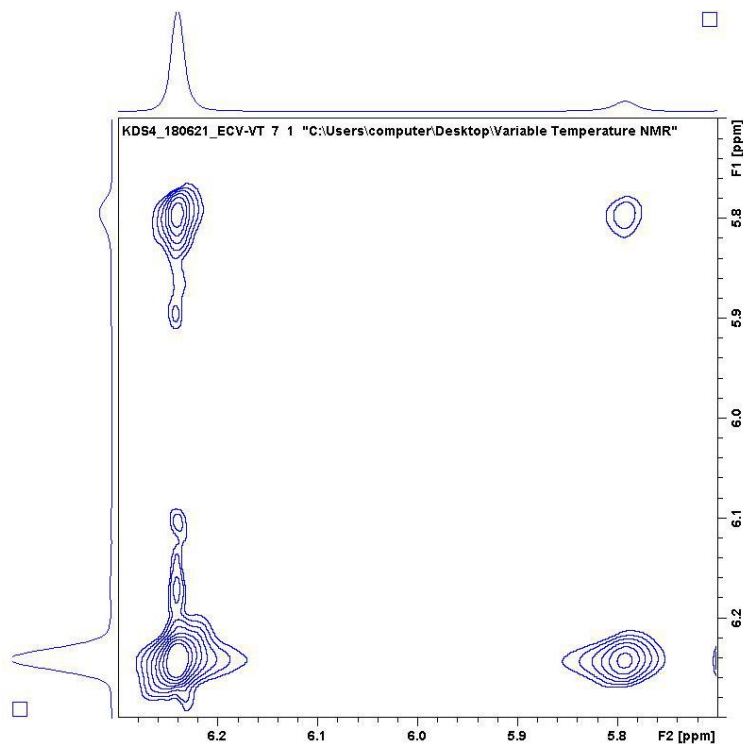


Figure 2.44 NOESY/EXSY spectra of rotor **1**(COPh) at -20 °C (400 MHz, dichloromethane-d²)

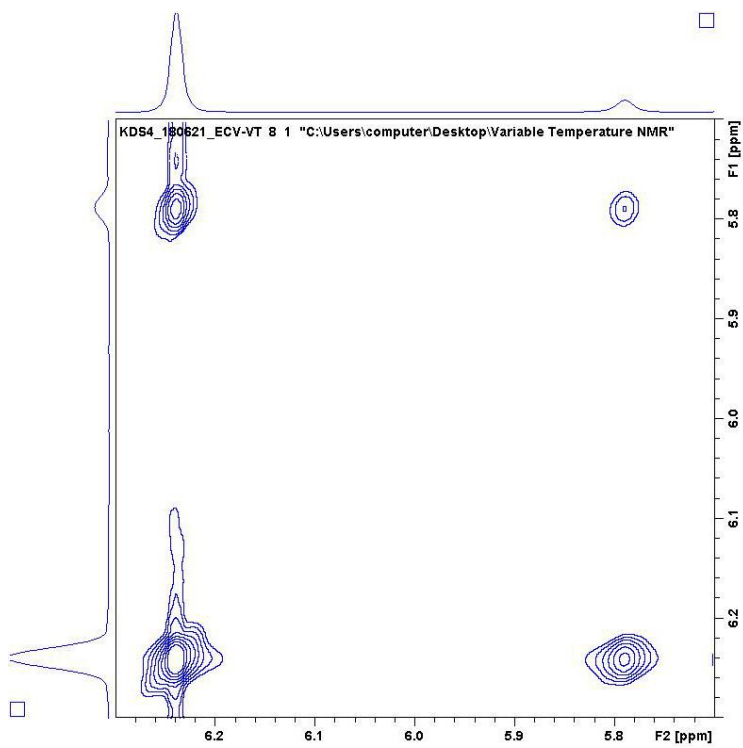


Figure 2.45 NOESY/EXSY spectra of rotor **1**(COPh) at -30 °C (400 MHz, dichloromethane-d²)

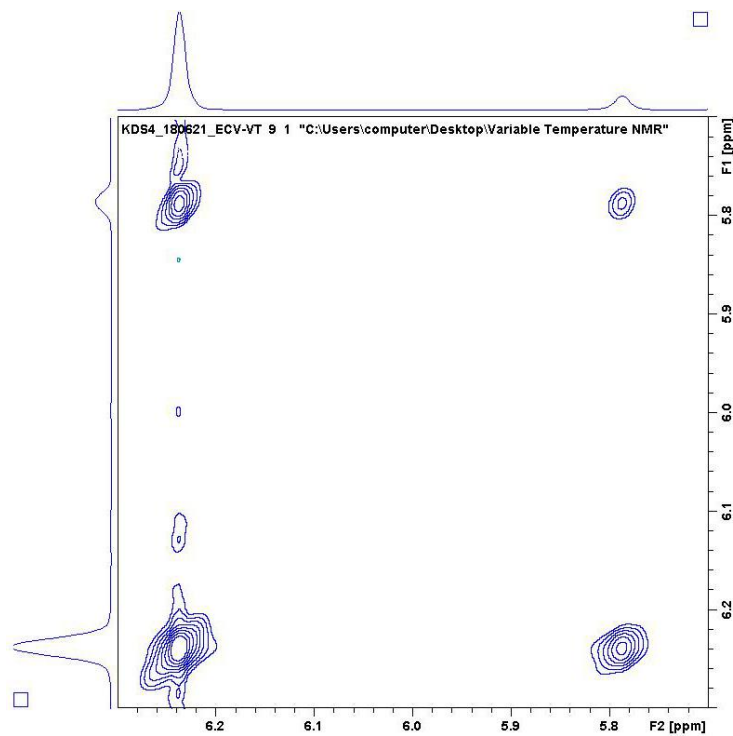


Figure 2.46 NOESY/EXSY spectra of rotor **1**(COPh) at $-25\text{ }^{\circ}\text{C}$ (400 MHz, dichloromethane- d_2)

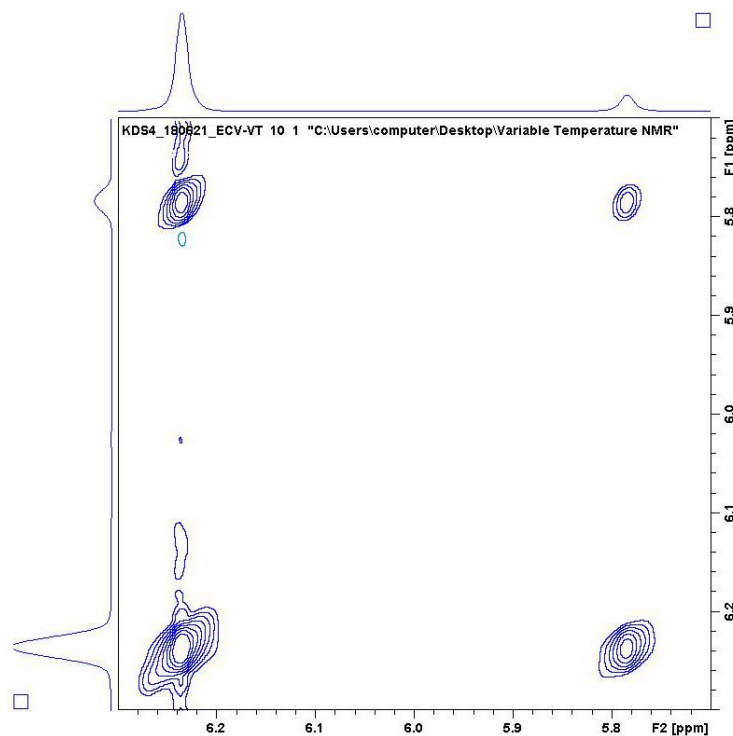


Figure 2.47 NOESY/EXSY spectra of rotor **1**(COPh) at $-35\text{ }^{\circ}\text{C}$ (400 MHz, dichloromethane- d_2)

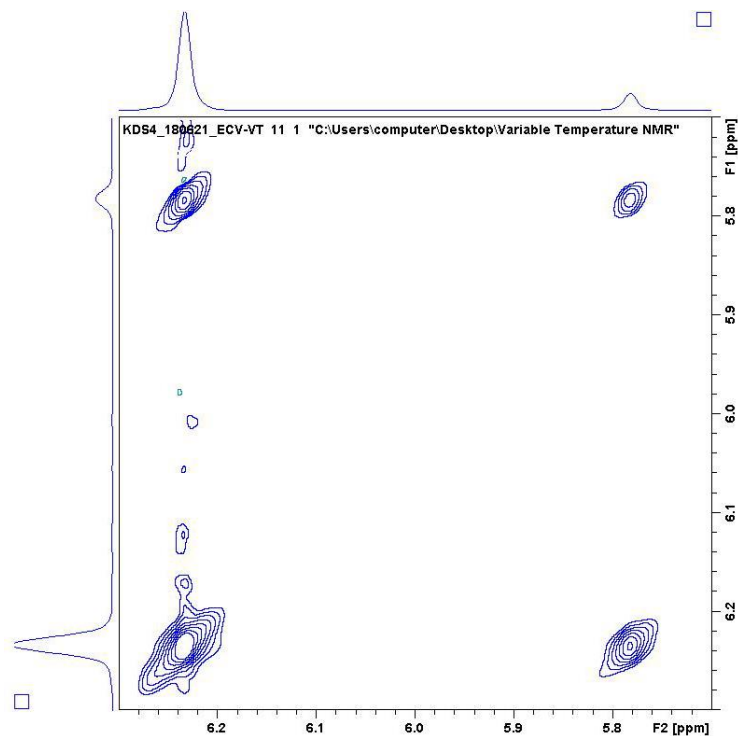


Figure 2.48 NOESY/EXSY spectra of rotor **1**(COPh) at $-40\text{ }^{\circ}\text{C}$ (400 MHz, dichloromethane- d_2)

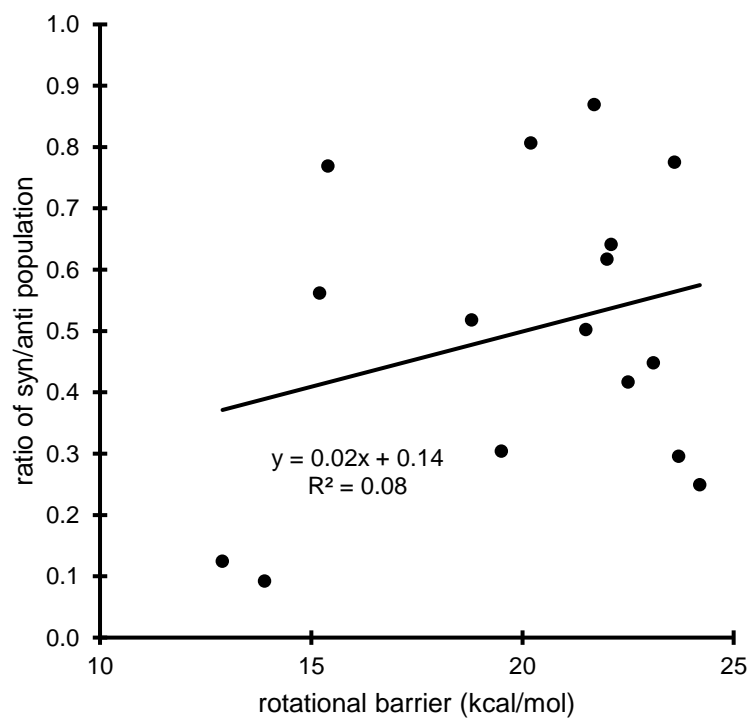


Figure 2.49 Correlation plot between ground state population ratios and rotational barrier energies (kcal/mol)

2.4.5 CALCULATION OF ROTATIONAL BARRIERS WITH TS AND GS GEOMETRIES

Following instructions from a benchmark study on the accuracy of different levels of theory for rotational barrier calculation, we optimized the ground state (GS) and transition state (TS) for our rotors using B3LYP-D3(0)/6-311G* and corrected for thermodynamic contributions.⁸⁹ All calculations were performed using *Spartan'18*. Convergence criteria were 10^{-4} Hartree and 10^{-4} atomic units as the maximum norm of the cartesian gradient. Vibrational analysis was also carried out at B3LYP-D3(0)/6-311G* and at 25 °C. To reduce error, the calculated GS energies for the *syn*- and *anti*- conformers were averaged. With thermodynamic corrections, the calculated barriers ($\Delta G^{\ddagger}_{\text{calc}}$) reproduced the experimental barriers ($\Delta G^{\ddagger}_{\text{exp}}$) with RMSD of ± 1.72 kcal/mol (Table 2.2 and Figure 2.50), suggesting that the calculated TS and GS geometries (Tables 2.3-2.32) were also accurate.

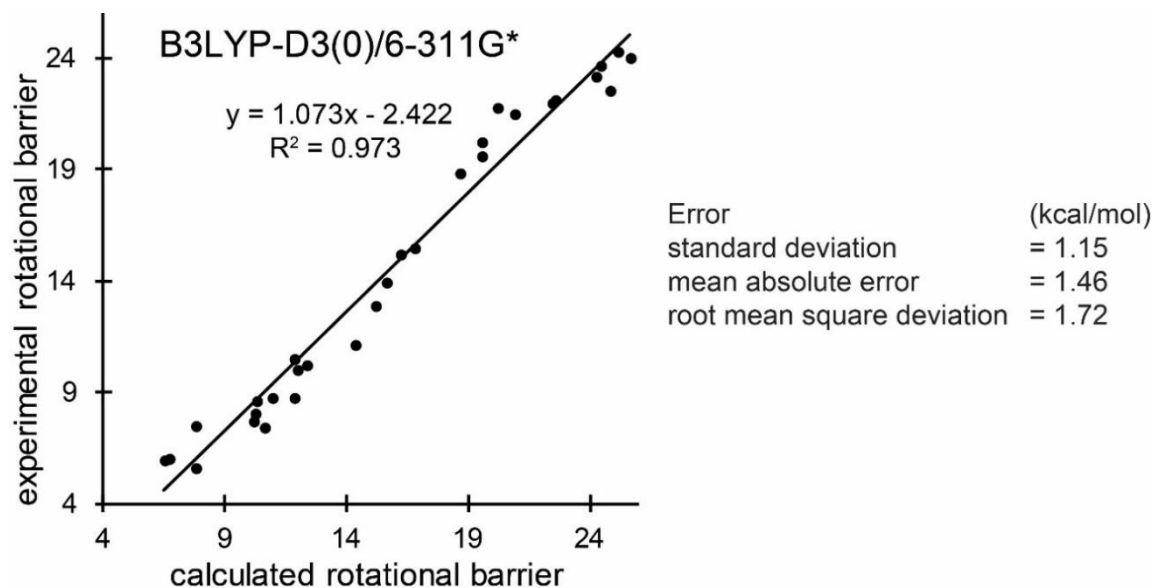


Figure 2.50 Correlation of the calculated ($\Delta G^{\ddagger}_{\text{calc}}$) and experimental ($\Delta G^{\ddagger}_{\text{exp}}$) rotational barriers for **1(R)**. Structures were calculated at the B3LYP-D3(0)/6-311G* level of theory with thermodynamic corrections.

Table 2.2 Calculated ($\Delta G^{\ddagger}_{\text{calc.}}$, kcal/mol)^a and experimental ($\Delta G^{\ddagger}_{\text{exp.}}$, kcal/mol)^b rotational barrier energies for rotors **1** and **2**, and the error (kcal/mol)^c reported as the difference between the calculated and experimental values.

Compound label	$\Delta G^{\ddagger}_{\text{calc.}}$ (kcal/mol) ^a	$\Delta G^{\ddagger}_{\text{exp.}}$ (kcal/mol) ^b	Error (kcal/mol) ^c
1 (COCH ₃)	15.6	13.9	1.7
1 (COPh)	15.1	12.9	2.2
1 (CHO)	16.2	15.2	1.0
1 (C(CH ₂)CH ₃)	19.5	19.5	0.0
1 (Ph)	20.8	21.5	-0.7
1 (CCH)	18.6	18.8	-0.2
1 (CN)	16.7	15.4	1.3
1 (OCH ₃)	19.5	20.2	-0.7
1 (SCH ₃)	24.8	22.5	2.3
1 (Cl)	22.5	22.1	0.4
1 (Br)	24.2	23.1	1.1
1 (I)	25.1	24.2	0.9
1 (CF ₃)	25.6	23.7	1.9
1 (CH ₃)	20.2	21.7	-1.5
1 (CH ₂ CH ₃)	22.4	22.0	0.4
1 (CH(CH ₃) ₂)	24.4	23.6	0.8
2 (COCH ₃)	10.2	8.0	2.2
2 (COPh)	8.8	-	-
2 (CHO)	12.3	10.2	2.1
2 (C(CH ₂)CH ₃)	9.1	-	-
2 (Ph)	7.8	7.5	0.3
2 (CCH)	6.7	6.0	0.7
2 (CN)	6.5	5.9	0.6
2 (OCH ₃)	7.8	5.6	2.2
2 (SCH ₃)	10.3	8.6	1.7
2 (Cl)	10.1	7.7	2.4
2 (Br)	10.9	8.7	2.2
2 (I)	11.9	10.0	1.9
2 (CF ₃)	11.8	10.5	1.3
2 (CH ₃)	10.6	7.4	3.2
2 (CH ₂ CH ₃)	11.8	8.7	3.1
2 (CH(CH ₃) ₂)	14.3	11.1	3.2

^a B3LYP-D3(0)/6-311G*; ^b via EXSY; ^c $\Delta G^{\ddagger}_{\text{calc.}} - \Delta G^{\ddagger}_{\text{exp.}}$

Table 2.3 XYZ coordinates of the GS and TS structures of **1**(Br)

H 0.357147 -1.901143 -5.447214 C 0.356879 -1.598440 -4.405510 C 0.326320 -0.818818 -1.720889 C -0.799852 -1.062444 -3.851032 C 1.503776 -1.738749 -3.628647 C 1.481537 -1.353222 -2.294771 C -0.813808 -0.665358 -2.516207 H -1.693243 -0.944031 -4.452123 H 2.409641 -2.151608 -4.058124 H 2.363900 -1.458479 -1.674715 N 0.361996 -0.449396 -0.347323 C 1.191003 0.580164 0.138841 C 1.039677 0.614921 1.646564 C 0.025110 -0.498701 1.987765 C -0.347164 -1.133367 0.662133 H 2.022233 0.469222 2.100326 O 1.885978 1.282835 -0.548740 O -1.095435 -2.054679 0.467848 C -1.131686 0.285186 2.717423 H -1.803078 -0.359315 3.281707 H 0.423397 -1.275774 2.643210 C 0.357902 1.913488 2.219521 H 1.044448 2.750450 2.331517 C -0.274225 1.312400 3.498953 H 0.454399 0.850682 4.172960 H -0.878666 2.034482 4.050842 C -0.891224 2.159336 1.388318 H -0.972727 2.903695 0.606481 C -1.770770 1.196944 1.682542 H -2.711284 0.996096 1.187748 Br -2.422181 0.113621 -1.839403	H -0.345452 5.525034 1.598755 C -0.254623 4.461378 1.405759 C -0.042535 1.722443 0.920702 C -0.560606 3.555068 2.417105 C 0.167612 4.006541 0.158612 C 0.269160 2.641745 -0.079763 C -0.444316 2.188643 2.176061 H -0.883318 3.902051 3.390885 H 0.411844 4.710635 -0.629046 H 0.590656 2.265243 -1.043608 N 0.056570 0.329063 0.646552 C -1.069349 -0.514146 0.541081 C -0.563090 -1.923258 0.307556 C 0.967797 -1.789156 0.145885 C 1.271663 -0.316073 0.343780 H -0.860931 -2.544058 1.155451 O -2.211634 -0.145553 0.610679 O 2.339248 0.233058 0.254095 C 1.221849 -2.353959 -1.300304 H 2.264298 -2.597102 -1.496573 H 1.539129 -2.362328 0.878906 C -1.017134 -2.574909 -1.048415 H -2.010301 -3.018179 -1.011603 C 0.192085 -3.513772 -1.290330 H 0.354578 -4.234350 -0.482681 H 0.137330 -4.038976 -2.245707 C -0.774481 -1.538054 -2.135262 H -1.551651 -0.946540 -2.602538 C 0.547960 -1.406686 -2.282558 H 1.071737 -0.688544 -2.901207 Br -0.814096 0.964742 3.597731	H 0.386467 -1.139857 -5.480701 C 0.322180 -1.073686 -4.400170 C 0.146354 -0.996086 -1.547515 C -0.675775 -1.748458 -3.721621 C 1.198063 -0.290300 -3.663920 C 1.102925 -0.260257 -2.284060 C -0.811175 -1.700491 -2.326484 H -1.406884 -2.316632 -4.282169 H 1.967039 0.298680 -4.151782 H 1.822395 0.335419 -1.753761 N 0.239782 -0.875137 -0.108453 C 1.388659 -0.318774 0.545746 C 1.005267 0.084458 1.945011 C -0.375933 -0.524617 2.175662 C -0.677120 -1.296467 0.915299 H 1.775297 -0.250191 2.640378 O 2.492742 -0.184221 0.081744 O -1.500564 -2.161232 0.831969 C -1.294737 0.738055 2.436740 H -2.249251 0.485132 2.894395 H -0.436259 -1.207655 3.022820 C 0.750820 1.641922 2.114981 H 1.665504 2.209216 2.275843 C -0.291287 1.584450 3.258753 H 0.071696 1.081386 4.160305 H -0.683660 2.568999 3.519657 C -0.138428 2.090418 0.966192 H 0.203082 2.641277 0.098379 C -1.347673 1.552026 1.155577 H -2.189112 1.573951 0.473936 Br -2.460415 -2.541325 -1.792751

Table 2.4 XYZ coordinates of the GS and TS structures of **1**(C(CH₂)CH₃)

H	1.101477	-1.639101	-5.185157	H	-0.695624	0.114062	-5.317846	H	0.697630	-0.167486	-5.219064
C	1.065952	-1.323843	-4.147320	C	-0.507048	0.054215	-4.250827	C	0.693277	-0.227390	-4.135770
C	0.946623	-0.509132	-1.489696	C	-0.005466	-0.081172	-1.523650	C	0.636253	-0.425949	-1.301654
C	-0.157839	-1.208916	-3.500946	C	0.045682	1.141883	-3.584577	C	-0.383605	-0.785473	-3.468002
C	2.242100	-1.022988	-3.463422	C	-0.811400	-1.111207	-3.550405	C	1.748312	0.258796	-3.379396
C	2.178951	-0.625973	-2.134614	C	-0.566825	-1.172112	-2.184527	C	1.713020	0.160997	-1.997211
C	-0.248316	-0.780370	-2.169928	C	0.324547	1.092774	-2.213447	C	-0.466435	-0.894423	-2.067292
H	-1.074255	-1.423682	-4.041542	H	0.294446	2.040673	-4.139250	H	-1.228665	-1.156123	-4.037201
H	3.202613	-1.104377	-3.960707	H	-1.241419	-1.965157	-4.063272	H	2.610406	0.717607	-3.852483
H	3.084403	-0.400535	-1.583749	H	-0.807664	-2.063088	-1.616442	H	2.557289	0.535484	-1.448926
N	0.957049	-0.134656	-0.109003	N	0.203615	-0.184109	-0.114790	N	0.729440	-0.409383	0.150733
C	1.485761	1.084162	0.354517	C	-0.513838	0.576254	0.819068	C	1.902436	-0.014358	0.867364
C	1.458312	1.052245	1.871251	C	-0.093732	0.121326	2.201150	C	1.523448	0.307958	2.289673
C	0.790306	-0.289241	2.240185	C	0.976382	-0.966167	1.968522	C	0.083001	-0.175611	2.443400
C	0.495375	-0.971108	0.919269	C	1.105627	-1.089113	0.463726	C	-0.295521	-0.722543	1.089081
H	2.482690	1.147747	2.238599	H	0.261925	0.981952	2.770354	H	2.239365	-0.159375	2.966209
O	1.884638	1.973618	-0.353763	O	-1.332841	1.416977	0.541459	O	3.026643	0.063707	0.437784
O	-0.032491	-2.042831	0.753270	O	1.826998	-1.833278	-0.152158	O	-1.301653	-1.340858	0.870762
C	-0.466982	0.154894	3.075416	C	0.362254	-2.234829	2.674587	C	-0.706233	1.134469	2.848211
H	-0.911533	-0.652067	3.654845	H	1.090714	-3.019786	2.867711	H	-1.681877	0.932638	3.285753
C	-1.601372	-0.601843	-1.565147	C	0.956237	2.260840	-1.538110	C	-1.767262	-1.514375	-1.639215
H	1.424625	-0.948975	2.836270	H	1.952645	-0.729337	2.394884	H	-0.060555	-0.952554	3.194845
C	0.525790	2.120217	2.553519	C	-1.211283	-0.644617	3.007811	C	1.419685	1.859135	2.597024
H	0.987304	3.100244	2.657995	H	-1.918813	0.016519	3.504435	H	2.383380	2.320113	2.804404
C	-0.805185	2.065816	1.820162	C	-1.801493	-1.691093	2.072980	C	0.582713	2.491305	1.497627
H	-1.129232	2.786348	1.080042	H	-2.758695	-1.600149	1.574654	H	0.980540	3.075370	0.676916
C	-1.389713	0.902792	2.126138	C	-0.872344	-2.633139	1.878482	C	-0.675406	2.064244	1.647168
H	-2.283669	0.484436	1.683700	H	-0.918777	-3.470991	1.193503	H	-1.507231	2.227390	0.973204
C	0.160082	1.344069	3.842985	C	-0.308599	-1.544010	3.886826	C	0.373314	1.797457	3.737235
H	1.028747	1.066512	4.449019	H	0.391167	-0.983174	4.514329	H	0.684791	1.178304	4.584290
H	-0.564911	1.874065	4.463302	H	-0.879003	-2.239271	4.506148	H	0.077851	2.786153	4.093119
C	-2.433472	-1.846410	-1.393981	C	0.150848	3.533280	-1.534157	C	-1.746548	-3.001084	-1.398131
H	-1.914178	-2.552956	-0.743410	H	-0.794473	3.364091	-1.011748	H	-0.990740	-3.271555	-0.659559
H	-2.599261	-2.348440	-2.353405	H	-0.096135	3.851086	-2.552804	H	-1.499664	-3.528581	-2.327341
H	-3.410126	-1.617969	-0.960682	H	0.687498	4.347720	-1.043056	H	-2.714518	-3.360432	-1.042808
C	-2.035343	0.616785	-1.243847	C	2.158877	2.145322	-0.972876	C	-2.892912	-0.803583	-1.689657
H	-1.417505	1.496148	-1.388873	H	2.709200	1.209906	-0.996010	H	-2.889550	0.255601	-1.925172
H	-3.027417	0.775316	-0.831292	H	2.636810	2.986920	-0.480678	H	-3.854420	-1.255593	-1.465922

Table 2.5 XYZ coordinates of the GS and TS structures of 1(CCH)

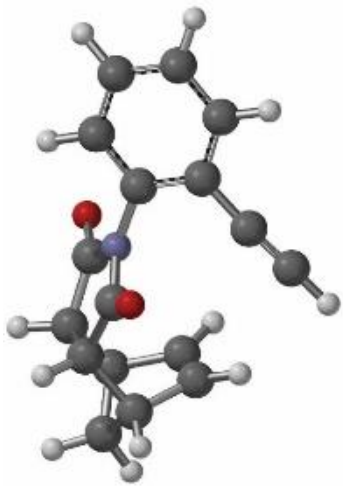
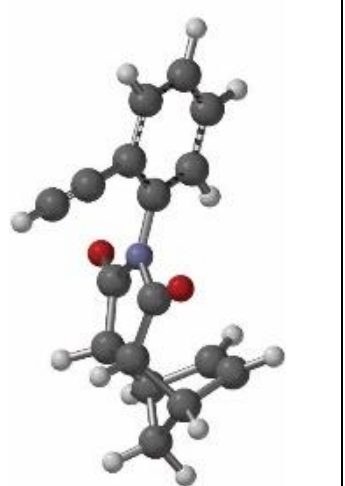
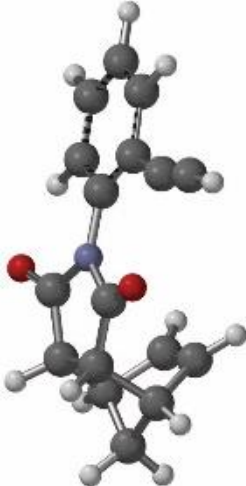
		
H 0.524105 -1.824303 -5.372848	H 0.476969 -1.085494 -5.498548	H 0.554231 -1.119706 -5.422823
C 0.531143 -1.550687 -4.323149	C 0.393172 -0.962588 -4.424005	C 0.501667 -1.034675 -4.342730
C 0.530365 -0.851376 -1.620403	C 0.165197 -0.647551 -1.664768	C 0.322371 -0.845701 -1.502948
C -0.641869 -1.129295 -3.714543	C -0.489006 -1.759290 -3.706885	C -0.651907 -1.386230 -3.671235
C 1.712139 -1.614917 -3.586030	C 1.171718 -0.013833 -3.763146	C 1.574742 -0.565756 -3.598472
C 1.706069 -1.270582 -2.239652	C 1.051948 0.144747 -2.386981	C 1.478691 -0.477847 -2.218852
C -0.665777 -0.760574 -2.357935	C -0.610990 -1.625999 -2.314121	C -0.798291 -1.302209 -2.264973
H -1.563632 -1.069013 -4.281840	H -1.092063 -2.505102 -4.212004	H -1.511724 -1.739361 -4.226942
H 2.634907 -1.936668 -4.056217	H 1.868075 0.605309 -4.318398	H 2.499396 -0.265968 -4.080284
H 2.617938 -1.314360 -1.657674	H 1.650007 0.877540 -1.859957	H 2.339713 -0.131395 -1.679483
N 0.575089 -0.510497 -0.237979	N 0.057392 -0.467343 -0.258153	N 0.376398 -0.678763 -0.061782
C 1.461959 0.453993 0.279912	C 1.158358 -0.560736 0.612644	C 1.549099 -0.287683 0.659376
C 1.260679 0.506974 1.780929	C 0.665787 -0.239662 2.008548	C 1.166425 0.073464 2.070880
C 0.164865 -0.535165 2.087793	C -0.841549 0.061921 1.859775	C -0.297469 -0.329398 2.214850
C -0.194252 -1.156998 0.753209	C -1.129746 -0.045571 0.376096	C -0.700489 -0.853722 0.858468
H 2.214030 0.305190 2.273528	H 0.888873 -1.081685 2.666258	H 1.849933 -0.424671 2.759151
O 2.232179 1.105600 -0.378487	O 2.283983 -0.826647 0.275456	O 2.681950 -0.233824 0.247882
O -0.976695 -2.045703 0.542909	O -2.158995 0.208954 -0.191201	O -1.768108 -1.340967 0.614697
C -0.971701 0.331720 2.757085	C -0.977801 1.521869 2.433444	C -1.016971 1.021141 2.612024
H -1.708085 -0.262382 3.294941	H -1.998783 1.797784 2.689512	H -2.003154 0.875398 3.047965
H 0.482946 -1.328417 2.767079	H -1.487805 -0.631132 2.401981	H -0.487684 -1.099158 2.963731
C 0.641463 1.854513 2.314758	C 1.236216 1.096790 2.619194	C 1.145219 1.629490 2.360193
H 1.376466 2.645300 2.451380	H 2.232135 0.989339 3.044635	H 2.131209 2.041484 2.565603
C -0.085278 1.310113 3.567403	C 0.066677 1.443081 3.574104	C 0.093456 1.636209 3.497316
H 0.581229 0.810581 4.278090	H -0.144422 0.657628 4.306357	H 0.370557 1.012185 4.352925
H -0.665725 2.075748 4.085517	H 0.206096 2.396601 4.087309	H -0.149812 2.643049 3.841857
C -0.550264 2.173164 1.425818	C 1.059247 2.183187 1.568622	C 0.346064 2.291123 1.249236
H -0.547404 2.911044 0.633516	H 1.857996 2.578581 0.953251	H 0.778347 2.845108 0.425058
C -1.501173 1.270323 1.685117	C -0.248866 2.439172 1.462256	C -0.934045 1.935450 1.399900
H -2.425413 1.123482 1.143622	H -0.737587 3.078891 0.738224	H -1.755215 2.135748 0.722978
C -1.891141 -0.288455 -1.805828	C -1.483354 -2.490859 -1.593336	C -2.120889 -1.683535 -1.871094
C -2.957543 0.116426 -1.422154	C -2.214154 -3.243341 -1.003503	C -3.276713 -2.023578 -1.840651
H -3.901622 0.455224 -1.067865	H -2.874722 -3.894562 -0.482660	H -4.286998 -2.315702 -1.681820

Table 2.6 XYZ coordinates of the GS and TS structures of **1**(CF₃)

H	0.759617	-2.161614	-5.170983	H	-0.452959	0.914576	-5.451789	H	0.687130	-1.012215	-5.306918
C	0.730500	-1.781931	-4.155575	C	-0.343345	0.803706	-4.378582	C	0.586177	-0.908280	-4.232492
C	0.634531	-0.803159	-1.545456	C	-0.059714	0.530776	-1.623797	C	0.333821	-0.756286	-1.396231
C	-0.445035	-1.225401	-3.661813	C	0.043625	1.897292	-3.608387	C	-0.422443	-1.574266	-3.559264
C	1.859749	-1.847720	-3.346915	C	-0.590670	-0.423837	-3.772309	C	1.414212	-0.075036	-3.500534
C	1.807670	-1.359118	-2.045046	C	-0.447274	-0.558209	-2.394492	C	1.281450	-0.007634	-2.123816
C	-0.502579	-0.732751	-2.359520	C	0.185246	1.767926	-2.229087	C	-0.613538	-1.495033	-2.170321
H	-1.325061	-1.170371	-4.289247	H	0.234965	2.853954	-4.076721	H	-1.122334	-2.160502	-4.135580
H	2.779733	-2.279395	-3.725641	H	-0.894789	-1.277287	-4.368910	H	2.177025	0.524687	-3.985549
H	2.677775	-1.405064	-1.400710	H	-0.635768	-1.504935	-1.901935	H	1.969131	0.627525	-1.597625
N	0.634438	-0.322840	-0.201025	N	0.065795	0.371920	-0.213125	N	0.438481	-0.627119	0.040189
C	1.130991	0.947478	0.156452	C	-1.039376	0.461001	0.653151	C	1.604050	-0.083730	0.683676
C	1.106082	1.033324	1.671071	C	-0.538060	0.177640	2.053553	C	1.236460	0.325928	2.084398
C	0.524528	-0.315068	2.154319	C	0.966088	-0.147121	1.899222	C	-0.133048	-0.299174	2.340198
C	0.281704	-1.130262	0.899957	C	1.253083	-0.054642	0.412989	C	-0.463299	-1.051104	1.075667
H	2.122533	1.222374	2.023209	H	-0.741027	1.044944	2.684658	H	2.022023	0.007309	2.769598
O	1.510945	1.776767	-0.627530	O	-2.166771	0.691082	0.301957	O	2.704948	0.029771	0.208736
O	-0.117250	-2.261679	0.815861	O	2.274953	-0.319281	-0.162859	O	-1.305127	-1.895215	0.986780
C	-0.764035	0.118893	2.951273	C	1.081642	-1.599347	2.496430	C	-1.060933	0.951145	2.629051
H	-1.159224	-0.664812	3.594937	H	2.100773	-1.890036	2.743294	H	-1.999388	0.684986	3.111362
C	-1.789123	-0.126040	-1.858618	C	0.583423	2.955079	-1.392659	C	-1.922782	-2.140642	-1.721790
H	1.196251	-0.877310	2.806335	H	1.623208	0.543122	2.431451	H	-0.167551	-0.993373	3.179718
C	0.107152	2.093241	2.270202	C	-1.121645	-1.130523	2.707421	C	0.962931	1.881658	2.251878
H	0.507888	3.104835	2.294035	H	-2.108266	-0.995502	3.146293	H	1.873381	2.462296	2.387355
C	-0.209034	1.402046	3.618655	C	0.056759	-1.476491	3.651013	C	-0.048546	1.812756	3.422329
H	0.674764	1.224726	4.240647	H	0.292851	-0.678702	4.362191	H	0.345148	1.317760	4.315554
H	-0.963621	1.936026	4.199192	H	-0.090451	-2.415262	4.188618	H	-0.447360	2.792645	3.690794
C	-1.214861	1.895597	1.546460	C	-0.982266	-2.243807	1.679537	C	0.038015	2.313434	1.124992
H	-1.574764	2.523824	0.742996	H	-1.799998	-2.639290	1.089809	H	0.349601	2.865386	0.246569
C	-1.727717	0.728513	1.946705	C	0.319650	-2.523965	1.556825	C	-1.158619	1.759462	1.347165
H	-2.586684	0.218466	1.532668	H	0.784516	-3.194021	0.844405	H	-2.015616	1.759589	0.684863
F	-1.627962	1.163695	-1.486476	F	1.721346	2.729705	-0.698149	F	-2.671566	-1.287800	-0.991443
F	-2.755492	-0.138845	-2.802159	F	0.792793	4.055849	-2.145044	F	-2.709113	-2.449718	-2.792048
F	-2.284410	-0.786425	-0.788262	F	-0.368335	3.273689	-0.484974	F	-1.762723	-3.299212	-1.067262

Table 2.7 XYZ coordinates of the GS and TS structures of 1(CHO)

H	0.214690	-5.550991	1.321610	H	0.312482	-0.668971	-5.559569	H	0.535176	-1.239018	-5.518980
C	0.129437	-4.484464	1.144456	C	0.266544	-0.635180	-4.476593	C	0.463114	-1.046114	-4.453894
C	-0.072257	-1.724113	0.693597	C	0.129535	-0.535720	-1.685628	C	0.261043	-0.608254	-1.662860
C	-0.810019	-3.725748	1.837232	C	-0.584233	-1.488692	-3.785171	C	-0.625980	-1.506987	-3.730862
C	0.951607	-3.860228	0.216314	C	1.064024	0.257473	-3.765032	C	1.442515	-0.328708	-3.783821
C	0.851921	-2.488099	-0.045041	C	0.989676	0.311464	-2.375051	C	1.348230	-0.126022	-2.413207
C	-0.900106	-2.353688	1.620391	C	-0.656757	-1.468868	-2.387774	C	-0.782024	-1.275091	-2.356022
H	-1.469261	-4.197407	2.558216	H	-1.198004	-2.199821	-4.331427	H	-1.412449	-2.056666	-4.235410
H	1.675821	-4.446385	-0.342303	H	1.740138	0.922916	-4.291333	H	2.300189	0.069621	-4.315529
N	-0.174217	-0.311143	0.565354	H	1.597678	1.011741	-1.816184	H	2.148054	0.391157	-1.915149
C	0.911472	0.567983	0.777138	N	0.049983	-0.433478	-0.273730	N	0.317653	-0.444270	-0.223507
C	0.374609	1.984017	0.700993	C	1.154648	-0.597449	0.577119	C	1.467895	-0.002214	0.506462
C	-1.137641	1.842248	0.425691	C	0.662243	-0.422828	1.998206	C	1.132506	0.035533	1.977082
C	-1.396824	0.352273	0.340480	C	-0.851417	-0.136027	1.883962	C	-0.302595	-0.478080	2.086087
H	0.604666	2.486831	1.642852	C	-1.144312	-0.105288	0.400196	C	-0.727211	-0.758360	0.668826
O	2.038144	0.216490	1.007439	H	0.901382	-1.323612	2.566236	H	1.870657	-0.560059	2.516346
O	-2.449671	-0.198174	0.137523	O	2.281066	-0.817694	0.208236	O	2.539854	0.308208	0.053436
C	-1.339829	2.649860	-0.911582	O	-2.177663	0.182416	-0.143063	O	-1.818865	-1.169515	0.359871
H	-2.378260	2.908458	-1.110910	C	-1.012408	1.253741	2.605647	C	-1.075209	0.721403	2.763167
H	-1.768088	2.254621	1.217139	H	-2.036625	1.482792	2.893046	H	-2.037279	0.436284	3.183405
C	0.877692	2.853763	-0.513828	C	-1.503346	-2.503089	-1.741322	H	-0.416462	-1.388764	2.676377
H	1.857237	3.299351	-0.350472	H	-1.480208	-0.898214	2.347607	C	1.045529	1.488370	2.591367
C	0.709637	2.009692	-1.766291	C	1.210415	0.854171	2.739733	H	2.015148	1.905282	2.855355
H	1.508886	1.476591	-2.259494	H	2.209759	0.723948	3.150485	C	0.176618	2.318614	1.658675
C	-0.600514	1.887194	-1.999676	H	1.007846	2.040162	1.807327	H	0.553538	3.057125	0.962042
H	-1.074533	1.246609	-2.732484	H	1.795548	2.511913	1.232786	C	-1.078030	1.867290	1.761961
C	-0.339571	3.801330	-0.654332	C	-0.305404	2.279962	1.731403	H	-1.933778	2.162603	1.167753
H	-0.554971	4.379957	0.250402	H	-0.810298	2.981772	1.079392	C	0.034415	1.204209	3.728434
H	-0.247325	4.476535	-1.507023	C	0.038647	1.079066	3.727644	H	0.368527	0.434784	4.431871
C	1.666778	-1.975449	-1.172101	H	-0.154582	0.220248	4.378478	H	-0.247475	2.104295	4.277360
H	2.427314	-2.702956	-1.531706	H	0.163859	1.977633	4.334781	C	-2.161989	-1.730069	-1.912015
O	1.535744	-0.912477	-1.727987	O	-1.587522	-2.737496	-0.558831	O	-2.538031	-2.867321	-2.047393
H	-1.622565	-1.762485	2.168405	H	-2.072697	-3.118990	-2.471574	H	-2.863284	-0.919266	-1.657227

Table 2.8 XYZ coordinates of the GS and TS structures of 1(Cl)

H	0.380161	-1.795100	-5.452200	H	-0.437629	1.481714	-5.492466	H	0.328579	-1.088505	-5.492717
C	0.386541	-1.520534	-4.402848	C	-0.322847	1.333555	-4.424019	C	0.290299	-1.045854	-4.409807
C	0.375852	-0.816246	-1.698493	C	-0.052721	0.962316	-1.671376	C	0.170897	-1.006816	-1.550137
C	-0.767958	-1.005581	-3.824991	C	-0.680266	2.354723	-3.549921	C	-0.713504	-1.701844	-3.722622
C	1.541071	-1.675440	-3.639432	C	0.180643	0.131991	-3.930671	C	1.216987	-0.320599	-3.675601
C	1.529213	-1.327599	-2.294696	C	0.309499	-0.049927	-2.559777	C	1.149552	-0.307899	-2.293122
C	-0.770477	-0.644832	-2.480826	C	-0.533775	2.172711	-2.178036	C	-0.811656	-1.678199	-2.325214
H	-1.670001	-0.871605	-4.409805	H	-1.067523	3.295039	-3.922668	H	-1.476347	-2.243040	-4.268284
H	2.445382	-2.070752	-4.088163	H	0.464621	-0.663970	-4.610420	H	2.005402	0.238322	-4.167861
H	2.417362	-1.444265	-1.685348	H	0.691761	-0.979466	-2.155881	H	1.906093	0.242783	-1.766771
N	0.404295	-0.478493	-0.317588	N	0.064804	0.737838	-0.273986	N	0.256231	-0.886048	-0.108081
C	1.233413	0.534360	0.201866	C	-1.055792	0.620428	0.573474	C	1.390635	-0.308404	0.551712
C	1.020173	0.574010	1.702166	C	-0.543610	0.322926	1.966868	C	0.998130	0.088827	1.949909
C	-0.022401	-0.525073	2.002670	C	0.988213	0.176097	1.821942	C	-0.378094	-0.529898	2.174225
C	-0.342163	-1.161921	0.665007	C	1.285003	0.428545	0.356904	C	-0.674533	-1.301615	0.912517
H	1.979692	0.420862	2.200447	H	-0.848791	1.127985	2.638295	H	1.768387	-0.241710	2.647109
O	1.966880	1.225678	-0.456804	O	-2.199103	0.712969	0.212526	O	2.495312	-0.150129	0.095156
O	-1.084526	-2.081502	0.442190	O	2.349405	0.359201	-0.201939	O	-1.507391	-2.156253	0.828525
C	-1.207230	0.279256	2.664617	C	1.250833	-1.298538	2.308127	C	-1.307441	0.725173	2.434155
H	-1.913962	-0.353651	3.197977	H	2.294357	-1.499855	2.542084	H	-2.261862	0.464342	2.887457
H	0.332846	-1.300874	2.683646	H	1.559658	0.882582	2.426928	H	-0.436990	-1.215187	3.019739
C	0.325511	1.885190	2.232416	C	-0.989830	-1.075048	2.534272	C	0.732904	1.644013	2.121464
H	1.016081	2.714528	2.372585	H	-1.985252	-1.070000	2.973830	H	1.642941	2.217472	2.286481
C	-0.379082	1.302879	3.481434	C	0.217815	-1.361588	3.461640	C	-0.313400	1.577902	3.260937
H	0.307515	0.838747	4.196923	H	0.370825	-0.594481	4.226963	H	0.049447	1.076555	4.163539
H	-1.003064	2.036792	3.994370	H	0.168198	-2.345597	3.931627	H	-0.713992	2.559312	3.521218
C	-0.875922	2.139485	1.335964	C	-0.736350	-2.097420	1.435911	C	-0.154785	2.086965	0.969313
H	-0.907904	2.879029	0.546030	H	-1.507180	-2.531324	0.811451	H	0.186829	2.640670	0.103433
C	-1.781715	1.190291	1.591707	C	0.587627	-2.228926	1.302065	C	-1.360903	1.539757	1.153319
H	-2.701425	1.000925	1.054541	H	1.118694	-2.798836	0.549622	H	-2.199823	1.556331	0.468439
Cl	-2.234157	0.051431	-1.815362	Cl	-0.941287	3.494354	-1.103367	Cl	-2.277904	-2.476423	-1.768429

Table 2.9 XYZ coordinates of the GS and TS structures of **1**(CN)

H 0.342052 -1.790612 -5.397215	H 0.272733 -5.520235 1.190121	H 0.318242 -1.425354 -5.489791
C 0.371941 -1.522426 -4.347045	C 0.248470 -4.441650 1.081227	C 0.308453 -1.274754 -4.416147
C 0.441677 -0.840567 -1.633997	C 0.169393 -1.666539 0.787641	C 0.244700 -0.897762 -1.586642
C -0.795309 -1.141933 -3.700135	C -0.408498 -3.667932 2.028766	C -0.773123 -1.688867 -3.663866
C 1.575701 -1.549324 -3.645648	C 0.877095 -3.831297 -0.002884	C 1.366335 -0.665009 -3.757963
C 1.608297 -1.215478 -2.295917	C 0.833975 -2.448938 -0.151307	C 1.329743 -0.485308 -2.383387
C -0.771976 -0.786031 -2.344150	C -0.445790 -2.273398 1.896229	C -0.847708 -1.520950 -2.262660
H -1.736724 -1.105125 -4.235982	H -0.894284 -4.130841 2.879676	H -1.617505 -2.164333 -4.147951
H 2.492416 -1.836166 -4.148890	H 1.394707 -4.433733 -0.741553	H 2.236298 -0.320217 -4.306617
H 2.540328 -1.233342 -1.746605	H 1.313921 -1.965469 -0.992399	H 2.172181 -0.015094 -1.911353
N 0.497534 -0.510422 -0.254304	N 0.100840 -0.259569 0.615002	N 0.333800 -0.637601 -0.168636
C 1.383193 0.455277 0.271345	C 1.235891 0.554653 0.424973	C 1.447429 -0.014767 0.483162
C 1.145863 0.528011 1.765081	C 0.746387 1.969470 0.193919	C 1.109279 0.210252 1.935328
C 0.052853 -0.520383 2.064963	C -0.795649 1.888992 0.215662	C -0.277964 -0.390961 2.138361
C -0.279676 -1.158869 0.734582	C -1.122543 0.427584 0.433242	C -0.682339 -0.921698 0.788306
H 2.089159 0.346341 2.284018	H 1.167266 2.620992 0.961904	H 1.894305 -0.233076 2.549645
O 2.169219 1.090334 -0.383409	O 2.372419 0.157428 0.425564	O 2.498695 0.308284 -0.010504
O -1.053012 -2.051984 0.511932	O -2.202715 -0.099058 0.427606	O -1.715771 -1.485132 0.558386
C -1.110637 0.345947 2.690497	C -1.208277 2.441228 -1.199485	C -1.147168 0.836272 2.625883
H -1.851424 -0.248871 3.221047	H -2.253792 2.734942 -1.265489	H -2.084485 0.542600 3.093218
H 0.362673 -1.300361 2.762953	H -1.257608 2.477209 1.010925	H -0.322208 -1.203070 2.865440
C 0.494893 1.878611 2.257570	C 1.051895 2.543269 -1.240827	C 0.905741 1.731559 2.318531
H 1.217952 2.680065 2.396128	H 2.063220 2.930281 -1.347986	H 1.839466 2.258136 2.504629
C -0.253572 1.348219 3.503070	C -0.128528 3.538376 -1.362807	C -0.082941 1.548237 3.495796
H 0.401205 0.870112 4.239234	H -0.148082 4.295416 -0.571888	H 0.308199 0.924283 4.305725
H -0.855307 2.116539 3.991501	H -0.167448 4.028956 -2.337198	H -0.435236 2.497838 3.902708
C -0.679802 2.165014 1.335807	C 0.616600 1.487728 -2.249064	C -0.023416 2.333667 1.275168
H -0.669940 2.894097 0.535344	H 1.293700 0.840469 -2.792857	H 0.295623 2.979751 0.466853
C -1.628373 1.257004 1.588359	C -0.719414 1.427413 -2.224638	C -1.238243 1.805609 1.458794
H -2.540852 1.092160 1.031304	H -1.356795 0.719201 -2.739106	H -2.111818 1.931230 0.831340
C -1.984476 -0.327839 -1.743623	C -1.078811 -1.485606 2.905501	C -2.099710 -2.042568 -1.786411
N -2.975874 0.072003 -1.307813	N -1.570280 -0.859340 3.741532	N -3.148851 -2.521197 -1.705345

Table 2.10 XYZ coordinates of the GS and TS structures of 1(COCH3)

H	0.907450	-1.493570	-5.250992	H	0.652661	-0.426242	-5.351354	H	0.562918	-1.004443	-5.440907
C	0.890985	-1.206714	-4.204867	C	0.597648	-0.398860	-4.268300	C	0.575466	-0.834156	-4.369598
C	0.827981	-0.457112	-1.518159	C	0.451780	-0.350016	-1.486411	C	0.595884	-0.448691	-1.563338
C	-0.318556	-1.140738	-3.521956	C	-0.315457	-1.208023	-3.599246	C	-0.300407	-1.517422	-3.541519
C	2.074380	-0.902148	-3.539434	C	1.435092	0.442079	-3.542239	C	1.460984	0.063535	-3.792466
C	2.042862	-0.543170	-2.196304	C	1.351697	0.476166	-2.153644	C	1.475899	0.243758	-2.416769
C	-0.374900	-0.747048	-2.181596	C	-0.392067	-1.214170	-2.204001	C	-0.339458	-1.335860	-2.150818
H	-1.239069	-1.366163	-4.049527	H	-0.958108	-1.866713	-4.172797	H	-0.995840	-2.229144	-3.973764
H	3.024273	-0.953962	-4.060515	H	2.147987	1.079709	-4.053978	H	2.158703	0.626365	-4.403629
H	2.959857	-0.318419	-1.667261	H	1.988847	1.135449	-1.578466	H	2.191435	0.926499	-1.996710
N	0.855796	-0.130963	-0.130739	N	0.365503	-0.264595	-0.069178	N	0.741355	-0.233351	-0.135177
C	1.549965	0.983172	0.389171	C	1.480058	-0.373500	0.783247	C	1.738869	0.590431	0.477728
C	1.415699	0.946551	1.896884	C	0.985931	-0.204683	2.204643	C	1.561158	0.550200	1.976067
C	0.569637	-0.306500	2.207397	C	-0.537521	0.017203	2.089940	C	0.386822	-0.393922	2.225472
C	0.238176	-0.910777	0.859362	C	-0.838093	-0.024982	0.609896	C	-0.068938	-0.822956	0.856745
H	2.415995	0.924187	2.334664	H	1.263606	-1.086635	2.784112	H	2.502145	0.234988	2.429655
O	2.144348	1.791702	-0.276038	O	2.614702	-0.538858	0.415045	O	2.588042	1.241669	-0.076029
O	-0.438956	-1.886811	0.639960	O	-1.910019	0.130663	0.076365	O	-1.014313	-1.545114	0.657757
C	-0.665055	0.275684	2.993746	C	-0.748413	1.427112	2.759425	C	-0.658074	0.511653	2.990021
H	-1.220214	-0.477524	3.549863	H	-1.781757	1.629775	3.033890	H	-1.431271	-0.056081	3.503097
C	-1.720574	-0.545194	-1.531566	C	-1.298380	-2.190419	-1.496346	C	-1.481865	-2.166557	-1.565218
H	1.092175	-1.053809	2.808386	H	-1.136343	-0.744829	2.591861	H	0.632209	-1.280214	2.812837
C	0.564496	2.116134	2.524503	C	1.485682	1.108030	2.917948	C	1.076675	1.911759	2.609036
H	1.126086	3.039767	2.652900	H	2.486479	1.022319	3.336545	H	1.882260	2.623758	2.775532
C	-0.721730	2.199288	1.718585	C	1.249265	2.259171	1.950602	C	-0.100939	2.398097	1.777505
H	-0.918346	2.927368	0.942498	H	2.023926	2.740692	1.366768	H	-0.050959	3.200286	1.051802
C	-1.450299	1.115085	1.999253	C	-0.070884	2.448828	1.858168	C	-1.126383	1.569632	2.002324
H	-2.346258	0.793037	1.487631	H	-0.594067	3.113906	1.182251	H	-2.085271	1.559088	1.499241
C	0.054140	1.389288	3.793245	C	0.301365	1.322181	3.893104	C	0.328429	1.348393	3.841313
H	0.856332	1.018768	4.439940	H	0.131858	0.477123	4.567838	H	0.961513	0.744770	4.499537
H	-0.637713	1.998126	4.378226	H	0.391320	2.242731	4.472657	H	-0.171324	2.124022	4.424267
C	-2.718677	-1.676544	-1.623700	C	-2.713747	-2.330155	-2.009338	C	-2.798319	-1.433739	-1.380483
H	-2.320988	-2.527768	-1.065456	H	-3.232574	-1.384449	-1.826520	H	-3.418614	-1.980358	-0.670948
H	-2.882138	-2.005788	-2.652958	H	-3.215650	-3.131309	-1.467945	H	-3.309842	-1.410743	-2.349695
H	-3.665898	-1.360208	-1.187807	H	-2.760895	-2.526623	-3.083069	H	-2.662575	-0.404934	-1.047116
O	-1.971263	0.492772	-0.957339	O	-0.901430	-2.808074	-0.531472	O	-1.406374	-3.371219	-1.535751

Table 2.11 XYZ coordinates of the GS and TS structures of **1**(C(CH₂)CH₃)

H 1.611542 -0.749356 -5.023226	H 2.418247 0.104673 -4.570541	H 1.448473 0.394253 -5.055646
C 1.598016 -0.477629 -3.973054	C 2.146758 0.040630 -3.522162	C 1.364965 0.333428 -3.975830
C 1.544916 0.227139 -1.273447	C 1.440632 -0.138254 -0.835576	C 1.096251 0.191428 -1.156943
C 0.411070 -0.551700 -3.251898	C 0.891676 -0.440552 -3.159770	C 0.130807 0.140082 -3.378157
C 2.761561 -0.048714 -3.341474	C 3.048000 0.434628 -2.537670	C 2.479761 0.447275 -3.157918
C 2.737918 0.287292 -1.991739	C 2.689598 0.357082 -1.194295	C 2.345640 0.382903 -1.778668
C 0.359884 -0.181041 -1.904937	C 0.526374 -0.554315 -1.816088	C -0.040777 0.048759 -1.988983
H -0.500908 -0.875071 -3.742035	H 0.190162 -0.755399 -3.924658	H -0.754743 0.051294 -3.998288
H 3.692244 0.015865 -3.895000	H 4.027902 0.809864 -2.812689	H 3.467098 0.594091 -3.582945
H 3.641514 0.609423 -1.491044	H 3.375378 0.668559 -0.416897	H 3.227678 0.481710 -1.172487
N 1.574138 0.530555 0.117897	N 1.082056 -0.192733 0.538742	N 1.058362 0.224668 0.291023
C 2.161571 1.697940 0.649492	C 1.830469 -0.884851 1.507429	C 2.191444 0.440621 1.136664
C 2.043263 1.625682 2.157791	C 1.091920 -0.764607 2.824873	C 1.709568 0.733839 2.535838
C 1.334532 0.287645 2.455738	C -0.159736 0.088307 2.520438	C 0.197387 0.520542 2.503673
C 1.057923 -0.329644 1.101722	C -0.079511 0.408851 1.045909	C -0.117016 0.176304 1.072466
H 3.043602 1.702970 2.589318	H 0.864001 -1.765979 3.193942	H 2.248999 0.096894 3.237819
O 2.669506 2.570583 -0.006547	O 2.879181 -1.439108 1.300081	O 3.352834 0.413946 0.815454
O 0.495737 -1.372776 0.871403	O -0.854892 1.062610 0.391745	O -1.222043 -0.080521 0.667272
C 0.049859 0.729758 3.256331	C 0.005725 1.325450 3.480437	C -0.385958 1.924408 2.942571
H -0.421211 -0.084326 3.804135	H -0.911216 1.894519 3.621414	H -1.424218 1.878724 3.264341
C -0.986124 -0.077365 -1.237423	C -0.762756 -1.238154 -1.440135	C -1.515048 -0.197067 -1.676923
H 1.934722 -0.409084 3.044882	H -1.102334 -0.428321 2.711501	H -0.168496 -0.272795 3.156636
C 1.081525 2.692031 2.806417	C 1.840203 0.078597 3.923425	C 1.849345 2.252247 2.957845
H 1.546638 3.666129 2.946233	H 2.594146 -0.485681 4.468994	H 2.850636 2.513890 3.294089
C -0.211486 2.654987 2.008284	C 2.304670 1.363212 3.253172	C 1.265221 3.091216 1.831299
H -0.486532 3.368818 1.242873	H 3.323812 1.560802 2.944668	H 1.851928 3.634583 1.101129
C -0.823651 1.497619 2.277587	C 1.220561 2.101222 2.992755	C -0.058567 2.902049 1.824838
H -1.686934 1.092635 1.768735	H 1.173650 3.021833 2.424367	H -0.769765 3.249996 1.085911
C 0.655310 1.899594 4.066434	C 0.613062 0.603041 4.707802	C 0.690033 2.318867 3.981614
H 1.495010 1.606821 4.705634	H -0.025059 -0.193149 5.103864	H 0.786760 1.603039 4.803983
H -0.091975 2.426913 4.662254	H 0.885543 1.289418 5.511816	H 0.539467 3.322377 4.383037
O -1.305093 0.965350 -0.694707	O -0.761539 -2.092747 -0.571384	O -2.312589 0.704845 -1.823894
C -1.933052 -1.228955 -1.318579	C -2.019261 -0.885938 -2.168070	C -1.954215 -1.617586 -1.482972
C -3.768088 -3.334705 -1.365070	C -4.450336 -0.284057 -3.408097	C -2.875364 -4.233529 -1.138107
C -1.494245 -2.541688 -1.525123	C -2.204898 0.353261 -2.791900	C -1.073879 -2.696138 -1.602214
C -3.298716 -0.981848 -1.126292	C -3.069386 -1.813682 -2.157191	C -3.302067 -1.859445 -1.195539
C -4.212228 -2.027857 -1.156418	C -4.274089 -1.519121 -2.781905	C -3.759320 -3.158727 -1.019060
C -2.409585 -3.589879 -1.543998	C -3.418524 0.652781 -3.404932	C -1.534247 -4.000548 -1.432927
H -0.435461 -2.741415 -1.632248	H -1.413799 1.092642 -2.764135	H -0.030428 -2.518792 -1.837359
H -3.623538 0.038131 -0.955186	H -2.920690 -2.758742 -1.647454	H -3.969688 -1.010288 -1.109134
H -5.269657 -1.829661 -1.013182	H -5.079424 -2.246819 -2.777530	H -4.804513 -3.339190 -0.787939
H -2.062567 -4.607751 -1.688708	H -3.561876 1.620733 -3.873819	H -0.846282 -4.834138 -1.532973
H -4.480950 -4.153415 -1.381823	H -5.394399 -0.050507 -3.890476	H -3.233432 -5.249514 -1.002598

Table 2.12 XYZ coordinates of the GS and TS structures of **1**(CH₂CH₃)

H	5.009347	-1.121596	-1.889185	H	0.523614	-0.184157	-5.233760	H	0.650606	-0.529077	-5.129699
C	3.986436	-1.090177	-1.527428	C	0.459951	-0.177679	-4.150239	C	0.652347	-0.500821	-4.044906
C	1.373503	-0.979587	-0.617375	C	0.273611	-0.188292	-1.388976	C	0.630533	-0.518769	-1.209243
C	3.326155	0.132319	-1.430680	C	-0.261652	-1.173898	-3.497618	C	-0.303603	-1.202179	-3.325892
C	3.339772	-2.265586	-1.158996	C	1.099249	0.817860	-3.418518	C	1.579375	0.246610	-3.342438
C	2.028300	-2.204933	-0.703928	C	1.000619	0.810116	-2.032446	C	1.559131	0.231165	-1.955972
C	2.008803	0.221589	-0.969912	C	-0.370385	-1.210405	-2.104267	C	-0.384321	-1.227130	-1.925048
H	3.852666	1.034662	-1.716416	H	-0.744546	-1.941669	-4.090423	H	-1.045541	-1.749645	-3.889407
H	3.846391	-3.222281	-1.228421	H	1.666151	1.594531	-3.920546	H	2.330115	0.840238	-3.853581
H	1.501468	-3.106098	-0.411639	H	1.485589	1.573813	-1.436205	H	2.315263	0.801232	-1.450679
N	0.016172	-0.984675	-0.148624	N	0.198269	-0.139188	0.040318	N	0.777280	-0.409470	0.245731
C	-0.344369	-1.409285	1.146043	C	1.336081	-0.191331	0.869099	C	1.907541	0.220723	0.868287
C	-1.856198	-1.338851	1.252444	C	0.880029	0.056676	2.293770	C	1.541792	0.610709	2.275913
C	-2.342410	-0.826813	-0.119531	C	-0.646442	0.271470	2.205254	C	0.225467	-0.106450	2.555798
C	-1.086140	-0.637694	-0.946545	C	-0.985957	0.148657	0.735279	C	-0.074169	-0.878978	1.294839
H	-2.236980	-2.327756	1.515621	H	1.177367	-0.786498	2.919843	H	2.360284	0.346101	2.945645
O	0.430623	-1.760776	1.997842	O	2.461633	-0.076740	0.483191	O	2.993003	0.417053	0.382122
O	-1.020462	-0.254280	-2.088344	O	-2.069707	0.290583	0.224863	O	-0.875109	-1.774072	1.245786
C	-3.120578	0.495944	0.244919	C	-0.840107	1.723180	2.785703	C	-0.781742	1.078811	2.862759
H	-3.774405	0.849775	-0.549924	H	-1.867260	1.945012	3.068365	H	-1.690714	0.750536	3.363225
C	1.277690	1.541290	-0.848148	C	-1.147058	-2.293101	-1.382533	C	-1.586392	-1.959379	-1.337278
H	0.505088	1.573065	-1.623309	H	-0.564809	-2.609782	-0.510000	H	-1.242068	-2.769288	-0.697723
H	0.732002	1.542380	0.100607	H	-2.058883	-1.843303	-0.977350	H	-2.114647	-1.281479	-0.666100
H	-3.005252	-1.518850	-0.642627	H	-1.233423	-0.449889	2.776841	H	0.252526	-0.801249	3.395250
C	-2.408279	-0.257284	2.256009	C	1.396472	1.411354	2.914063	C	1.168343	2.143009	2.449216
H	-2.415069	-0.587815	3.292847	H	2.406634	1.349171	3.313970	H	2.039046	2.784800	2.568258
C	-1.673023	1.041837	1.960707	C	1.139305	2.499306	1.881979	C	0.197718	2.509535	1.339407
H	-0.870007	1.443086	2.566206	H	1.901004	2.941341	1.251733	H	0.458448	3.074076	0.452693
C	-2.096695	1.488235	0.774158	C	-0.182710	2.683336	1.805369	C	-0.956063	1.880150	1.584612
H	-1.712350	2.330529	0.213154	H	-0.720706	3.300794	1.096938	H	-1.824528	1.832152	0.939009
C	-3.768360	0.035575	1.574717	C	0.234687	1.687723	3.900188	C	0.184145	2.007363	3.637392
H	-4.404080	-0.849149	1.467151	H	0.080249	0.886038	4.628963	H	0.626197	1.541101	4.523687
H	-4.328418	0.830792	2.070530	H	0.337129	2.642442	4.419334	H	-0.276624	2.957800	3.912485
C	2.144284	2.796709	-0.936462	C	-1.514921	-3.524231	-2.212740	C	-2.613588	-2.524742	-2.324129
H	2.601130	2.910481	-1.923113	H	-0.634043	-3.990831	-2.662813	H	-2.195142	-3.300406	-2.971379
H	2.946880	2.787719	-0.193332	H	-2.214528	-3.281352	-3.016968	H	-3.058101	-1.754395	-2.961442
H	1.536366	3.687496	-0.759017	H	-2.000503	-4.271058	-1.579664	H	-3.426806	-2.985632	-1.757196

Table 2.13 XYZ coordinates of the GS and TS structures of **1(I)**

H	0.531067	-1.975426	-5.443040	H	0.259520	-1.270944	-5.487320	H	0.503400	-1.323425	-5.475726
C	0.485420	-1.645764	-4.410463	C	0.238237	-1.183022	-4.406254	C	0.399416	-1.188968	-4.404505
C	0.336590	-0.794648	-1.752665	C	0.162713	-0.984518	-1.621853	C	0.128885	-0.961103	-1.573177
C	-0.685152	-1.069557	-3.929139	C	-0.140867	-2.280062	-3.640508	C	-0.608728	-1.843695	-3.719536
C	1.587542	-1.792011	-3.573059	C	0.585501	0.014609	-3.787605	C	1.220793	-0.329887	-3.692291
C	1.506508	-1.370849	-2.252598	C	0.542856	0.108841	-2.403376	C	1.082138	-0.231263	-2.319461
C	-0.761041	-0.637203	-2.605484	C	-0.171283	-2.189470	-2.249481	C	-0.807209	-1.715743	-2.334752
H	-1.539517	-0.951790	-4.584822	H	-0.411235	-3.209595	-4.125702	H	-1.300664	-2.455296	-4.282384
H	2.503595	-2.237036	-3.945052	H	0.880448	0.872811	-4.381018	H	1.981897	0.260591	-4.190627
H	2.352828	-1.481873	-1.584763	H	0.802479	1.033446	-1.902457	H	1.766053	0.414196	-1.800021
N	0.324763	-0.399922	-0.384098	N	0.126181	-0.818198	-0.210246	N	0.221986	-0.802545	-0.139658
C	1.129024	0.647656	0.105990	C	1.266875	-0.469601	0.538389	C	1.373557	-0.246447	0.511668
C	0.998426	0.655105	1.615739	C	0.806860	-0.155240	1.946764	C	1.005972	0.106455	1.928722
C	0.018295	-0.490037	1.954922	C	-0.720469	-0.382795	1.949404	C	-0.371212	-0.513827	2.156921
C	-0.374690	-1.098999	0.622157	C	-1.075503	-0.744827	0.521906	C	-0.682459	-1.243357	0.874179
H	1.993126	0.521615	2.046611	H	1.355562	-0.778176	2.654873	H	1.786093	-0.250738	2.601537
O	1.797414	1.375739	-0.581092	O	2.384596	-0.403178	0.096127	O	2.467744	-0.078688	0.035450
O	-1.128174	-2.014624	0.420182	O	-2.172738	-0.901738	0.055088	O	-1.515643	-2.098481	0.759501
C	-1.127086	0.242963	2.749036	C	-1.296175	1.016814	2.390685	C	-1.288211	0.738812	2.470795
H	-1.760631	-0.432087	3.321224	H	-2.325137	0.973716	2.741990	H	-2.236613	0.469947	2.932032
H	0.458501	-1.276725	2.571506	H	-1.052079	-1.174697	2.623212	H	-0.419235	-1.225556	2.981256
C	0.302696	1.921272	2.238640	C	0.937231	1.365648	2.342763	C	0.752400	1.656244	2.153679
H	0.970013	2.774168	2.347082	H	1.942292	1.649269	2.648871	H	1.668608	2.219276	2.321401
C	-0.266926	1.272412	3.525179	C	-0.196918	1.441682	3.394178	C	-0.274786	1.559097	3.307650
O	0.497716	0.813540	4.160107	H	-0.070923	0.743371	4.227392	H	0.100494	1.025720	4.186683
H	-0.868175	1.964704	4.117517	H	-0.346437	2.451549	3.781085	H	-0.664257	2.533891	3.607290
C	-0.981969	2.153685	1.459003	C	0.315160	2.181870	1.217692	C	-0.151214	2.139019	1.030220
H	-1.111583	2.914775	0.700140	H	0.878596	2.728393	0.471442	H	0.179748	2.717016	0.176069
C	-1.827337	1.164328	1.763771	C	-1.006484	1.980668	1.248572	C	-1.357155	1.591861	1.216744
H	-2.783212	0.953601	1.303627	H	-1.742286	2.317468	0.529048	H	-2.206802	1.633013	0.546179
I	-2.578034	0.292988	-1.976158	I	-0.756572	-3.934093	-1.163660	I	-2.755000	-2.556119	-1.865842

Table 2.14 XYZ coordinates of the GS and TS structures of **1**(*i*-Pr)


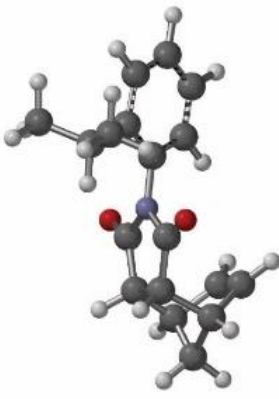
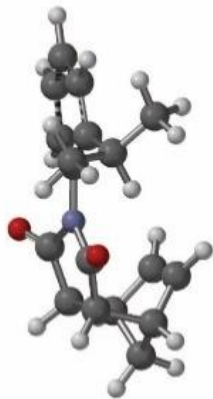
		
H 0.398278 -1.966543 -5.023063	H 0.053629 -0.123938 -5.139282	H 0.237597 -0.534118 -5.124417
C 0.549515 -1.586847 -4.017559	C 0.114273 -0.115192 -4.055691	C 0.313637 -0.447350 -4.045447
C 0.901475 -0.622685 -1.442863	C 0.233357 -0.107578 -1.284295	C 0.496518 -0.346653 -1.215984
C -0.548397 -1.274864 -3.225355	C -0.693841 -0.965108 -3.311430	C -0.678845 -0.958894 -3.228706
C 1.839718 -1.409224 -3.522518	C 1.001610 0.742919 -3.409198	C 1.372948 0.212499 -3.443650
C 2.010615 -0.929381 -2.231157	C 1.053564 0.747028 -2.022885	C 1.453859 0.252841 -2.061768
C -0.403408 -0.777857 -1.924724	C -0.649902 -0.993731 -1.911523	C -0.675129 -0.886926 -1.825091
H -1.546502 -1.417140 -3.627233	H -1.378028 -1.630023 -3.828409	H -1.535616 -1.420110 -3.703324
H 2.702611 -1.645648 -4.135772	H 1.642241 1.406689 -3.980080	H 2.149482 0.687692 -4.033813
H 3.003448 -0.787174 -1.819260	H 1.730185 1.409986 -1.496775	H 2.311028 0.741520 -1.638564
N 1.148974 -0.146675 -0.113642	N 0.320519 -0.028590 0.142757	N 0.824488 -0.286978 0.211579
C 1.589927 1.158273 0.166644	C 1.500357 -0.310662 0.854649	C 2.138691 0.056512 0.689347
C 1.807695 1.255268 1.665379	C 1.269152 0.078533 2.301810	C 2.050891 0.422927 2.147761
C 1.418201 -0.128888 2.228830	C -0.169906 0.636841 2.351948	C 0.658939 -0.024894 2.582120
C 0.973527 -0.941251 1.028579	C -0.696275 0.522822 0.936583	C 0.040495 -0.633131 1.349723
H 2.847711 1.532114 1.850520	H 1.435613 -0.787386 2.944685	H 2.873529 -0.049232 2.685158
O 1.750446 2.021688 -0.657581	O 2.509032 -0.754447 0.368317	O 3.165688 0.050670 0.060329
O 0.528983 -2.062260 1.026901	O -1.782598 0.855389 0.531773	O -0.941137 -1.329689 1.382896
C 0.282126 0.207322 3.263653	C 0.037732 2.121894 2.838660	C -0.024004 1.320388 3.070558
H 0.084048 -0.596084 3.970213	H -0.874832 2.592534 3.199098	H -0.910611 1.153952 3.679672
C -1.628097 -0.437318 -1.092780	C -1.532501 -1.967535 -1.146889	C -1.979077 -1.365918 -1.175877
H -1.280467 0.028714 -0.169867	H -1.302314 -1.870827 -0.083251	H -2.066169 -0.915798 -0.198083
H 2.240838 -0.651023 2.722422	H -0.834328 0.102603 3.033349	H 0.644903 -0.763346 3.383945
C 0.840702 2.234746 2.427595	C 2.144554 1.301254 2.779791	C 2.039582 1.983125 2.430828
H 1.146479 3.277813 2.373919	H 3.150427 1.021887 3.086752	H 3.035006 2.422408 2.454650
C -0.573557 1.916729 1.964697	C 2.033878 2.369049 1.701552	C 1.035520 2.617329 1.482860
H -1.138462 2.513755 1.259475	H 2.804517 2.587217 0.972677	H 1.294671 3.176290 0.592093
C -0.905655 0.720812 2.463928	C 0.787276 2.851482 1.733559	C -0.185002 2.224002 1.861894
H -1.798234 0.145282 2.253058	H 0.331455 3.540568 1.033357	H -1.119050 2.398416 1.341789
C 0.835787 1.544532 3.814917	C 1.189351 1.889235 3.846655	C 1.212081 1.972945 3.738515
H 1.830683 1.455605 4.262755	H 0.934525 1.183866 4.643925	H 1.652482 1.362374 4.532814
H 0.155855 2.022172 4.522701	H 1.563028 2.817532 4.282831	H 1.006744 2.976455 4.115529
C -2.405494 -1.707368 -0.708883	C -1.230870 -3.423933 -1.542780	C -1.974890 -2.890137 -0.985453
H -1.756856 -2.414042 -0.189197	H -0.174670 -3.665739 -1.398751	H -1.128049 -3.206418 -0.376447
H -2.813651 -2.202282 -1.595794	H -1.475364 -3.615038 -2.591261	H -1.917895 -3.405377 -1.950228
H -3.246126 -1.461064 -0.052208	H -1.824623 -4.114346 -0.936169	H -2.889038 -3.217256 -0.480729
C -2.533024 0.586074 -1.797441	C -3.022469 -1.635131 -1.328222	C -3.242152 -0.921652 -1.940886
H -3.346935 0.893753 -1.133578	H -3.640192 -2.301529 -0.718285	H -4.118659 -1.104930 -1.312249
H -2.990421 0.172025 -2.700810	H -3.331664 -1.761981 -2.370481	H -3.406706 -1.468432 -2.873876
H -1.972356 1.478944 -2.084901	H -3.225900 -0.606616 -1.029076	H -3.216753 0.144894 -2.179466

Table 2.15 XYZ coordinates of the GS and TS structures of 1(CH₃)

H	0.665488	-1.942392	-5.247933	H	-0.287216	0.918146	-5.414424	H	0.510995	-0.895336	-5.354960
C	0.665446	-1.624855	-4.210093	C	-0.247668	0.827965	-4.333582	C	0.494938	-0.851471	-4.270868
C	0.632960	-0.809945	-1.558255	C	-0.132707	0.622483	-1.571946	C	0.402201	-0.795572	-1.431665
C	-0.530211	-1.262423	-3.598480	C	0.277335	1.867103	-3.571378	C	-0.527049	-1.457537	-3.559545
C	1.857530	-1.571999	-3.492697	C	-0.725791	-0.321657	-3.709863	C	1.476646	-0.186480	-3.557190
C	1.836814	-1.164831	-2.163988	C	-0.665314	-0.421497	-2.325407	C	1.422326	-0.164817	-2.171932
C	-0.576127	-0.841606	-2.266106	C	0.343326	1.792127	-2.176874	C	-0.634726	-1.454377	-2.157531
H	-1.454955	-1.299029	-4.166851	H	0.642445	2.761652	-4.066907	H	-1.308424	-1.963843	-4.116148
H	2.795962	-1.845890	-3.962482	H	-1.140769	-1.135237	-4.295483	H	2.295097	0.317330	-4.060914
H	2.753231	-1.113406	-1.587659	H	-1.031989	-1.304857	-1.815928	H	2.215875	0.339948	-1.655194
N	0.665702	-0.390805	-0.189069	N	-0.090842	0.471236	-0.149190	N	0.493471	-0.635699	0.023578
C	1.330136	0.775720	0.235776	C	-1.248637	0.295597	0.631274	C	1.605048	-0.016963	0.684937
C	1.186880	0.863939	1.742008	C	-0.809422	0.031148	2.057732	C	1.209768	0.346465	2.092717
C	0.366303	-0.376844	2.152758	C	0.732688	0.014482	2.014192	C	-0.150514	-0.302682	2.308874
C	0.065681	-1.107499	0.858163	C	1.102102	0.310167	0.574057	C	-0.448336	-1.029992	1.021538
H	2.183170	0.904450	2.187243	H	-1.229022	0.796786	2.713090	H	1.990487	0.017220	2.779070
O	1.897414	1.548800	-0.492829	O	-2.376269	0.327517	0.209099	O	2.702306	0.200706	0.233501
O	-0.580577	-2.116633	0.722692	O	2.209108	0.381867	0.101618	O	-1.332861	-1.835849	0.910341
C	-0.885002	0.242007	2.880256	C	1.085558	-1.443986	2.496269	C	-1.102951	0.926362	2.608804
H	-1.430394	-0.472907	3.493177	H	2.126087	-1.563927	2.791225	H	-2.047745	0.636438	3.064556
C	-1.882557	-0.443242	-1.632876	C	0.911633	2.924675	-1.365816	C	-1.887322	-2.148000	-1.653808
H	-2.239198	-1.228579	-0.961491	C	0.285547	3.146549	-0.497057	H	-1.669097	-3.005404	-1.022848
H	-2.646700	-0.265508	-2.392028	H	0.992524	3.833941	-1.964016	H	-2.464967	-2.494698	-2.512508
H	-1.775429	0.465682	-1.037437	H	1.906065	2.667576	-0.992985	H	-2.529331	-1.487860	-1.073584
H	0.897686	-1.054413	2.824173	H	1.205305	0.751416	2.666204	H	-0.192529	-1.017364	3.131244
C	0.309361	2.061775	2.264109	C	-1.174803	-1.408169	2.585948	C	0.916552	1.890934	2.297492
H	0.848698	3.005628	2.315723	H	-2.192350	-1.488868	2.963081	H	1.815845	2.479954	2.466128
C	-0.195140	1.434878	3.587990	C	-0.006621	-1.611487	3.581399	C	-0.118673	1.781870	3.443798
H	0.611182	1.137976	4.266468	H	0.035399	-0.850623	4.367804	H	0.261928	1.269096	4.332768
H	-0.900400	2.077401	4.118408	H	-0.004894	-2.604911	4.034182	H	-0.536156	2.749585	3.728076
C	-0.980417	2.059811	1.456502	C	-0.772367	-2.391061	1.496367	C	0.011129	2.336780	1.160113
H	-1.201603	2.749932	0.651758	H	-1.465465	-2.881373	0.824011	H	0.336286	2.910141	0.300874
C	-1.687177	0.985515	1.823617	C	0.563667	-2.406527	1.437994	C	-1.182891	1.763805	1.344236
H	-2.603758	0.619294	1.379454	H	1.183360	-2.908253	0.705308	H	-2.027324	1.777308	0.666051

Table 2.16 XYZ coordinates of the GS and TS structures of **1**(OCH₃)

H 0.865606 -1.903122 -5.049350	H -0.974257 -0.240921 -5.276401	H 0.401621 -0.552443 -5.318380
C 0.905693 -1.537912 -4.028154	C -0.788554 -0.107334 -4.215498	C 0.412388 -0.548496 -4.233960
C 0.983703 -0.619334 -1.408613	C -0.336088 0.210419 -1.496298	C 0.411152 -0.556184 -1.387619
C -0.279605 -1.423370 -3.303240	C -1.871267 -0.060906 -3.338667	C -0.579103 -1.189575 -3.516753
C 2.124367 -1.185687 -3.459791	C 0.514388 0.017659 -3.746196	C 1.404853 0.108760 -3.524452
C 2.155462 -0.730000 -2.143553	C 0.734327 0.171604 -2.379718	C 1.397172 0.107435 -2.138640
C -0.253246 -0.948105 -1.990399	C -1.655426 0.116180 -1.969971	C -0.608018 -1.200019 -2.122050
H -1.217948 -1.693246 -3.770619	H -2.877206 -0.150639 -3.728246	H -1.402967 -1.689974 -4.015175
H 3.042714 -1.268817 -4.029785	H 1.352466 -0.013147 -4.433301	H 2.198625 0.638157 -4.040302
H 3.091775 -0.453639 -1.673202	H 1.738957 0.257992 -1.983519	H 2.194515 0.620535 -1.632258
N 1.019291 -0.155277 -0.063663	N -0.108155 0.329636 -0.097719	N 0.473650 -0.451854 0.061620
C 1.359583 1.162750 0.284697	C -0.452494 -0.684316 0.813478	C 1.571297 0.148734 0.734437
C 1.198191 1.295085 1.786826	C 0.013971 -0.242978 2.186002	C 1.168631 0.502568 2.143145
C 0.712137 -0.088437 2.273460	C 0.684165 1.130269 1.971455	C -0.216460 -0.101308 2.323837
C 0.623389 -0.948103 1.028149	C 0.555879 1.418342 0.488705	C -0.503113 -0.838122 1.038372
H 2.147204 1.611345 2.224131	H -0.835495 -0.223101 2.871134	H 1.923235 0.131434 2.838178
O 1.704909 2.015026 -0.493775	O -0.983303 -1.724815 0.521145	O 2.667852 0.365167 0.285339
O 0.278760 -2.099351 0.954157	O 0.967956 2.380696 -0.108382	O -1.377019 -1.646927 0.923536
C -0.676561 0.236081 2.945928	C 2.164647 0.884708 2.458599	C -1.128221 1.152803 2.577283
H -1.041797 -0.557657 3.595012	H 2.717621 1.802588 2.648730	H -2.101537 0.903503 2.996014
O -1.352013 -0.753918 -1.217216	O -2.635617 0.219256 -1.038297	O -1.699680 -1.811046 -1.570734
H 1.380889 -0.566815 2.991533	H 0.227419 1.944489 2.536796	H -0.302141 -0.805345 3.152455
C 0.035241 2.261384 2.233544	C 1.177921 -1.125405 2.775921	C 0.928731 2.043951 2.345279
H 0.319586 3.311929 2.234891	H 0.831879 -2.038213 3.256846	H 1.838980 2.603605 2.551862
C -0.327861 1.601822 3.585074	C 1.878362 -0.058678 3.652690	C -0.152867 1.977734 3.441889
H 0.509495 1.554166 4.288885	H 1.223311 0.380975 4.411585	H 0.174608 1.455083 4.346452
H -1.185733 2.073255 4.068866	H 2.789556 -0.430594 4.125477	H -0.548982 2.961176 3.700928
C -1.186978 1.884917 1.409673	C 2.212927 -1.288978 1.672303	C 0.089822 2.513610 1.169934
H -1.536760 2.432671 0.543943	H 2.337966 -2.184092 1.075885	H 0.467040 3.073813 0.322533
C -1.606608 0.688030 1.829781	C 2.794128 -0.099752 1.483002	C -1.126073 1.980148 1.304663
H -2.362119 0.063655 1.371678	H 3.497550 0.170734 0.705136	H -1.939108 2.018071 0.589375
C -2.607079 -1.228077 -1.681047	C -3.963368 -0.125529 -1.406761	C -1.531205 -3.209613 -1.379236
H -2.576945 -2.304040 -1.880526	H -4.010473 -1.143374 -1.807352	H -0.666806 -3.421434 -0.744100
H -2.933311 -0.695412 -2.581170	H -4.376302 0.577965 -2.138577	H -1.410306 -3.718763 -2.342743
H -3.313428 -1.031796 -0.876126	H -4.547392 -0.070740 -0.489989	H -2.430564 -3.565181 -0.880730

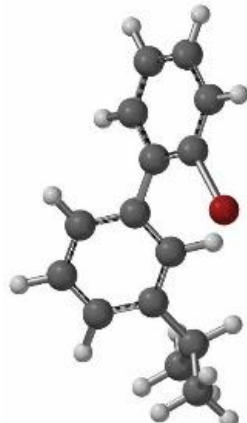
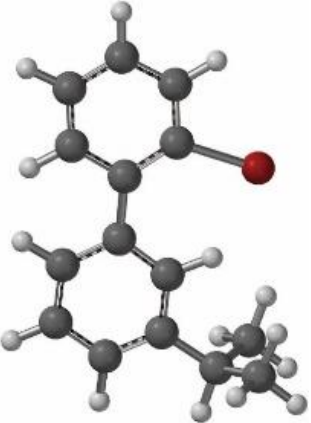
Table 2.17 XYZ coordinates of the GS and TS structures of **1(Ph)**

H 1.661563 -1.676816 -5.123458	H -0.878954 -0.047771 -5.348401	H 1.207405 -0.532076 -5.164829
C 1.601236 -1.288040 -4.112030	C -0.780015 -0.094835 -4.268771	C 1.171757 -0.420939 -4.086208
C 1.425679 -0.304375 -1.519930	C -0.515082 -0.198508 -1.507667	C 1.057242 -0.198493 -1.253909
C 0.403481 -1.370909 -3.409830	C 0.043349 0.812400 -3.609968	C 0.183675 -1.049101 -3.347662
C 2.715266 -0.697604 -3.520423	C -1.481712 -1.054980 -3.543526	C 2.087487 0.369391 -3.408365
C 2.626743 -0.212864 -2.221047	C -1.340253 -1.109105 -2.161503	C 2.027443 0.472417 -2.027606
C 0.289181 -0.868755 -2.108952	C 0.182696 0.785854 -2.217797	C 0.068943 -0.947753 -1.949060
H -0.471024 -1.814154 -3.874886	H 0.576815 1.570991 -4.172924	H -0.571632 -1.635780 -3.858648
H 3.649849 -0.621204 -4.065749	H -2.128612 -1.762847 -4.050946	H 2.862530 0.909164 -3.942597
H 3.486210 0.237228 -1.737417	H -1.855974 -1.863762 -1.578561	H 2.774409 1.069284 -1.538765
N 1.391343 0.162468 -0.169990	N -0.343334 -0.330173 -0.093743	N 1.146999 -0.015581 0.185886
C 1.464607 1.519755 0.183969	C -1.219828 0.215568 0.849837	C 2.260601 0.599138 0.838465
C 1.498155 1.596202 1.699611	C -0.765320 -0.244451 2.219829	C 1.886181 0.915238 2.264095
C 1.385026 0.132909 2.185976	C 0.489179 -1.112367 1.967338	C 0.527614 0.258640 2.482845
C 1.319202 -0.708612 0.928899	C 0.690761 -1.102002 0.465122	C 0.204861 -0.426810 1.178155
H 2.420548 2.092519 2.008751	H -0.582609 0.628035 2.849541	H 2.677629 0.565766 2.927933
O 1.485854 2.433502 -0.601726	O -2.167844 0.914694 0.586839	O 3.340868 0.849391 0.363335
O 1.219500 -1.907229 0.848837	O 1.546900 -1.662744 -0.168881	O -0.694337 -1.207455 1.034084
C 0.066597 0.143208 3.046536	C 0.080509 -2.513483 2.559980	C -0.419050 1.477940 2.833709
H -0.035906 -0.724322 3.695868	H 0.925532 -3.177294 2.732310	H -1.357145 1.174763 3.294342
H 2.231253 -0.201442 2.789618	H 1.391625 -0.741011 2.455746	H 0.499641 -0.481063 3.283577
C 0.245931 2.290634 2.356784	C -1.755276 -1.244621 2.932460	C 1.595387 2.452389 2.519531
H 0.310718 3.376789 2.378012	H -2.579691 -0.751267 3.443769	H 2.496676 3.037429 2.691461
C 0.218938 1.535022 3.707005	C -0.731906 -2.033417 3.787620	C 0.577718 2.309794 3.677317
H 1.139069 1.644266 4.290698	H -0.156421 -1.402564 4.472685	H 0.971734 1.771057 4.544841
H -0.639731 1.804895 4.324829	H -1.188490 -2.855893 4.341884	H 0.165184 3.268778 3.996535
C -0.977198 1.688482 1.684873	C -2.127645 -2.307967 1.910759	C 0.673045 2.928310 1.407881
H -1.556853 2.171136 0.909023	H -3.073988 -2.349263 1.385756	H 0.986219 3.523988 0.559431
C -1.079585 0.417616 2.085647	C -1.043185 -3.058456 1.690485	C -0.517391 2.348254 1.593284
H -1.753176 -0.333602 1.694833	H -0.922358 -3.837746 0.948179	H -1.371367 2.375367 0.927594
C -1.037511 -0.909100 -1.427707	C 1.039562 1.785711 -1.533026	C -1.182434 -1.611364 -1.457163
C -3.597240 -0.993636 -0.289643	C 2.647914 3.706962 -0.283292	C -3.603406 -2.865331 -0.806717
C -1.510138 -2.084731 -0.837580	C 0.482436 2.691641 -0.622958	C -1.241626 -2.996846 -1.294800
C -1.853201 0.226653 -1.428339	C 2.408295 1.852874 -1.811509	C -2.357737 -0.865749 -1.333433
C -3.126915 0.184750 -0.866299	C 3.208240 2.807471 -1.188289	C -3.558584 -1.486606 -1.001868
C -2.783190 -2.125504 -0.271447	C 1.283375 3.646533 -0.002824	C -2.441187 -3.618311 -0.960379
H -0.867560 -2.956595 -0.806691	H -0.581726 2.649911 -0.417389	H -0.337689 -3.585818 -1.411789
H -1.485105 1.142147 -1.879680	H 2.843413 1.139816 -2.504234	H -2.327081 0.207685 -1.493032
H -3.752500 1.071613 -0.880648	H 4.270548 2.845659 -1.407532	H -4.462380 -0.893342 -0.899611
H -3.139500 -3.043691 0.184922	H 0.837985 4.349515 0.694121	H -2.469387 -4.694851 -0.821315
H -4.589616 -1.028608 0.148782	H 3.271088 4.452890 0.199484	H -4.538816 -3.350912 -0.546548

Table 2.18 XYZ coordinates of the GS and TS structures of **1**(SCH₃)

H	0.714145	-2.418221	-5.068968	H	0.906066	-0.872051	-5.299518	H	0.946430	-1.141207	-5.063835
C	0.718277	-2.007014	-4.064853	C	0.782128	-0.776342	-4.225725	C	0.817623	-0.956401	-4.002423
C	0.707724	-0.964162	-1.481588	C	0.461544	-0.552938	-1.471114	C	0.515795	-0.635773	-1.203838
C	-0.485754	-1.689145	-3.443568	C	0.102926	-1.762734	-3.519462	C	-0.161698	-1.636833	-3.298253
C	1.921425	-1.794359	-3.397788	C	1.316301	0.320502	-3.552842	C	1.591870	-0.026848	-3.329681
C	1.912359	-1.277708	-2.106663	C	1.154172	0.429438	-2.177566	C	1.439830	0.109158	-1.959200
C	-0.508577	-1.156554	-2.152023	C	-0.070518	-1.667599	-2.135101	C	-0.411021	-1.456036	-1.925458
H	-1.426760	-1.848060	-3.958222	H	-0.292143	-2.629521	-4.038112	H	-0.777541	-2.330938	-3.850426
H	2.863848	-2.036067	-3.877198	H	1.856562	1.087153	-4.097678	H	2.329610	0.576571	-3.846988
H	2.839356	-1.117826	-1.567591	H	1.559749	1.274226	-1.633579	H	2.091756	0.799660	-1.456090
N	0.754583	-0.461766	-0.146207	N	0.312047	-0.389827	-0.063737	N	0.606764	-0.444664	0.233842
C	1.091216	0.861682	0.170517	C	1.400995	-0.415582	0.825951	C	1.753026	0.127311	0.878143
C	1.163567	0.967486	1.682687	C	0.864990	-0.112592	2.210027	C	1.393406	0.459611	2.304056
C	0.713799	-0.414130	2.209943	C	-0.655683	0.091493	2.029882	C	0.026794	-0.180548	2.535292
C	0.468211	-1.261296	0.977564	C	-0.908916	-0.073140	0.545813	C	-0.297764	-0.876667	1.238893
H	2.184394	1.234149	1.966483	H	1.127841	-0.930729	2.882636	H	2.183600	0.102597	2.965080
O	1.271631	1.737014	-0.640574	O	2.544316	-0.618169	0.506943	O	2.837564	0.324275	0.391724
O	0.107584	-2.407680	0.927813	O	-1.955839	0.075054	-0.035435	O	-1.165419	-1.698464	1.110772
C	-0.556514	-0.067531	3.070087	C	-0.888183	1.556325	2.559064	C	-0.903837	1.054073	2.879466
H	-0.861111	-0.871344	3.737644	H	-1.929336	1.779069	2.783923	H	-1.844222	0.764933	3.344604
H	1.460366	-0.914512	2.830168	H	-1.269045	-0.623242	2.581566	H	-0.005771	-0.911173	3.343825
C	0.128627	1.959124	2.331154	C	1.341808	1.265566	2.806710	C	1.121921	2.001883	2.555945
H	0.455964	2.997047	2.328479	H	2.331311	1.224480	3.257692	H	2.031414	2.575333	2.723991
C	-0.062461	1.259496	3.700238	C	0.130860	1.564986	3.725790	C	0.106757	1.874731	3.717983
H	0.865555	1.153590	4.271621	H	-0.053206	0.785234	4.471058	H	0.496551	1.333010	4.585493
H	-0.820382	1.743048	4.319399	H	0.202175	2.536666	4.218344	H	-0.292394	2.839673	4.036090
C	-1.215855	1.662891	1.687118	C	1.128877	2.317173	1.727938	C	0.201550	2.487972	1.447784
H	-1.673343	2.269988	0.917067	H	1.918467	2.743511	1.121398	H	0.517925	3.078757	0.597063
C	-1.614743	0.461045	2.114069	C	-0.188870	2.491247	1.582602	C	-0.995246	1.922755	1.637680
H	-2.457246	-0.114371	1.755322	H	-0.694866	3.082487	0.829588	H	-1.849856	1.958717	0.973323
S	-2.080987	-0.730808	-1.402583	S	-0.917449	-2.985358	-1.256179	S	-1.955512	-2.173186	-1.310320
C	-2.127186	1.047813	-1.861652	C	-2.649749	-2.598183	-1.731450	C	-2.911875	-2.436821	-2.851066
H	-1.217434	1.548605	-1.531968	H	-2.898382	-1.590761	-1.405895	H	-2.942137	-1.542065	-3.474356
H	-2.990982	1.483182	-1.356795	H	-3.282338	-3.322206	-1.215746	H	-3.920799	-2.649975	-2.491986
H	-2.243293	1.166396	-2.939130	H	-2.788611	-2.703636	-2.807786	H	-2.575096	-3.293422	-3.437126

Table 2.19 XYZ coordinates of the GS and TS structures of 2(Br)^a

							
C	-1.004483	1.781060	-0.807301	C	0.689718	1.886829	0.133640
C	-3.000707	3.734527	-1.231201	C	2.574416	4.061181	0.175081
C	-2.266693	1.441187	-1.320006	C	2.087975	1.690246	0.007993
C	-0.779336	3.137783	-0.523842	C	0.321078	3.245711	0.281973
C	-1.756351	4.104825	-0.728744	C	1.212701	4.303769	0.303808
C	-3.254784	2.400445	-1.530600	C	2.999395	2.751032	0.028456
H	0.186161	3.419908	-0.117626	H	-0.723302	3.495634	0.387047
H	-1.548780	5.142633	-0.491293	H	0.836286	5.314443	0.420621
H	-4.213694	2.100821	-1.935616	H	4.055893	2.536603	-0.073166
H	-3.775138	4.476222	-1.395889	H	3.297140	4.869588	0.187653
C	0.089582	0.803873	-0.564328	C	-0.412047	0.857426	0.126030
C	2.167868	-1.003850	-0.091446	C	-2.546310	-1.023386	0.116958
C	1.332437	0.984482	-1.176520	C	-1.760946	1.256325	0.264829
C	-0.088749	-0.288613	0.292584	C	-0.200302	-0.522649	-0.015631
C	0.932723	-1.205084	0.537419	C	-1.234761	-1.465127	-0.022996
C	2.365327	0.081422	-0.938295	C	-2.799507	0.337796	0.259796
H	1.478328	1.818027	-1.855398	H	-2.037123	2.293817	0.380902
H	-1.052757	-0.429992	0.770927	H	0.797518	-0.902231	-0.125602
H	2.980534	-1.703766	0.075269	H	-3.366325	-1.736004	0.114919
Br	-2.702270	-0.366961	-1.827982	Br	3.000450	-0.009737	-0.207497
H	3.325730	0.220843	-1.424655	H	-3.820347	0.691075	0.368346
C	0.684569	-2.411934	1.428443	C	-0.922994	-2.944859	-0.191964
H	-0.311993	-2.290804	1.869426	H	-1.874652	-3.486056	-0.122139
C	1.692996	-2.507567	2.583141	C	-0.324143	-3.241499	-1.576558
H	1.695628	-1.594373	3.183400	H	0.636798	-2.735593	-1.709417
H	2.709939	-2.666356	2.213144	H	-0.989001	-2.905439	-2.376400
H	1.449831	-3.346690	3.241692	H	-0.154543	-4.315077	-1.704390
C	0.667313	-3.709042	0.599832	C	-0.011605	-3.472883	0.928063
H	1.645978	-3.902444	0.149993	H	0.969548	-2.990162	0.905642
H	-0.063197	-3.651024	-0.211115	H	0.147740	-4.550142	0.820866
H	0.413986	-4.569559	1.226588	H	-0.448745	-3.290632	1.913136

^a The version with an *i*-Pr reporter group was used in consistent with the original work by A. Mazzanti and co-workers.

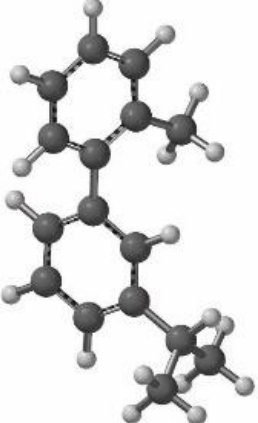
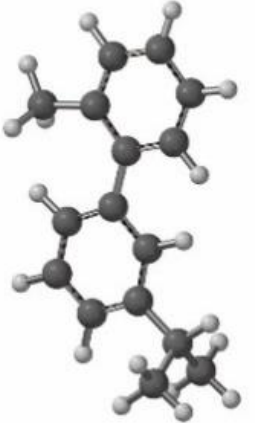
Table 2.20 XYZ coordinates of the GS and TS structures of 2(CCH)

C	3.141696	0.531425	-0.627241	C	2.640694	-0.329673	-0.031771
C	5.603649	1.808267	-0.113433	C	5.236721	0.873470	-0.053375
C	3.546816	0.798210	0.703921	C	2.809897	1.073504	0.166376
C	3.997311	0.912107	-1.668241	C	3.823819	-1.063553	-0.245071
C	5.212686	1.541240	-1.423920	C	5.088059	-0.494744	-0.257345
C	4.776538	1.438420	0.938141	C	4.102624	1.638303	0.152702
H	3.684909	0.726512	-2.690614	H	3.766905	-2.129495	-0.411477
H	5.847788	1.829262	-2.255457	H	5.954899	-1.125569	-0.426188
H	5.074360	1.631876	1.962457	H	4.188819	2.707228	0.310270
H	6.548209	2.302386	0.088088	H	6.217467	1.336511	-0.057071
C	1.857294	-0.139614	-0.955576	C	1.329350	-1.058653	-0.023462
C	-0.557066	-1.400929	-1.611140	C	-1.136680	-2.468487	-0.007549
C	0.647115	0.275025	-0.386263	C	0.097125	-0.413442	0.164225
C	1.832985	-1.200955	-1.870443	C	1.271861	-2.457092	-0.202245
C	0.633195	-1.823484	-2.197947	C	0.066158	-3.144492	-0.196914
C	-0.573463	-0.344285	-0.688793	C	-1.135421	-1.083756	0.181751
H	0.667467	1.104883	0.311379	H	0.087615	0.653460	0.306727
H	2.761801	-1.553859	-2.306895	H	2.169419	-3.042744	-0.346515
H	0.628114	-2.649782	-2.902519	H	0.068348	-4.221085	-0.340291
H	-1.479828	-1.910175	-1.873405	H	-2.068441	-3.027297	-0.006659
Si	-2.168515	0.240860	0.148961	Si	-2.710097	-0.077389	0.461149
C	2.760302	0.405157	1.829106	C	-2.556527	0.830578	2.109403
H	1.538954	-0.200809	3.641016	H	-3.449451	1.420837	2.335173
C	2.120897	0.087521	2.798727	H	-1.698739	1.510073	2.107712
C	-3.489780	-1.130025	0.058767	H	-2.408713	0.125385	2.932450
H	-3.620126	-1.372141	-1.005806	C	-4.218742	-1.210152	0.487544
C	-1.794487	0.637162	1.956227	H	-4.349646	-1.746942	-0.456454
H	-1.032806	1.415067	2.057751	H	-5.131347	-0.632596	0.662230
H	-1.427441	-0.247391	2.483622	H	-4.150178	-1.955095	1.285817
H	-2.690803	0.989242	2.475333	C	-2.871901	1.194418	-0.949279
C	-2.814495	1.790215	-0.717782	H	-1.932895	1.766641	-0.938751
H	-2.036220	2.554432	-0.800241	C	-4.030911	2.178143	-0.717973
H	-3.653766	2.231924	-0.172563	H	-4.997949	1.663093	-0.712028
H	-3.158270	1.563333	-1.731525	H	-4.076353	2.931057	-1.513608
C	-3.058873	-2.411954	0.792843	H	-3.937537	2.713249	0.231534
H	-2.106666	-2.805440	0.427369	C	-2.992129	0.512901	-2.322719
H	-3.808181	-3.203606	0.677722	H	-3.924723	-0.056452	-2.403291
H	-2.946459	-2.233918	1.867556	H	-2.165953	-0.179032	-2.509238
C	-4.848726	-0.637552	0.588385	H	-2.995232	1.250565	-3.133118
H	-4.786035	-0.349878	1.643284	C	1.771841	2.033650	0.384451
H	-5.607877	-1.424877	0.517498	H	0.293828	3.720770	0.727882
H	-5.222204	0.226147	0.031653	C	1.004085	2.944918	0.568169

Table 2.21 XYZ coordinates of the GS and TS structures of 2(CF₃)

C	-2.119849	0.957657	-0.148485	C	2.353491	-0.776677	-0.098822
C	-4.454236	0.977956	-1.732709	C	5.094245	0.042166	-0.360715
C	-2.759441	-0.245518	-0.507911	C	2.738991	0.599624	-0.034148
C	-2.696529	2.157816	-0.586084	C	3.421604	-1.674697	-0.300374
C	-3.846377	2.175026	-1.368003	C	4.749560	-1.297911	-0.428812
C	-3.911206	-0.224786	-1.297344	C	4.082958	0.970154	-0.165560
H	-2.211602	3.090046	-0.317821	H	3.221466	-2.732210	-0.366007
H	-4.261609	3.121834	-1.697471	H	5.505717	-2.060966	-0.582357
H	-4.392857	-1.158804	-1.557681	H	4.343785	2.017415	-0.113880
H	-5.349417	0.975742	-2.345157	H	6.123910	0.367124	-0.458244
C	-0.868286	1.035540	0.653424	C	0.967982	-1.374899	0.013865
C	1.505239	1.285443	2.110635	C	-1.609520	-2.590415	0.176711
C	0.309707	0.424564	0.216695	C	-0.210805	-0.634663	0.197279
C	-0.840593	1.783248	1.835486	C	0.786170	-2.774205	-0.074337
C	0.340411	1.905103	2.560161	C	-0.466585	-3.365917	0.006201
C	1.510000	0.529283	0.929681	C	-1.490814	-1.203310	0.277174
H	0.282094	-0.140208	-0.708146	H	-0.170163	0.429788	0.286109
H	-1.752692	2.252630	2.190489	H	1.620636	-3.446501	-0.207682
H	0.350006	2.482884	3.479209	H	-0.545539	-4.446359	-0.069570
H	2.416882	1.394720	2.690697	H	-2.583266	-3.068991	0.230290
Si	3.031346	-0.399875	0.302224	Si	-2.972126	-0.040094	0.458274
C	2.864363	-2.215129	0.785392	C	-2.713675	1.039479	1.982434
H	3.728120	-2.807006	0.467859	H	-3.541327	1.739619	2.129499
H	1.969998	-2.655422	0.334022	H	-1.794126	1.626655	1.901903
H	2.768109	-2.325010	1.869565	H	-2.630947	0.428892	2.886289
C	4.585270	0.349528	1.066083	C	-4.563538	-1.038837	0.621623
H	4.663947	1.417673	0.843362	H	-4.734371	-1.685224	-0.243948
H	5.486155	-0.135392	0.679018	H	-5.428042	-0.373738	0.707684
H	4.600662	0.235152	2.154017	H	-4.553736	-1.673653	1.512580
C	3.097434	-0.248649	-1.596407	C	-3.016426	1.044249	-1.105106
H	2.199916	-0.755966	-1.977518	H	-2.014632	1.492254	-1.171438
C	4.321198	-0.974618	-2.181441	C	-4.038287	2.190889	-1.016110
H	5.256657	-0.523072	-1.834938	H	-5.063170	1.811735	-0.935821
H	4.325202	-0.918172	-3.275844	H	-4.000295	2.819444	-1.912985
H	4.344561	-2.034083	-1.910225	H	-3.857097	2.841299	-0.155601
C	3.047952	1.214584	-2.068264	C	-3.239583	0.204212	-2.373894
H	3.914626	1.779921	-1.708685	H	-4.232952	-0.257254	-2.376503
H	2.150288	1.728870	-1.714794	H	-2.501393	-0.596889	-2.470611
H	3.056512	1.276339	-3.162609	H	-3.172650	0.825580	-3.274095
C	-2.247630	-1.594437	-0.058340	C	1.797046	1.770768	0.165808
F	-1.197571	-2.019293	-0.814363	F	1.121349	1.701554	1.341454
F	-1.835657	-1.599894	1.223065	F	0.877177	1.874614	-0.828158
F	-3.194644	-2.555085	-0.166085	F	2.434798	2.960358	0.189279

Table 2.22 XYZ coordinates of the GS and TS structures of 2(CH₃)^a

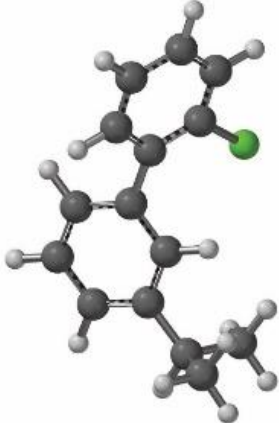
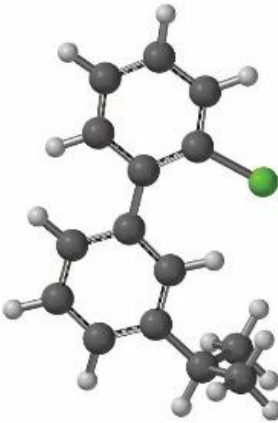
							
H	1.566312	-0.054672	-3.274985	H	-1.770477	-0.000262	-3.183726
C	1.310188	-0.166110	-2.225852	C	-1.389518	-0.000202	-2.167034
C	0.682309	-0.479809	0.488245	C	-0.430595	-0.000089	0.518173
C	2.053814	-1.031457	-1.430279	C	-2.269147	-0.000257	-1.096023
C	0.241887	0.559670	-1.684736	C	-0.012099	-0.000111	-1.922698
C	-0.054814	0.385539	-0.331322	C	0.430852	-0.000024	-0.602473
C	1.747174	-1.187367	-0.080291	C	-1.804505	-0.000214	0.217636
H	2.877483	-1.590700	-1.863773	H	-3.340395	-0.000360	-1.274225
H	-0.868409	0.957071	0.106453	H	1.503553	0.000124	-0.467396
H	2.325205	-1.870012	0.534525	H	-2.545983	-0.000266	0.994061
C	0.373428	-0.618066	1.942243	C	0.134775	-0.000009	1.915773
C	-0.081992	-0.836656	4.703455	C	1.438698	0.000266	4.455691
C	-0.870107	-1.093135	2.409613	C	-0.622348	0.000026	3.124609
C	1.365195	-0.272829	2.870787	C	1.538559	0.000070	2.060733
C	1.146394	-0.375504	4.240387	C	2.186636	0.000215	3.286291
C	-1.069702	-1.193709	3.790783	C	0.055815	0.000160	4.352221
H	2.317181	0.097743	2.503608	H	2.168966	0.000018	1.184208
H	1.928836	-0.095288	4.938588	H	3.271563	0.000290	3.319093
H	-2.020836	-1.571284	4.156443	H	-0.536893	0.000178	5.262119
H	-0.269641	-0.926483	5.768939	H	1.917443	0.000380	5.429580
C	-1.976578	-1.522491	1.472615	C	-2.133371	-0.000067	3.232972
H	-1.589131	-2.037310	0.591146	H	-2.588186	0.883175	2.776108
H	-2.561474	-0.670489	1.111428	H	-2.427926	-0.000010	4.283819
H	-2.670547	-2.196159	1.980077	H	-2.588071	-0.883439	2.776239
C	-0.575356	1.521572	-2.536149	C	0.991750	-0.000150	-3.067300
H	-1.347488	1.947313	-1.884365	H	1.992472	-0.000556	-2.618286
C	-1.296438	0.801664	-3.688540	C	0.875936	1.268201	-3.930351
H	-0.587084	0.358197	-4.393894	H	-0.095295	1.323460	-4.431223
H	-1.922804	1.502019	-4.249200	H	1.647355	1.282013	-4.706525
H	-1.936635	-0.001867	-3.315820	H	0.987963	2.171665	-3.325465
C	0.277437	2.689956	-3.060141	C	0.875202	-1.268013	-3.930983
H	1.071089	2.339199	-3.726517	H	-0.096009	-1.322415	-4.431983
H	0.752885	3.233430	-2.239579	H	0.986603	-2.171853	-3.326543
H	-0.337781	3.398022	-3.623892	H	1.646676	-1.281944	-4.707091

^a The version with an *i*-Pr reporter group was used in consistent with the original work by A. Mazzanti and co-workers.

Table 2.23 XYZ coordinates of the GS and TS structures of 2(CHO)

C	2.670960	-0.425065	-0.102953	C	2.305359	0.342298	0.261664
C	5.246362	0.676917	-0.406009	C	4.329662	2.343904	0.023256
C	3.123764	0.593093	0.763836	C	3.621035	0.018670	-0.177359
C	3.542460	-0.890466	-1.096369	C	2.104226	1.678255	0.659539
C	4.814695	-0.350885	-1.247164	C	3.083431	2.657209	0.554480
C	4.402151	1.141566	0.590463	C	4.584010	1.028243	-0.329950
H	3.197770	-1.663415	-1.775763	H	1.150194	1.974895	1.073035
H	5.466902	-0.725024	-2.030059	H	2.862459	3.667790	0.882719
H	4.713975	1.925166	1.272019	H	5.556853	0.738389	-0.709889
H	6.235835	1.104440	-0.528430	H	5.096139	3.102595	-0.091184
C	1.299874	-0.992546	-0.016634	C	1.122144	-0.583122	0.242036
C	-1.280773	-2.056006	0.184582	C	-1.184475	-2.240615	0.207398
C	0.172149	-0.158570	-0.026682	C	-0.184005	-0.062249	0.344273
C	1.107807	-2.376573	0.067887	C	1.212172	-1.976689	0.075058
C	-0.176228	-2.903396	0.170254	C	0.084388	-2.788803	0.065723
C	-1.130615	-0.663868	0.077803	C	-1.339063	-0.855233	0.339357
H	0.326941	0.911940	-0.122461	H	-0.321233	1.010510	0.400110
H	1.969419	-3.036321	0.084771	H	2.161261	-2.466698	-0.061518
H	-0.313833	-3.977062	0.255462	H	0.205010	-3.860286	-0.062115
H	-2.271442	-2.489594	0.286900	H	-2.051777	-2.893448	0.194992
Si	-2.636195	0.485182	0.105002	Si	-3.050711	-0.058108	0.483097
C	-2.046189	2.244122	0.447006	C	-3.188430	0.812187	2.152647
H	-2.890151	2.916058	0.624466	H	-4.183545	1.239959	2.306142
H	-1.476883	2.654480	-0.392677	H	-2.463742	1.626842	2.246140
H	-1.404783	2.288376	1.332133	H	-3.000231	0.113826	2.973372
C	-3.805864	-0.080933	1.473553	C	-4.388116	-1.381627	0.348606
H	-4.211226	-1.079139	1.285687	H	-4.334025	-1.930823	-0.595467
H	-4.654944	0.602294	1.568597	H	-5.380916	-0.925422	0.404501
H	-3.297293	-0.110950	2.441160	H	-4.321894	-2.110538	1.161526
C	-3.547010	0.431057	-1.567654	C	-3.245797	1.209723	-0.926470
H	-2.813218	0.757547	-2.318317	H	-2.404256	1.909555	-0.819496
C	-4.727584	1.418511	-1.594790	C	-4.548566	2.017589	-0.806615
H	-5.484618	1.156530	-0.847899	H	-5.428994	1.372726	-0.900314
H	-5.224722	1.409625	-2.571343	H	-4.619852	2.771232	-1.599092
H	-4.412582	2.447327	-1.398916	H	-4.623736	2.541761	0.150238
C	-4.013247	-0.984027	-1.949900	C	-3.134938	0.544302	-2.309248
H	-4.737537	-1.376314	-1.227677	H	-3.966128	-0.147378	-2.482964
H	-3.182410	-1.692297	-2.004883	H	-2.206322	-0.022416	-2.419856
H	-4.508116	-0.981754	-2.927544	H	-3.165729	1.290091	-3.111365
C	2.320974	1.065778	1.923521	C	4.183457	-1.348638	-0.410523
H	1.435028	0.454687	2.178155	H	3.895333	-2.124877	0.322743
O	2.605331	2.035838	2.591872	O	5.006936	-1.605753	-1.257355

Table 2.24 XYZ coordinates of the GS and TS structures of **2(Cl)**^a

							
C	1.868528	0.588443	-0.445928	C	2.007999	-0.011806	-0.129417
C	4.238666	2.026263	0.087167	C	4.704082	0.977723	0.032386
C	2.640858	0.329999	0.695232	C	2.316287	1.311166	0.270889
C	2.331181	1.590963	-1.312135	C	3.149034	-0.790263	-0.436044
C	3.496615	2.303176	-1.058154	C	4.452785	-0.330615	-0.363295
C	3.810441	1.035964	0.964856	C	3.626657	1.788953	0.347003
H	1.742152	1.814445	-2.195627	H	3.016344	-1.815206	-0.747295
H	3.820498	3.073516	-1.750085	H	5.267695	-1.000313	-0.617100
H	4.382840	0.795981	1.852609	H	3.786910	2.813335	0.659594
H	5.151400	2.572969	0.298916	H	5.715438	1.363446	0.097749
C	0.618362	-0.140571	-0.787260	C	0.652101	-0.653564	-0.258915
C	-1.749608	-1.449272	-1.478308	C	-1.869652	-1.934750	-0.533091
C	-0.461226	-0.181971	0.099239	C	-0.559290	0.003967	0.011128
C	0.494576	-0.762838	-2.035664	C	0.540305	-1.999552	-0.674462
C	-0.684447	-1.417118	-2.374954	C	-0.691073	-2.622274	-0.807753
C	-1.655094	-0.829928	-0.229446	C	-1.810874	-0.607897	-0.118399
H	-0.365126	0.308455	1.061266	H	-0.551077	1.026391	0.335996
H	1.329361	-0.745651	-2.728551	H	1.411341	-2.595800	-0.903620
H	-0.773883	-1.906772	-3.339718	H	-0.730275	-3.658338	-1.130093
H	-2.667435	-1.962456	-1.751925	H	-2.829802	-2.431573	-0.640883
Cl	2.191693	-0.957254	1.818211	Cl	1.123173	2.545589	0.732332
C	-2.822315	-0.863501	0.743689	C	-3.081262	0.163540	0.205987
H	-3.639127	-1.406832	0.253212	H	-3.928225	-0.491117	-0.033042
C	-2.459443	-1.628322	2.026948	C	-3.164481	0.497426	1.705130
H	-1.651140	-1.128831	2.568713	H	-2.342661	1.151174	2.010819
H	-2.125471	-2.644210	1.800672	H	-3.110639	-0.408693	2.314331
H	-3.319705	-1.695066	2.699964	H	-4.102815	1.009135	1.939740
C	-3.336804	0.548862	1.065628	C	-3.221740	1.430475	-0.653692
H	-2.571894	1.143691	1.573017	H	-2.420963	2.144957	-0.443818
H	-4.210855	0.504572	1.722329	H	-4.172931	1.932570	-0.452542
H	-3.623599	1.083296	0.156088	H	-3.182391	1.191912	-1.719623

^a The version with an *i*-Pr reporter group was used in consistent with the original work by A. Mazzanti and co-workers

Table 2.25 XYZ coordinates of the GS and TS structures of 2(CN)

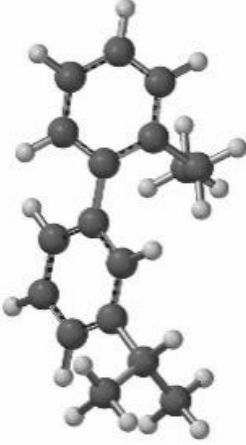
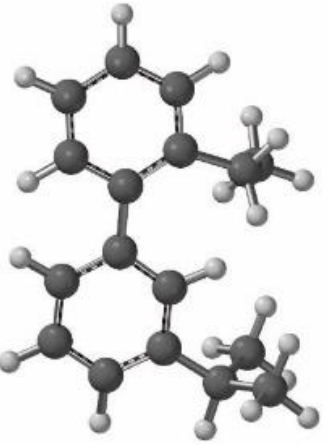
C	0.312497	-0.144595	3.148843	C	3.070381	-0.296461	0.046001
C	0.098053	1.080527	5.685431	C	5.654739	0.945161	0.035009
C	-0.668532	0.841556	3.400771	C	3.236711	1.100592	0.266793
C	1.167573	-0.494350	4.200933	C	4.262088	-1.011415	-0.178955
C	1.065633	0.104622	5.451599	C	5.517718	-0.421815	-0.185895
C	-0.765755	1.447343	4.662789	C	4.513118	1.694306	0.258438
H	1.936060	-1.237420	4.018622	H	4.218944	-2.075954	-0.356860
H	1.747775	-0.186256	6.243643	H	6.392090	-1.039093	-0.364836
H	-1.531648	2.195819	4.830616	H	4.584651	2.761665	0.433151
H	0.015652	1.551449	6.658675	H	6.630197	1.418050	0.033181
C	0.445360	-0.813953	1.831266	C	1.761613	-1.026961	0.041284
C	0.686458	-2.091891	-0.643881	C	-0.695814	-2.441680	0.030569
C	0.475119	-0.076485	0.639749	C	0.529420	-0.389987	0.256788
C	0.549871	-2.208463	1.760491	C	1.710882	-2.418706	-0.181354
C	0.672367	-2.842517	0.527938	C	0.507162	-3.109150	-0.187646
C	0.586107	-0.692337	-0.612042	C	-0.701261	-1.062822	0.260629
H	0.411882	1.004313	0.697308	H	0.505256	0.671611	0.434306
H	0.504121	-2.799243	2.669637	H	2.610075	-2.994613	-0.352897
H	0.742436	-3.925066	0.482548	H	0.510664	-4.180708	-0.363759
H	0.767700	-2.609593	-1.596783	H	-1.625314	-3.003830	0.020729
Si	0.522379	0.294243	-2.227233	Si	-2.281974	-0.062128	0.563390
C	-1.613763	1.224470	2.394756	C	-2.081038	0.899608	2.173871
N	-2.383152	1.554966	1.598632	H	-2.996279	1.438029	2.436766
C	0.320003	2.125657	-1.838332	H	-1.277099	1.637632	2.092968
H	1.180339	2.521154	-1.290151	H	-1.836764	0.235089	3.007541
H	-0.572459	2.311977	-1.234336	C	-3.765677	-1.223303	0.667328
H	0.225465	2.711641	-2.757247	H	-3.923715	-1.781646	-0.260093
C	-0.968827	-0.342618	-3.224453	H	-4.681565	-0.658453	0.864689
H	-0.782186	-1.414316	-3.388491	H	-3.653722	-1.950685	1.476955
C	2.109885	-0.007896	-3.204508	C	-2.493416	1.162792	-0.879254
H	2.992119	0.293955	-2.632675	H	-1.565306	1.751433	-0.899557
H	2.116227	0.553986	-4.143230	C	-3.662554	2.134609	-0.647389
H	2.228422	-1.066899	-3.454123	H	-4.621955	1.606654	-0.608260
C	-1.077221	0.329534	-4.604723	H	-3.733872	2.866478	-1.460262
H	-1.265547	1.404500	-4.513095	H	-3.554482	2.695854	0.284826
H	-1.908017	-0.091277	-5.182235	C	-2.630785	0.444936	-2.232120
H	-0.168641	0.202569	-5.200843	H	-3.558800	-0.135241	-2.282934
C	-2.284018	-0.206319	-2.439081	H	-1.801106	-0.243507	-2.417302
H	-2.242258	-0.719571	-1.475193	H	-2.655756	1.162149	-3.060261
H	-3.124306	-0.625976	-3.003702	C	2.181294	2.036552	0.514214
H	-2.523168	0.842763	-2.237889	N	1.401250	2.864960	0.720210

Table 2.26 XYZ coordinates of the GS and TS structures of **2**(COCH₃)^a

C	2.076878	-0.131289	-0.386035	C	1.871443	-0.646005	-0.106931
C	4.622989	1.040429	-0.610469	C	4.563900	0.220189	-0.451865
C	2.462194	0.903173	0.492021	C	2.210212	0.728882	-0.098935
C	2.995295	-0.577916	-1.344091	C	2.931327	-1.542855	-0.343117
C	4.259759	-0.009879	-1.452009	C	4.245529	-1.131670	-0.513487
C	3.723124	1.495810	0.344240	C	3.539323	1.136322	-0.253339
H	2.691181	-1.358304	-2.034622	H	2.730875	-2.603612	-0.408219
H	4.951696	-0.374281	-2.204824	H	5.017738	-1.872873	-0.692108
H	3.985254	2.311780	1.007872	H	3.767612	2.197437	-0.216140
H	5.601528	1.500470	-0.699386	H	5.588272	0.558034	-0.566087
C	0.708778	-0.711043	-0.373231	C	0.493533	-1.186377	0.135566
C	-1.877308	-1.766376	-0.266590	C	-2.097221	-2.242250	0.591454
C	-0.413375	0.121213	-0.478575	C	-0.643908	-0.370831	0.220462
C	0.515101	-2.090302	-0.247342	C	0.280954	-2.568520	0.313283
C	-0.774695	-2.610999	-0.187849	C	-0.989113	-3.083383	0.531369
C	-1.712356	-0.385207	-0.424420	C	-1.931299	-0.867173	0.443755
H	-0.264078	1.189954	-0.604155	H	-0.556689	0.698765	0.140244
H	1.374683	-2.747398	-0.163316	H	1.108218	-3.265231	0.305479
H	-0.920799	-3.680233	-0.069188	H	-1.114556	-4.153647	0.664377
H	-2.876090	-2.186907	-0.207172	H	-3.086946	-2.655145	0.764898
C	1.616808	1.417808	1.630307	C	1.239545	1.884986	0.024401
O	1.665503	2.591749	1.938172	O	1.029375	2.444369	1.075532
C	0.788233	0.450789	2.465118	C	0.652087	2.369466	-1.289869
H	1.006581	-0.598798	2.273312	H	0.285457	1.536723	-1.894858
H	-0.274501	0.614481	2.273484	H	1.444889	2.854728	-1.869170
H	0.973391	0.686269	3.515043	H	-0.145458	3.089394	-1.103777
C	-2.914641	0.542609	-0.506006	C	-3.116382	0.082172	0.527081
H	-2.537701	1.545616	-0.736840	H	-4.004490	-0.525297	0.739087
C	-3.643651	0.620142	0.847139	C	-2.954632	1.090514	1.677264
H	-2.971633	0.949736	1.643633	H	-2.089792	1.741627	1.521282
H	-4.044448	-0.356767	1.133844	H	-2.813373	0.579175	2.632670
H	-4.481309	1.322376	0.798214	H	-3.839242	1.729073	1.761160
C	-3.887851	0.144939	-1.627896	C	-3.358262	0.802818	-0.809910
H	-3.380775	0.086729	-2.594096	H	-2.514182	1.448963	-1.068202
H	-4.695410	0.877908	-1.710278	H	-4.251637	1.432186	-0.756474
H	-4.348356	-0.828277	-1.434008	H	-3.493108	0.089045	-1.626873

^a The version with an *i*-Pr reporter group was used in consistent with the original work by A. Mazzanti and co-workers

Table 2.27 XYZ coordinates of the GS and TS structures of $2(\text{CH}_2\text{CH}_3)^a$

							
C	-1.669536	0.894847	0.378416	C	0.460561	-0.934557	1.661380
C	-3.960862	2.404517	-0.195526	C	-0.493589	-2.735756	3.664986
C	-2.346119	0.696872	-0.842128	C	-0.917642	-1.301906	1.716241
C	-2.158358	1.838119	1.290396	C	1.290877	-1.493251	2.657890
C	-3.294610	2.591456	1.012127	C	0.844930	-2.369454	3.634778
C	-3.485927	1.464255	-1.104357	C	-1.342539	-2.193039	2.713537
H	-1.627053	1.983259	2.225852	H	2.339692	-1.239836	2.686520
H	-3.653636	3.321104	1.731004	H	1.545443	-2.760506	4.365796
H	-4.015079	1.314254	-2.042155	H	-2.393392	-2.467377	2.735247
H	-4.847616	2.985422	-0.430001	H	-0.873476	-3.422028	4.415043
C	-0.448017	0.119988	0.742255	C	1.110158	-0.020278	0.650641
C	1.863244	-1.284893	1.460018	C	2.404639	1.689115	-1.229429
C	0.764077	0.338897	0.077692	C	0.421167	0.631557	-0.384942
C	-0.485380	-0.817489	1.777316	C	2.501281	0.224811	0.691749
C	0.667513	-1.515895	2.131673	C	3.129048	1.057994	-0.221996
C	1.927972	-0.350317	0.419354	C	1.033000	1.473624	-1.319041
H	0.795390	1.075325	-0.720774	H	-0.636343	0.493773	-0.498252
H	-1.421134	-1.001909	2.295665	H	3.130112	-0.237680	1.438221
H	0.629758	-2.245563	2.934844	H	4.201109	1.212636	-0.147028
H	2.752453	-1.836609	1.747776	H	2.905286	2.337149	-1.942960
C	-1.937741	-0.377517	-1.829388	C	-2.028913	-0.862979	0.773126
H	-2.261162	-0.083426	-2.833553	H	-2.981989	-1.021814	1.286027
H	-0.851015	-0.472158	-1.870959	H	-2.000215	0.210951	0.586229
C	-2.544353	-1.746371	-1.479597	C	-2.061976	-1.657994	-0.543548
H	-3.636885	-1.699466	-1.463914	H	-2.253097	-2.714875	-0.340394
H	-2.210054	-2.080602	-0.493990	H	-1.116745	-1.599330	-1.086829
H	-2.248284	-2.505072	-2.210209	H	-2.855119	-1.294043	-1.203975
C	3.229796	-0.074400	-0.314419	C	0.206787	2.115154	-2.424563
H	3.007597	0.651821	-1.105328	H	0.882425	2.757027	-3.002570
C	4.272437	0.562627	0.618501	C	-0.364718	1.058049	-3.385708
H	5.184442	0.815566	0.069483	H	0.423679	0.416930	-3.787991
H	4.550049	-0.119167	1.428341	H	-0.878843	1.533268	-4.226786
H	3.885115	1.477193	1.074800	H	-1.089117	0.414446	-2.877540
C	3.785035	-1.338502	-0.990674	C	-0.916792	3.005452	-1.868255
H	4.690554	-1.109210	-1.560442	H	-0.525494	3.762694	-1.184335
H	3.053179	-1.774364	-1.675700	H	-1.657425	2.413337	-1.322264
H	4.044209	-2.102591	-0.252397	H	-1.442767	3.518738	-2.679004

^a The version with an *i*-Pr reporter group was used in consistent with the original work by A. Mazzanti and co-workers

Table 2.28 XYZ coordinates of the GS and TS structures of **2(i-Pr)**^a

C	1.065441	0.966775	-0.476385	C	0.216604	1.066245	1.589744
C	3.194404	2.711909	0.042743	C	2.314512	1.777472	3.395141
C	2.244589	0.466151	0.111587	C	1.570612	0.683376	1.324064
C	0.966107	2.334000	-0.769148	C	0.010216	1.833076	2.757517
C	2.017724	3.206037	-0.515032	C	1.013658	2.185905	3.645440
C	3.295642	1.360049	0.351600	C	2.565197	1.045258	2.244078
H	0.051310	2.703763	-1.221959	H	-0.979662	2.187401	3.000725
H	1.922047	4.259395	-0.758237	H	0.769847	2.777009	4.522475
H	4.212895	0.989542	0.797715	H	3.586731	0.745695	2.050664
H	4.029323	3.376852	0.240193	H	3.124132	2.029325	4.072446
C	-0.090994	0.084006	-0.809507	C	-1.012918	0.738910	0.765588
C	-2.268661	-1.562762	-1.422561	C	-3.394338	0.167537	-0.711361
C	-1.323812	0.256602	-0.173982	C	-2.294040	1.151816	1.202003
C	0.030346	-0.923086	-1.776351	C	-1.011276	0.017830	-0.442462
C	-1.052128	-1.740541	-2.078186	C	-2.162733	-0.272158	-1.183144
C	-2.424507	-0.558808	-0.464728	C	-3.448189	0.877517	0.484022
H	-1.416686	1.037397	0.574530	H	-2.425244	1.694188	2.125787
H	0.974443	-1.054882	-2.293552	H	-0.095017	-0.356809	-0.851994
H	-0.950742	-2.518749	-2.828506	H	-4.303302	-0.045956	-1.266806
H	-3.108555	-2.209533	-1.661228	C	2.032069	-0.131489	0.111801
C	2.392879	-0.998308	0.512683	H	1.484718	0.232201	-0.757264
H	1.429605	-1.489232	0.357345	C	1.735979	-1.630577	0.322287
C	2.733609	-1.150993	2.004766	H	0.703341	-1.815241	0.622417
H	1.988406	-0.654009	2.631012	H	2.380473	-2.024360	1.113405
H	3.710484	-0.723451	2.246235	H	1.932972	-2.205378	-0.588589
H	2.759321	-2.208422	2.285036	C	3.509728	0.048771	-0.272922
C	3.425041	-1.723913	-0.366150	H	3.779979	1.103911	-0.359298
H	3.149651	-1.679096	-1.422802	H	3.686757	-0.424011	-1.243035
H	3.503191	-2.778300	-0.083830	H	4.194021	-0.423172	0.436793
H	4.418627	-1.277123	-0.265789	H	-4.404099	1.220470	0.868342
C	-3.763807	-0.355087	0.226527	C	-2.062267	-1.070654	-2.476076
H	-4.426035	-1.163004	-0.107371	H	-3.075324	-1.142884	-2.889704
C	-3.653650	-0.457351	1.756485	C	-1.188160	-0.365599	-3.526367
H	-3.035628	0.345573	2.168166	H	-0.146010	-0.300590	-3.199476
H	-3.207201	-1.408203	2.058028	H	-1.539739	0.651212	-3.717703
H	-4.641390	-0.381638	2.220900	H	-1.200833	-0.913985	-4.473132
C	-4.413655	0.974182	-0.193520	C	-1.564219	-2.503492	-2.221376
H	-3.801855	1.827026	0.114861	H	-0.546010	-2.502903	-1.821962
H	-5.399950	1.088521	0.266764	H	-1.556032	-3.082568	-3.149966
H	-4.535829	1.028710	-1.278352	H	-2.202132	-3.023299	-1.502103

^a The version with an *i*-Pr reporter group was used in consistent with the original work by A. Mazzanti and co-workers

Table 2.29 XYZ coordinates of the GS and TS structures of **2(I)**^a

C	-0.770265	0.137964	2.062239	C	-0.582200	0.875207	1.714862
C	-1.120057	1.064734	4.696154	C	-1.048894	1.229199	4.530718
C	-1.718208	1.124075	2.364268	C	-0.290757	-0.137525	2.666472
C	0.000293	-0.367037	3.117529	C	-1.148095	2.043976	2.279791
C	-0.169152	0.085439	4.421673	C	-1.382086	2.231662	3.630341
C	-1.896145	1.590058	3.666496	C	-0.509724	0.052175	4.037098
H	0.733632	-1.135581	2.896244	H	-1.430431	2.855048	1.626721
H	0.436150	-0.329991	5.220323	H	-1.824346	3.161731	3.970883
H	-2.636698	2.352180	3.875753	H	-0.262827	-0.742013	4.729408
H	-1.264908	1.422982	5.709928	H	-1.212381	1.345771	5.596522
C	-0.584963	-0.402198	0.684773	C	-0.363572	0.867917	0.222389
C	-0.289807	-1.368248	-1.913498	C	0.040393	0.923525	-2.593853
C	0.361463	0.155899	-0.179408	C	-0.671107	2.008145	-0.554063
C	-1.377024	-1.462015	0.238346	C	0.154755	-0.222114	-0.488331
C	-1.225810	-1.941858	-1.059892	C	0.363968	-0.220378	-1.871630
C	0.520904	-0.310713	-1.485942	C	-0.475872	2.031048	-1.926731
H	0.964497	0.988074	0.170288	H	-1.063617	2.910010	-0.108817
H	-2.119626	-1.894490	0.900402	H	0.414264	-1.124493	0.031545
H	-1.847183	-2.760278	-1.410101	H	0.191382	0.952958	-3.669188
H	-0.194076	-1.744037	-2.927379	I	0.463900	-2.156585	2.322795
I	-2.948893	1.966435	0.806925	H	-0.728520	2.928833	-2.482417
C	1.516894	0.339208	-2.432159	C	0.926180	-1.453846	-2.562758
C	2.536066	-0.669959	-2.987144	H	1.048330	-1.203745	-3.623602
H	2.051428	-1.427113	-3.610628	C	-0.044201	-2.644916	-2.477329
H	3.060105	-1.190047	-2.181123	H	0.343367	-3.500861	-3.038506
H	3.282227	-0.163818	-3.606606	H	-1.025977	-2.388947	-2.884258
C	0.793645	1.074248	-3.574431	H	-0.186643	-2.965685	-1.441207
H	0.246352	0.371352	-4.210094	C	2.310953	-1.837683	-2.014450
H	1.509995	1.606093	-4.208019	H	2.731937	-2.675999	-2.577750
H	0.074293	1.799486	-3.185984	H	2.251820	-2.142283	-0.965645
H	2.074871	1.089155	-1.858934	H	3.010001	-1.000132	-2.079008

^a The version with an *i*-Pr reporter group was used in consistent with the original work by A. Mazzanti and co-workers

Table 2.30 XYZ coordinates of the GS and TS structures of 2(OCH³)

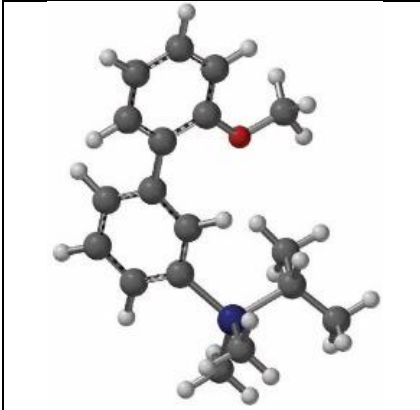
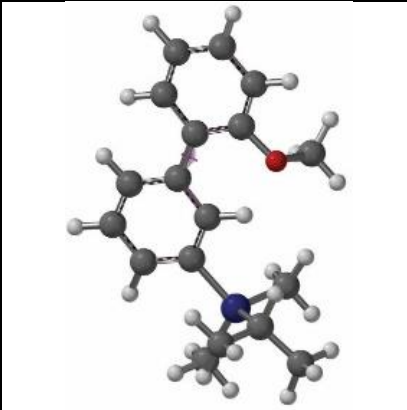
							
C	-2.362499	1.303259	-0.985225	C	0.512987	-1.530280	2.475142
C	-4.797376	0.632869	-2.224651	C	-0.519849	-2.214014	5.051893
C	-2.947179	0.030908	-0.785043	C	-0.767956	-1.109317	2.906082
C	-3.034590	2.208979	-1.809545	C	1.223098	-2.328495	3.396984
C	-4.240284	1.888331	-2.430635	C	0.730919	-2.671927	4.647451
C	-4.156474	-0.294083	-1.403459	C	-1.257367	-1.437223	4.171685
H	-2.582540	3.180252	-1.982116	H	2.194131	-2.718456	3.124806
H	-4.731890	2.610401	-3.073633	H	1.328852	-3.294065	5.305337
H	-4.609128	-1.264872	-1.248191	H	-2.232674	-1.050694	4.448353
H	-5.733992	0.361431	-2.701441	H	-0.915865	-2.459851	6.031609
C	-1.085775	1.686204	-0.331910	C	1.135665	-1.183962	1.156783
C	1.313311	2.391857	0.937569	C	2.347439	-0.594971	-1.344240
C	0.027261	0.839776	-0.363715	C	0.450520	-0.505393	0.133865
C	-0.967173	2.911970	0.334014	C	2.472327	-1.534396	0.878113
C	0.226465	3.264067	0.957405	C	3.063896	-1.249772	-0.345425
C	1.231402	1.159147	0.272803	C	1.024114	-0.207773	-1.111257
H	-0.074520	-0.108386	-0.879753	H	-0.555768	-0.173468	0.325093
H	-1.826057	3.573773	0.387077	H	3.082326	-2.028183	1.622805
H	0.300263	4.213059	1.479991	H	4.096493	-1.539603	-0.515782
H	2.224149	2.671746	1.459141	H	2.824304	-0.383252	-2.296678
Si	2.616332	-0.123361	0.274327	Si	-0.014737	0.742564	-2.371824
C	1.841581	-1.830008	0.638323	C	-1.572998	-0.248269	-2.770234
H	1.224355	-2.076905	-0.237602	H	-2.181194	0.241032	-3.536531
C	3.876300	0.319167	1.606521	H	-2.198529	-0.369341	-1.880381
H	4.337363	1.292395	1.412674	H	-1.323859	-1.249029	-3.134706
H	4.685928	-0.414685	1.654618	C	0.983350	1.045709	-3.944292
H	3.413105	0.367051	2.596317	H	1.912265	1.583746	-3.735612
C	3.450798	-0.175658	-1.418314	H	0.410674	1.646872	-4.657086
H	2.736834	-0.455916	-2.199105	H	1.245371	0.108726	-4.444764
C	0.918939	-1.811527	1.868594	C	-0.507382	2.401343	-1.578658
H	0.078004	-1.127084	1.736869	H	-1.030368	2.140324	-0.647183
H	1.458737	-1.505963	2.771748	C	-1.476946	3.213988	-2.454576
H	0.510367	-2.810409	2.065225	H	-1.024284	3.477469	-3.416908
C	2.915175	-2.923425	0.773705	H	-1.754437	4.154385	-1.964949
H	2.458218	-3.908947	0.919962	H	-2.402738	2.669970	-2.664214
H	3.563068	-2.740960	1.637374	C	0.725765	3.240005	-1.201304
H	3.556090	-2.992086	-0.110512	H	1.297346	3.531847	-2.089388
H	4.274203	-0.895794	-1.448322	H	1.401754	2.696177	-0.536303
H	3.858888	0.802728	-1.688631	H	0.432219	4.164087	-0.690595
O	-2.273836	-0.825954	0.038693	O	-1.593610	-0.328986	2.114527
C	-2.825349	-2.104095	0.311167	C	-2.677380	-1.036516	1.508246
H	-3.801437	-2.025534	0.802856	H	-2.312963	-1.804893	0.816538
H	-2.121065	-2.589072	0.984894	H	-3.258184	-0.296691	0.957013
H	-2.925968	-2.704647	-0.600062	H	-3.316730	-1.509422	2.260563

Table 2.31 XYZ coordinates of the GS and TS structures of 2(Ph)

C	-2.099092	1.523729	0.132090	C	0.921510	-1.185269	2.669199
C	-4.445591	1.807404	-1.399022	C	-0.258598	-2.379073	4.980092
C	-2.657285	0.401432	-0.524240	C	-0.469743	-1.478688	2.716162
C	-2.745542	2.761685	0.009809	C	1.660145	-1.506293	3.827491
C	-3.905994	2.909601	-0.742257	C	1.099471	-2.086922	4.955269
C	-3.820372	0.570824	-1.286099	C	-1.020185	-2.068588	3.863097
H	-2.305057	3.628371	0.491806	H	2.720269	-1.300478	3.862887
H	-4.380487	3.882326	-0.822057	H	1.728935	-2.310432	5.810742
H	-4.253221	-0.298190	-1.771861	H	-2.083938	-2.283475	3.861251
H	-5.350507	1.905089	-1.990327	H	-0.718935	-2.837067	5.849430
C	-0.835235	1.446050	0.912352	C	1.648911	-0.585152	1.496160
C	1.558182	1.285225	2.360508	C	3.068844	0.530080	-0.703519
C	0.290279	0.802760	0.385502	C	1.015937	-0.215252	0.297994
C	-0.736445	2.020078	2.184766	C	3.042531	-0.372884	1.538495
C	0.455406	1.942938	2.900635	C	3.734662	0.174474	0.466710
C	1.493531	0.695979	1.087929	C	1.688831	0.332032	-0.804297
H	0.204256	0.365595	-0.603383	H	-0.045709	-0.360193	0.201256
H	-1.603484	2.507437	2.620330	H	3.621488	-0.638870	2.411916
H	0.518862	2.390337	3.888075	H	4.807982	0.319020	0.547689
H	2.474639	1.231220	2.941433	H	3.629264	0.953330	-1.531984
Si	2.899658	-0.338531	0.364731	Si	0.697154	0.737703	-2.362572
C	2.635127	-2.129808	0.896963	C	-0.107376	-0.846291	-2.999904
H	3.438620	-2.787575	0.551726	H	-0.636311	-0.678681	-3.942783
H	1.689443	-2.509872	0.498876	H	-0.828573	-1.243942	-2.279896
H	2.585107	-2.212118	1.986984	H	0.643621	-1.621831	-3.177446
C	4.553532	0.300691	1.010828	C	1.842307	1.444006	-3.685995
H	4.721923	1.342082	0.722263	H	2.361066	2.345901	-3.348619
H	5.386592	-0.291032	0.620738	H	1.275088	1.710641	-4.582554
H	4.607374	0.248793	2.102375	H	2.603451	0.718558	-3.988427
C	2.844195	-0.231582	-1.536486	C	-0.661776	2.000661	-1.932514
H	1.874170	-0.650682	-1.838953	H	-1.289068	1.515690	-1.172325
C	3.940943	-1.095096	-2.184889	C	-1.556661	2.319553	-3.142871
H	4.941749	-0.736998	-1.920621	H	-0.983585	2.777862	-3.956240
H	3.869849	-1.064237	-3.278157	H	-2.346994	3.028973	-2.870703
H	3.874951	-2.144495	-1.883430	H	-2.044091	1.426366	-3.543991
C	2.919463	1.218477	-2.044670	C	-0.089219	3.289666	-1.319596
H	3.870876	1.685728	-1.769037	H	0.557479	3.818536	-2.028310
H	2.118352	1.841022	-1.637752	H	0.500929	3.089461	-0.421164
H	2.847298	1.258471	-3.137739	H	-0.892534	3.982371	-1.042649
C	-2.082775	-0.970635	-0.418622	C	-1.474950	-1.217872	1.633335
C	-0.992832	-3.555922	-0.236929	C	-3.438278	-0.763646	-0.324266
C	-1.768167	-1.699454	-1.572841	C	-2.167946	-0.002881	1.585430
C	-1.858155	-1.568003	0.828015	C	-1.798096	-2.211331	0.702225
C	-1.320342	-2.847476	0.918817	C	-2.767411	-1.984143	-0.272822
C	-1.223011	-2.978890	-1.483805	C	-3.137448	0.224930	0.611208
H	-1.931717	-1.248887	-2.546817	H	-1.929788	0.771770	2.306577
H	-2.100832	-1.018537	1.730371	H	-1.271897	-3.159693	0.733727
H	-1.151111	-3.291777	1.894369	H	-2.999382	-2.763185	-0.992168
H	-0.974433	-3.523193	-2.389664	H	-3.660069	1.175827	0.584225
H	-0.563736	-4.550250	-0.165321	H	-4.191312	-0.585276	-1.084951

Table 2.32 XYZ coordinates of the GS and TS structures of 2(SCH₃)

C	-2.664213	0.836849	-0.454769	C	0.427571	-1.504588	2.598581
C	-4.576139	1.021273	-2.517099	C	-0.504874	-2.362534	5.170033
C	-3.904735	0.174258	-0.341542	C	-0.927518	-1.308466	3.003924
C	-2.406489	1.561183	-1.627167	C	1.237476	-2.192694	3.528065
C	-3.346767	1.659507	-2.647864	C	0.802010	-2.613443	4.775174
C	-4.844386	0.276962	-1.372343	C	-1.350153	-1.722394	4.276021
H	-1.455190	2.075142	-1.718868	H	2.261467	-2.420822	3.272886
H	-3.120195	2.235782	-3.539284	H	1.489073	-3.137360	5.431736
H	-5.787034	-0.250356	-1.275346	H	-2.382920	-1.543158	4.551957
H	-5.318899	1.087518	-3.305802	H	-0.870207	-2.672920	6.143307
C	-1.607881	0.804215	0.592814	C	1.068880	-1.059999	1.310176
C	0.457544	0.856343	2.474070	C	2.319239	-0.264274	-1.121222
C	-0.324311	0.350118	0.266434	C	0.369562	-0.420629	0.273934
C	-1.847440	1.274291	1.886860	C	2.445708	-1.263162	1.076967
C	-0.816252	1.301396	2.820484	C	3.054559	-0.875415	-0.109367
C	0.731029	0.365075	1.187296	C	0.954728	-0.022304	-0.936437
H	-0.169465	-0.030937	-0.738563	H	-0.673468	-0.200328	0.423969
H	-2.838483	1.622893	2.152275	H	3.080444	-1.722894	1.821218
H	-1.007909	1.677141	3.820855	H	4.117276	-1.055781	-0.241314
H	1.245072	0.892331	3.222784	H	2.812863	0.021479	-2.045567
Si	2.456581	-0.278005	0.761087	Si	-0.116615	0.857321	-2.224144
C	2.799018	-1.797196	1.829232	C	-1.838691	0.082040	-2.235457
H	3.827896	-2.151988	1.719534	H	-2.455790	0.501304	-3.035521
H	2.130415	-2.624864	1.573405	H	-2.360354	0.264947	-1.291575
H	2.639326	-1.568996	2.887410	H	-1.792186	-1.000146	-2.385704
C	3.720396	1.064206	1.164152	C	0.683700	0.713253	-3.927079
H	3.518871	1.981876	0.605089	H	1.651132	1.221705	-3.963599
H	4.738340	0.742413	0.924196	H	0.051414	1.165897	-4.696384
H	3.701582	1.320632	2.227726	H	0.847337	-0.331127	-4.207947
C	2.559222	-0.729317	-1.085881	C	-0.264715	2.689780	-1.726908
H	1.694597	-1.373289	-1.300109	H	-0.697934	2.678670	-0.716621
C	3.829324	-1.539595	-1.399404	C	-1.213943	3.476202	-2.646463
H	4.735587	-0.969421	-1.167804	H	-0.842342	3.500400	-3.676898
H	3.877631	-1.797978	-2.463133	H	-1.309688	4.517031	-2.316761
H	3.873295	-2.473904	-0.833537	H	-2.219940	3.046962	-2.667752
C	2.477347	0.509034	-1.997482	C	1.111183	3.371809	-1.642444
H	3.345554	1.159532	-1.851825	H	1.586309	3.434279	-2.627735
H	1.585395	1.113942	-1.812255	H	1.794604	2.833092	-0.980101
H	2.464563	0.220470	-3.054593	H	1.022261	4.396655	-1.264741
S	-4.347307	-0.839756	1.078820	S	-2.277025	-0.554252	2.051338
C	-3.173288	-2.227936	0.849584	C	-2.696692	-1.934301	0.919083
H	-3.340931	-2.711764	-0.112691	H	-1.871357	-2.159791	0.242260
H	-3.367581	-2.940352	1.652431	H	-3.555004	-1.604918	0.331702
H	-2.143691	-1.878727	0.920824	H	-2.967380	-2.825128	1.485412

2.4.6 THROUGH-BOND (MESOMERIC) EFFECTS

One common concern regarding the origins of the large reductions in rotational barriers is the through-bond (mesomeric) effects of the R-groups. The argument is that the electron-withdrawing groups at the *ortho*- and/or *para*-position could reduce the net atomic charge of the imide carbonyl oxygen and/or enhance the double bond character of the C_{aryl}-N_{imide} bond in the TS, lowering the TS energy. However, this concern has been addressed by K. Kishikawa and co-workers in an earlier study on a similar succinimide rotor model.⁸⁰ Various electron-donating (NEt₂, OMe, and Me) and -withdrawing groups (F, Cl, CO₂Me, and NO₂) were introduced to the *para*-position of the *N*-(*o*-tolyl) ring of **3**(CH₃), and their rotational barriers were measured in both polar (toluene) and non-polar (DMSO) solvents. Rotational barriers ($\Delta G_{\text{exp}}^{\ddagger}$) were found to decrease only slightly (~ 1 kcal/mol) when electron-withdrawing groups (such as CO₂Me and NO₂) were introduced (Table 2.33). Furthermore, the rotational barriers of **3**(CH₃) were found to be little sensitive to the solvent environment, varying less than 1.7 kcal/mol from non-polar octane to polar DMSO. These results suggested the mesomeric effects of electron-withdrawing substituents exert *little* influence on the rotational barrier of *N*-phenylimide rotors.

To account for the possible bias between model systems, we also have examined the through-bond effects of *para*-substituent on the rotational barriers of our rotor **1**(CH₃). Specifically, three electron withdrawing groups (NO₂, CHO, and CN) with sizable Hammett σ_{para} values (0.78, 0.42, and 0.66) were introduced to the *para*-position of *N*-phenyl ring in rotor **1**(CH₃), which has an *ortho*-methyl group that does not form a stabilizing TS interaction. The idea was to test whether the through bond interactions of these EWGs could explain the large changes in barriers seen for rotors with ketone or

aldehyde groups in the *ortho*-position. The rotational barriers were calculated at the B3LYP-D3/6-311G* level of theory. Efficacy of such DFT calculation in evaluating the rotational barrier of rotors **1**(R) is demonstrated in section 2.4.5. The results shown in the Table 2.33 suggest the mesomeric effects are small (less than 1 kcal/mol) corroborating the statement: “The through-bond (mesomeric) effects of these groups are relatively small and thus cannot explain the large reductions in rotational barriers.” Note that similar calculations were able to replicate the large (5-10 kcal/mol) TS stabilization for rotors with strong electron-acceptor groups such as ketones, aldehydes, and nitriles in the *ortho*-position. Our calculations are also in good agreement with the previous study by Kishikawa and co-workers on the succinimide rotors **3**(CH₃) (Table 2.33), which showed the similar small influences (less than ~1 kcal/mol) of the *para*-substituents (NO₂ and CO₂Me) on the rotational barriers in both polar (DMSO) and non-polar (toluene) solvents.⁸⁰

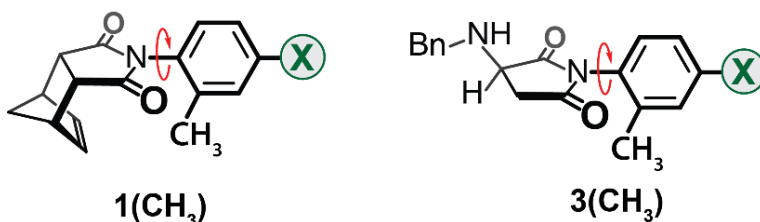


Figure 2.51 Structures of the para-substituted *N*-(*o*-tolyl)imide rotors **1**(CH₃) and **3**(CH₃)

Table 2.33 Experimental ($\Delta G_{\text{exp}}^{\ddagger}$) and calculated ($\Delta G_{\text{calc}}^{\ddagger}$) barriers for para-substituted **1**(CH₃) and **3**(CH₃)

X	σ_{para}	$\Delta G_{\text{exp}}^{\ddagger}$ of 3 (CH ₃)		$\Delta G_{\text{calc}}^{\ddagger}$ of 1 (CH ₃)
		in toluene	in DMSO	
H	0	19.3 kcal/mol	20.6 kcal/mol	20.2 kcal/mol
NO ₂	0.78	18.4 kcal/mol	19.6 kcal/mol	19.5 kcal/mol
CHO	0.42	N/A	N/A	19.8 kcal/mol
COOMe	0.49	18.6 kcal/mol	19.7 kcal/mol	N/A
CN	0.66	N/A	N/A	19.4 kcal/mol

2.4.7 INTRAMOLECULAR $n \rightarrow \sigma^*$ INTERACTIONS

One viable concern regarding the seemingly steric driven barrier of **1**(SCH₃) is the possible $n \rightarrow \sigma^*$ interactions between the carbonyl oxygen and *ortho*-thioether group in the TS.^{90,91} The calculated TS geometry (B3LYP-D3/6-311G*) of **1**(SCH₃) featured a short O-to-S distance of 2.59 Å (significantly shorter than the sum of vdW between O and S) and $\angle O \cdots S-C$ of $\sim 166^\circ$, which is indicative of a strong $n \rightarrow \sigma^*$ interaction (Figure 2.52). We then conducted the NBO analysis (ω B97M-V/6-311G*) on *this* TS geometry (**TS_I**) and found that the stabilizing $n \rightarrow \sigma^*$ interaction of 5.8 kcal/mol between the imide carbonyl oxygen and the sulfur of the *ortho*-SCH₃ group.

We then further investigated why the stabilizing $n \rightarrow \sigma^*$ interaction was *not* reflected in the observed or calculated rotational barriers for **1**(SCH₃). We hypothesized that the SCH₃ group had to orient itself into an unfavorable geometry to form the intramolecular $n \rightarrow \sigma^*$ interaction. Thus, the steric strain in the unfavorable geometry might have reduced or negated the stabilizing effects of the $n \rightarrow \sigma^*$ interaction. Support for this hypothesis was first provided by the identification of a second TS geometry (**TS_{II}**) that was very close in energy to **TS_I**, with an $n \rightarrow \sigma^*$ interaction (Figure 2.52). This second TS geometry (**TS_{II}**) is only slightly higher in energy (0.06 kcal/mol) but cannot accommodate the intramolecular $n \rightarrow \sigma^*$ interaction. The SCH₃ group in **TS_{II}** is perpendicular to the phenyl rotor and thus, the sulfur σ^* is not aligned with the donor lone-pair on the imide carbonyl oxygen. This relieves the steric strain present in **TS_I**, that arises from fixing the thioether group into a geometry to accommodate the $n \rightarrow \sigma^*$ interaction. Additional support for the absence of steric strain in **TS_{II}** and the presence of steric strain in the original TS (**TS_I**) was provided by a computational analysis of the phenyl rotor units of the two transition states (Figure

2.52). The imide stator unit of the two transition states were deleted, and the remaining phenylthioether units fixed in their TS geometries were capped with a hydrogen and subjected to single-point energy calculations. The phenylthioether of **TS_{II}** was 7.7 kcal/mol lower in energy than the phenylthioether of **TS_I** confirming that the transition state geometry with $n \rightarrow \sigma^*$ interaction (**TS_I**) contained significant adversarial steric strain.

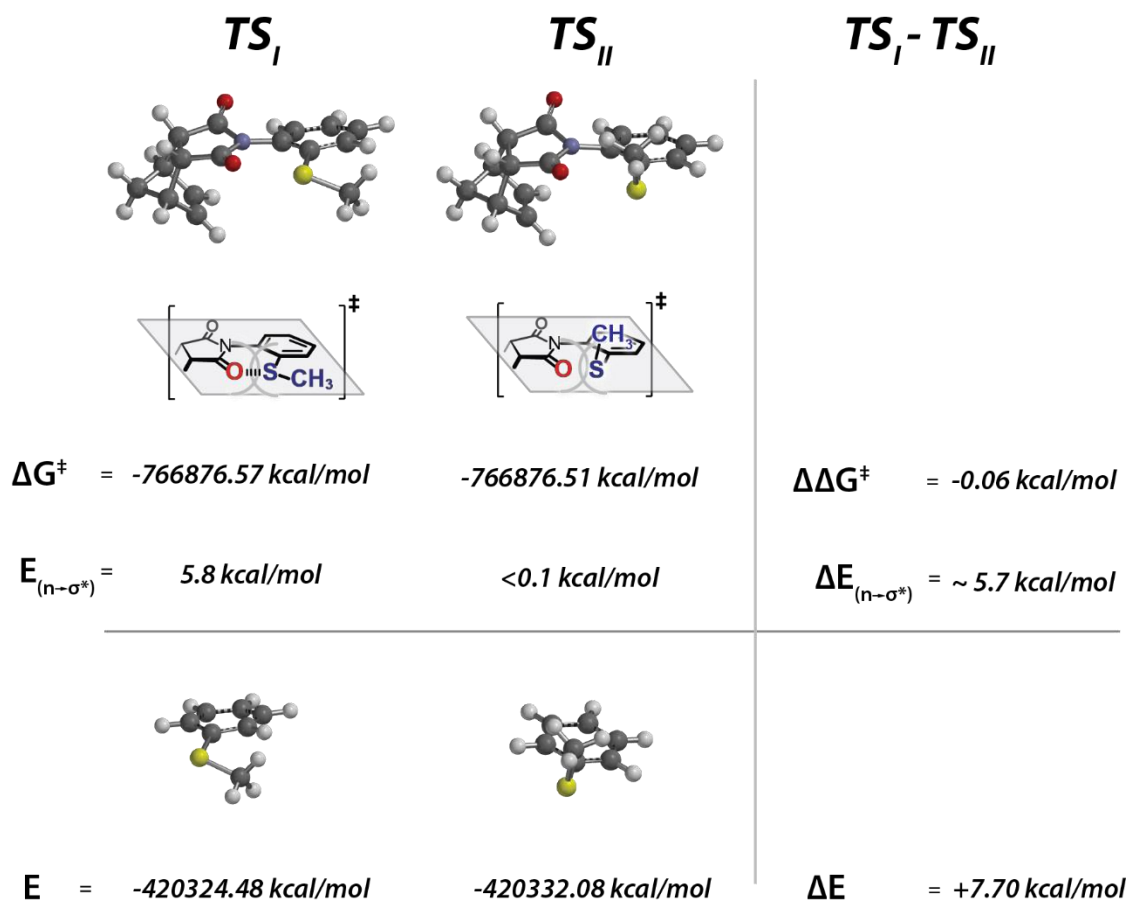


Figure 2.52 The two calculated TS geometries (**TS_I** and **TS_{II}**, B3LYP-D3/6-311G*) for **1(SCH₃)** and the corresponding conformations of the thioether motif (capped with hydrogen). The calculated $n \rightarrow \sigma^*$ stabilization ($E_{(n \rightarrow \sigma^*)}$, ω B97M-V/6-311G*) associated with **TS_I** and **TS_{II}** as well as the single point energies (E , B3LYP-D3/6-311G*) for the corresponding hydrogen-capped thioethers.

2.4.8 ASSOCIATED XYZ COORDINATES

Table 2.34 XYZ coordinates of the GS and TS structures of **1**(CH₃) with para-NO₂

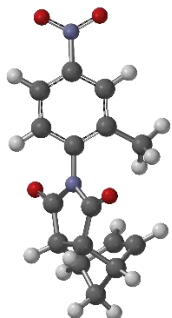
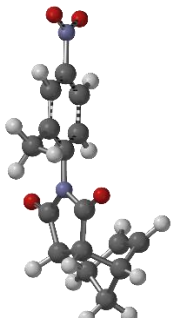
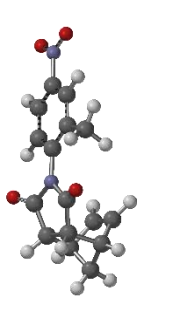
		
C -1.475794 -0.632852 -3.828684	C 0.248507 -0.762641 -3.929159	C 0.459020 -0.763390 -3.848533
C -0.676259 -0.570728 -1.200747	C 0.181188 -0.592720 -1.188274	C 0.390737 -0.775423 -1.036657
C -1.188926 0.587187 -3.232175	C -0.371316 -1.766024 -3.198796	C -0.564478 -1.392989 -3.166645
C -1.360715 -1.834914 -3.142254	C 0.855004 0.328037 -3.317617	C 1.461797 -0.116546 -3.152423
C -0.958141 -1.791042 -1.817203	C 0.813480 0.404556 -1.934788	C 1.413211 -0.133873 -1.770673
C -0.771561 0.642305 -1.901945	C -0.410951 -1.706185 -1.805597	C -0.654098 -1.420552 -1.768947
H -1.280295 1.491664 -3.818986	H -0.815906 -2.599729 -3.726357	H -1.334562 -1.875848 -3.752103
H -0.852456 -2.707945 -1.251646	H 1.274176 1.238123 -1.421588	H 2.215112 0.353126 -1.249706
N -0.264855 -0.599498 0.165234	N 0.148532 -0.447434 0.229414	N 0.479543 -0.634911 0.407624
C 0.860985 -1.328799 0.607780	C 1.306324 -0.216549 1.005167	C 1.596908 -0.025125 1.079652
C 0.952378 -1.163557 2.109891	C 0.859207 0.060832 2.425181	C 1.173752 0.391601 2.462696
C -0.257049 -0.290052 2.506379	C -0.682648 -0.014108 2.397454	C -0.196076 -0.245273 2.673923
C -0.977687 0.017811 1.210117	C -1.047813 -0.312268 0.959232	C -0.479283 -1.007866 1.405710
H 0.955900 -2.152398 2.572328	H 1.330011 -0.655729 3.100226	H 1.937369 0.086479 3.178217
O 1.594762 -1.957033 -0.110058	O 2.430011 -0.219092 0.574555	O 2.706227 0.138714 0.640103
O -1.980527 0.669640 1.064271	O -2.152899 -0.391763 0.485620	O -1.355475 -1.820770 1.299035
C 0.411046 0.952045 3.211161	C -1.123462 1.421115 2.878506	C -1.147465 0.998898 2.918620
H -0.282798 1.534793 3.813514	H -2.161966 1.472625 3.198715	H -2.099735 0.727588 3.369905
C -0.426235 1.963486 -1.273080	C -1.068820 -2.813114 -1.026410	C -1.899480 -2.130359 -1.271626
H -1.232063 2.295612 -0.615315	H -0.517453 -3.039987 -0.110903	H -1.671409 -2.985222 -0.641353
H -0.260716 2.725758 -2.035529	H -1.126520 -3.725469 -1.621940	H -2.468234 -2.482769 -2.132961
H 0.476530 1.883147 -0.664580	H -2.080081 -2.525122 -0.732272	H -2.550232 -1.476851 -0.694016
H -0.954595 -0.781522 3.187124	H -1.104200 -0.783334 3.047098	H -0.256510 -0.933389 3.517114
C 2.184189 -0.322324 2.617655	C 1.135451 1.536800 2.909014	C 0.881091 1.944303 2.604548
H 3.105994 -0.896989 2.679946	H 2.153914 1.695405 3.257272	H 1.779558 2.535849 2.767522
C 1.575052 0.227436 3.931777	C -0.018541 1.679788 3.931496	C -0.170927 1.877409 3.738534
H 1.244541 -0.554434 4.622698	H 0.009046 0.932996 4.731176	H 0.195025 1.394846 4.650071
H 2.243418 0.916159 4.451519	H -0.075090 2.679375 4.366196	H -0.588346 2.855570 3.983562
C 2.232011 0.952656 1.788718	C 0.638629 2.466247 1.810432	C -0.004915 2.354144 1.439519
H 2.934505 1.136616 0.985394	H 1.279556 2.990049 1.112179	H 0.334213 2.901436 0.568669
C 1.186534 1.707502 2.143015	C -0.696841 2.398394 1.792307	C -1.205293 1.795070 1.625794
H 0.861964 2.636186 1.691488	H -1.369360 2.848421 1.072924	H -2.042374 1.796931 0.938430
H -1.583812 -2.767990 -3.640669	H 1.335069 1.088060 -3.918079	H 2.262469 0.387287 -3.676133
N -1.902886 -0.656073 -5.246912	N 0.269858 -0.864589 -5.406696	N 0.465213 -0.772075 -5.323624
O -2.145377 -1.746416 -5.746707	O -0.270026 -1.836503 -5.918333	O 1.376604 -0.178980 -5.886704
O -1.987062 0.414563 -5.833520	O 0.825932 0.031537 -6.027353	O -0.438961 -1.367042 -5.897142

Table 2.35 XYZ coordinates of the GS and TS structures of **1**(CH₃) with para-CHO

C 0.616394 -1.487158 -3.856404	C 0.251780 -0.755336 -3.955399	C 0.455488 -0.736012 -3.876121
C 0.589124 -0.678214 -1.202055	C 0.181355 -0.590591 -1.186959	C 0.391483 -0.770109 -1.036673
C -0.586941 -1.165148 -3.224640	C -0.358040 -1.755353 -3.198971	C -0.559843 -1.365624 -3.168447
C 1.817228 -1.389392 -3.150064	C 0.846569 0.336095 -3.312534	C 1.452909 -0.095708 -3.147831
C 1.799867 -0.985403 -1.822744	C 0.807966 0.414564 -1.932629	C 1.412844 -0.118866 -1.768748
C -0.631575 -0.748298 -1.897789	C -0.403448 -1.705709 -1.804270	C -0.654458 -1.407339 -1.769768
H -1.500892 -1.237056 -3.805167	H -0.807240 -2.604473 -3.708472	H -1.346776 -1.853619 -3.736592
H 2.758278 -1.629416 -3.635982	H 1.322891 1.103503 -3.911677	H 2.254612 0.415289 -3.668771
H 2.720124 -0.899989 -1.258211	H 1.261384 1.249232 -1.413419	H 2.213336 0.366234 -1.243352
N 0.624189 -0.267559 0.166058	N 0.146442 -0.446353 0.232564	N 0.483616 -0.641306 0.410509
C 1.325727 0.875981 0.602710	C 1.303230 -0.223659 1.010540	C 1.603329 -0.040526 1.085148
C 1.164522 0.966774 2.106109	C 0.855447 0.057557 2.430033	C 1.179037 0.377667 2.467993
C 0.311581 -0.255711 2.506959	C -0.686211 -0.014409 2.400463	C -0.190012 -0.261498 2.678021
C 0.008530 -0.980040 1.210988	C -1.049328 -0.311884 0.961111	C -0.470660 -1.021864 1.407278
H 2.155064 0.985539 2.564818	H 1.324148 -0.658814 3.106783	H 1.942399 0.073934 3.184368
O 1.930609 1.626233 -0.118587	O 2.428879 -0.235941 0.584638	O 2.715634 0.114217 0.649887
O -0.642551 -1.984199 1.068239	O -2.155399 -0.392644 0.488879	O -1.343150 -1.839880 1.301217
H -0.935778 0.392498 3.220364	C -1.125106 1.421482 2.881137	C -1.143252 0.980774 2.924567
H -1.503485 -0.310078 3.827019	H -2.163765 1.474845 3.200732	H -2.094924 0.707586 3.376119
C -1.943349 -0.379289 -1.258920	C -1.057223 -2.815019 -1.024098	C -1.900504 -2.115738 -1.272030
H -2.280419 -1.172030 -0.587424	H -0.502791 -3.044074 -0.110770	H -1.675303 -2.978483 -0.651293
H -2.711329 -0.217456 -2.016849	H -1.115438 -3.727603 -1.620112	H -2.476711 -2.457210 -2.133682
H -1.851676 0.531547 -0.663941	H -2.068296 -2.530718 -0.725249	H -2.546508 -1.465603 -0.684922
H 0.817767 -0.946265 3.184217	H -1.110105 -0.782939 3.049489	H -0.249543 -0.951165 3.520023
C 0.306795 2.185011 2.617797	C 1.133851 1.533376 2.912943	C 0.883514 1.929682 2.610354
H 0.866778 3.116142 2.676018	H 2.152415 1.690573 3.261714	H 1.780887 2.522960 2.773444
C -0.224693 1.568079 3.935898	C -0.020465 1.678910 3.934722	C -0.168014 1.860471 3.744697
H 0.567203 1.249836 4.621299	H 0.005437 0.932229 4.734643	H 0.199195 1.377670 4.655625
H -0.919772 2.226027 4.460536	H -0.075659 2.678787 4.369108	H -0.586935 2.837781 3.990777
C -0.974623 2.212399 1.797546	C 0.639298 2.463100 1.813698	C -0.003518 2.338717 1.445983
H -1.174590 2.910667 0.994366	H 1.281338 2.983266 1.113779	H 0.335082 2.884154 0.573799
C -1.710915 1.155715 2.157481	C -0.696253 2.397701 1.794936	C -1.203001 1.777908 1.632559
H -2.636496 0.815715 1.711034	H -1.367100 2.846669 1.073346	H -2.039111 1.776694 0.944042
C 0.612025 -1.916530 -5.274553	C 0.271380 -0.857252 -5.432738	C 0.455085 -0.737761 -5.353678
H 1.615490 -2.148497 -5.694954	H -0.225456 -1.764361 -5.843721	H -0.397733 -1.281107 -5.819678
O -0.378210 -2.020434 -5.961173	O 0.773512 -0.044757 -6.174239	O 1.291508 -0.202321 -6.044827

Table 2.36 XYZ coordinates of the GS and TS structures of **1**(CH₃) with para-CN

C	0.651177	-1.542870	-4.008836	C	0.806189	0.257783	-4.119595	C	0.468413	-0.775299	-4.045139
C	0.607695	-0.730172	-1.354074	C	0.629239	0.203082	-1.349076	C	0.398629	-0.784651	-1.202796
C	-0.559160	-1.228902	-3.381624	C	1.801852	-0.361613	-3.356794	C	-0.554105	-1.399838	-3.334492
C	1.853666	-1.434118	-3.299335	C	-0.278832	0.873604	-3.482928	C	1.466983	-0.131578	-3.319880
C	1.821154	-1.029033	-1.974687	C	-0.359327	0.839957	-2.101315	C	1.418987	-0.145180	-1.938772
C	-0.606762	-0.809227	-2.053031	C	1.739374	-0.396630	-1.963630	C	-0.645022	-1.427270	-1.936628
H	-1.480815	-1.303966	-3.948159	H	2.641788	-0.824383	-3.862948	H	-1.336908	-1.888894	-3.901478
H	2.794233	-1.667013	-3.783430	H	-1.049038	1.360552	-4.068945	H	2.279757	0.376723	-3.824866
H	2.740700	-0.936562	-1.410659	H	-1.192351	1.307104	-1.592683	H	2.221325	0.342757	-1.419122
N	0.637603	-0.321062	0.013269	N	0.472273	0.168462	0.068667	N	0.490595	-0.645942	0.244019
C	1.342149	0.820276	0.453131	C	0.221400	1.323144	0.843028	C	1.608995	-0.037231	0.913211
C	1.177830	0.908922	1.955902	C	-0.048541	0.874239	2.264035	C	1.195893	0.362792	2.304249
C	0.319372	-0.311220	2.353150	C	0.037657	-0.666868	2.236048	C	-0.169102	-0.281740	2.519747
C	0.016434	-1.032872	1.055979	C	0.329030	-1.028982	0.795353	C	-0.463550	-1.025167	1.242380
H	2.167325	0.923599	2.416890	H	0.669204	1.349657	2.934819	H	1.967070	0.052465	3.009394
O	1.949172	1.569002	-0.267601	O	0.203730	2.446754	0.412015	O	2.714532	0.139051	0.467876
O	-0.637908	-2.034176	0.908879	O	0.399156	-2.133623	0.318936	O	-1.348111	-1.828915	1.130986
C	-0.927115	0.340482	3.064896	C	-1.388492	-1.118702	2.731597	C	-1.122483	0.954549	2.792579
H	-1.498535	-0.360790	3.669492	H	-1.428599	-2.156913	3.054442	H	-2.068442	0.673473	3.251032
C	-1.924962	-0.449452	-1.422540	C	2.833581	-1.067576	-1.178421	C	-1.891370	-2.135335	-1.438959
H	-2.266099	-1.251178	-0.764084	H	3.058591	-0.520813	-0.259782	H	-1.664152	-2.991116	-0.809565
H	-2.687617	-0.276733	-2.183581	H	3.750228	-1.134224	-1.766398	H	-2.463244	-2.486759	-2.299003
H	-1.837468	0.452965	-0.814692	H	2.530973	-2.075957	-0.888939	H	-2.539945	-1.481022	-0.859832
H	0.821916	-1.004389	3.030426	H	0.816860	-1.081154	2.878690	H	-0.218412	-0.983279	3.352580
C	0.323173	2.129482	2.467400	C	-1.522175	1.139425	2.759284	C	0.898583	1.912213	2.467622
H	0.886491	3.058396	2.528011	H	-1.686448	2.157037	3.107478	H	1.796267	2.505751	2.627795
C	-0.213028	1.512425	3.783524	C	-1.646189	-0.013959	3.785257	C	-0.140488	1.827096	3.612334
H	0.576379	1.190422	4.469958	H	-0.891772	0.021246	4.577537	H	0.237738	1.334837	4.513614
H	-0.906708	2.172057	4.307781	H	-2.640826	-0.077936	4.230103	H	-0.559074	2.800384	3.874215
C	-0.956604	2.162739	1.644729	C	-2.457782	0.632928	1.670254	C	-0.002060	2.332331	1.317546
H	-1.153322	2.864545	0.843806	H	-2.994152	1.268166	0.976383	H	0.325231	2.890900	0.449363
C	-1.697464	1.108156	2.001635	C	-2.379862	-0.702024	1.654229	C	-1.198206	1.766517	1.510518
H	-2.625035	0.773690	1.555030	H	-2.832623	-1.379732	0.941476	H	-2.042767	1.772761	0.832454
C	0.650580	-1.962726	-5.376549	C	0.895233	0.259887	-5.547443	C	0.471236	-0.791659	-5.473835
N	0.641553	-2.300695	-6.481009	N	0.960652	0.258062	-6.700733	N	0.467207	-0.803724	-6.629149

Table 2.37 XYZ coordinates of the TSII of **1**(SCH₃) and two thioether conformers.

H 0.656510 -0.509630 -5.320196	H 0.823971 0.808697 -2.877963	H 1.290718 0.063395 -2.336509
C 0.577833 -0.479015 -4.238796	C 0.672190 0.831738 -1.803382	C 1.161911 0.248201 -1.275097
C 0.364050 -0.483144 -1.395809	C 0.268769 0.897695 0.953219	C 0.860083 0.568829 1.523488
C -0.405297 -1.203107 -3.585773	C -0.431904 0.188270 -1.248153	C 0.182590 -0.432231 -0.570927
C 1.417801 0.311918 -3.471257	C 1.575421 1.506728 -0.984208	C 1.936159 1.177754 -0.602355
C 1.307403 0.302407 -2.089955	C 1.371854 1.539779 0.393932	C 1.784119 1.313760 0.768126
C -0.574857 -1.208001 -2.188972	C -0.636227 0.213979 0.134104	C -0.066733 -0.251434 0.801868
H -1.116032 -1.776263 -4.168553	H -1.141432 -0.331390 -1.883105	H -0.433252 -1.126336 -1.123100
H 2.170016 0.941939 -3.934246	H 2.432338 2.010118 -1.420240	H 2.673899 1.781173 -1.119662
H 1.999350 0.912365 -1.538454	H 2.068834 2.070444 1.034566	H 2.436045 2.004262 1.271237
N 0.439107 -0.396843 0.049458	S -2.070303 -0.601769 0.852421	S -1.611224 -0.968585 1.417006
C 1.583829 0.138902 0.726617	C -1.352459 -2.264116 1.154624	C -2.567587 -1.232219 -0.123740
C 1.176625 0.549720 2.117242	H -0.506043 -2.199287 1.838778	H -2.597849 -0.337463 -0.747030
C -0.213525 -0.051086 2.321858	H -2.136389 -2.870061 1.611289	H -3.576511 -1.445373 0.235340
C -0.495468 -0.817103 1.052630	H -1.037991 -2.729313 0.219976	H -2.230807 -2.088820 -0.709799
H 1.930197 0.214139 2.829973	H 0.099370 0.928488 2.024142	H 0.758440 0.725085 2.591153
O 2.698217 0.250560 0.282073		
O -1.322073 -1.679566 0.954216		
C -1.129086 1.216783 2.568225		
H -2.092203 0.969381 3.010644		
H -0.293276 -0.734948 3.166875		
C 0.926275 2.109212 2.278196		
H 1.840814 2.672614 2.453305		
C -0.134475 2.059016 3.405116		
H 0.211351 1.555498 4.313115		
H -0.525923 3.046027 3.658045		
C 0.057860 2.560526 1.114719		
H 0.415599 3.108020 0.251276		
C -1.157463 2.029642 1.285571		
H -1.987164 2.053035 0.589740		
S -2.140673 -1.984520 -1.732059		
C -1.605850 -3.667672 -1.261581		
H -1.044408 -3.640148 -0.330224		
H -2.517263 -4.249339 -1.112794		
H -1.017800 -4.121318 -2.060223		

2.4.9 ADDITIONAL TABLES AND FIGURES

Table 2.38 Experimentally measured ($\Delta G_{\text{exp}}^{\ddagger}$, kcal/mol) and calculated ($\Delta G_{\text{calc}}^{\ddagger}$, kcal/mol) rotational barriers for rotor **1** with various R-groups at 25 °C, experimentally quantified TS stabilization ($\Delta\Delta G_{\text{exp}}^{\ddagger}$, kcal/mol)^c, calculated TS NBO energies (E_{NBO} , kcal/mol) between the imide carbonyl oxygens and R-groups, and natural bond orbital atomic charges (NBO charge, a.u.) for the accepting carbon atoms as a phenyl substituent.

R-group	$\Delta G_{\text{exp}}^{\ddagger a}$	$\Delta G_{\text{calc}}^{\ddagger b}$	$\Delta\Delta G_{\text{exp}}^{\ddagger c}$	E_{NBO}^d	NBO charge ^e
COCH ₃	13.9	15.6	-8.2	-18.3	0.596
COPh	12.9	15.1	-9.7	-17.1	0.574
CHO	15.2	16.2	-8.4	-16.4	0.439
C(CH ₂)CH ₃	19.5	19.5	-3.3	-5.7	-0.014
Ph	21.5	20.8	-0.3	-3.1	-0.047
CN	15.4	16.7	-5.3	-9.0	0.289
CCH	18.8	19.6	-1.9	-5.3	-0.022
CH ₃	21.7	20.2	-	-	-
CH ₂ CH ₃	22.0	22.4	-	-	-
CH(CH ₃) ₂	23.6	24.4	-	-	-
OCH ₃	20.2	19.5	-	-	-
SCH ₃	22.5	24.8	-	-	-
Cl	22.1	22.5	-	-	-
Br	23.1	24.2	-	-	-
I	24.2	25.1	-	-	-
CF ₃	23.7	25.6	-	-	-

^aError in the EXSY rotational barriers was ± 0.1 kcal/mol;⁹² ^bB3LYP-D3/6-311G*; ^cMeasured as the difference in $\Delta G_{\text{exp}}^{\ddagger}$ and the steric trendline (Figure 1) at the corresponding B-value; ^d ω B97M-V/6-311G*, ^eNatural bond orbital charge or natural charge;

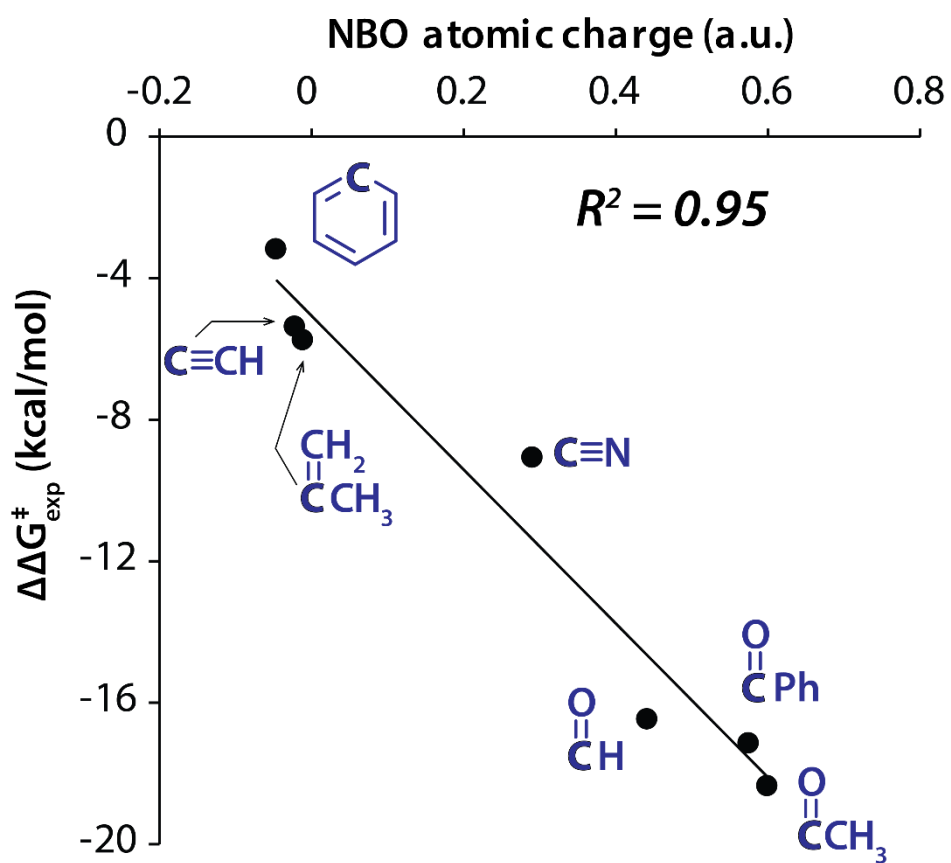


Figure 2.53 Correlation plot of the measured TS stabilization ($\Delta\Delta G_{\text{exp}}^{\ddagger}$) and the calculated NBO atomic charges (B3LYP-D3/6-311G*) of the first carbon atom of the *ortho* R-groups.

CHAPTER 3 ORIGINS OF A LARGE TRANSITION STATE STABILIZATION BY A
WEAK HYDROGEN BOND

3.1 ABSTRACT

A series of molecular rotors were designed to measure and study the transition stabilizing effect of a weak neutral hydrogen bond. The rotors formed an intramolecular hydrogen bond in the planar transition state, which dramatically lowered the rotational barrier and speed up the rate of rotation in comparison to similar rotors which could not form the TS hydrogen bonds. The magnitude of the TS stabilization (9.9 kcal/mol) was significantly larger than predicted by the independently measured hydrogen bond strength (1.5 kcal/mol) between a phenol donor and an imide or amide carbonyl acceptor. Substituent experimental and computational studies attributed the TS stabilization to the rigid constrained environment and preorganization of the interacting groups in the TS. The enhanced TS effects for the hydrogen bond were attributed to the reduction in the large steric term of the hydrogen bond due to preorganization and rigidity of the rotor framework. This study demonstrates that the insertion of a hydrogen bonding proton can lead to large TS stabilizing effects which has potential applications in catalyst design and mechanistic studies of enzyme catalysis.

3.2 MAIN TEXT

Hydrogen bonds are key contributors to the large rate accelerations observed in reactions catalyzed by enzyme and synthetic organocatalysts. However, measuring the stabilizing effect of hydrogen bonds in transition states (TS) is challenging due to the instability and crowded structure of transition states. In this work, we designed a series of molecular rotors to measure and study the TS stabilizing effects of a weak neutral hydrogen bond. Molecular rotor **1** (Figure 3.1A) consists of an *N*-phenyl rotor attached to a cyclic imide stator via a C-N single bond. Substituents on the *ortho*-position of the rotor are forced

into close proximity to the imide carbonyls in the planar transition state. The rotational barriers for molecular rotors are strongly correlated with the steric interactions formed in the TS, leading to the development of new steric parameters. The exception are rotors with substituents that can form stabilizing interactions such as hydrogen bonds in the transition state. These hydrogen bond accelerated rotors have been used as molecular devices where modulation of the hydrogen bonding interaction provides a mechanism to control the rate of rotation. In the course of studying these molecular devices, we observed that the hydrogen bonding TS stabilizing effects were significantly greater than expected. For example, the TS stabilization by the phenol hydrogen bond in rotor **1** was estimated to be 9.9 kcal/mol from the difference in rotational barriers of rotor **1** (10.9 kcal/mol) and control rotor **2** (20.8 kcal/mol) which as an ortho-OCH₃ group that cannot form a TS hydrogen bond. The magnitude of the TS stabilization was surprising given the thermodynamic strength of the phenol•••carbonyl hydrogen bond in similar solvent systems was 1.0 to 3.0 kcal/mol.⁹³ The ability of hydrogen bonds to have amplified effects in TS could have applications in the design of new hydrogen bonding catalysts and in enzyme catalysis. Therefore, we examined the origins of the hydrogen bonding TS stabilization in rotor **1** experimentally and computationally via substituted derivatives which varied the hydrogen bond strength.

The use of molecular rotors to study transition states has a number of unique advantages. First, bond rotation is a unimolecular process which reduces the number of experimental variables and simplifies kinetic analysis. The rates of bond rotation can be easily and accurately measured by dynamic NMR experiments including line shape, exchange, or coalescence experiments conducted over a range of temperatures. Second, the

TS for the bond rotation process is very simple with minimal degrees of freedom, enabling accurate computational modeling of the TS geometries and energies. The rigid framework fixes the position of the interacting groups into close proximity in the planar TS mimicking the compact structure and short atom-atom distance generally found in more complex bond forming or bond breaking transition states. Finally, hydrogen bond strengths can easily be modulated using electron withdrawing substituents on the phenyl rotor ($X = \text{H}, p\text{-Cl}, m\text{-Cl}, p\text{-CN}, m\text{-NO}_2, p\text{-NO}_2$), which increase the acidity and hydrogen bond donating ability of the phenol proton.

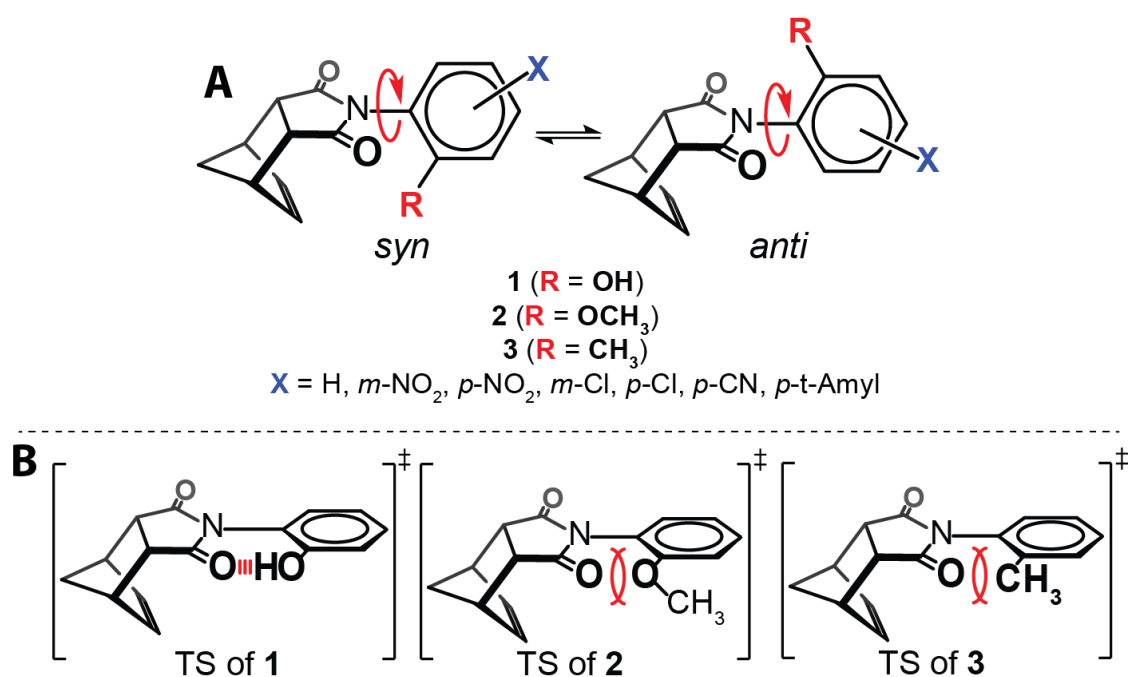


Figure 3.1 (A) The *syn-anti* conformational equilibrium of molecular rotors **1**, **2**, and **3** designed to isolate and measure the TS stabilization of the intramolecular hydrogen bond via changes in the rate of rotation. (B) Representations of the TS geometries and the non-covalent and steric interactions formed in the TS

Sternhill, Mazzanti, Rousell, and others have shown that the rotational barrier of molecular rotors are primarily governed by the steric size of the *ortho*-substituents that are adjacent to the rotatable bond.^{16–21,94} An exception are rotors capable of forming stabilizing non-covalent interactions in the planar transition state such as hydrogen bonding rotor **1**. Thus, our first approach to isolating the stabilizing effects of the TS hydrogen bond was to compare the rotational barrier for rotor **1** to the rotational barriers for rotors **2** and **3** which have similar sized groups *ortho*-groups (Figure 3.1B). Rotor **1** has an *ortho*-OH group that could form an intramolecular TS hydrogen bond with the imide carbonyl oxygen. Whereas rotors **2** and **3** have *ortho*-OCH₃, and *ortho*-CH₃ groups that lack hydrogen bond donating groups and cannot form hydrogen bonds. The similarity in the steric size of the *ortho*-groups was assessed using the B-value steric parameter developed by Mazzanti. The B-values for the OCH₃, OH, and CH₃ groups are fairly similar at 5.6, 5.4, and 7.4 kcal/mol, respectively.^{17,20} Mazzanti's steric parameter is particularly relevant to this study, because the B-value parameters are directly measured from the rotational barrier of a very similar biphenyl rotor with a varying *ortho*-substituents.

Rotors **1**, **2**, and **3** were synthesized in one step via the thermal condensation of the appropriately substituted aniline with *cis*-5-norbornene-*endo*-2,3-dicarboxylic anhydride. The large difference in rotational barriers of hydrogen bonding rotor **1** versus non-hydrogen bonding control rotors **2** and **3** was immediately evident by the large difference in their coalescence temperatures. At room temperature (23 °C), rotor **1** was in fast exchange in the ¹H NMR spectra as the peaks for the *syn* and *anti*-rotamers were coalesced into one set of peaks. In contrast, rotors **2** and **3** were in slow exchange at 23 °C, as the *syn* and *anti*-rotamers displayed separate sets of peaks. The precise barriers were measured by

¹H NMR variable temperature lineshape analysis. Non-hydrogen bonding rotors **2** and **3** had high rotational barriers of 20.8 kcal/mol and 21.7 kcal/mol. The similarity in barrier of the non-hydrogen bonding rotors confirms that their ortho-groups are of similar size as predicted by their B-values. In contrast, hydrogen bonding rotor **1** had a significantly lower rotational barrier of 10.9 kcal/mol. To confirm the large difference in rotational barriers of the hydrogen bonding and non-hydrogen bonding rotors, the coalescence temperatures (T_C) of **1** and **2** were measured. A similarly large difference in T_C was observed with a much lower T_C for **1** (-55 °C) than for **2** (113 °C), which was consistent with rotational barrier measurements. Rotor **2** was selected as the control rotor due to the similarity in steric size of the OCH₃ and the OH groups. Thus, the magnitude of the hydrogen bonding stabilization was estimated from the difference in barriers of **2** and **1**, which was 9.9 kcal/mol.

Alternative explanations for the large TS stabilization in **1** were explored. First, the possibility that the different solvent systems used in the NMR studies was examined. Different solvents were required because of the large differences in the coalescence temperatures of the hydrogen bonding and non-hydrogen bonding rotors. Rotor **1** had a low coalescence temperature and thus a solvent such as CD₂Cl₂ with a low freezing point (-95 °C) was required. Rotors **2** and **3** had much higher coalescence temperatures. Therefore, TCE-d₂, which has a much higher boiling point (146.5 °C), was used. Previous studies of hydrogen bond accelerated rotors established that solvents or guests that can form hydrogen bonds and disrupt the intramolecular hydrogen bonding will alter the rotational barriers.^{9,10} However, CD₂Cl₂ and TCE-d₂ have very similar hydrogen bonding abilities and thus, significant differences due to solvent interactions or solvent environment are expected. Both solvents are poor hydrogen bonding donors and acceptors.

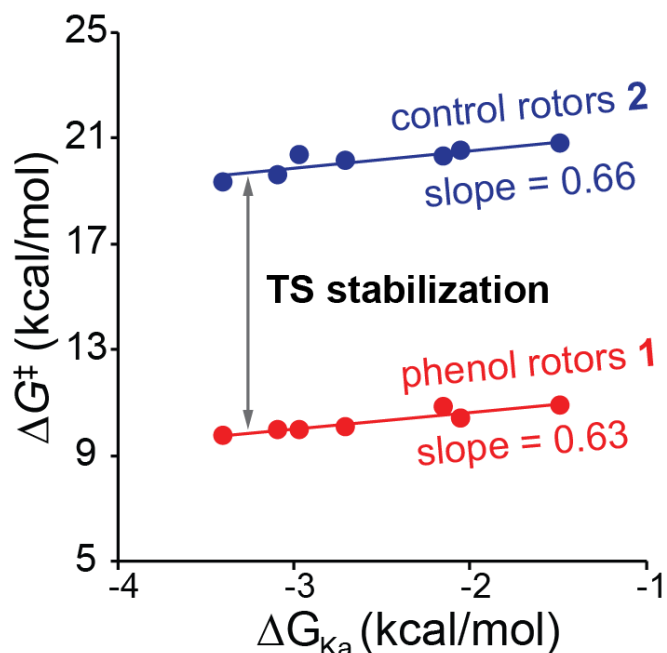


Figure 3.2 ^1H NMR measured rotational barriers (ΔG^\ddagger) of substituted rotors **1**, **2** (left to right, X = *p*-NO₂, *m*-NO₂, *p*-CN, *m*-Cl, *p*-*t*-Amyl, *p*-Cl, and H) plotted against the measured association energies of the analogously substituted phenol•NMP complexes in CD₂Cl₂. The difference in the rotational barrier between **1** and **2** corresponds to the TS stabilization of the hydrogen bond.

Next, the possibility that the difference in barriers was due to the presence or absence of repulsive lone pair-lone pair (lp-lp) interactions was explored. The high barrier of **2** could be due to enhanced repulsion between the lone pairs on the carbonyl oxygen and the lone pairs on the *ortho*-OCH₃ group. The formation of the intramolecular hydrogen bond in **1** between the carbonyl oxygen and the *ortho*-group could eliminate these repulsive lp-lp interactions leading to a significantly lower barrier. However, non-hydrogen bonding control rotor **3** has a very similar barrier to rotor **2** which can form lp-lp interactions even though the *ortho*-CH₃ group in **3** lacks lone pairs and cannot form lp-lp interactions. Thus, the higher barrier of rotor **2** is not due to the presence of destabilizing lp-lp interactions, and the lower barrier of rotor **1** is not due to the absence of lp-lp interactions. The above

analyses rule out alternative explanations leaving the differences in intramolecular TS hydrogen bonding as the most likely explanation for large TS stabilization in rotor **1**.

To study the role of hydrogen bonding in stabilizing the TS of rotor **1**, the strength of the phenol hydrogen was systematically varied and the resulting changes in the rotational barriers were measured. Electron donating and withdrawing substituents ($X = \text{H}, p\text{-Cl}, p\text{-}t\text{-Amyl}, m\text{-Cl}, p\text{-CN}, m\text{-NO}_2, p\text{-NO}_2$) were placed on the *para*- and *meta*-positions of rotor **1** to vary the acidity and hydrogen bonding ability of the phenolic OH proton (Figure 3.2). An analogous series of similarly substituted control rotors **2** were synthesized and their rotational barriers measured to assess the ability of the substituent to modulate the rotational barrier in the absence of the hydrogen bond. The strength of the phenol•••carbonyl hydrogen bond and the ability to modulate the interaction strengths via substituents was assessed by measuring the association energies of similarly substituted bimolecular hydrogen bonding complexes. The bimolecular phenol•NMP complex forms a similar phenol•••carbonyl hydrogen bond as rotor **1** (Figure 3.3). The association energies (ΔG_{Ka}) were measured via ^1H NMR titration in CD_2Cl_2 (Figure 3.4). The hydrogen bond in the unsubstituted phenol•NMP complex had an association energy of 1.5 kcal/mol, which was consistent with previous reports of intermolecular phenol•carbonyl hydrogen bonds (1-3 kcal/mol) in chlorinated organic solvents.⁹³ More importantly, the phenol•NMP hydrogen bond was 6 times smaller than the TS hydrogen bond stabilization of unsubstituted phenol rotor **1** (9.9 kcal/mol). Part of the difference can be attributed to the intramolecular versus intermolecular hydrogen bonds in rotor **1** and the phenol•NMP. However, even when the entropic penalty of 1.4 kcal/mol for intermolecular versus an

intramolecular interaction is taken into account, a significant difference remains between the strength of the hydrogen bonding interaction and the observed TS stabilization.⁹⁵

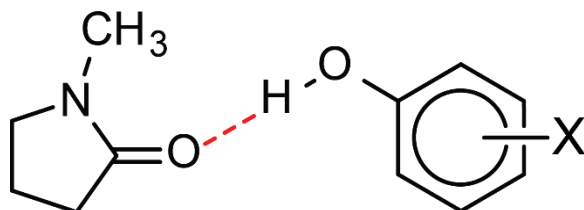


Figure 3.3 The bimolecular complexes between *N*-methyl pyrrolidone (NMP) and substituted phenols used to independently measure the phenol-carbonyl hydrogen bond strengths.

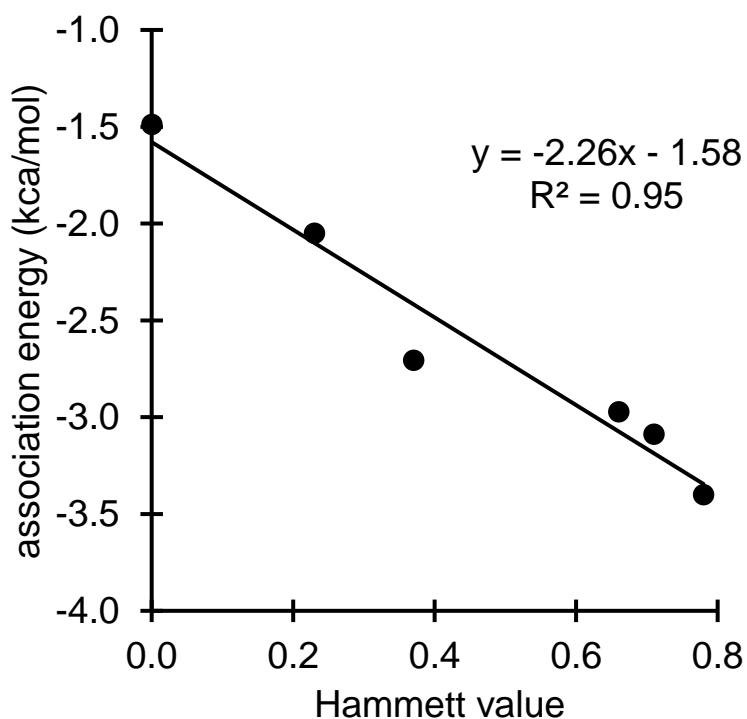


Figure 3.4 Hammett plot correlating the intermolecular hydrogen bond strength

Substituent studies of the phenol•NMP complex also quantified the ability of the substituents to modulate the hydrogen bond strengths. The hydrogen bond strengths varied as expected from 1.5 to 3.4 kcal/mol. Electron withdrawing groups (NO₂, CN, Cl)

systematically increased the acidity of the phenol proton depending the electron withdrawing strength and substitution position. The electrostatic effects of the phenolic substituents were verified by the linear free-energy relationship (Figure 3.4) between the measured association constants and the electrostatic Hammett *meta*- or *para*-substituent parameter. Similar trends are expected for the intramolecular hydrogen bonding strengths of the substituted phenol rotors **1**.

With the ability to vary the hydrogen bond strengths established, the correlation between hydrogen bond strength and TS stabilization was analyzed by measuring the rotational barriers of substituted rotors **1** and **2**. As expected, the rotational barriers of the substituted hydrogen bonding rotors **1** decreased with increasing hydrogen bond strength. A linear correlation was observed between the barriers of substituted **1** and the hydrogen bonding strength of a similarly substituted phenol (ΔG_{Ka}) in a bimolecular phenol•NMP complex (Figure 3.2). For example, the rotation barrier of *para*-nitro substituted **1** ($X = p\text{-NO}_2$), which can form the strongest hydrogen bond, was 1.2 kcal/mol lower than unsubstituted **1** ($X = \text{H}$). However, we were also surprised to observe a nearly identical substituent trend was for the barriers of the non-hydrogen bonding rotors **2**. A linear correlation with an almost identical slope was measured between the rotational barriers and the hydrogen bonding strength of a similarly substituted phenol (Figure 3.2, blue circles). Therefore, the overall TS stabilization as measured by the difference in barrier of rotors **2** and **1** remained constant over the series of substituted rotors (9.9 ± 0.3 kcal/mol).

Computational studies were conducted to gain further insight into the origins of the larger than expected TS stabilization.⁸⁹ The GS and TS geometries of rotors **1** and **2** were optimized at the B3LYP-D3(BJ)/def2-TZVP level of theory and confirmed by vibrational

analysis. The energies were recalculated at the B2GP-PLYP-D3(BJ)/def2-TZVP level. The calculated barriers (ΔG_{calc}) based on the difference in energy of the TS and GS were able to reproduce the measured barriers for the complete series of substituted rotors **1** and **2** with a RMSD of ± 0.66 kcal/mol. The excellent accuracy provided support for the ability to accurately model the bond rotation process and the TS and GS geometries. In the TS of **1** (X = H), well-defined hydrogen bonds were formed with O-H...O bond angles of 165.76° and very short O...O distances of 2.50 ± 0.006 Å (Figure 3.5). Interestingly, the TS geometry of **2** is nearly identical despite the absence of the intramolecular hydrogen bond, providing support for the ability of the rigid framework to preorganize and fix the position of the interacting groups. For example, the average O...O distances of **2** across the series of substituted rotors was only 0.02 Å shorter (2.48 ± 0.003 Å) than the substituted **1** rotors.

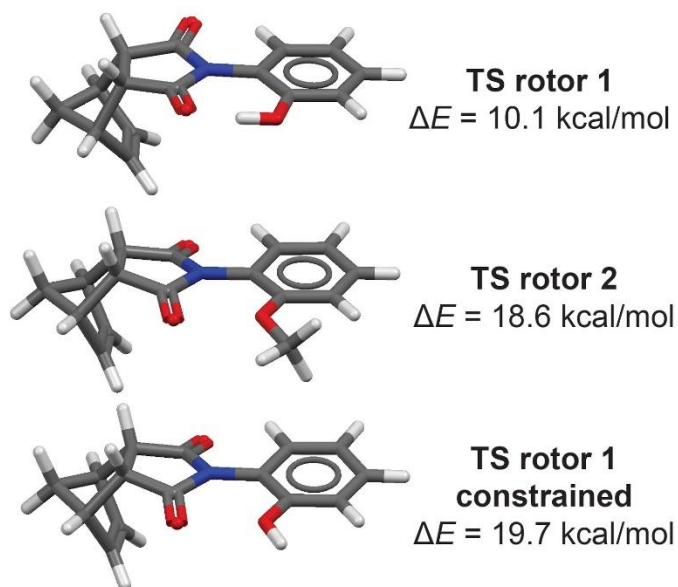


Figure 3.5 The optimized TS structures (B3LYP-D3(BJ)/def2-TZVP) and energies (B2GP-PLYP-D3(BJ)/def2-TZVP) for rotors **1** and **2** and rotor **1** constrained with the phenol hydrogen fixed in a non-hydrogen bonding geometry.

The computational studies also provided the ability to test whether steric differences between the OH and OCH₃ groups in rotors **1** and **2** played a role in the large

differences in rotational barriers. The OH proton in rotor **1** was fixed in a non-hydrogen bonding geometry pointing away from the imide carbonyl (Figure 3.5, bottom structure) and the barrier was recalculated. In this case, due to constraining rotor **1** in the TS only a potential energy (ΔE) can be calculated rather than a Gibb's free energy (ΔG). The barrier for non-hydrogen bonding **1** was 19.7 kcal/mol, which was very similar to the barrier for the non-hydrogen bonding control rotor **2** (18.6 kcal/mol) and was much higher than the barrier of hydrogen bonding **1** (10.1 kcal/mol). The result confirms that OH and OCH₃ groups have similar steric effects, and the difference in barrier between **1** and **2** is due to the presence and absence of the intramolecular hydrogen bond.

Symmetry-adapted perturbation theory (SAPT) analysis was employed to examine the components and origins of the TS stabilizing effects of the hydrogen bonds. SAPT is commonly used to estimate and study intermolecular interactions, and thus, the method was applied to study the hydrogen bond and steric interactions in the bimolecular phenol•NMP complex (Figure 3.6A). The atoms of the NMP amide and phenol were constrained in a planar geometry, and the O-to-O distance was fixed at 2.5 Å to mimic the TS distances in the rotors (Figure 3.5). A hydrogen bonding (HB) and non-hydrogen bonding (nHB) geometry of the phenol•NMP complexes were compared to isolate the energy contributions from the hydrogen bond. In the HB structure, the phenol proton was allowed to form a hydrogen bond with the NMP carbonyl oxygen. In the nHB structure, the phenol proton was fixed in a non-hydrogen bonding position pointing away from the NMP carbonyl. For both complexes, the total SAPT interaction energy (E_{total}) as well as the electrostatic (E_{elst}), exchange repulsion (E_{exch}), induction (E_{ind}), and dispersion (E_{disp}) component energies were obtained (Figure 3.6B).

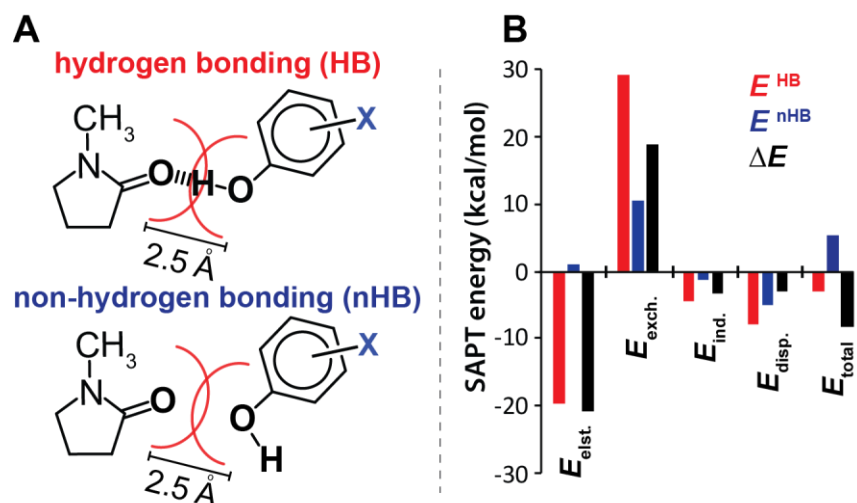


Figure 3.6 (A) Hydrogen bonding and non-hydrogen bonding bimolecular complexes used in the SAPT analyses with the overlapping VDW radii of the oxygen atoms highlighted in red. (B) SAPT energies ($E_{\text{elst.}}$ = electrostatic, $E_{\text{exch.}}$ = exchange, $E_{\text{ind.}}$ = induction, $E_{\text{disp.}}$ = dispersion, E_{total} = sum of all component energies) calculated (CCSD/cc-pVTZ) for the phenol•NMP complex (X = H) in the hydrogen bonding and non-hydrogen bonding geometries, and the difference energies: ΔE = (hydrogen bonding E) - (non-hydrogen bonding E).

The SAPT analysis of the phenol-NMP complex was consistent with previous component analyses of hydrogen bonding interactions.⁹⁶ The intermolecular hydrogen bond (Figure 3.6B, red bars) has a large attractive term (-32.1 kcal/mol) made up primarily of the electrostatic component between the phenol hydrogen and carbonyl oxygen with smaller contributions from the induction, and dispersion components. The attractive term is balanced by an almost equally as large repulsive exchange term (+29.2 kcal/mol). Thus, the overall hydrogen bonding interaction is only weakly attractive (-2.9 kcal/mol). The repulsive exchange component in **1** is a combination of the H•••O repulsion (65%) and the O•••O interactions (35%). The significant repulsive interaction between the non-adjacent oxygens was initially surprising, but an analysis found that most hydrogen bonds place the heavy atoms within vdw radii, leading to significant repulsive interactions. These heavy

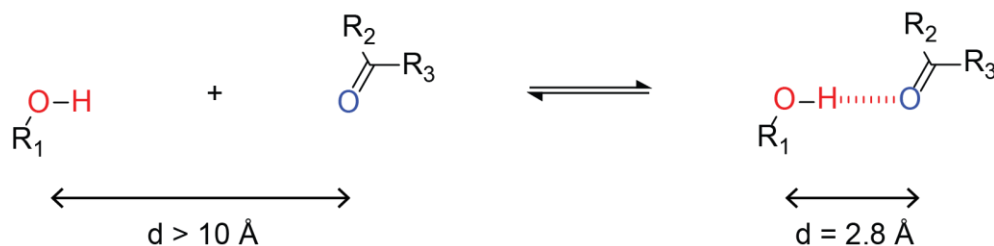
atom-heavy atom interactions played a significant role in the large TS stabilization of the hydrogen bonds.

The total SAPT energy of the hydrogen bonding ($E(\text{HB})$) and non-hydrogen bonding ($E(\text{nHB})$) complexes, and difference energy ($\Delta E = E(\text{HB}) - E(\text{nHB})$) follow the rotational barrier trends observed in our molecular rotors. Specifically, the total SAPT hydrogen bonding interaction energy in the bimolecular complex is only weakly stabilizing; whereas ΔE , which is analogous to the energy difference in rotors **2** and **1**, is significantly more stabilizing. Some caution must be applied in not overinterpreting these similarities as the hydrogen bonds in the TS of the rotors and in the constrained bimolecular complexes differ in solvent environment and intra- vs intermolecular nature of the interactions. Nevertheless, the SAPT component energies provide insight into the origins of the differences in $E(\text{HB})$ and ΔE .

Analysis of the component SAPT energies revealed that the difference in ΔE and $E(\text{HB})$ was primarily due to the repulsive exchange component. The attractive SAPT components (E_{elst} , E_{ind} , and E_{disp}) of $E(\text{HB})$ and ΔE are similar in magnitude as the attractive components are mainly associated with the interactions of the phenolic proton with the carbonyl oxygen. Thus, the nHB complex lacks these attractive components of the hydrogen bond in the HB complex due to the phenolic proton being positioned further away from the carbonyl oxygen. In contrast, the nHB complex contains a significant portion of the repulsive exchange component of the hydrogen bond in the HB complex, as the phenolic oxygen and carbonyl oxygen are at similar positions and distances in the nHB and HB complexes. Thus, the ΔE contains most of the attractive components of the hydrogen bond but only two thirds of the repulsive components, leading to a larger ΔE than the

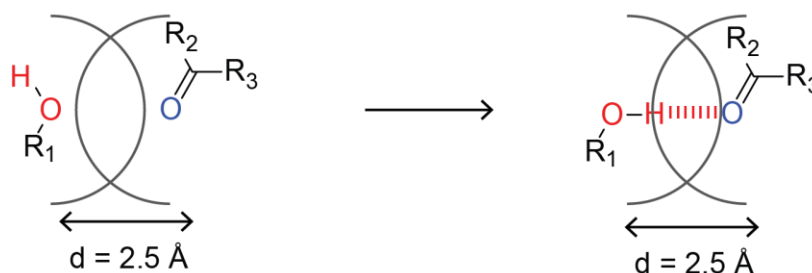
hydrogen bonding interaction strength, $E(\text{HB})$. Similar stability and TS stabilizing effects are expected for the hydrogen bonding interactions

in thermodynamic GS



$$\text{GS NCI strength} = 100\% \Delta E_{\text{attraction}} + 100\% \Delta E_{\text{repulsion}} \quad \text{Equation 3.1}$$

in kinetic TS



$$\text{TS NCI strength} = 100\% \Delta E_{\text{attraction}} + 70\% \Delta E_{\text{repulsion}} \quad \text{Equation 3.2}$$

Figure 3.7 State equations for calculating the thermodynamic (Eq. 1) and TS NCI (Eq. 2) interaction energies. The energies are calculated from the difference between the NCI structures (right) and non-NCI control structures (left).

Another way to understand the disparity between the total SAPT energies for $E(\text{HB})$ and ΔE are to consider the atoms involved in the interactions in the HB and nHB complexes (Figure 3.7). Normally, hydrogen bond strengths are based on equilibrium shown in equation 1. On the left hand side of the equilibrium, the hydrogen bond donor and acceptor groups are positioned far apart so that they do not form any interactions. On

the right-hand side of the equilibrium, donor and acceptor are closer the heavy atoms and proton can form interactions. Thus, equation 1 corresponds to the calculated energy ($E(\text{HB})$) or the measured association energies (ΔG_{Ka}) for the HB complexes. In contrast, equation 2 describes the energy corresponding to the TS stabilization of the hydrogen bond as defined by the difference energies in the nHB and HB complexes (ΔE) or in the barriers of rotors **2** and **1**. Like equation 1, the hydrogen-bond not formed in the left-hand complex in equation 2 and is formed in the right-hand complex. However, the heavy atoms of the donor and acceptor still form an interaction in the left-hand structure. This oxygen-oxygen interaction is part of the hydrogen bonding interaction energy in equation 1 but is removed from the interaction energy in equation 2. Thus, the TS stabilization energy as defined by equation 2 is much larger than the hydrogen bond interaction as defined by equation 1 because the TS stabilization contains all of the attractive components of the hydrogen bond but only two-thirds of the repulsive components. This analysis demonstrates that the insertion or positioning of a hydrogen to form a hydrogen bond can greatly stabilize

3.3 CONCLUSION

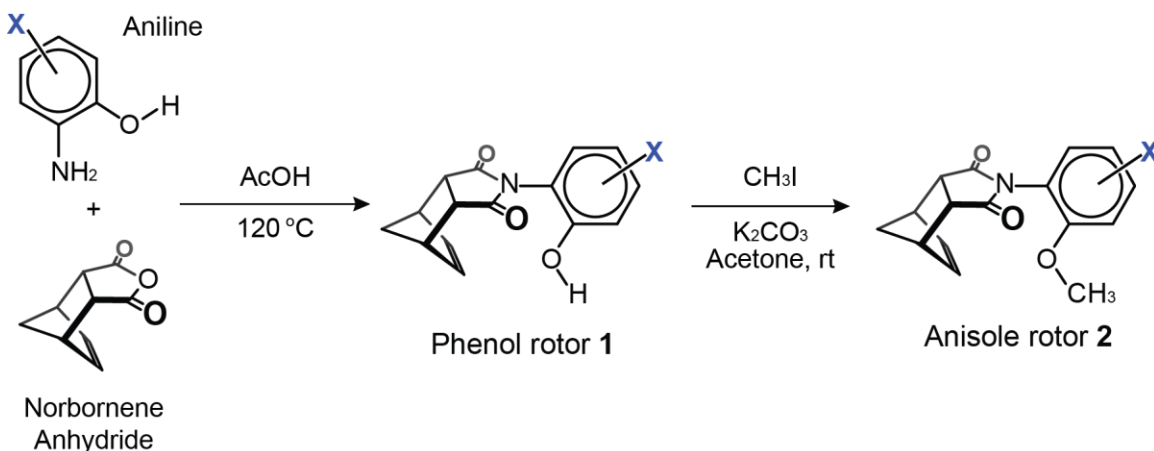
Study of the hydrogen bond stabilization in molecular rotor **1** demonstrates that a single neutral hydrogen bond can have a TS stabilization that is significantly greater than the strength of the hydrogen bond. The origins of the TS stabilization provide a new design strategy for hydrogen bond catalysts. The traditional approach is to optimize the attractive component of hydrogen bonding interactions. However, the molecular rotors demonstrate that large rate accelerations can be affected by targeting the large repulsive energy term of the hydrogen bonding interaction. The key is to rigidly position the interacting groups in close proximity in order to ‘prepay’ the repulsive interactions and reduce their destabilizing

influence on the transition state. In addition, similarly constrained hydrogen bonds could play a role in enzyme active sites. For example, Warshel has proposed an electrostatic analog of the TS preorganization hypothesis for enzymatic systems.⁹⁷ The protein framework holds key catalytic and recognition groups in proximity to the enzyme active site, overcoming the large repulsive electrostatic penalty for their organization in the crowded TS. We propose that the protein framework can also perform a similar preorganizing function in reducing the large repulsive component of hydrogen bonds allowing them to amplify the catalytic effects.

3.4 SUPPLEMENTAL INFORMATION

3.4.1 GENERAL EXPERIMENTAL INFORMATION

NMR spectra were recorded on a Bruker 400 MHz spectrometer. Chemical shifts are reported in ppm (δ) referenced to solvent residue. All spectra given for characterization purposes were taken at room temperature. All chemicals and solvents were purchased from commercial suppliers and used as received. Flash chromatography was performed using silica gel from Sorbent Technologies (60 Å, 200 – 400 mesh).



Scheme 3.1 General route for synthesizing molecular rotors

3.4.2 SYNTHESIS

Phenol rotors **1** (X = H, *p*-NO₂, *m*-NO₂, *p*-Cl, *m*-Cl, *p*-CN, *p*-*t*-amyl) were prepared via a thermal condensation between a substituted aniline and a bicyclic anhydride, and anisole rotors **2** (X = H, *p*-NO₂, *m*-NO₂, *p*-Cl, *m*-Cl, *p*-CN, *p*-*t*-amyl) were prepared via a subsequent methylation reaction of the corresponding phenol rotors (Scheme 3.1). Methyl Rotor **3** was prepared as described previously and matched the previous characterization.⁸⁷

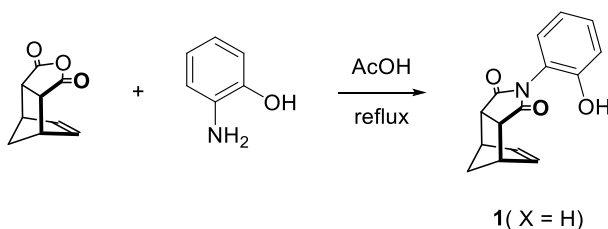


Figure 3.8 Synthesis of rotor **1** (X = H)

Anhydride (100 mg, 0.61 mmol) and aniline (X = H) (73 mg, 0.67 mmol) were added to acetic acid (10 mL) in a round bottom flask with a magnetic stir bar. The round bottom flask was then heated to 120 °C in a silicon oil bath for 12 hours while stirring. After letting the round bottom flask cool to room temperature, the acetic acid was removed *in vacuo*. The crude material was then purified by column chromatography (ethyl acetate/hexanes = 1:1, v/v) to give **1** (X = H) as a white powder (135 mg, 87%). ¹H NMR (400 MHz, dichloromethane-*d*₂) δ 7.29 (ddd, *J* = 10.8, 9.0, 3.3 Hz, 1H), 7.04-6.95 (m, 3H), 6.27 (s, 2H), 5.76 (s, 1H), 3.46 (br, 4H), 1.78 (d, *J* = 11.9 Hz, 1H), 1.62 (d, *J* = 11.9 Hz, 1H). ¹³C NMR (100 MHz, dichloromethane-*d*₂) 177.33, 151.19, 134.86, 130.35, 128.26, 120.95, 120.20, 118.51, 52.27, 46.20, 45.51. HRMS (EI) *m/z* calculated for [C₁₅H₁₃NO₃]⁺ (M⁺): 255.0895; found 255.0886.

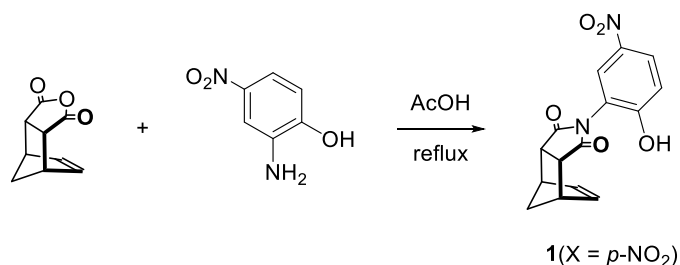


Figure 3.9 Synthesis of rotor **1** (X = *p*-NO₂)

Anhydride (100 mg, 0.61 mmol) and aniline (X = *p*-NO₂) (103 mg, 0.67 mmol) were added to acetic acid (10 mL) in a round bottom flask with a magnetic stir bar. The round bottom flask was then heated to 120 °C in a silicon oil bath for 12 hours while stirring. After letting the round bottom flask cool to room temperature, the acetic acid was removed *in vacuo*. The crude material was then purified by column chromatography (ethyl acetate/hexanes = 1:1, v/v) to give **1** (X = *p*-NO₂) as an orange powder (123 mg, 67%). ¹H NMR (400 MHz, acetone-d₆) δ 10.06 (br, 1H), 8.07 (dd, *J* = 2.8, 9.0 Hz, 1H), 7.75 (d, *J* = 2.8 Hz, 1H), 7.06 (d, *J* = 9.0 Hz, 1H), 6.15 (t, *J* = 1.7 Hz, 1H), 3.45-3.44 (m, 2H), 3.27-3.25 (m, 2H), 1.59-1.55 (m, 2H). ¹³C NMR (100 MHz, acetone-d₆) δ 175.76, 159.40, 140.29, 134.65, 126.05, 125.89, 120.39, 116.80, 51.79, 46.24, 45.12. HRMS (EI) *m/z* calculated for [C₁₅H₁₂N₂O₅]⁺ (M⁺): 300.0746; found 300.0748.

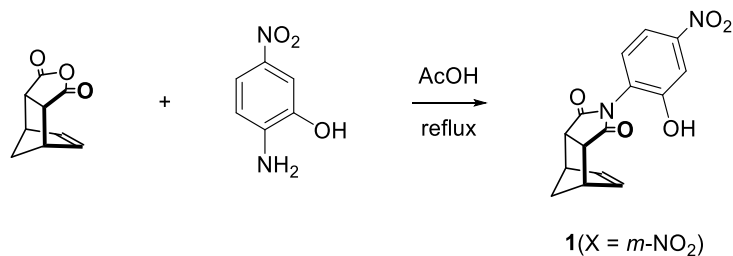


Figure 3.10 Synthesis of rotor **1** (X = *m*-NO₂)

Anhydride (100 mg, 0.61 mmol) and aniline (X = *m*-NO₂) (103 mg, 0.67 mmol) were added to acetic acid (10 mL) in a round bottom flask with a magnetic stir bar. The round bottom flask was then heated to 120 °C in a silicon oil bath for 12 hours while stirring. After letting the round bottom flask cool to room temperature, the acetic acid was removed *in vacuo*. The crude material was then purified by column chromatography (ethyl acetate/hexanes = 1:1, v/v) to give **1**(X = *m*-NO₂) as an orange powder (128 mg, 70%). ¹H NMR (400 MHz, acetone-d₆) δ 9.50 (br, 1H), 7.67 (d, *J* = 2.5 Hz, 1H), 7.63 (dd, *J* = 2.5, 8.6 Hz, 1H), 7.11 (d, *J* = 8.6 Hz, 1H), 6.13 (t, *J* = 1.8 Hz, 2H), 3.44-3.43 (m, 2H), 3.27-3.25 (m, 2H), 1.56 (t, *J* = 1.5 Hz, 2H). ¹³C NMR (100 MHz, acetone-d₆) 175.65, 154.02, 148.79, 134.64, 130.69, 126.29, 114.32, 111.31, 51.76, 46.24, 45.17. HRMS (EI) *m/z* calculated for [C₁₅H₁₂N₂O₅]⁺ (M⁺): 300.0746; found 300.0752.

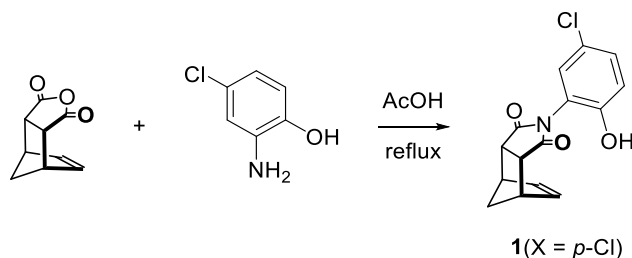


Figure 3.11 Synthesis of rotor **1**(X = *p*-Cl)

Anhydride (100 mg, 0.61 mmol) and aniline (X = *p*-Cl) (96 mg, 0.67 mmol) were added to acetic acid (10 mL) in a round bottom flask with a magnetic stir bar. The round bottom flask was then heated to 120 °C in a silicon oil bath for 12 hours while stirring. After letting the round bottom flask cool to room temperature, the acetic acid was removed *in vacuo*. The crude material was then purified by column chromatography (ethyl acetate/hexanes = 1:1, v/v) to give **1**(X = *p*-Cl) as a white powder (150 mg, 85%). ¹H NMR

(400 MHz, acetone-d₆) δ 8.83 (br, 1H), 7.28 (dd, *J* = 2.6, 8.8 Hz, 1H), 7.00 (d, *J* = 8.8 Hz, 1H), 6.97 (d, *J* = 2.6 Hz, 1H), 6.28 (t, *J* = 1.9 Hz, 2H), 3.53-3.52 (m, 2H), 3.39-3.38 (m, 2H), 1.72-1.67 (m, 2H). ¹³C NMR (100 MHz, acetone-d₆) δ 175.93, 152.48, 134.62, 129.84, 129.11, 123.07, 121.28, 117.98, 51.72, 46.03, 45.10. HRMS *m/z* calculated for [C₁₅H₁₂ClNO₃]⁺ (M⁺): 289.0506; found 289.0516.

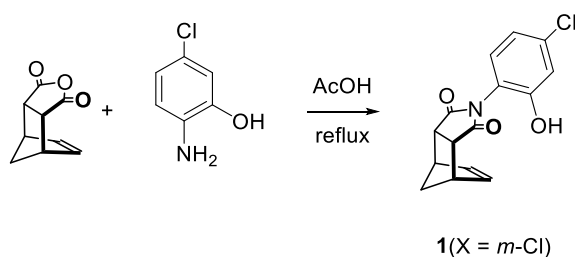


Figure 3.12 Synthesis of rotor **1**(X = *m*-Cl)

Anhydride (100 mg, 0.61 mmol) and aniline (X = *m*-Cl) (96 mg, 0.67 mmol) were added to acetic acid (10 mL) in a round bottom flask with a magnetic stir bar. The round bottom flask was then heated to 120 °C in a silicon oil bath for 12 hours while stirring. After letting the round bottom flask cool to room temperature, the acetic acid was removed *in vacuo*. The crude material was then purified by column chromatography (ethyl acetate/hexanes = 1:1, v/v) to give **1**(X = *m*-Cl) as a white powder (144 mg, 82%). ¹H NMR (400 MHz, acetone-d₆) δ 9.01 (br, 1H), 7.01 (d, *J* = 2.2 Hz, 1H), 6.96-6.90 (m, 2H), 6.24 (t, *J* = 1.8 Hz, 2H), 3.52-3.51 (m, 2H), 3.39-3.36 (m, 2H), 1.71-1.66 (m, 2H). ¹³C NMR (100 MHz, acetone-d₆) δ 175.93, 152.48, 134.62, 129.84, 129.11, 123.07, 121.28, 117.98, 51.72, 46.03, 45.10. HRMS *m/z* calculated for [C₁₅H₁₂ClNO₃]⁺ (M⁺): 289.0506; found 289.0509.

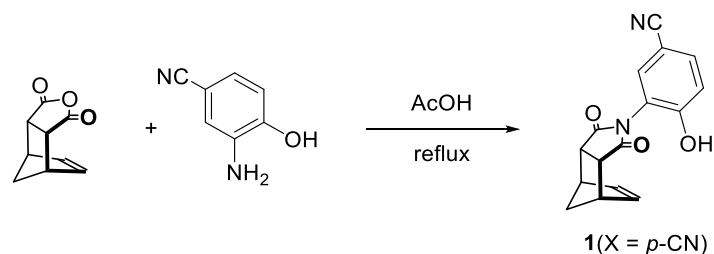


Figure 3.13 Synthesis of rotor **1**(X = *p*-CN)

Anhydride (100 mg, 0.61 mmol) and aniline (X = *p*-CN) (96 mg, 0.67 mmol) were added to acetic acid (10 mL) in a round bottom flask with a magnetic stir bar. The round bottom flask was then heated to 120 °C in a silicon oil bath for 12 hours while stirring. After letting the round bottom flask cool to room temperature, the acetic acid was removed *in vacuo*. The crude material was then purified by column chromatography (ethyl acetate/hexanes = 1:1, v/v) to give **1**(X = *p*-CN) as a white powder (123 mg, 72%). ¹H NMR (400 MHz, acetone-*d*₆) δ 9.81 (br, 1H), 7.68 (dd, *J* = 2.0, 8.6 Hz, 1H), 7.41 (d, *J* = 2.0 Hz, 1H), 7.16 (d, *J* = 8.6 Hz, 1H), 6.30 (t, *J* = 1.6 Hz, 2H), 3.56-3.55 (m, 2H), 3.40-3.38 (m, 2H), 1.72-1.68 (m, 2H). ¹³C NMR (100 MHz, acetone-*d*₆) δ 175.85, 157.57, 134.67, 134.35, 134.02, 121.08, 117.96, 117.80, 102.87, 51.70, 46.10, 45.15. HRMS *m/z* calculated for [C₁₆H₁₂N₂O₃]⁺ (M⁺): 280.0848; found 280.0860.

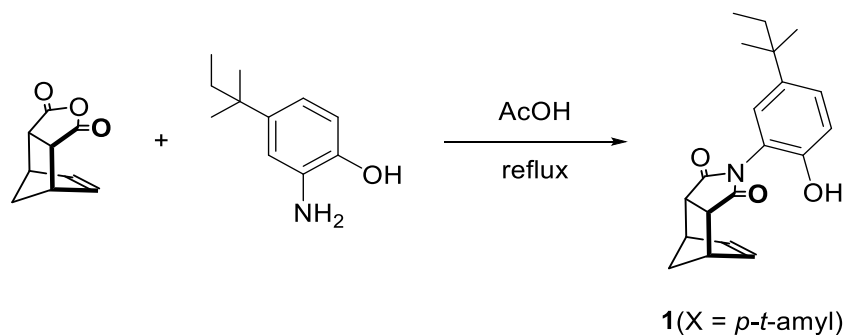


Figure 3.14 Synthesis of rotor **1**(X = *p*-*t*-amyl)

Anhydride (100 mg, 0.61 mmol) and aniline (X = *p-t*-amyl) (120 mg, 0.67 mmol) were added to acetic acid (10 mL) in a round bottom flask with a magnetic stir bar. The round bottom flask was then heated to 120 °C in a silicon oil bath for 12 hours while stirring. After letting the round bottom flask cool to room temperature, the acetic acid was removed *in vacuo*. The crude material was then purified by column chromatography (ethyl acetate/hexanes = 1:1, v/v) to give **1**(X = *p-t*-amyl) as a white powder (188 mg, 95%). ¹H NMR (400 MHz, chloroform-d₁) δ 7.26 (dd, *J* = 2.4, 8.8 Hz, 1H), 6.99-6.97 (m, 2H), 6.31 (t, *J* = 1.6 Hz, 2H), 5.44 (br, 1H), 3.54-3.50 (m, 4H), 1.84 (dt, *J* = 9.0, 1.6 Hz, 1H), 1.66 (d, *J* = 9.0 Hz, 1H), 1.61 (q, *J* = 7.6 Hz, 2H), 1.26 (s, 6H), 0.72 (t, *J* = 7.6 Hz, 3H). ¹³C NMR (100 MHz, chloroform-d₁) δ 177.56, 148.40, 142.56, 134.88, 127.99, 125.41, 119.50, 118.52, 52.31, 46.19, 45.45, 37.38, 36.83, 28.39, 9.07. HRMS *m/z* calculated for [C₂₀H₂₃NO₃]⁺ (M⁺): 325.1678; found 325.1687.

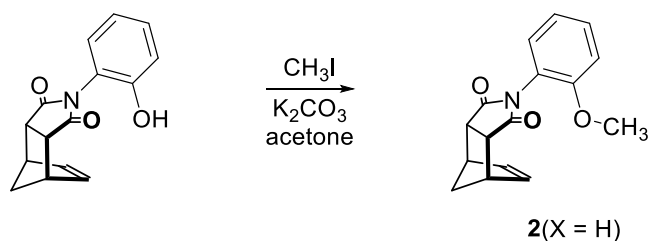


Figure 3.15 Synthesis of rotor **2**(X = H)

Potassium carbonate (223 mg, 1.83 mmol) and iodomethane (0.095 mL, 1.52 mmol) were both added to **1**(X = H) (50 mg, 0.20 mmol) in a round bottom flask with 25 mL of acetone and a stir bar. The round bottom was then stirred at room temperature for 12 hours. The acetone was removed using a rotary evaporator. The crude product was then purified by column chromatography (ethyl acetate/hexanes = 1:3, v/v) to yield **2**(X = H) as a white powder (52 mg, 99%). ¹H NMR (400 MHz, dichloromethane-d₂) δ 7.41-7.28 (m,

1H *folded* and *unfolded*), 7.08-6.91 (m, 3H *folded* and *unfolded*), 6.30 (s, 2H *unfolded*), 6.23 (s, 2H *folded*), 3.80 (s, 3H *folded* and *unfolded*), 3.50-3.43 (m, 4H *folded* and *unfolded*), 1.82-1.77 (m, 1H *folded* and *unfolded*), 1.64-1.59 (m, 1H *folded* and *unfolded*). ¹³C NMR has been reported previously.⁸⁷ HRMS *m/z* calculated for [C₁₆H₁₅NO₃]⁺ (M⁺): 269.1052; found 269.1057.

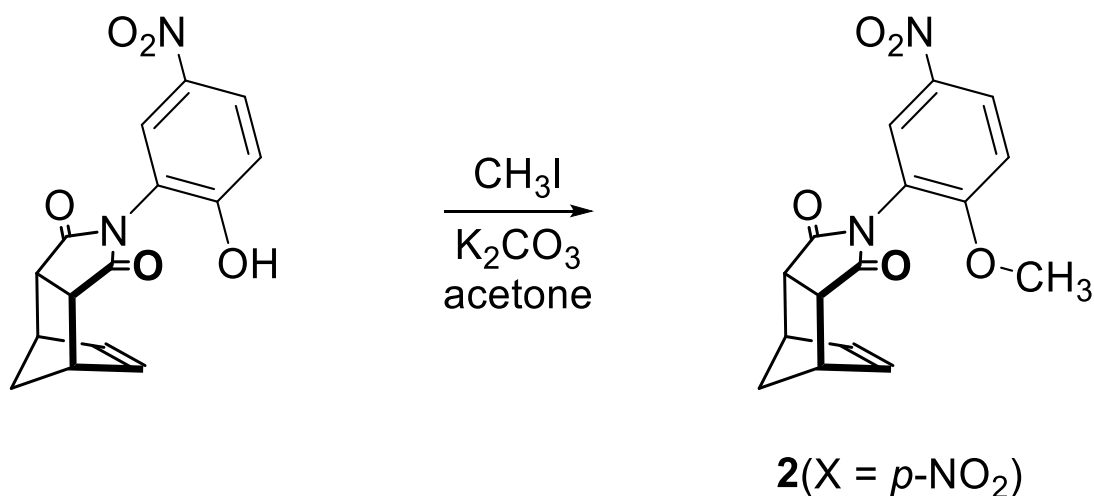


Figure 3.16 Synthesis of rotor **2**(X = *p*-NO₂)

Potassium carbonate (223 mg, 1.83 mmol) and iodomethane (0.095 mL, 1.52 mmol) were both added to **1**(X = *p*-NO₂) (50 mg, 0.17 mmol) in a round bottom flask with 25 mL of acetone and a stir bar. The round bottom was then stirred at room temperature for 12 hours. The acetone was removed using a rotary evaporator. The crude product was then purified by column chromatography (ethyl acetate/hexanes = 1:3, v/v) to yield **2**(X = *p*-NO₂) as a white powder (52 mg, 99%). ¹H NMR (400 MHz, tetrachloroethane-*d*₂) δ 8.36-8.33 (m, 1H *folded* and *unfolded*), 8.03 (d, *J* = 2.7 Hz, 1H *folded*), 7.83 (d, *J* = 2.7 Hz, 1H *unfolded*), 7.12-7.09 (m, 1H *folded* and *unfolded*), 6.36 (s, 2H *unfolded*), 6.23 (s, 2H *folded*), 3.94 (s, 3H *unfolded*), 3.93 (s, 3H *folded*), 3.55-3.50 (m, 4H *folded* and *unfolded*),

1.86-1.81 (m, 1H *folded* and *unfolded*), 1.66-1.63 (m, 1H *folded* and *unfolded*). ^{13}C NMR (100 MHz, chloroform- d_1) δ 176.02, 175.86, 160.02, 159.89, 141.10, 140.98, 134.77, 134.53, 126.74, 126.65, 126.05, 125.55, 121.17, 121.08, 111.65, 111.64, 56.70, 56.42, 52.51, 52.18, 46.71, 46.23, 45.44, 45.36. HRMS m/z calculated for $[\text{C}_{16}\text{H}_{14}\text{N}_2\text{O}_5]^+$ (M^+): 314.0903; found 314.0911.

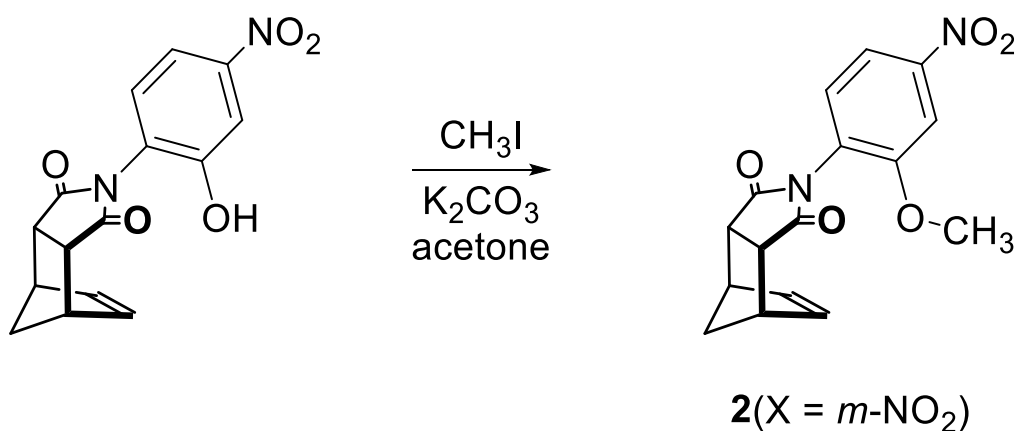


Figure 3.17 Synthesis of rotor **2**(X = *m*-NO₂)

Potassium carbonate (223 mg, 1.83 mmol) and iodomethane (0.095 mL, 1.52 mmol) were both added to **1**(X = *m*-NO₂) (50 mg, 0.17 mmol) in a round bottom flask with 25 mL of acetone and a stir bar. The round bottom was then stirred at room temperature for 12 hours. The acetone was removed using a rotary evaporator. The crude product was then purified by column chromatography (ethyl acetate/hexanes = 1:3, v/v) to yield **2**(X = *m*-NO₂) as a white powder (52 mg, 99%). ^1H NMR (400 MHz, chloroform- d_1) δ 7.84-7.79 (m, 1H *folded* and *unfolded*), 7.77-7.76 (m, 1H *folded* and *unfolded*), 7.17 (d, J = 8.6 Hz, 1H *folded*), 7.02 (d, J = 8.6 Hz, 1H *unfolded*), 6.23 (s, 2H *unfolded*), 6.15 (s, 2H *folded*), 3.83 (s, 3H *folded* and *unfolded*), 3.44-3.39 (m, 4H *folded* and *unfolded*), 1.76-1.71 (m, 1H *folded* and *unfolded*), 1.58-1.53 (m, 1H *folded* and *unfolded*). ^{13}C NMR (100 MHz,

chloroform-d₁) δ 175.85, 175.68, 155.44, 155.31, 149.09, 149.03, 134.75, 134.51, 130.21, 129.82, 126.74, 126.67, 115.90, 115.86, 107.39, 107.36, 56.52, 56.28, 52.50, 52.19, 46.77, 46.31, 45.42. HRMS m/z calculated for [C₁₆H₁₄N₂O₅]⁺ (M⁺): 314.0903; found 314.0915.

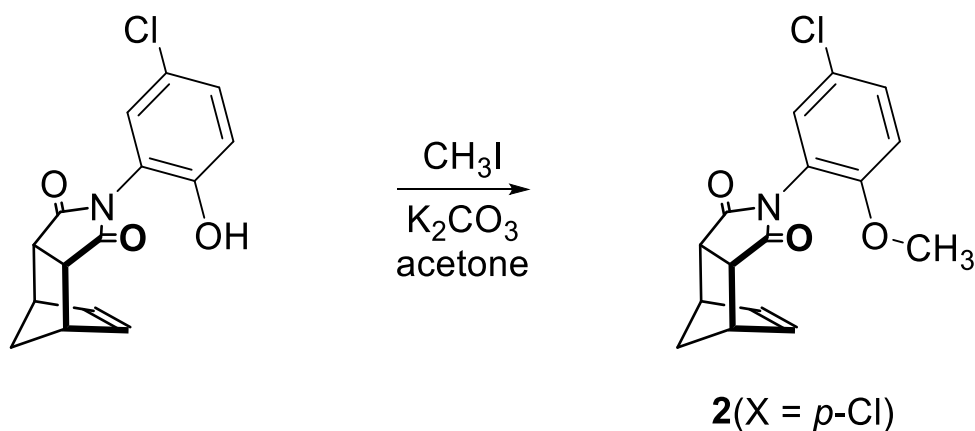


Figure 3.18 Synthesis of rotor **2**(X = *p*-Cl)

Potassium carbonate (223 mg, 1.83 mmol) and iodomethane (0.095 mL, 1.52 mmol) were both added to **1**(X = *p*-Cl) (50 mg, 0.17 mmol) in a round bottom flask with 25 mL of acetone and a stir bar. The round bottom was then stirred at room temperature for 12 hours. The acetone was removed using a rotary evaporator. The crude product was then purified by column chromatography (ethyl acetate/hexanes = 1:3, v/v) to yield **2**(X = *p*-Cl) as a white powder (52 mg, 99%). ¹H NMR (400 MHz, tetrachloroethane-d₂) δ 7.31-7.28 (m, 1H *folded* and *unfolded*), 6.99 (d, *J* = 2.6 Hz, 1H *folded*), 6.87-6.84 (m, 1H *folded* and *unfolded*), 6.80 (d, *J* = 2.6 Hz, 1H *unfolded*), 6.19 (br, 2H *unfolded*), 6.10 (t, *J* = 1.6 Hz, 1H *folded*), 3.69 (s, 3H *unfolded*), 3.68 (s, 3H *folded*), 3.40-3.32 (m, 4H *folded* and *unfolded*), 1.72-1.67 (m, 1H *folded* and *unfolded*), 1.53-1.48 (m, 1H *folded* and *unfolded*). ¹³C NMR (101 MHz, tetrachloroethane -d₂) δ 176.43, 176.30, 153.84, 153.74, 134.77, 134.56, 130.62, 130.53, 129.63, 129.13, 125.24, 125.10, 121.80, 121.67, 113.40, 113.36,

56.39, 56.15, 52.57, 52.23, 46.70, 46.18, 45.49, 45.46. HRMS m/z calculated for $[C_{16}H_{14}ClNO_3]^+$ (M^+): 303.0662; found 303.0675.

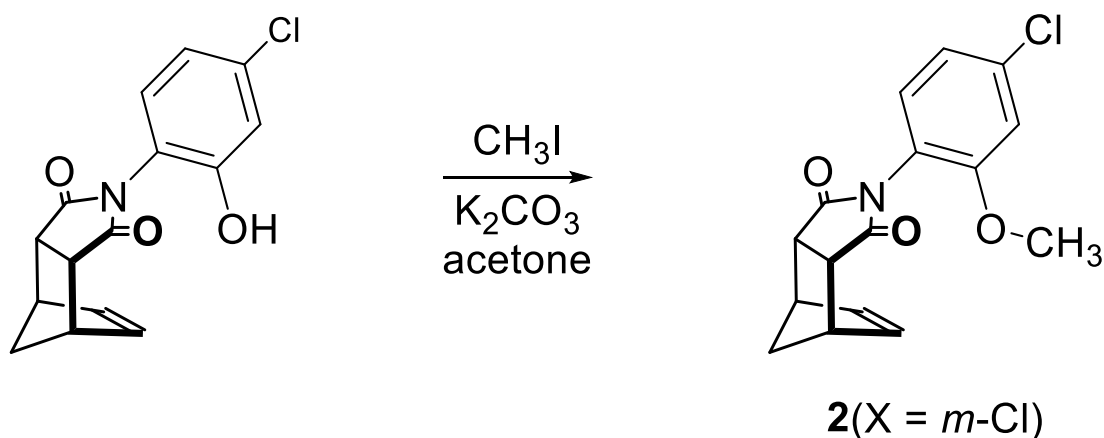


Figure 3.19 Synthesis of rotor **2**(X = *m*-Cl)

Potassium carbonate (223 mg, 1.83 mmol) and iodomethane (0.095 mL, 1.52 mmol) were both added to **1**(X = *m*-Cl) (50 mg, 0.17 mmol) in a round bottom flask with 25 mL of acetone and a stir bar. The round bottom was then stirred at room temperature for 12 hours. The acetone was removed using a rotary evaporator. The crude product was then purified by column chromatography (ethyl acetate/hexanes = 1:3, v/v) to yield **2**(X = *m*-Cl) as a white powder (52 mg, 99%). 1H NMR (400 MHz, acetone- d_6) δ 7.84-7.80 (m, 1H *folded* and *unfolded*), 7.52 (d, $J = 2.2$ Hz, 1H *folded*), 7.38 (d, $J = 2.2$ Hz, 1H *unfolded*), 7.34-7.29 (m, 1H *folded* and *unfolded*), 6.34 (t, $J = 1.8$ Hz, *unfolded*), 6.18 (t, $J = 1.8$ Hz, *folded*), 3.91 (s, 3H *folded*), 3.89 (s, 3H *unfolded*), 3.58-3.50 (m, 2H *folded* and *unfolded*), 3.40-3.35 (m, 2H *folded* and *unfolded*), 1.72-1.65 (m, 2H *folded* and *unfolded*). ^{13}C NMR (100 MHz, acetone- d_6) δ 175.52, 175.40, 158.88, 158.87, 134.95, 134.69, 134.42, 133.58, 133.18, 122.80, 122.44, 117.83, 117.72, 113.25, 113.19, 103.73, 103.54, 56.00, 55.69,

51.77, 51.65, 46.50, 45.78, 45.23, 45.03. HRMS m/z calculated for $[C_{16}H_{14}ClNO_3]^+$ (M^+): 303.0662; found 303.0674.

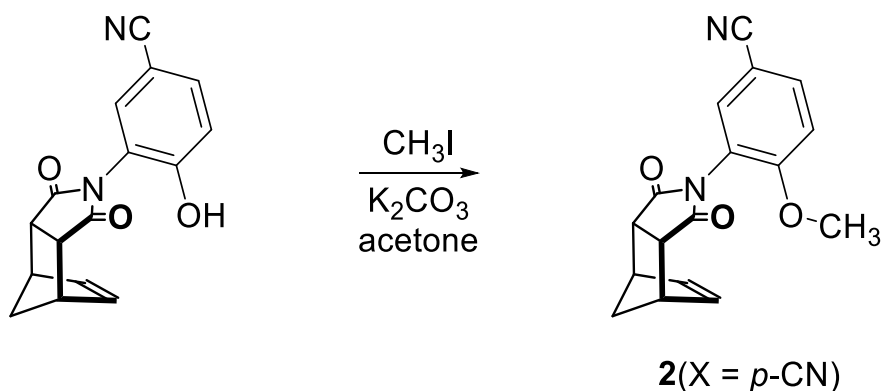


Figure 3.20 Synthesis of rotor **2**(X = *p*-CN)

Potassium carbonate (223 mg, 1.83 mmol) and iodomethane (0.095 mL, 1.52 mmol) were both added to **1**(X = *p*-CN) (50 mg, 0.18 mmol) in a round bottom flask with 25 mL of acetone and a stir bar. The round bottom was then stirred at room temperature for 12 hours. The acetone was removed using a rotary evaporator. The crude product was then purified by column chromatography (ethyl acetate/hexanes = 1:3, v/v) to yield **2**(X = *p*-CN) as a white powder (52 mg, 99%). 1H NMR (400 MHz, acetone- d_6) δ 7.16 (d, $J = 2.1$ Hz, 1H *unfolded*), 7.13 (d, $J = 2.1$ Hz, 1H *folded*), 7.08 (d, $J = 8.3$ Hz, 1H *unfolded*), 7.02-7.00 (m, 1H *folded* and *unfolded*), 6.93 (d, $J = 8.3$ Hz, 1H *folded*), 6.25 (t, $J = 1.8$ Hz, 2H *unfolded*), 6.16 (t, $J = 1.8$ Hz, 2H *folded*), 3.82 (s, 3H, *folded*), 3.81 (s, 3H, *unfolded*), 3.53-3.46 (m, 2H *folded* and *unfolded*), 3.38-3.34 (m, 2H *folded* and *unfolded*), 1.70-1.63 (m, 2H *folded* and *unfolded*). ^{13}C NMR (100 MHz, acetone- d_6) δ 175.73, 175.61, 156.04, 156.03, 135.06, 134.88, 134.56, 134.37, 130.80, 130.48, 120.91, 120.59, 120.30, 120.21, 112.79, 112.75, 55.81, 55.53, 51.81, 51.60, 46.39, 45.67, 45.18, 44.98. HRMS m/z calculated for $[C_{17}H_{14}N_2O_3]^+$ (M^+): 294.1004; found 294.1010.

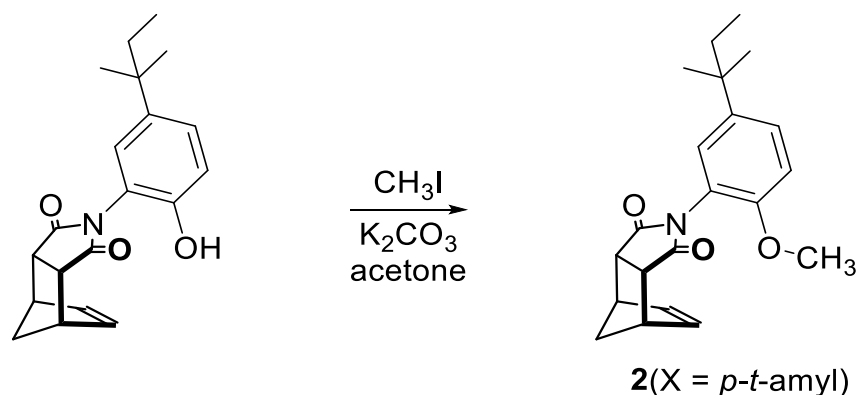


Figure 3.21 Synthesis of rotor **2** (X = *p-t*-amyl)

Potassium carbonate (223 mg, 1.83 mmol) and iodomethane (0.095 mL, 1.52 mmol) were both added to **1** (X = *p-t*-amyl) (50 mg, 0.15 mmol) in a round bottom flask with 25 mL of acetone and a stir bar. The round bottom was then stirred at room temperature for 12 hours. The acetone was removed using a rotary evaporator. The crude product was then purified by column chromatography (ethyl acetate/hexanes = 1:3, v/v) to yield **2** (X = *p-t*-amyl) as a white powder (52 mg, 99%). ¹H NMR (400 MHz, acetone-d₆) 7.37-7.32 (m, 1H *folded* and *unfolded*), 7.04-6.99 (m, 2H *unfolded* and 1H *folded*), 6.83 (d, *J* = 2.4 Hz, 1H *folded*), 6.27 (t, *J* = 1.6 Hz, *unfolded*), 6.15 (t, *J* = 1.6 Hz, *folded*), 3.74 (s, 3H *folded*), 3.73 (s, 1H *folded*), 3.50-3.43 (m, 2H *folded* and *unfolded*), 3.37-3.33 (m, 2H *folded* and *unfolded*), 1.71-1.58 (m, 4H *folded* and *unfolded*), 1.23 (s, 6H *folded* and *unfolded*), 0.69-0.65 (m, 3H *folded* and *unfolded*). ¹³C NMR (100 MHz, acetone-d₆) 175.99, 175.85, 152.97, 152.95, 141.36, 141.20, 134.51, 134.34, 127.43, 127.23, 127.20, 126.75, 121.42, 121.17, 111.68, 111.64, 55.28, 55.07, 51.83, 51.52, 46.30, 45.59, 45.17, 44.96, 37.02, 36.93, 36.54, 36.50, 27.97, 27.87, 8.52, 8.50. HRMS *m/z* calculated for [C₂₁H₂₅NO₃]⁺ (M⁺): 339.1844; found 339.1834.

3.4.3 ^1H AND ^{13}C NMR SPECTRA

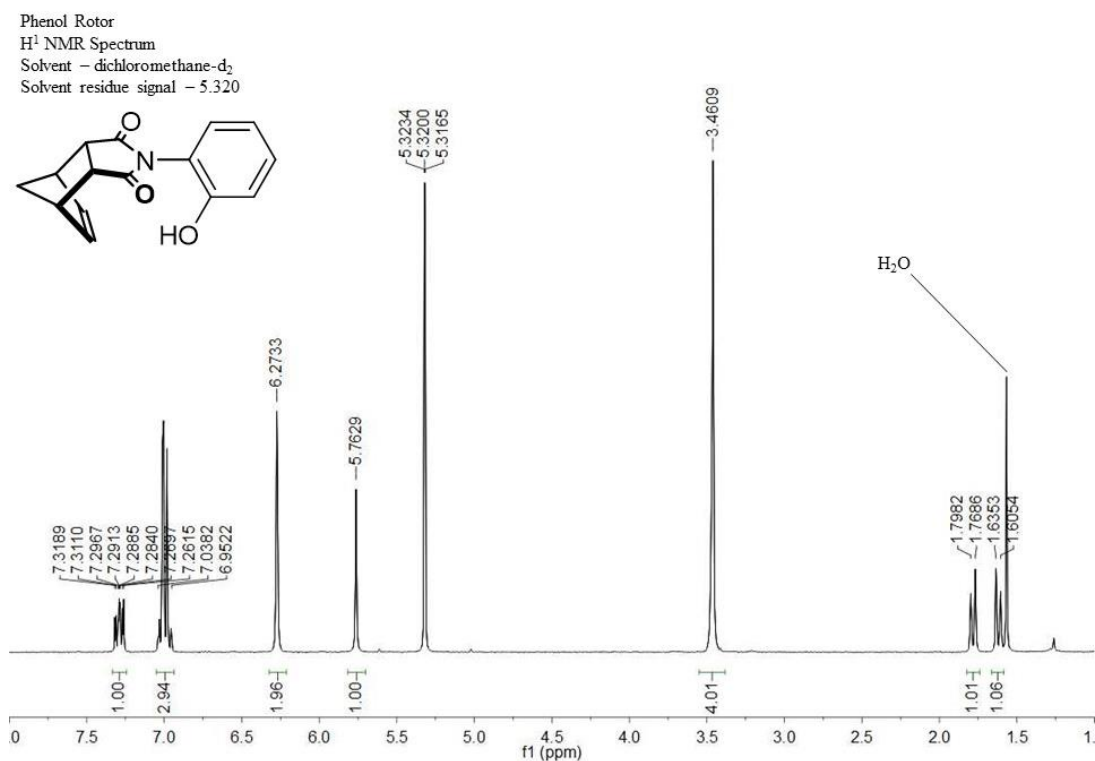


Figure 3.22 ^1H NMR spectra of rotor **1**(X = H) (400 MHz, dichloromethane- d_2)

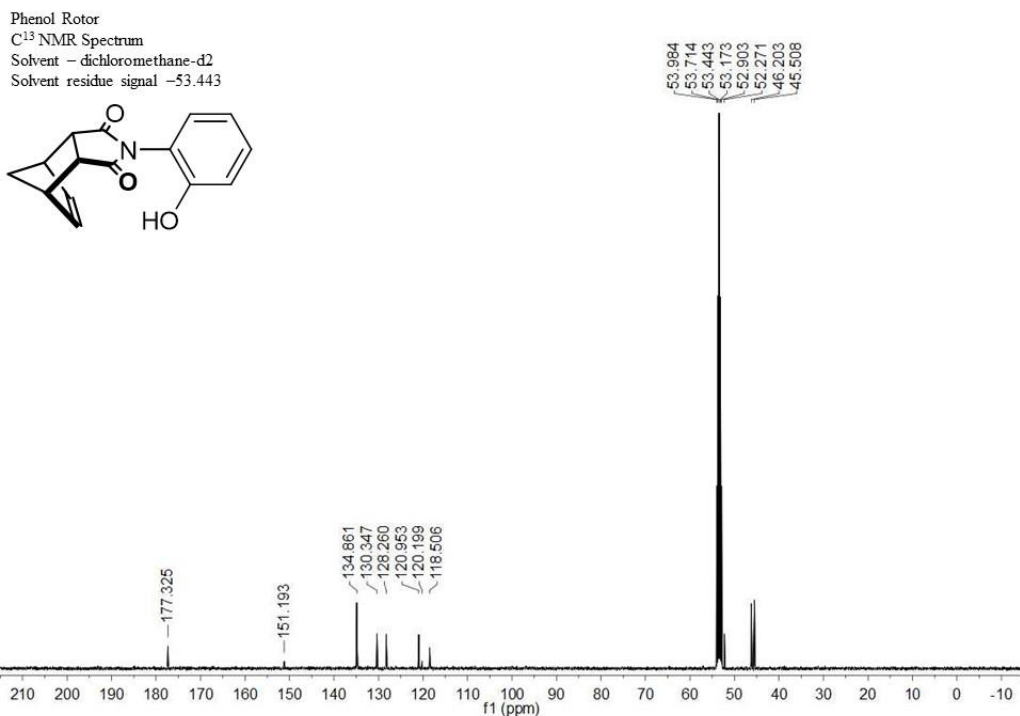


Figure 3.23 ^{13}C NMR spectra of rotor **1**(X = H) (100 MHz, dichloromethane- d_2)

p-NO₂ phenol rotor
 H¹ NMR Spectrum
 Solvent – acetone-d₆
 Solvent residue signal – 2.05

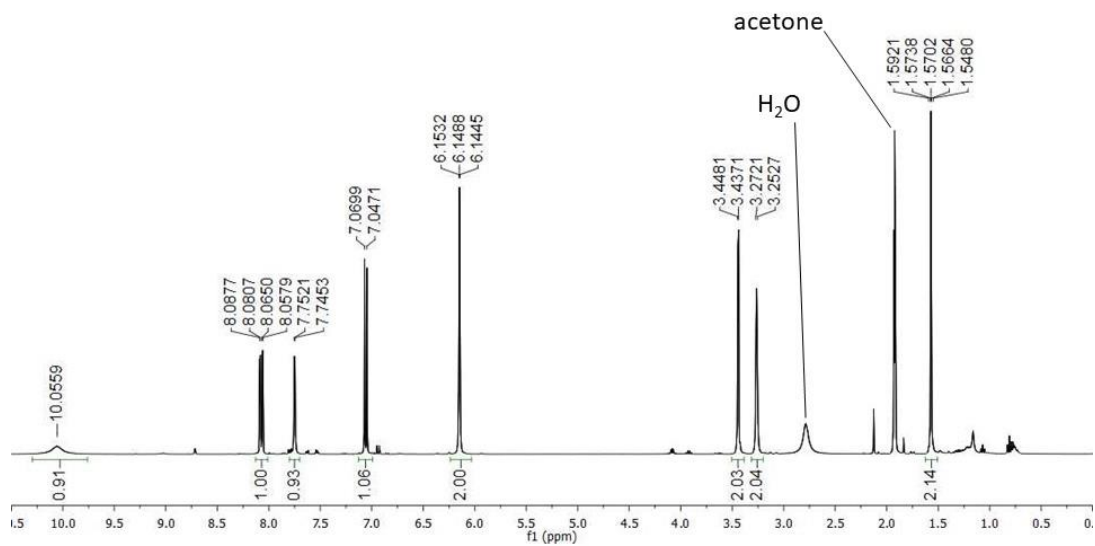
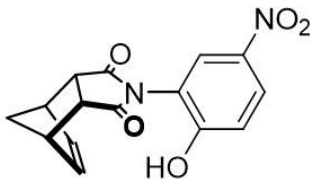


Figure 3.24 ¹H NMR spectra of rotor **1** (X = *p*-NO₂) (400 MHz, acetone-d₆)

p-NO₂ phenol rotor
 C¹³ NMR Spectrum
 Solvent – acetone-d₆
 Solvent residue signal – 205 & 28

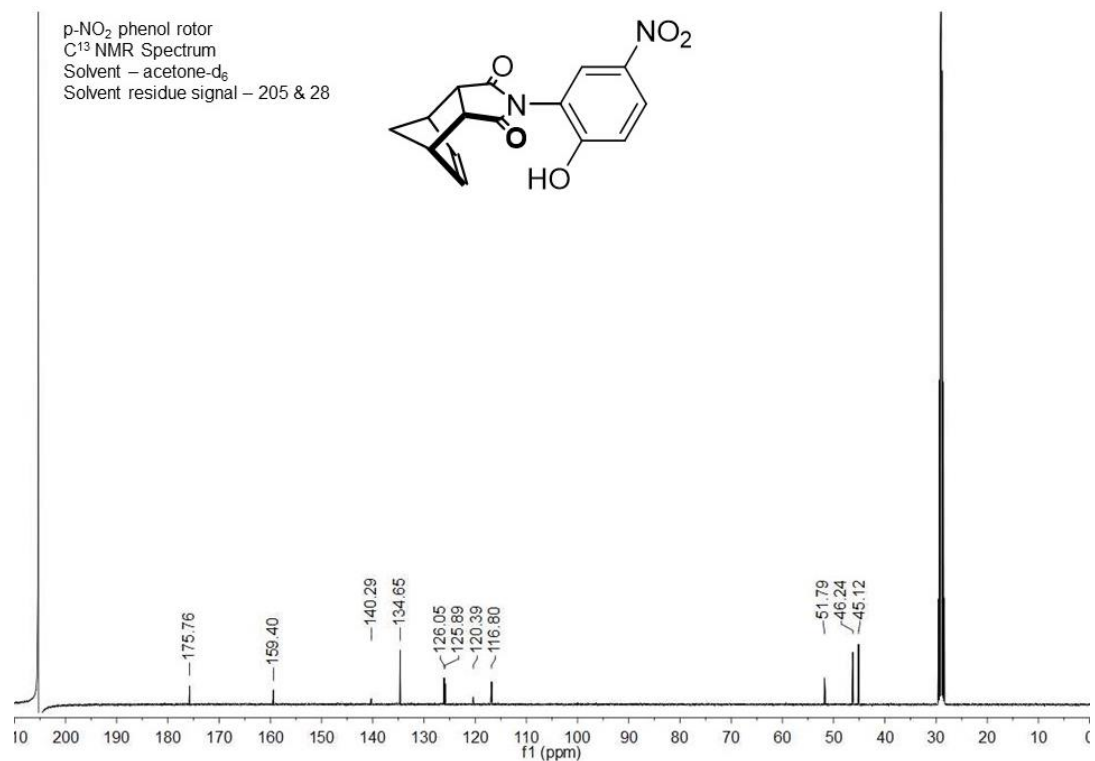
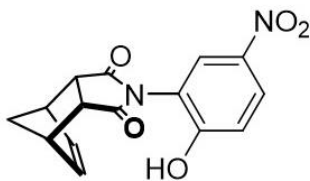


Figure 3.25 ¹³C NMR spectra of rotor **1** (X = *p*-NO₂) (100 MHz, acetone-d₆)

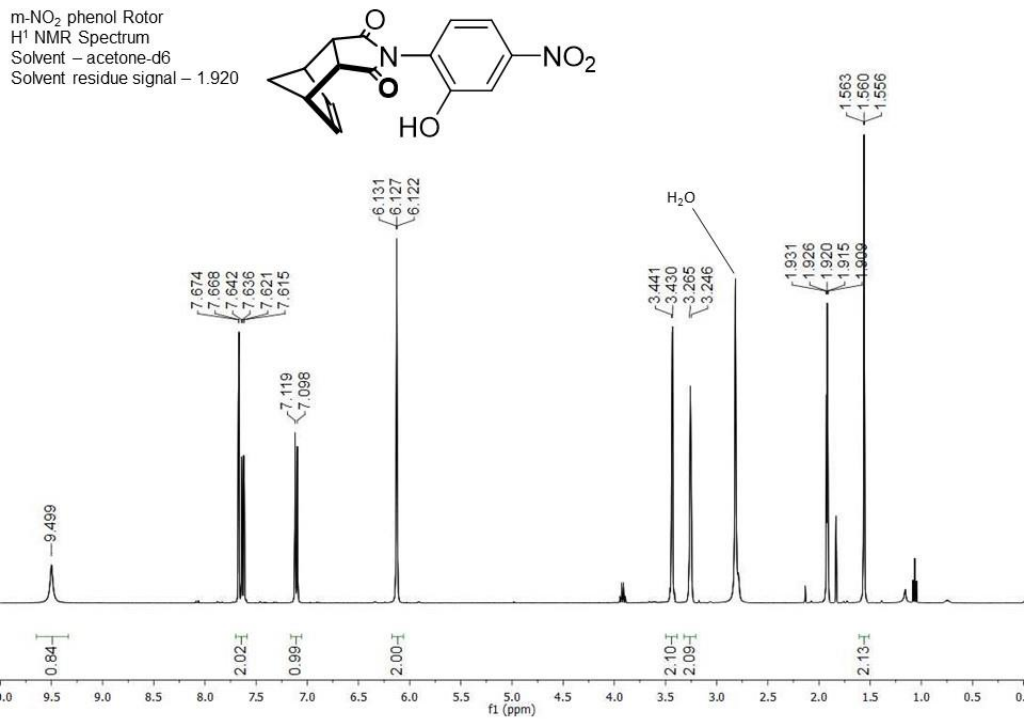


Figure 3.26 ¹H NMR spectra of rotor 1(X = *m*-NO₂) (400 MHz, acetone-d₆)

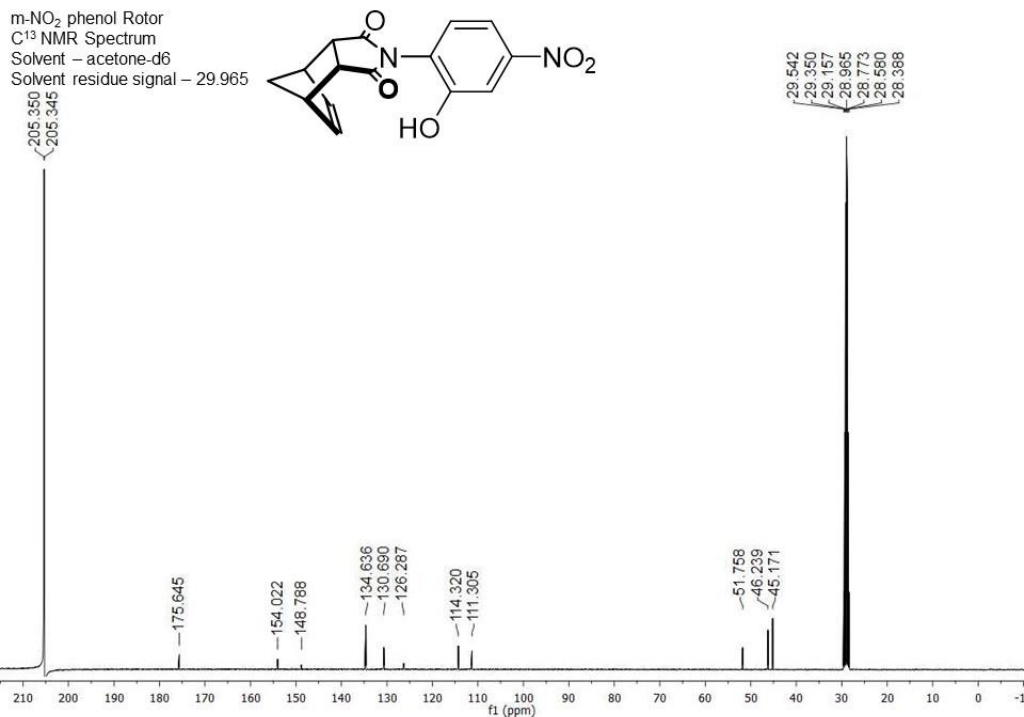


Figure 3.27 ¹³C NMR spectra of rotor 1(X = *m*-NO₂) (100 MHz, acetone-d₆)

p-Cl phenol Rotor
¹H NMR Spectrum
 Solvent – acetone-d6
 Solvent residue signal – 2.07

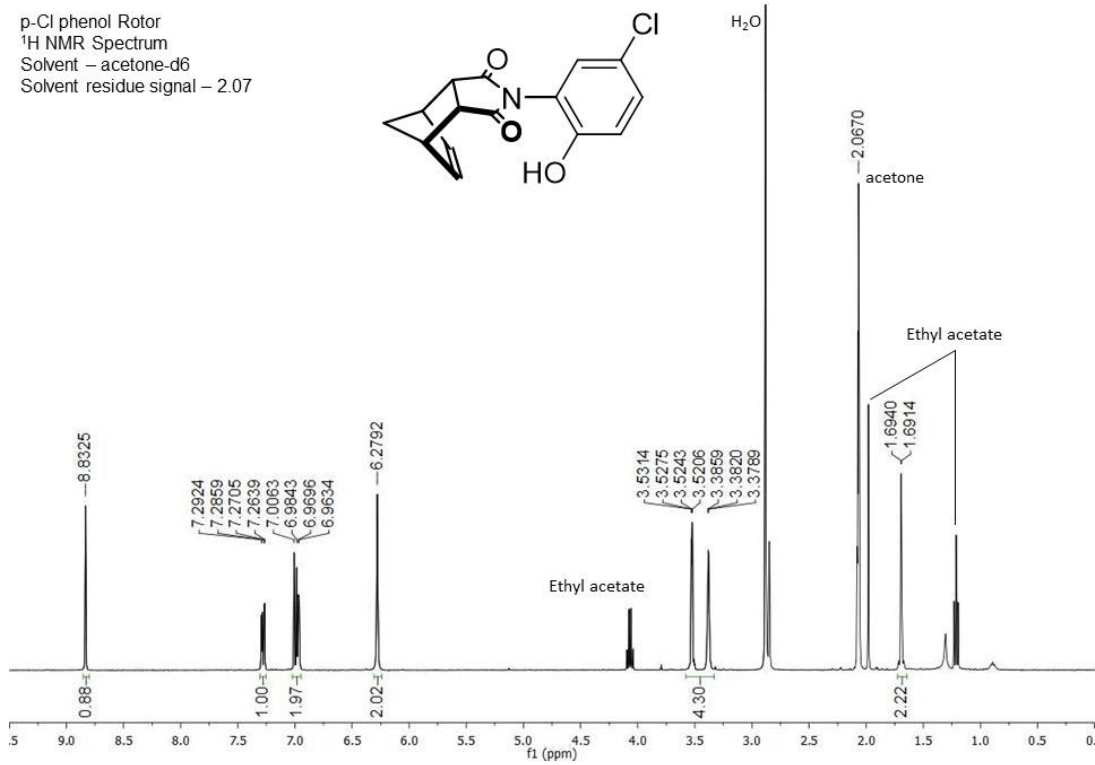


Figure 3.28 ¹H NMR spectra of rotor 1 (X = p-Cl) (400 MHz, acetone-d6)

p-Cl phenol Rotor
¹³C NMR Spectrum
 Solvent – acetone-d6
 Solvent residue signal – 205 & 28

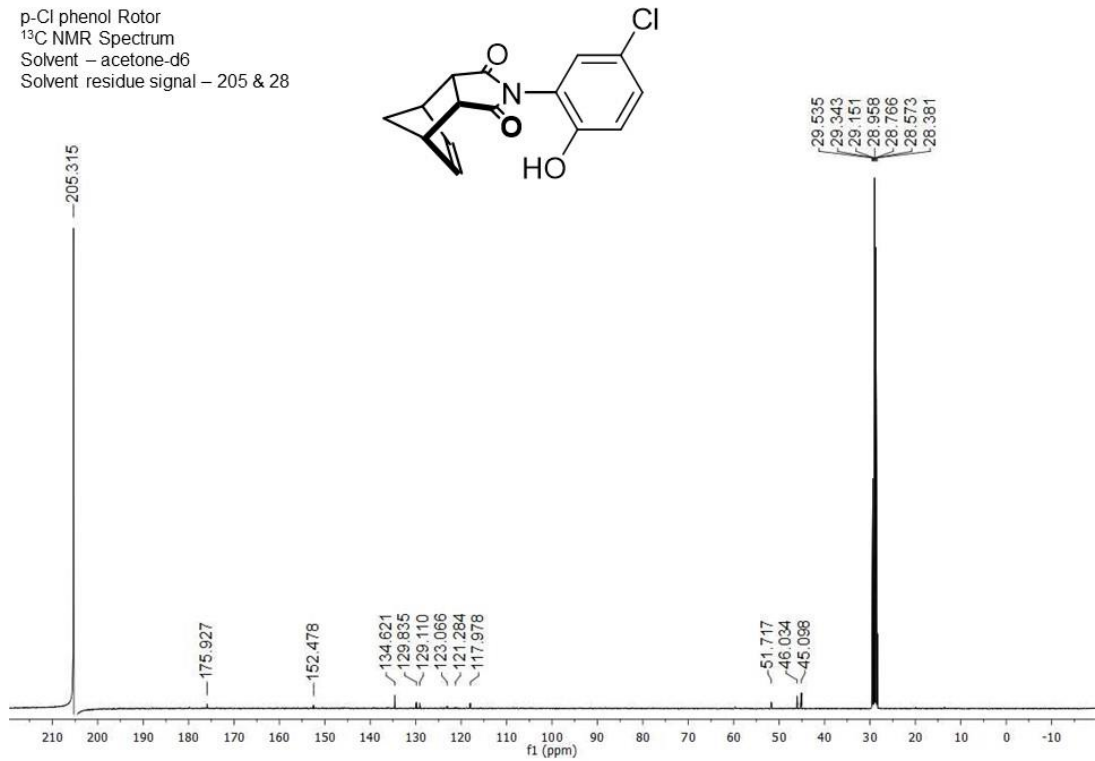


Figure 3.29 ¹³C NMR spectra of rotor 1 (X = p-Cl) (100 MHz, acetone-d6)

m-Cl phenol Rotor
 ^1H NMR Spectrum
 Solvent – acetone- d_6
 Solvent residue signal – 2.07

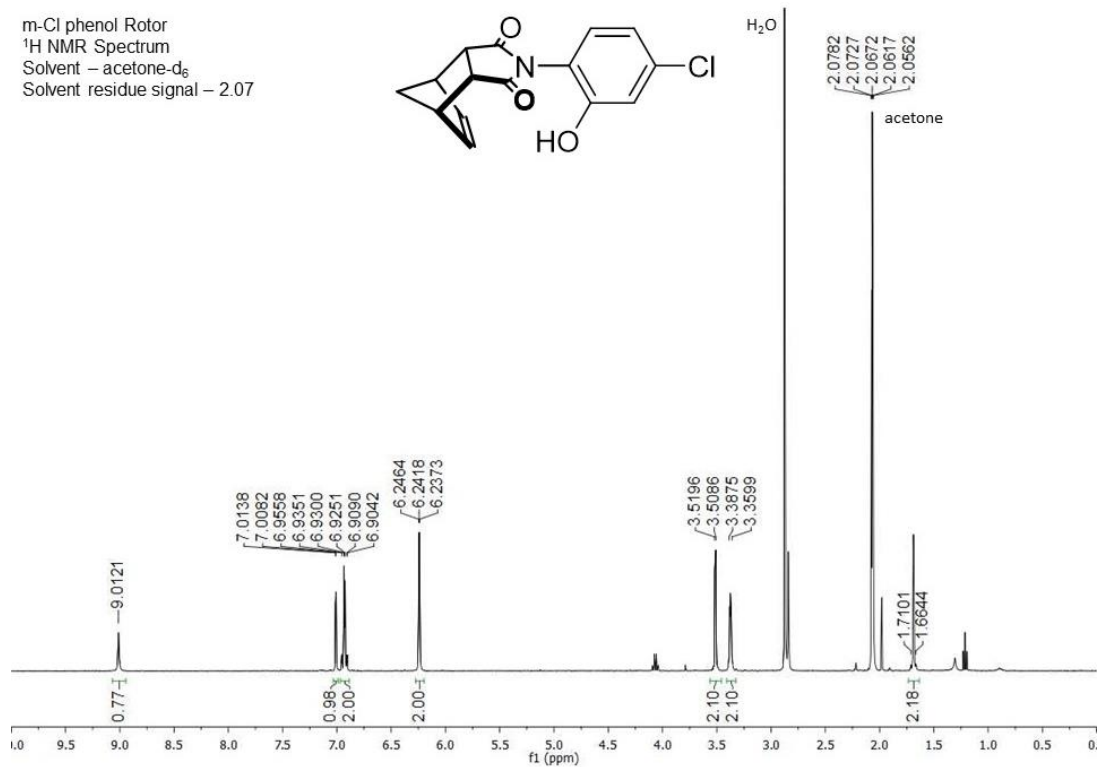


Figure 3.30 ^1H NMR spectra of rotor **1** (X = *m*-Cl) (400 MHz, acetone- d_6)

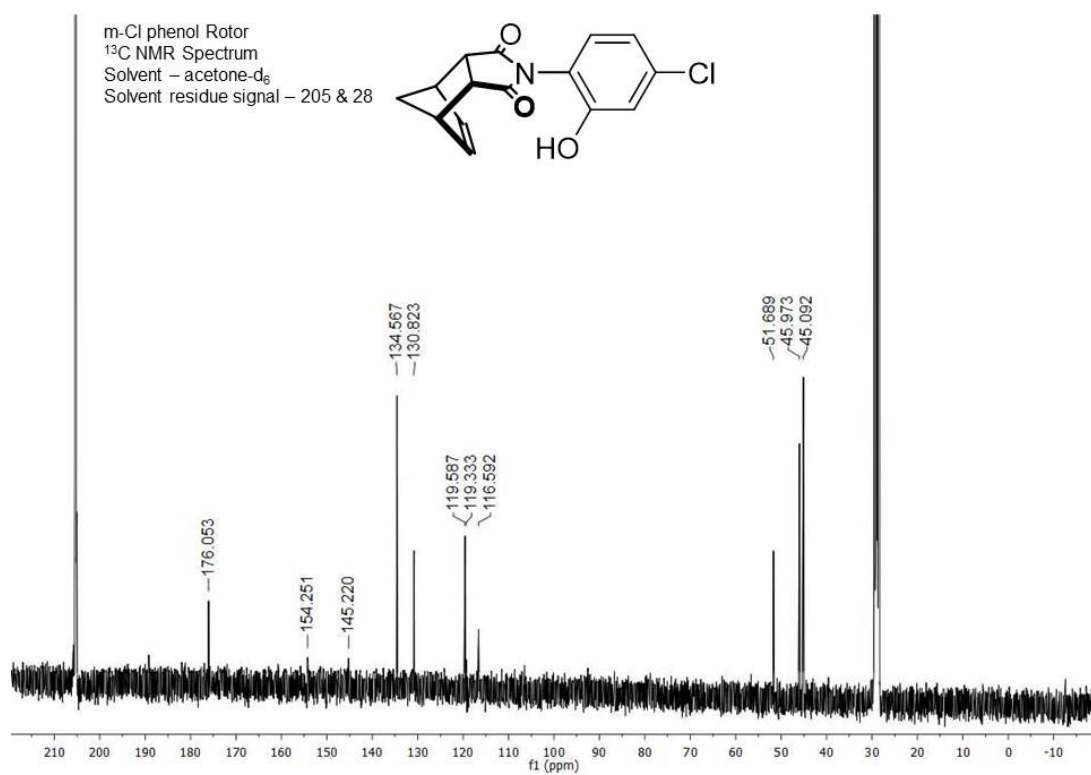


Figure 3.31 ^{13}C NMR spectra of rotor **1** (X = *m*-Cl) (100 MHz, acetone- d_6)

p-CN phenol Rotor
¹H NMR Spectrum
 Solvent – acetone-d₆
 Solvent residue signal – 2.05

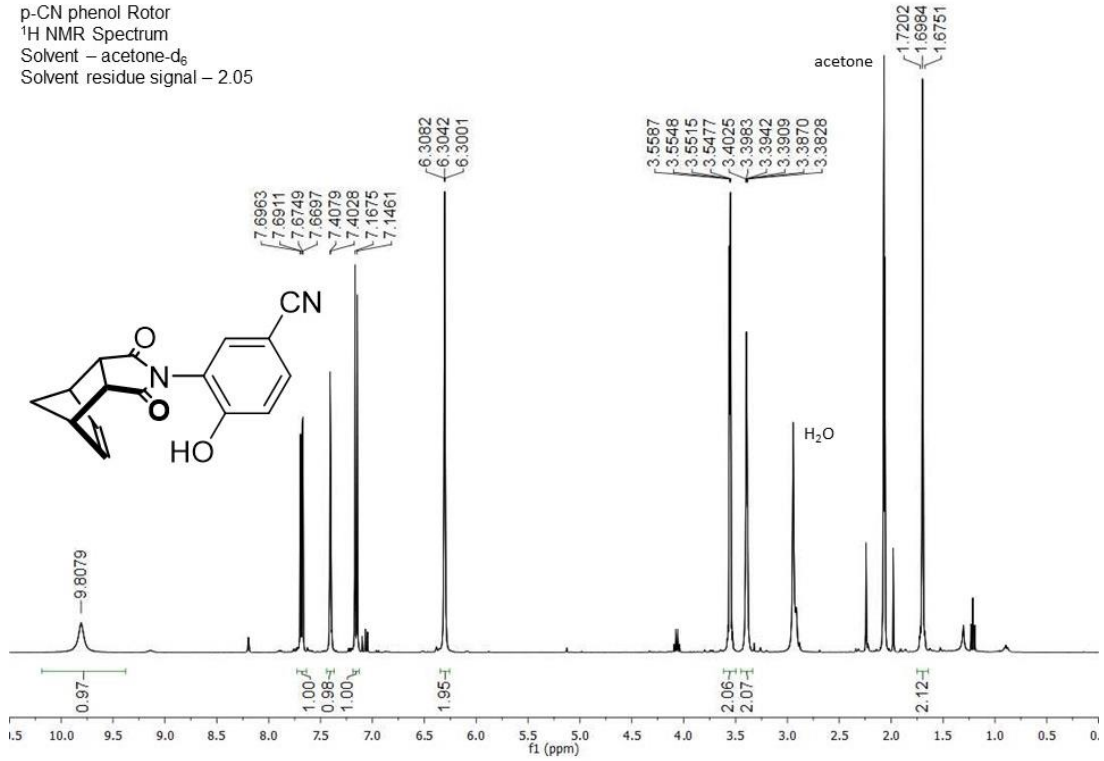


Figure 3.32 ¹H NMR spectra of rotor 1 (X = *p*-CN) (400 MHz, acetone-d₆)

p-CN phenol Rotor
¹³C NMR Spectrum
 Solvent – acetone-d₆
 Solvent residue signal – 205 & 28

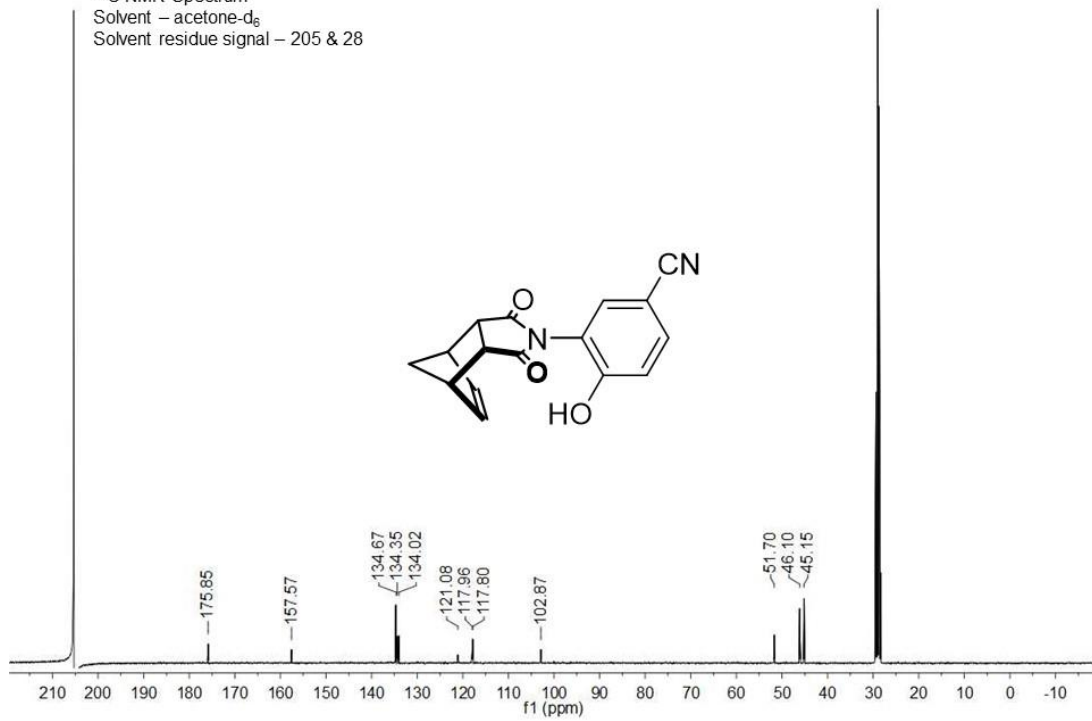


Figure 3.33 ¹³C NMR spectra of rotor 1 (X = *p*-CN) (100 MHz, acetone-d₆)

Tert-amyl phenol rotor
¹H NMR Spectrum
 Solvent – chloroform-d1
 Solvent residue signal – 7.285

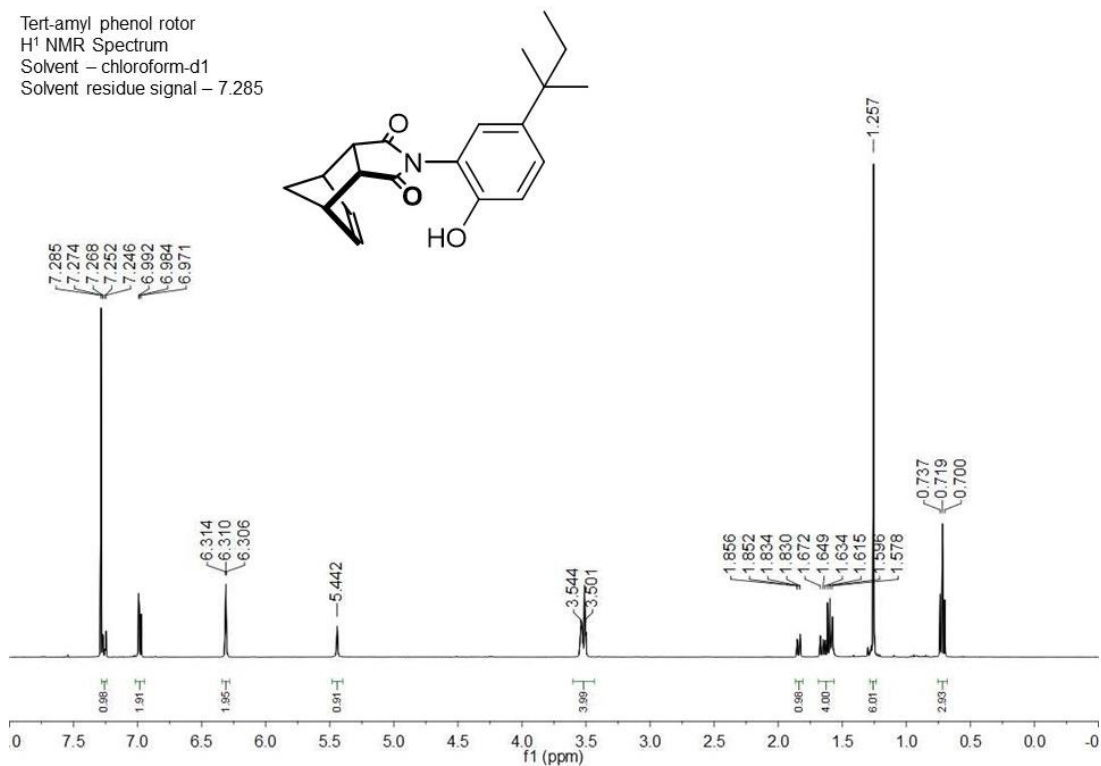


Figure 3.34 ¹H NMR spectra of rotor **1** (X = *p-t*-amyl) (400 MHz, chloroform-d₁)

Tert-amyl phenol rotor
¹³C NMR Spectrum
 Solvent – chloroform-d1
 Solvent residue signal – 77.36, 77.04, 76.72

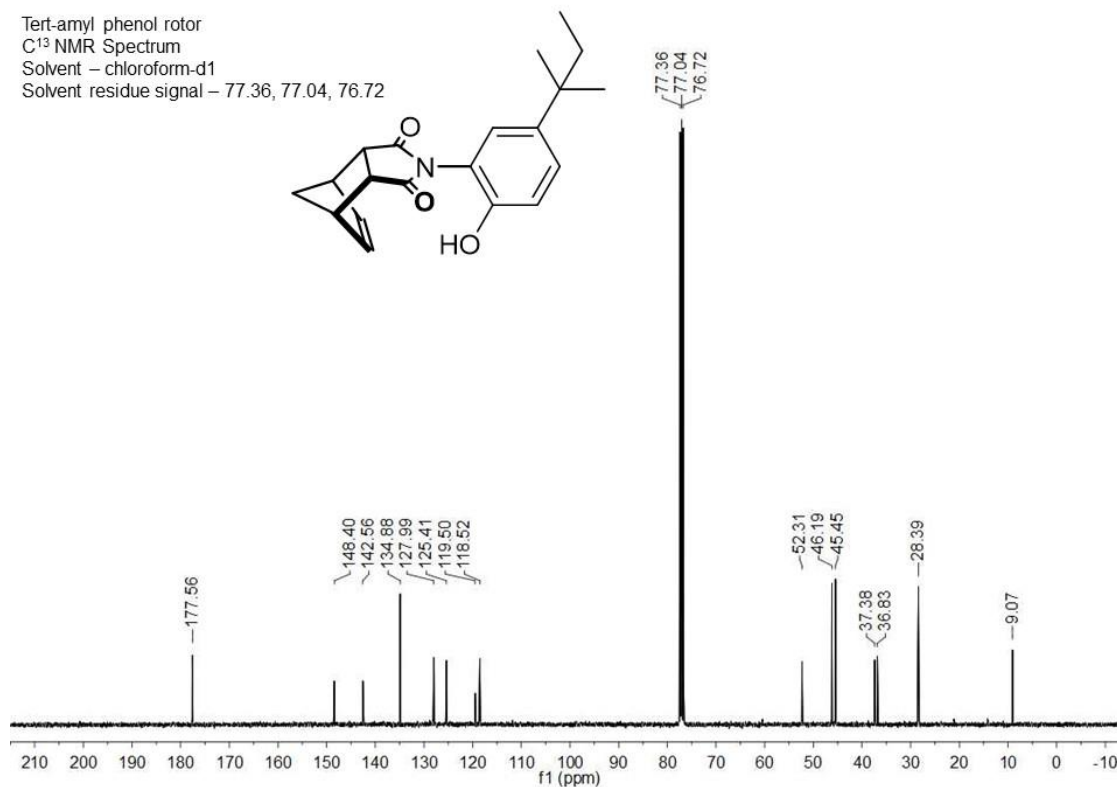


Figure 3.35 ¹³C NMR spectra of rotor **1** (X = *p-t*-amyl) (100 MHz, chloroform-d₁)

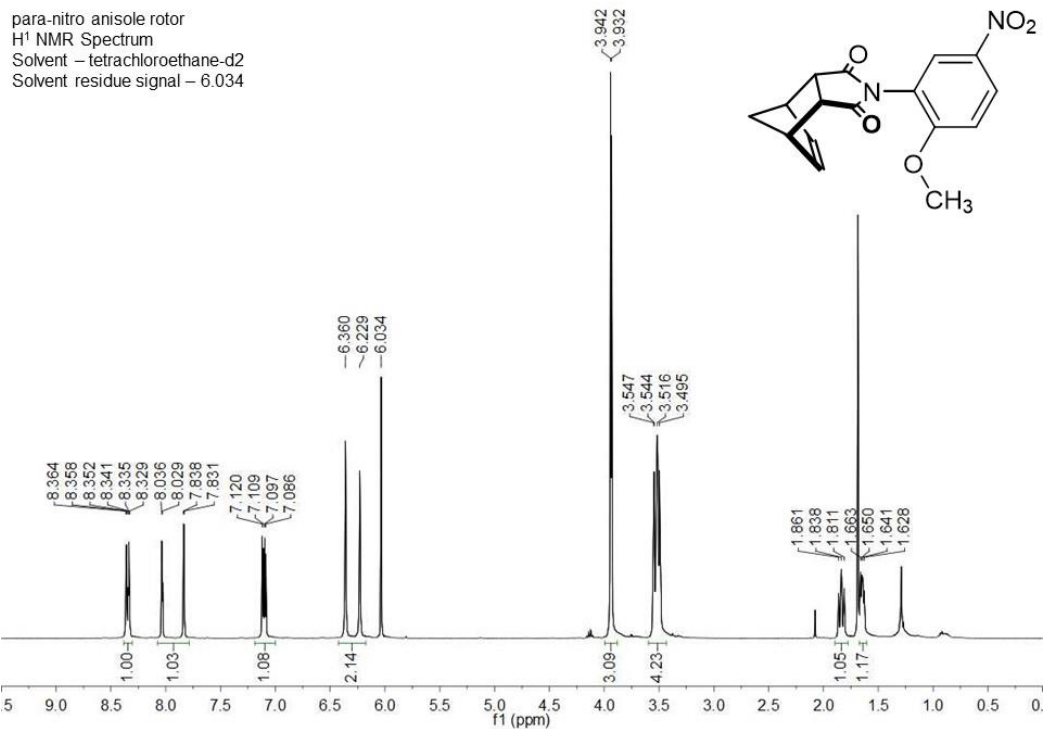


Figure 3.36 ^1H NMR spectra of rotor **2** (X = *p*-NO₂) (400 MHz, tetrachloroethane- d_4)

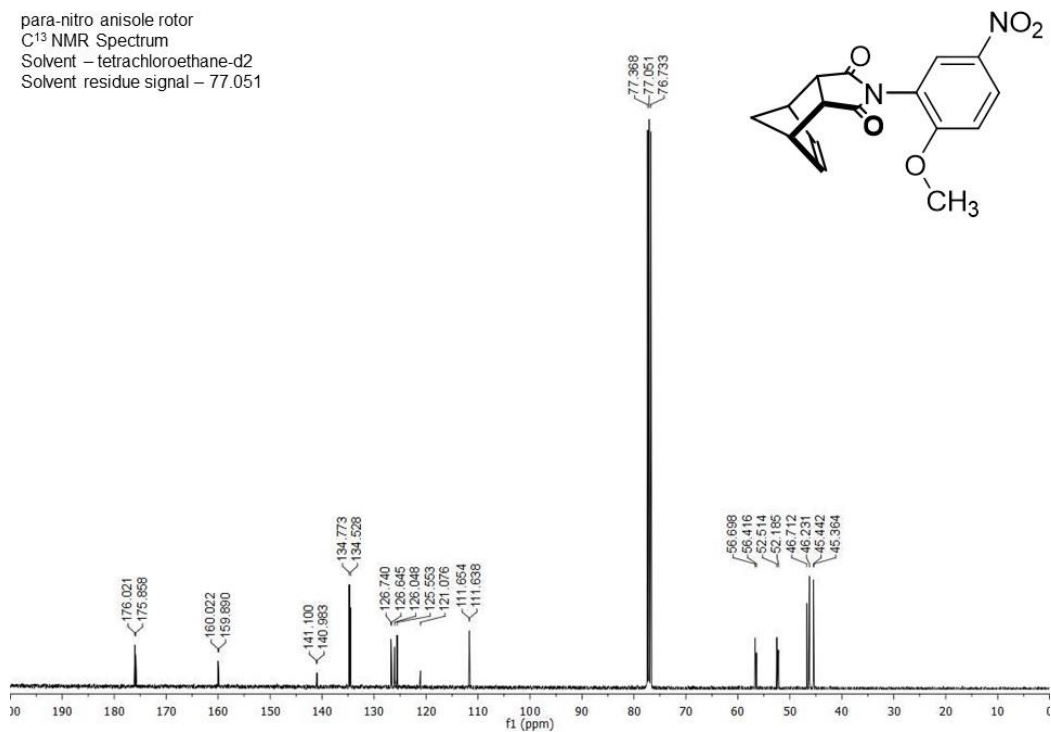


Figure 3.37 ^{13}C NMR spectra of rotor **2** (X = *p*-NO₂) (400 MHz, tetrachloroethane- d_4)

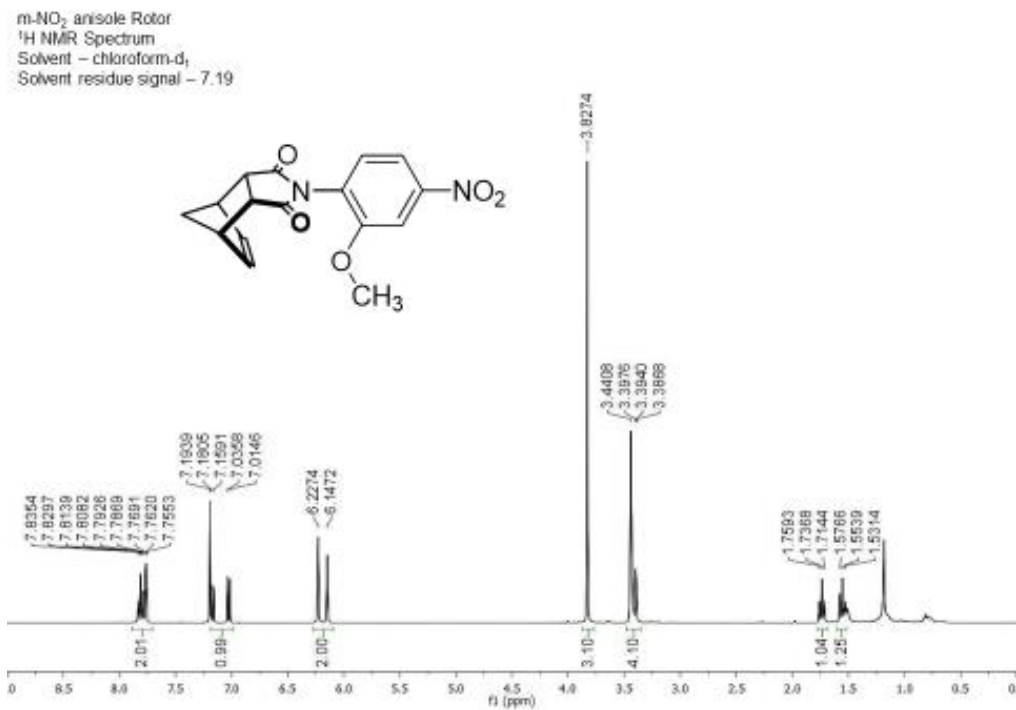


Figure 3.38 ¹H NMR spectra of rotor **2**(X = *m*-NO₂) (400 MHz, chloroform-d₁)

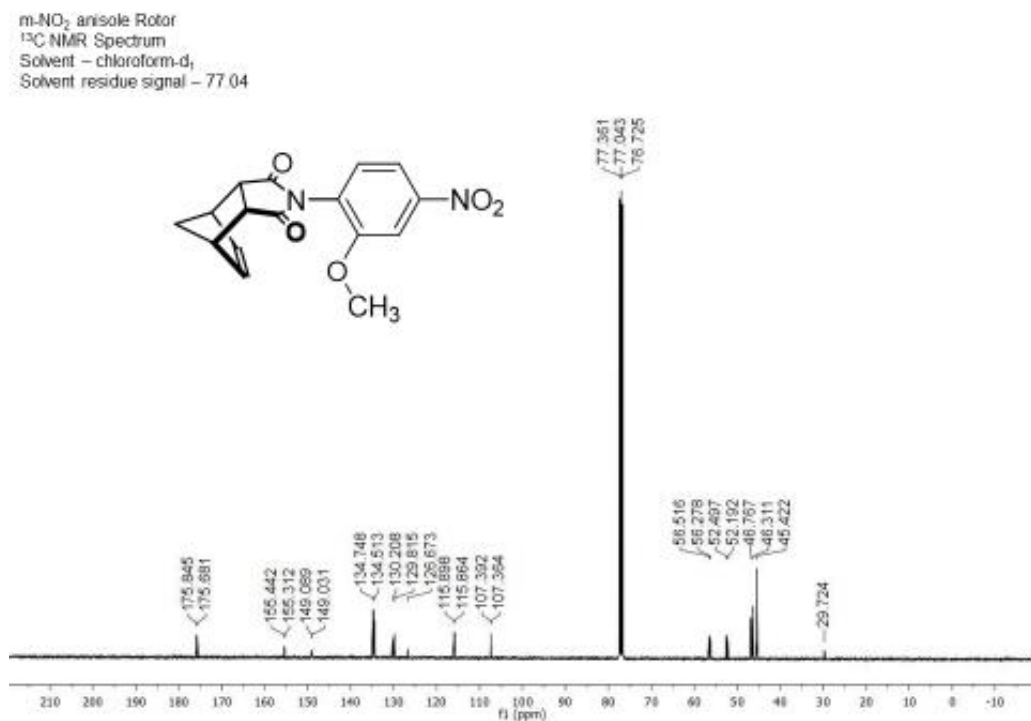


Figure 3.39 ¹³C NMR spectra of rotor **2**(X = *m*-NO₂) (100 MHz, chloroform-d₁)

p-Cl anisole Rotor
¹H NMR Spectrum
 Solvent – tetrachloroethane-d₂
 Solvent residue signal – 5.92

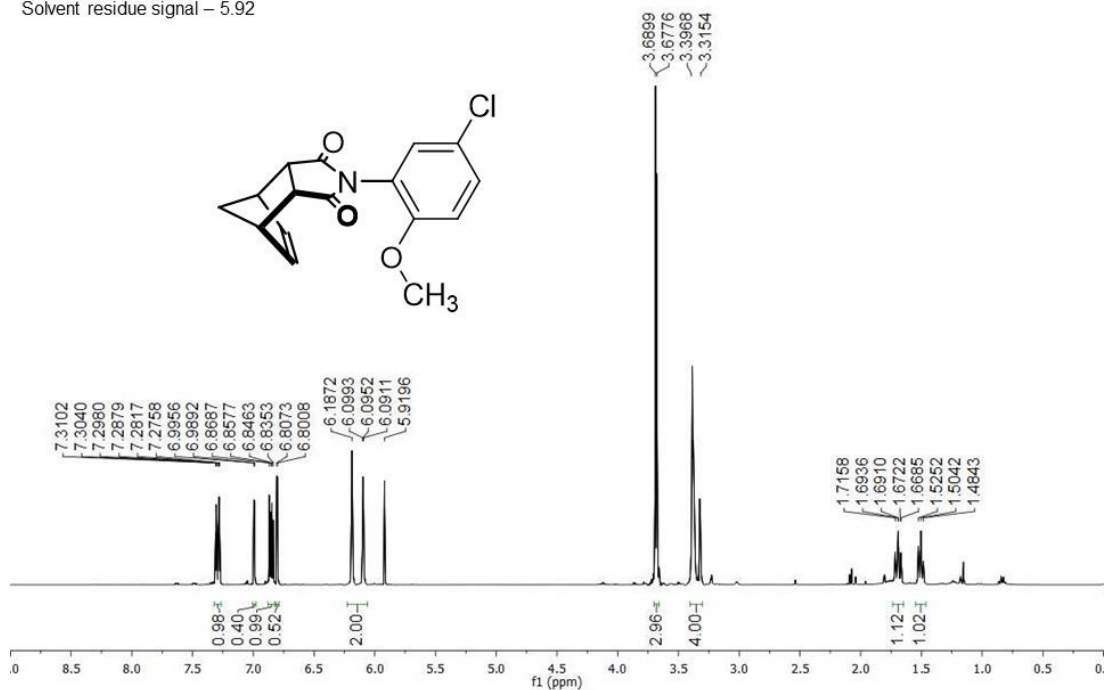


Figure 3.40 ¹H NMR spectra of rotor 2 (X = p-Cl) (100 MHz, acetone-d₆)

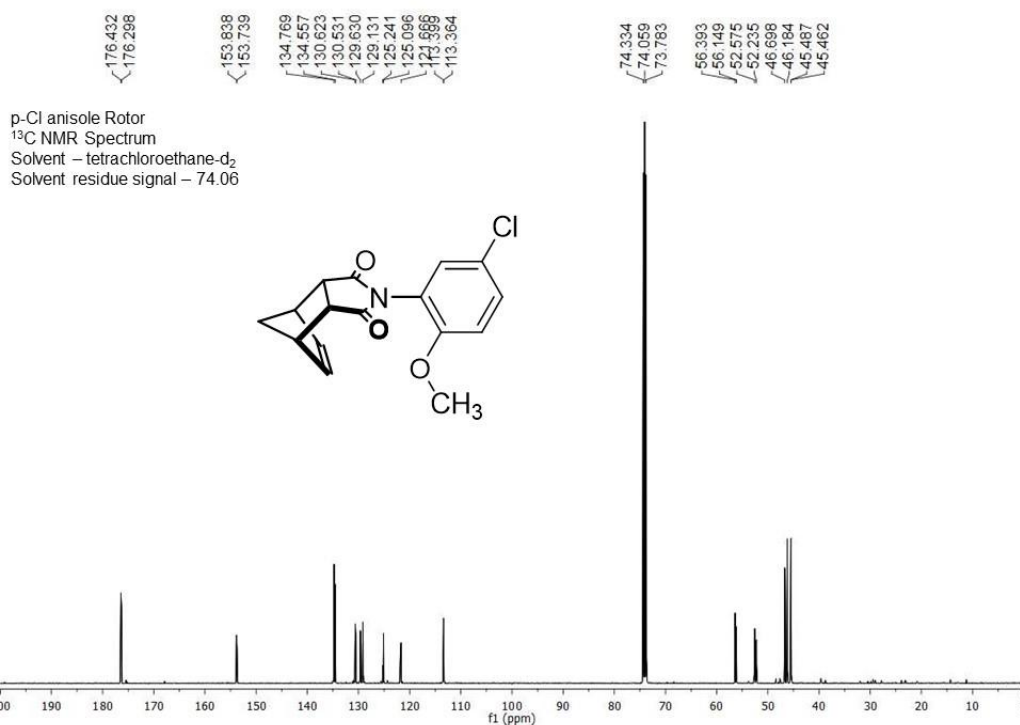


Figure 3.41 ¹³C NMR spectra of rotor 2 (X = p-Cl) (100 MHz, acetone-d₆)

m-Cl anisole Rotor
¹H NMR Spectrum
 Solvent – acetone-d₆
 Solvent residue signal – 2.07

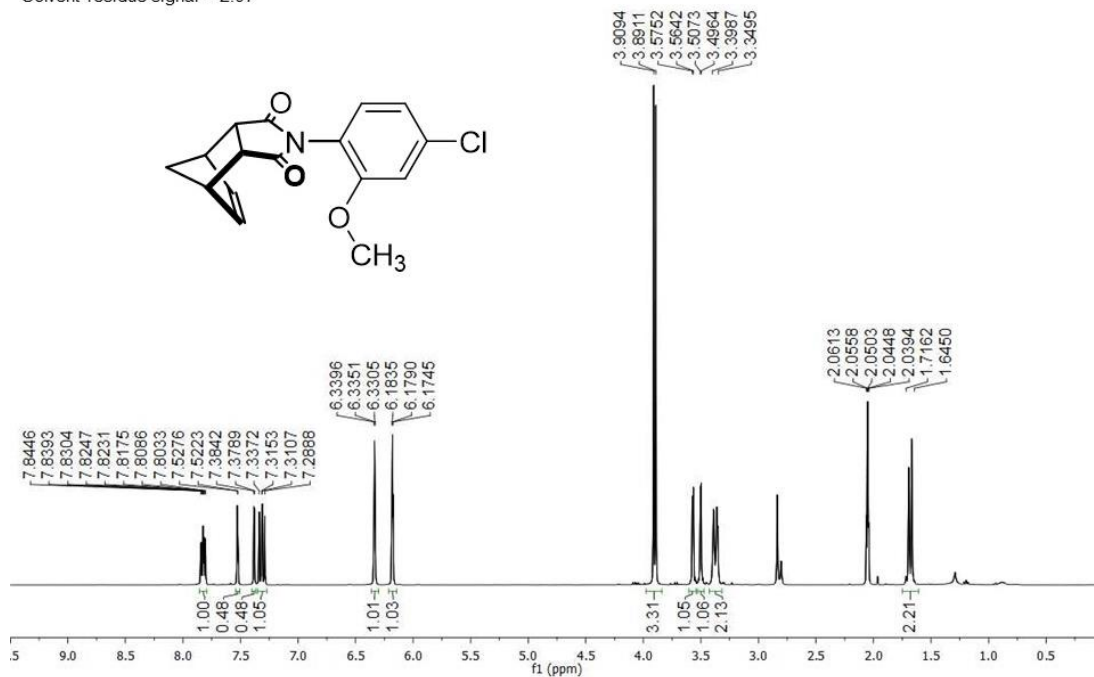


Figure 3.42 ¹H NMR spectra of rotor 2(X = m-Cl) (400 MHz, acetone-d₆)

m-Cl anisole Rotor
¹H NMR Spectrum
 Solvent – acetone-d₆
 Solvent residue signal – 2.07

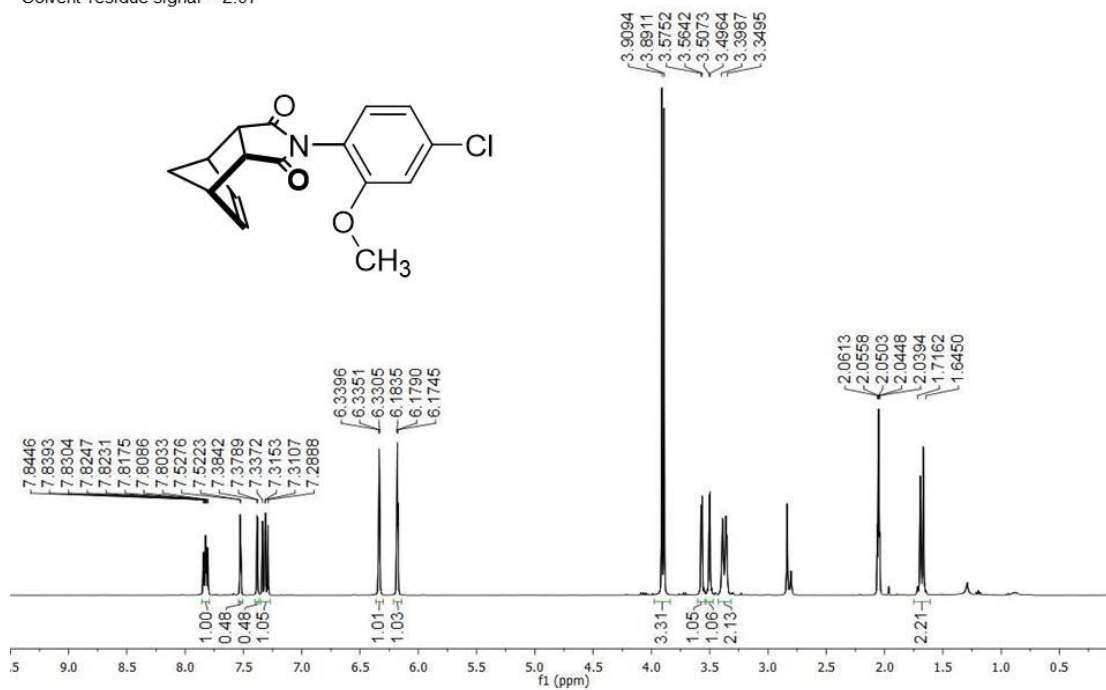


Figure 3.43 ¹³C NMR spectra of rotor 2(X = m-Cl) (100 MHz, acetone-d₆)

p-CN anisole Rotor
¹H NMR Spectrum
 Solvent – acetone-d₆
 Solvent residue signal – 2.05

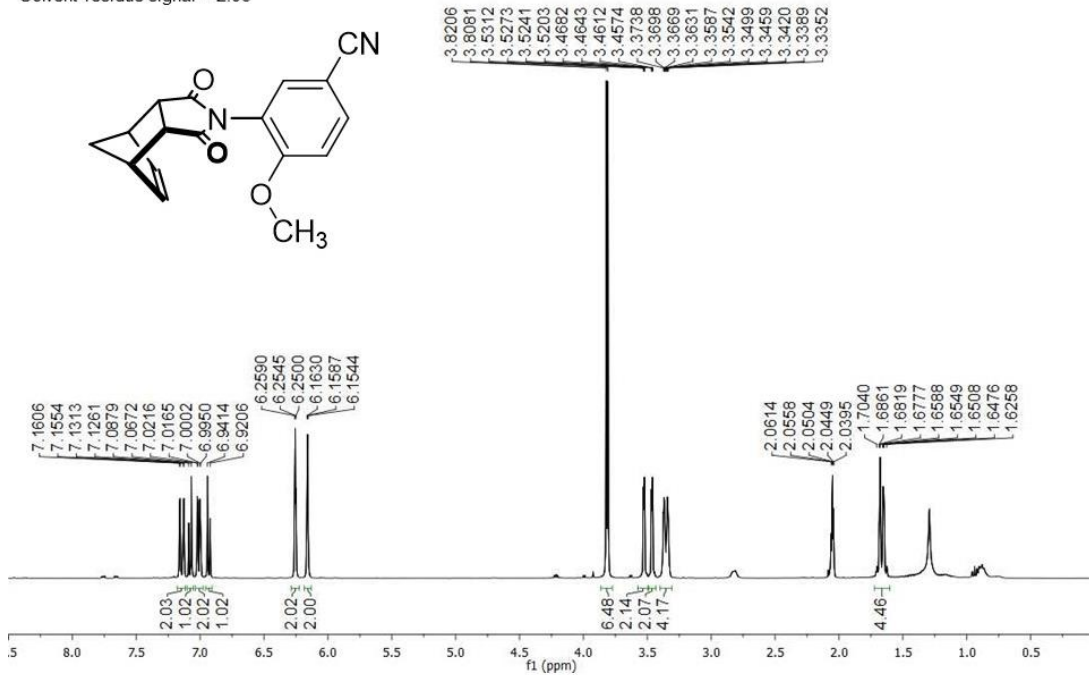


Figure 3.44 ¹H NMR spectra of rotor 2 (X = p-CN) (400 MHz, acetone-d₆)

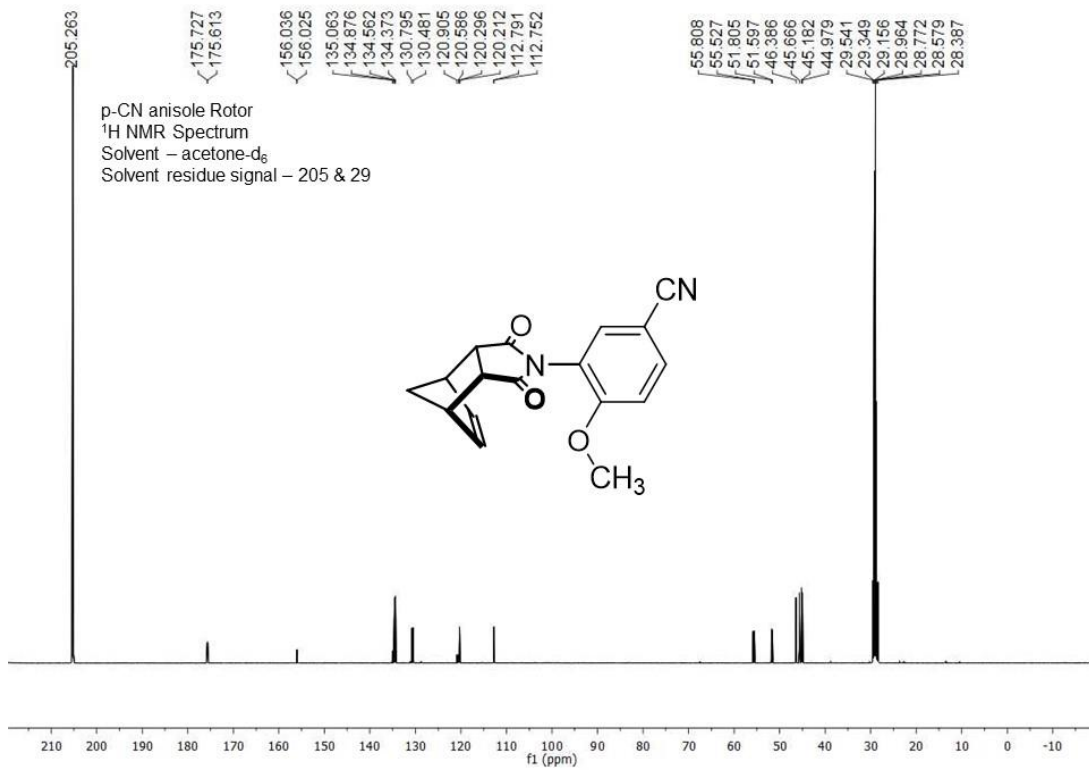


Figure 3.45 ¹³C NMR spectra of rotor 2 (X = p-CN) (100 MHz, acetone-d₆)

tert-amyl anisole rotor
¹H NMR Spectrum
 Solvent – acetone-d₆
 Solvent residue signal – 2.050

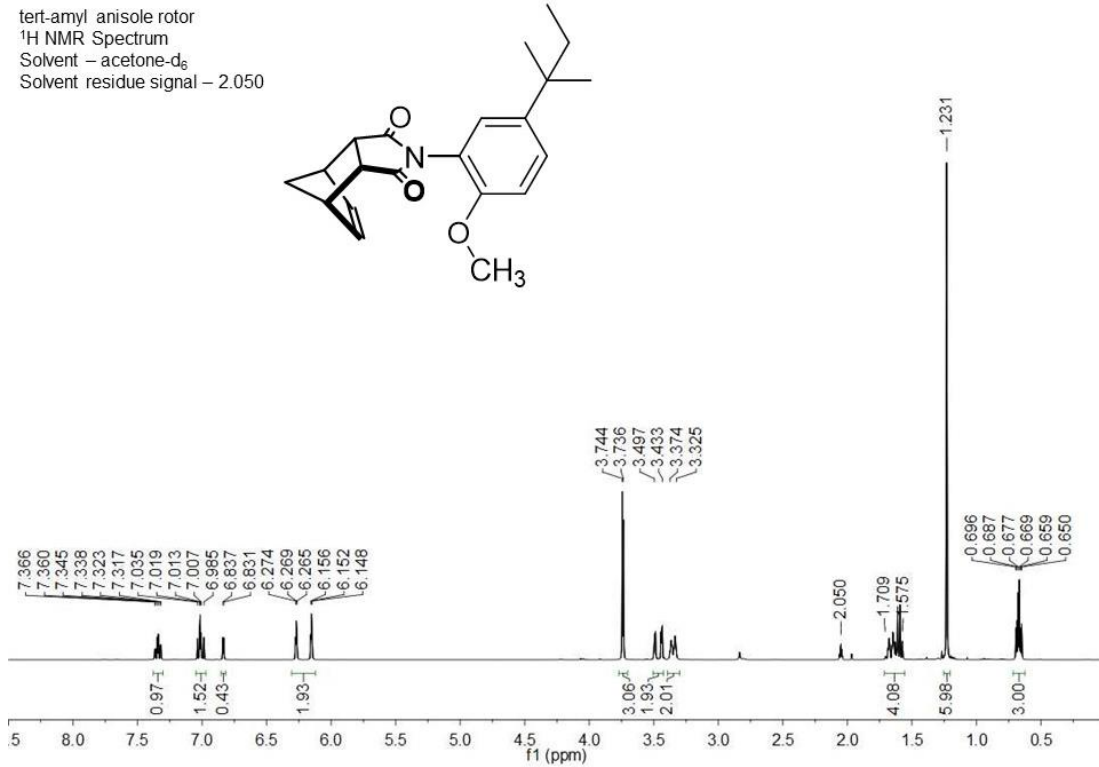


Figure 3.46 ¹H NMR spectra of rotor 2(X = p-t-amyl) (400 MHz, acetone-d₆)

tert-amyl anisole rotor
¹H NMR Spectrum
 Solvent – acetone-d₆
 Solvent residue signal – 2.050

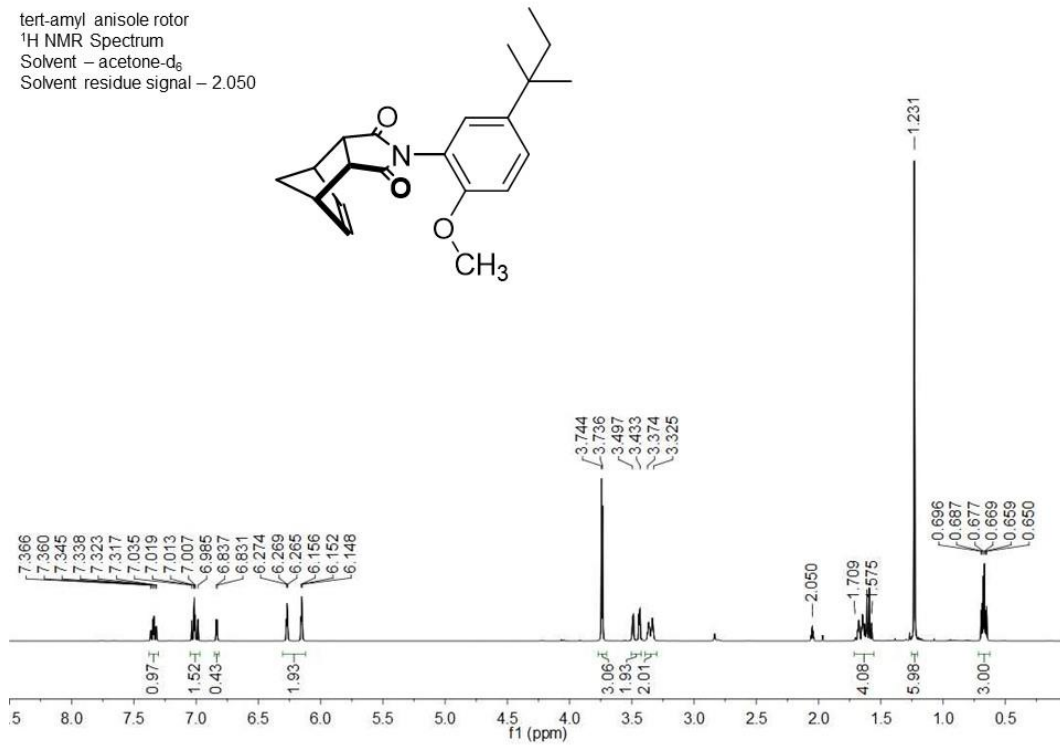


Figure 3.47 ¹³C NMR spectra of rotor 2(X = p-t-amyl) (100 MHz, acetone-d₆)

3.4.4 EXPERIMENTAL DETERMINATION OF ROTATIONAL BARRIERS

The rotational barriers of rotors **1** and **2** (Table 3.1) were determined via coalescence temperature analysis (Figure 3.48) and corroborated by NMR line-shape analysis of chemical exchange signals (Figure 3.49). The coalescence temperature and line-shape analyses were carried out in accordance with literature precedence.^{16,80} Line-shape analysis was performed using the Bruker Topspin software. The rotational barrier for each rotor was obtained from the coalescence temperature analysis using Equations 3.3-3.4. The TS enthalpy (ΔH^\ddagger) and entropy (ΔS^\ddagger) for the unsubstituted phenol and anisole rotors were obtained from the Eyring plots (Figure 3.50) following Equation 3.5. The rotation barriers were determined by plugging the enthalpy and entropy along with a temperature into Equation 3.6.

Due to the large difference in coalescence temperatures for the phenol and anisole rotors two different solvents with similar chemical properties but different melting/boiling temperatures were chosen. Dichloromethane-d₂ (melting point = -95, boiling point = 40 °C) was an appropriate choice as a solvent for the phenol rotors **1** which have an average coalescence temperature of -61 °C. Meanwhile, tetrachloroethane-d₂ (melting point = -45, boiling point = 145 °C) was an appropriate choice as a solvent for the anisole rotors **2** which have an average coalescence temperature of 97 °C.

$$\Delta G^\ddagger = -RT \ln \left(\frac{k_c h}{k_B T_c} \right) \dots \dots \dots \text{Equation 3.3}$$

$$k_c = \frac{\pi \Delta \nu}{\sqrt{2}} \dots \dots \dots \text{Equation 3.4}$$

$$\ln \left(\frac{k_{ex}}{T} \right) = \frac{-\Delta H^\ddagger}{R} \cdot \frac{1}{T} + \ln \left(\frac{k_B}{h} \right) + \frac{-\Delta S^\ddagger}{R} \dots \dots \dots \text{Equation 3.5}$$

$$\Delta G^\ddagger = \Delta H^\ddagger - T \Delta S^\ddagger \dots \dots \dots \text{Equation 3.6}$$

Table 3.1 Experimental rotational barrier (ΔG^\ddagger , kcal/mol) for rotors **1** and **2** via coalescence temperature and exchange line-shape analyses.

Rotor		coalescence temperature			exchange line-shape analysis			Isotope effect
label	X	ΔG^\ddagger ^a	Temperature (Celsius)	Rate (k _c)	ΔG^\ddagger ^{ab}	ΔH^\ddagger ^a	ΔS^\ddagger ^a	k _H /k _D
1	H	10.89	-55	54.40	10.75	10.58	-5.68 x 10 ⁻⁴	0.926 ^e
1	H	10.91	-55	52.26				
1 ^c	H	10.91	-55	52.27				
1 ^d	H	10.77	-57	56.71				
1 ^d	H	10.87	-55	58.04				
1	p-NO ₂	9.73	-67	202.12				
1	m-NO ₂	9.99	-62	196.26				
1	p-Cl	10.39	-60	97.15				
1	m-Cl	10.08	-65	111.99				
1	p-CN	9.96	-65	147.19				
1	p-t-amyl	10.91	-55	52.71				
2	H	20.77	113	12.89	20.14	20.16	6.19 x 10 ⁻⁵	
2	p-NO ₂	19.35	82	8.98				
2	m-NO ₂	19.58	86	8.98				
2	p-Cl	20.11	98	10.93				
2	m-Cl	20.15	95	8.18				
2	p-CN	20.36	103	11.47				
2	p-t-amyl	20.35	105	13.33				

^a energy in kcal/mol. ^b at 298.15 K. ^c mixed with H₂O. ^d mixed with D₂O, no phenolic signal was observed in the ¹H NMR spectra. ^e Average isotope effect.

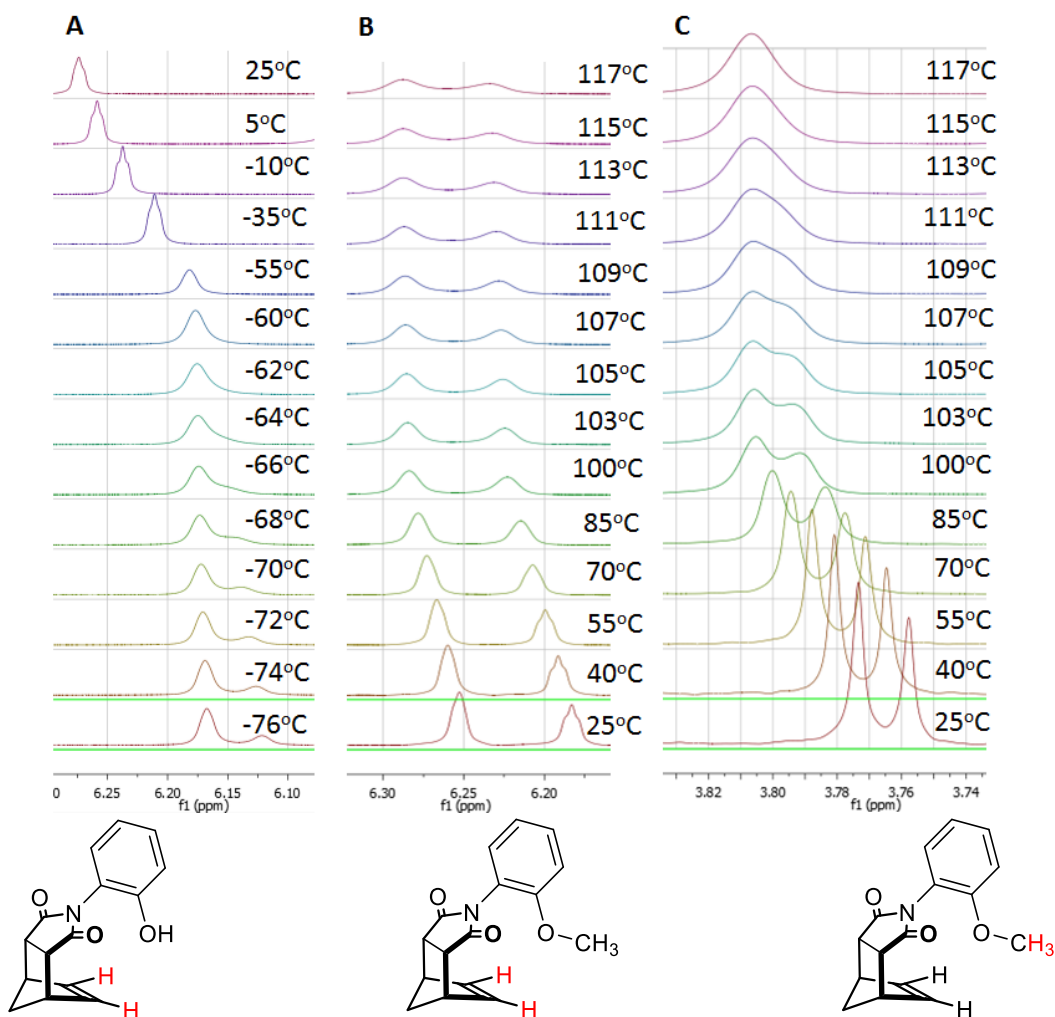


Figure 3.48 Spectral regions of rotor **1** (**A**) and rotor **2** (**B** and **C**) in VT NMR experiment: **A**) ethene protons on rotor **1** coalesced at -55 °C (dichloromethane- d_2); **B**) ethene protons on rotor **2** did not reach coalescence up to 117 °C; **C**) methoxy protons on rotor **2** coalesced at 113 °C (tetrachloroethane- d_2).

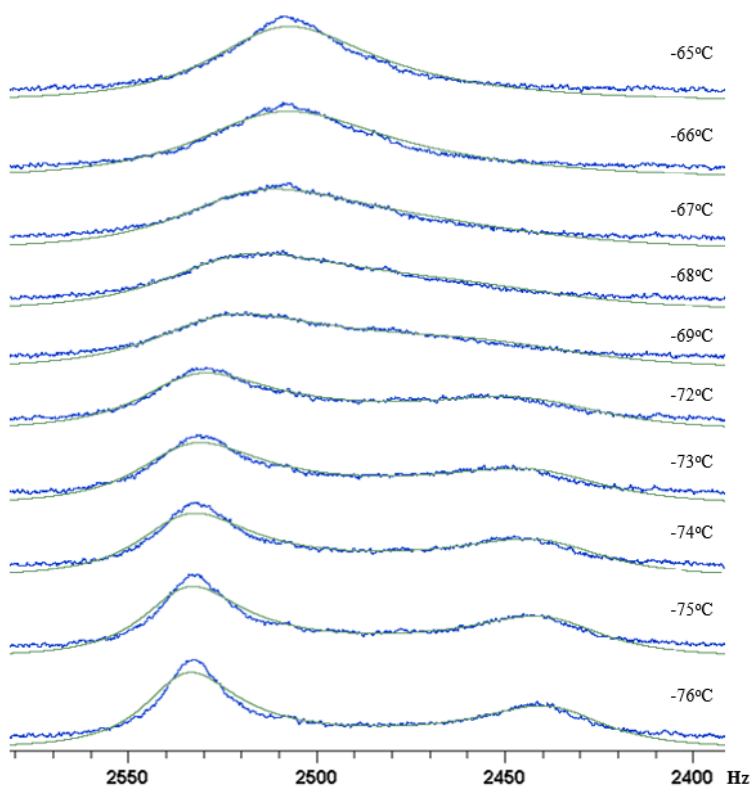


Figure 3.49 ^1H NMR exchange line-shape analysis for unsubstituted phenol rotor **1** in dichloromethane- d_2 showing the overlaid experimental (blue lines) and simulated (green lines) traces

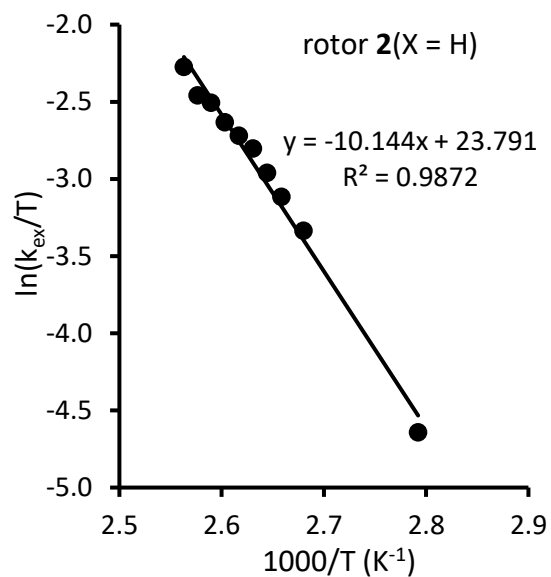
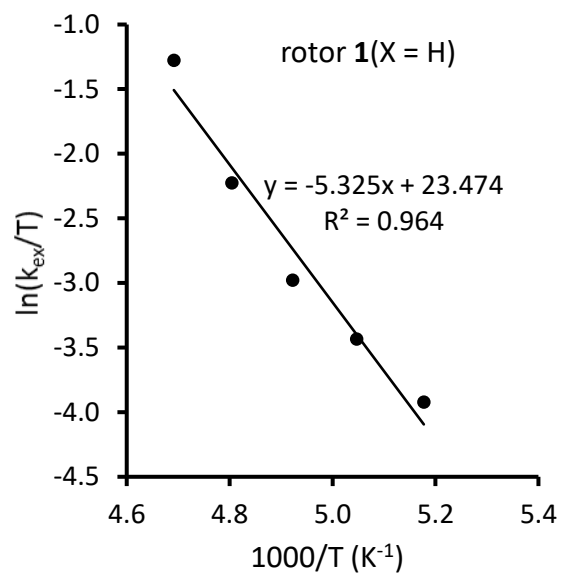


Figure 3.50 Eyring plots for rotors 1 and 2

3.4.5 INTERMOLECULAR HYDROGEN BOND ASSOCIATION MEASUREMENTS

The intermolecular hydrogen bond strength between *N*-methylpyrrolidone (NMP) and substituted phenols ($X = \text{H}, p\text{-NO}_2, m\text{-NO}_2, p\text{-Cl}, m\text{-Cl}, p\text{-CN}, p\text{-t-amyl}$) were measured (Figure 3.51) in dichloromethane- d_2 to gauge the strength of the intramolecular hydrogen bond in phenol rotors **1**. NMP was chosen due to its structural similarity to the hydrogen bond acceptor imide in the phenol rotors and its convenience of handling in titration experiment.

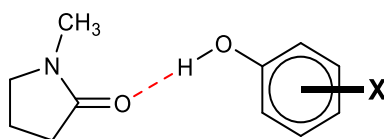


Figure 3.51 Intermolecular hydrogen bond between *N*-methylpyrrolidone (NMP) and substituted phenols.

The association constants for the hydrogen bonded complexes of NMP with (substituted) phenols in dichloromethane- d_2 were measured via ^1H NMR titration experiments. The change in chemical shift ($\Delta\delta$) of phenolic proton was monitored as NMP guest was gradually added into the (substituted) phenol host solution (20 mmol/L) in dichloromethane- d_2 . Subsequent addition of NMP continued until the phenol protons chemical shift remained constant.⁹⁸ The association constants (K_a) were obtained through fitting the experimental binding isotherm using Equations 3.6-3.10. An example of the fitted and experimental isotherms for the host-guest complex of *m*-nitrophenol and NMP is shown in Figure 3.52. The Gibbs free association energies (ΔG_{K_a}) of the hydrogen bonded host-guest complexes were then calculated from the measured association constants ($\Delta G_{K_a} = -R \times T \times \ln K_a$) and tabulated in Table 3.2.

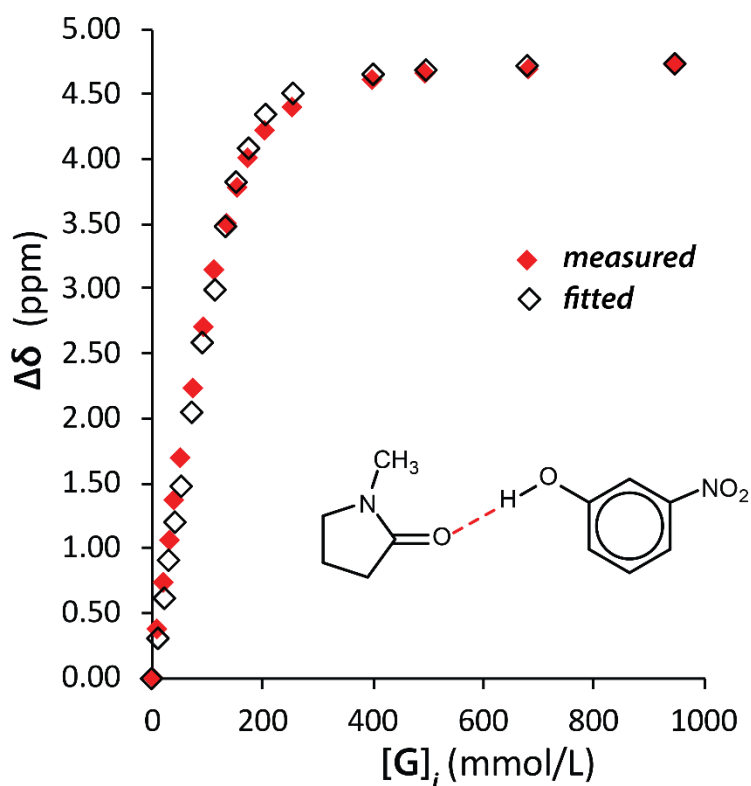


Figure 3.52 Experimentally measured and fitted isotherms (in dichloromethane-d₂) of NMP (guest) binding of m-nitrophenol (host) based on chemical shift change ($\Delta\delta$) of the phenolic proton as NMP guest was gradually added.

Table 3.2 Gibbs free association energy (ΔG_{Ka} , kcal/mol)^a for the hydrogen bonded host-guest complexes of *N*-methyl pyrrolidone and (substituted) phenols in dichloromethane-d₂

Guest	Substituent on phenol host	ΔG_{Ka} (kcal/mol)
NMP	<i>p</i> -NO ₂	-3.40
NMP	<i>m</i> -NO ₂	-3.09
NMP	<i>p</i> -Cl	-2.05
NMP	<i>m</i> -Cl	-2.71
NMP	<i>p</i> -CN	-2.97
NMP	<i>p-t</i> -Amyl	-2.15
NMP	H	-1.49

^a ΔG_{Ka} values were measured at 25 °C with an error of less than ± 10 %.

$$\Delta\delta_i = \frac{[H]_{free}}{[H]_i} \cdot \Delta\delta_{HG} + \Delta\delta_{HG} \dots \dots \dots \text{Equation 3.6}$$

$$[H]_i = \frac{[H]_0 V_0}{V_i} \dots \dots \dots \text{Equation 3.7}$$

$$[G]_i = \frac{[G]_0 \cdot (V_i - V_0)}{V_i} \dots \dots \dots \text{Equation 3.8}$$

$$[H]_{free} = \frac{\sqrt{b^2 - 4 \cdot \left(\frac{K_a}{1000}\right) \cdot V_i}}{2 \cdot \left(\frac{K_a}{1000}\right)} \dots \dots \dots \text{Equation 3.9}$$

$$b = [G]_i \cdot \left(\frac{K_a}{1000}\right) - [H]_i \cdot \left(\frac{K_a}{1000}\right) + 1 \dots \dots \dots \text{Equation 3.10}$$

3.4.6 CRYSTALLOGRAPHIC STRUCTURES

3.4.6.1 X-RAY STRUCTURE DETERMINATION FOR PHENOL ROTOR **1** (X = H), C₁₅H₁₃NO₃

X-ray intensity data from a colorless needle were collected at 100(2) K using a Bruker D8 QUEST diffractometer equipped with a PHOTON-100 CMOS area detector and an Incoatec microfocus source (Mo K α radiation, $\lambda = 0.71073$ Å). The raw area detector data frames were reduced and corrected for absorption effects using the Bruker APEX3, SAINT+ and SADABS programs.^{99,100} Final unit cell parameters were determined by least-squares refinement of 9106 reflections taken from the data set. The structure was

solved with SHELXT.^{101,102} Subsequent difference Fourier calculations and full-matrix least-squares refinement against F^2 were performed with SHELXL-2016^{101,102} using OLEX2.¹⁰³

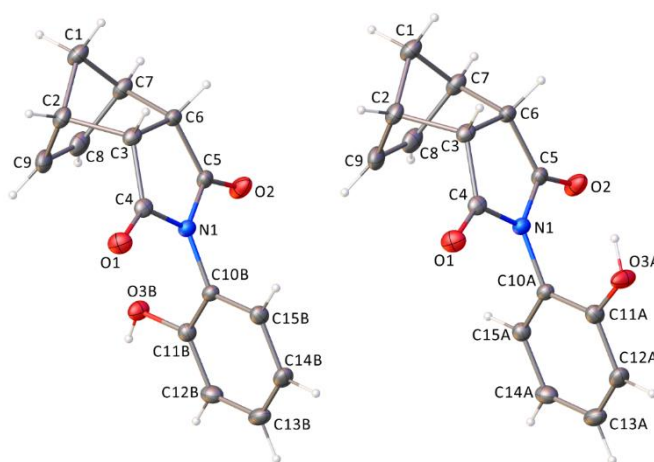


Figure 3.53 Crystal structure of rotor **1** (X = H)

The compound crystallizes in the space group $P2_1/n$ of the monoclinic system. The asymmetric unit consists of one $C_{15}H_{13}NO_3$ molecule, which is disordered. The $-C_6H_4OH$ substituent is disordered over two orientations *via* a 180° rotation about the N1-C10 bond. Only the hydroxyl group atoms are affected; all other atoms are exactly superimposed. The major component occupancy fraction (atom label suffixes A) refined to 0.685(3). All non-hydrogen atoms were refined with anisotropic displacement parameters. Hydrogen atoms bonded to carbon were located in Fourier difference maps before being placed in geometrically idealized positions and included as riding atoms with $d(C-H) = 1.00 \text{ \AA}$ and $U_{iso}(H) = 1.2U_{eq}(C)$ for methine hydrogen atoms, $d(C-H) = 0.95 \text{ \AA}$ and $U_{iso}(H) = 1.2U_{eq}(C)$ for aromatic hydrogen atoms and $d(C-H) = 0.99 \text{ \AA}$ and $U_{iso}(H) = 1.2U_{eq}(C)$ for methylene hydrogens. Hydroxyl hydrogen atoms were located in difference maps. They were refined isotropically with a similar distance restraints (SHELX SADI). The largest

residual electron density peak in the final difference map is $0.39 \text{ e}^-/\text{\AA}^3$, located 0.75 \AA from C5.

3.4.6.2 X-RAY STRUCTURE DETERMINATION FOR PHENOL ROTOR **1** ($X = P\text{-CL}$), $\text{C}_{15}\text{H}_{12}\text{CLNO}_3$

X-ray intensity data from a colorless needle were collected at $100(2) \text{ K}$ using a Bruker D8 QUEST diffractometer equipped with a PHOTON-100 CMOS area detector and an Incoatec microfocus source (Mo $K\alpha$ radiation, $\lambda = 0.71073 \text{ \AA}$). The raw area detector data frames were reduced and corrected for absorption effects using the Bruker APEX3, SAINT+ and SADABS programs.^{99,100} Final unit cell parameters were determined by least-squares refinement of 9958 reflections taken from the data set. The structure was solved with SHELXT.^{101,104} Subsequent difference Fourier calculations and full-matrix least-squares refinement against F^2 were performed with SHELXL-2017^{101,104} using OLEX2.¹⁰³

The compound crystallizes in the monoclinic system. The pattern of systematic absences in the intensity data was consistent with the space group $P2_1/c$, which was verified by structure solution. The asymmetric unit consists of two crystallographically independent but chemically identical molecules. The molecules were numbered identically except for label suffixes A or B. All non-hydrogen atoms were refined with anisotropic displacement parameters. Hydrogen atoms bonded to carbon were located in Fourier difference maps before being placed in geometrically idealized positions and included as riding atoms with $d(\text{C-H}) = 1.00 \text{ \AA}$ and $U_{\text{iso}}(\text{H}) = 1.2U_{\text{eq}}(\text{C})$ for methine hydrogen atoms, $d(\text{C-H}) = 0.95 \text{ \AA}$ and $U_{\text{iso}}(\text{H}) = 1.2U_{\text{eq}}(\text{C})$ for aromatic hydrogen atoms, $d(\text{C-H}) = 0.99 \text{ \AA}$ and $U_{\text{iso}}(\text{H}) = 1.2U_{\text{eq}}(\text{C})$ for methylene hydrogen atoms, and $d(\text{C-H}) = 0.98 \text{ \AA}$ and $U_{\text{iso}}(\text{H}) = 1.5U_{\text{eq}}(\text{C})$ for methyl hydrogens. The methyl hydrogens were allowed to rotate as a rigid group to the

orientation of maximum observed electron density. The two independent hydroxy hydrogen atoms were located in difference Fourier maps and refined freely. The largest residual electron density peak in the final difference map is $0.42 \text{ e}^-/\text{\AA}^3$, located 0.74 \AA from C6A.

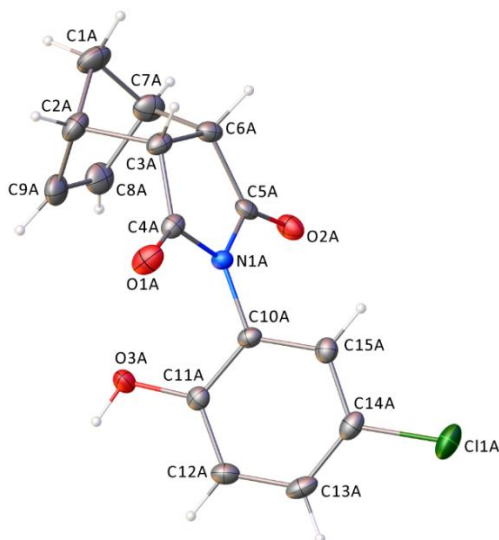


Figure 3.54 Crystal structure of rotor **1** ($X = p\text{-Cl}$)

3.4.6.3 X-RAY STRUCTURE DETERMINATION FOR PHENOL ROTOR **1** ($X = m\text{-Cl}$), $\text{C}_{15}\text{H}_{12}\text{ClNO}_3$

X-ray intensity data from a colorless plate were collected at $100(2) \text{ K}$ using a Bruker D8 QUEST diffractometer equipped with a PHOTON-100 CMOS area detector and an Incoatec microfocus source ($\text{Mo K}\alpha$ radiation, $\lambda = 0.71073 \text{ \AA}$). The raw area detector data frames were reduced and corrected for absorption effects using the Bruker APEX3, SAINT+ and SADABS programs.^{99,100} Final unit cell parameters were determined by least-squares refinement of 9909 reflections taken from the data set. The structure was solved with SHELXT.^{102,104} Subsequent difference Fourier calculations and full-matrix

least-squares refinement against F^2 were performed with SHELXL-2016^{102,104} using OLEX2.¹⁰³

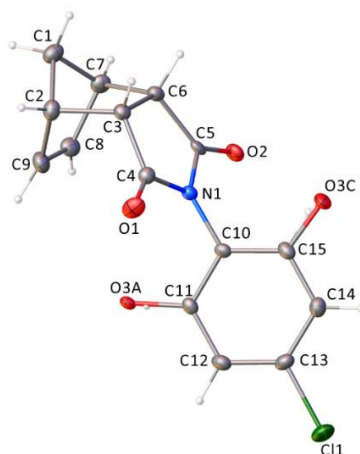


Figure 3.55 Crystal structure of rotor **1** ($X = m\text{-Cl}$)

The compound crystallizes in the monoclinic system. The pattern of systematic absences in the intensity data was consistent with the space groups Ia and $I2/a$. A reasonable solution and refinement was obtained in $I2/a$. The refinement was hampered by whole-molecule disorder present in the crystal. This was suggested by the appearance of diffuse streaking between Bragg peaks in the area detector diffraction pattern images of several surveyed crystals, both at low and at room temperature. Initial structure solutions returned a pattern of electron density consistent with one molecule in the asymmetric unit. A single molecule model refined poorly, giving high R -values and a pattern of residual electron density eventually seen to correspond to another complete molecule in a different orientation, but partially overlapped with the main molecule. The two disorder components are related by an apparent non-crystallographic mirror plane perpendicular to the b axis at $y = 0.25$. The whole-molecular disorder was also observed in the lower symmetry space groups Ia and $I2$. Examination of the diffraction pattern for an alternative unit cell or for

twinning was fruitless. The disordered asymmetric unit in $I2/a$ consists of one $C_{15}H_{12}ClNO_3$ molecule, with disorder population fractions of 0.879(2) (no atom label suffix) and 0.121(2) (atom label suffixes B). A further structural complication is that the $-C_6H_3ClOH$ substituent of each disorder component is itself disordered over two conformations within each component. This is manifested only in the position of the $-OH$ group. For stability, $-OH$ group occupancies were fixed at values providing the most reasonable displacement parameter values, and are: main whole-molecule component, $O3A/O3C = 50/50$ (0.44/0.44), minor component $O3B/O3D = 60/40$ (0.07/0.05). A total of 64 restraints were used in the disorder modeling. The geometry of the minor component was restrained to be similar to that of the major using SHELX SAME instructions. The two $N1-C10$ distances and all $C-O(\text{hydroxyl})$ distances between components were further restrained to be similar to those of the same type. All non-hydrogen atoms of the major disorder component were refined with anisotropic displacement parameters. Those of the minor were refined isotropically except when they were nearly superimposed with an atom from the major component, in which case both atoms were refined with equal anisotropic displacement parameters. Hydrogen atoms bonded to carbon placed in geometrically idealized positions and included as riding atoms with $d(C-H) = 1.00 \text{ \AA}$ and $U_{iso}(H) = 1.2U_{eq}(C)$ for methine hydrogen atoms, $d(C-H) = 0.95 \text{ \AA}$ and $U_{iso}(H) = 1.2U_{eq}(C)$ for aromatic hydrogen atoms and $d(C-H) = 0.99 \text{ \AA}$ and $U_{iso}(H) = 1.2U_{eq}(C)$ for methylene hydrogen atoms. Hydroxyl hydrogen atoms could not be reliably located and were not calculated. The largest residual electron density peak in the final difference map is $0.35 e^-/\text{\AA}^3$, located 0.91 \AA from O3B.

3.4.6.4 X-RAY STRUCTURE DETERMINATION FOR ANISOLE ROTOR **2**(X = *p*-NO₂), C₁₆H₁₄N₂O₅

X-ray intensity data from a colorless block were collected at 100(2) K using a Bruker D8 QUEST diffractometer equipped with a PHOTON-100 CMOS area detector and an Incoatec microfocus source (Mo K α radiation, $\lambda = 0.71073$ Å). The raw area detector data frames were reduced and corrected for absorption effects using the Bruker APEX3, SAINT+ and SADABS programs.^{99,100} Final unit cell parameters were determined by least-squares refinement of 9963 reflections taken from the data set. The structure was solved with SHELXT.^{101,104} Subsequent difference Fourier calculations and full-matrix least-squares refinement against F^2 were performed with SHELXL-2017^{101,104} using OLEX2.¹⁰³

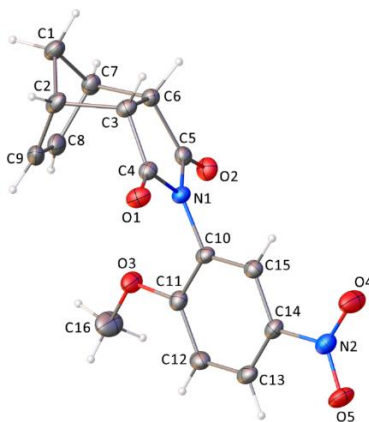


Figure 3.56 Crystal structure of rotor **2**(X = *p*-NO₂)

The compound crystallizes in the triclinic system. The space group *P*-1 (No. 2) was confirmed by structure solution. The asymmetric unit consists of one molecule. All non-hydrogen atoms were refined with anisotropic displacement parameters. Hydrogen atoms bonded to carbon were located in difference Fourier maps before being placed in geometrically idealized positions and included as riding atoms with $d(\text{C-H}) = 1.00$ Å and

$U_{iso}(H) = 1.2U_{eq}(C)$ for methine hydrogen atoms, $d(C-H) = 0.95 \text{ \AA}$ and $U_{iso}(H) = 1.2U_{eq}(C)$ for aromatic hydrogen atoms, and $d(C-H) = 0.98 \text{ \AA}$ and $U_{iso}(H) = 1.5U_{eq}(C)$ for methyl hydrogens. The methyl hydrogens were allowed to rotate as a rigid group to the orientation of maximum observed electron density. The largest residual electron density peak in the final difference map is $0.38 \text{ e}^-/\text{\AA}^3$, located 0.62 \AA from C14.

3.4.6.5 X-RAY STRUCTURE DETERMINATION FOR ANISOLE ROTOR **2**(X = M-CL), $C_{16}H_{14}CLNO_3$

X-ray intensity data from a colorless block were collected at 100(2) K using a Bruker D8 QUEST diffractometer equipped with a PHOTON-100 CMOS area detector and an Incoatec microfocus source (Mo $K\alpha$ radiation, $\lambda = 0.71073 \text{ \AA}$). The raw area detector data frames were reduced and corrected for absorption effects using the Bruker APEX3, SAINT+ and SADABS programs.^{99,100} Final unit cell parameters were determined by least-squares refinement of 9800 reflections taken from the data set. The structure was solved with SHELXT.^{101,104} Subsequent difference Fourier calculations and full-matrix least-squares refinement against F^2 were performed with SHELXL-2017^{101,104} using OLEX2.¹⁰³

The compound crystallizes in the orthorhombic system. The pattern of systematic absences in the intensity data was consistent with the space group $P2_12_12_1$, which was confirmed by structure solution. The asymmetric unit consists of one molecule. All non-hydrogen atoms were refined with anisotropic displacement parameters. Hydrogen atoms bonded to carbon were located in Fourier difference maps before being placed in geometrically idealized positions and included as riding atoms with $d(C-H) = 1.00 \text{ \AA}$ and $U_{iso}(H) = 1.2U_{eq}(C)$ for methine hydrogen atoms, $d(C-H) = 0.95 \text{ \AA}$ and $U_{iso}(H) =$

1.2Ueq(C) for aromatic hydrogen atoms, $d(\text{C-H}) = 0.99 \text{ \AA}$ and $U_{\text{iso}}(\text{H}) = 1.2U_{\text{eq}}(\text{C})$ for methylene hydrogen atoms, and $d(\text{C-H}) = 0.98 \text{ \AA}$ and $U_{\text{iso}}(\text{H}) = 1.5U_{\text{eq}}(\text{C})$ for methyl hydrogens. The methyl hydrogens were allowed to rotate as a rigid group to the orientation of maximum observed electron density. The largest residual electron density peak in the final difference map is 0.26 e-/\AA^3 , located 0.68 \AA from C13. The absolute structure (Flack) parameter after the final refinement cycle was 0.013(13), indicating the correct absolute structure and the absence of racemic twinning.

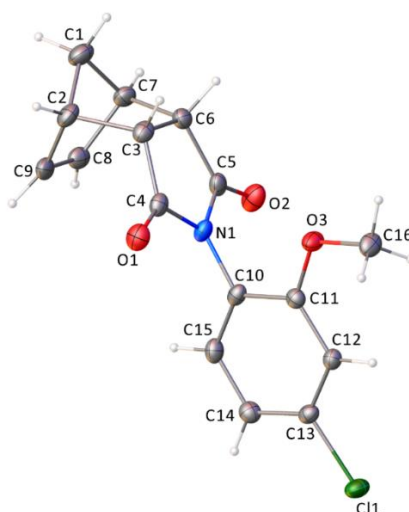


Figure 3.57 Crystal structure of rotor **2** ($X = m\text{-Cl}$)

3.4.6.6 X-RAY STRUCTURE DETERMINATION FOR ANISOLE ROTOR **2** ($X = P\text{-CN}$), $\text{C}_{17}\text{H}_{14}\text{N}_2\text{O}_3$

X-ray intensity data from a colorless rectangular plate were collected at 100(2) K using a Bruker D8 QUEST diffractometer equipped with a PHOTON-100 CMOS area detector and an Incoatec microfocus source (Mo $K\alpha$ radiation, $\lambda = 0.71073 \text{ \AA}$). The raw area detector data frames were reduced and corrected for absorption effects using the Bruker APEX3, SAINT+ and SADABS programs.^{99,100} Final unit cell parameters were determined by least-squares refinement of 9963 reflections taken from the data set. The structure was solved with SHELXT.^{101,104} Subsequent difference Fourier calculations and

full-matrix least-squares refinement against F^2 were performed with SHELXL-2017^{101,104} using OLEX2.¹⁰³

The compound crystallizes in the orthorhombic system. The pattern of systematic absences in the intensity data was consistent with the space groups $Pna2_1$ and $Pnma$. Intensity statistics suggested an acentric structure. $Pna2_1$ was assigned by SHELXT and was confirmed by structure refinement and with ADDSYM.^{105–108} The asymmetric unit consists of one molecule. All non-hydrogen atoms were refined with anisotropic displacement parameters. Hydrogen atoms were located in Fourier difference maps before being placed in geometrically idealized positions and included as riding atoms with $d(\text{C-H}) = 1.00 \text{ \AA}$ and $U_{\text{iso}}(\text{H}) = 1.2U_{\text{eq}}(\text{C})$ for methine hydrogen atoms, $d(\text{C-H}) = 0.95 \text{ \AA}$ and $U_{\text{iso}}(\text{H}) = 1.2U_{\text{eq}}(\text{C})$ for aromatic hydrogen atoms, and $d(\text{C-H}) = 0.98 \text{ \AA}$ and $U_{\text{iso}}(\text{H}) = 1.5U_{\text{eq}}(\text{C})$ for methyl hydrogens. The methyl hydrogens were allowed to rotate as a rigid group to the orientation of maximum observed electron density. Though lacking any atoms heavier than oxygen, the final absolute structure (Flack) parameter of 0.11(14) suggests the correct absolute structure has been established. This was aided by the high-quality, relatively high resolution data ($d_{\text{max}} = 0.71 \text{ \AA}$). The largest residual electron density peak in the final difference map is $0.28 \text{ e}^-/\text{\AA}^3$, located 0.70 \AA from C11.

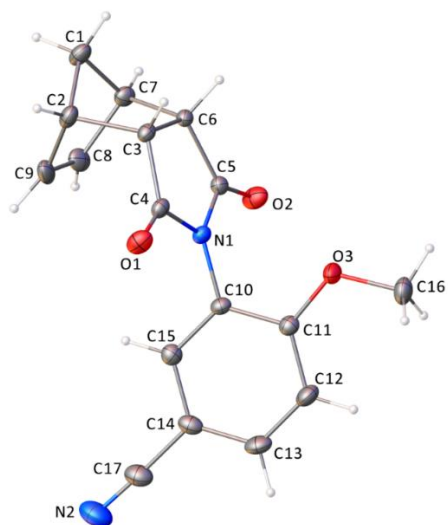


Figure 3.58 Crystal structure of rotor **2** ($X = p\text{-CN}$)

Table 3.3 Crystal data and structure refinement for **1**(X = H)

Empirical formula	C ₁₅ H ₁₃ NO ₁₃
Formula weight	255.26
Temperature/K	100(2)
Crystal system	monoclinic
Space group	P2 ₁ /n
a/Å	10.7032(5)
b/Å	6.6627(3)
c/Å	16.9382(8)
α/°	90
β/°	92.303(2)
γ/°	90
Volume/Å ³	1206.92(10)
Z	4
ρ _{calc} /g/cm ³	1.405
μ/mm ⁻¹	0.099
F(000)	536.0
Crystal size/mm ³	0.52 × 0.26 × 0.2
Radiation	MoKα (λ = 0.71073)
2θ range for data collection/°	4.422 to 60.36
Index ranges	-15 ≤ h ≤ 15, -9 ≤ k ≤ 9, -23 ≤ l ≤ 23
Reflections collected	56388
Independent reflections	3575 [R _{int} = 0.0454, R _{sigma} = 0.0223]
Data/restraints/parameters	3575/1/191
Goodness-of-fit on F ²	1.046
Final R indexes [I ≥ 2σ (I)]	R ₁ = 0.0401, wR ₂ = 0.0967
Final R indexes [all data]	R ₁ = 0.0525, wR ₂ = 0.1027
Largest diff. peak/hole / e Å ⁻³	0.39/-0.21

Table 3.4 Crystal data and structure refinement for **1**(X = *p*-Cl)

Empirical formula	C ₁₅ H ₁₂ ClNO ₃
Formula weight	289.71
Temperature/K	100(2)
Crystal system	monoclinic
Space group	P2 ₁ /c
a/Å	21.3570(9)
b/Å	6.8190(3)
c/Å	20.0691(8)
α/°	90
β/°	115.0080(10)
γ/°	90
Volume/Å ³	2648.72(19)
Z	8
ρ _{calc} /g/cm ³	1.453
μ/mm ⁻¹	0.295
F(000)	1200.0
Crystal size/mm ³	0.6 × 0.14 × 0.08
Radiation	MoKα (λ = 0.71073)
2θ range for data collection/°	4.48 to 60.106
Index ranges	-30 ≤ h ≤ 29, -9 ≤ k ≤ 9, -28 ≤ l ≤ 28
Reflections collected	61497
Independent reflections	7769 [R _{int} = 0.0490, R _{sigma} = 0.0344]
Data/restraints/parameters	7769/0/370
Goodness-of-fit on F ²	1.017
Final R indexes [I ≥ 2σ (I)]	R ₁ = 0.0426, wR ₂ = 0.0909
Final R indexes [all data]	R ₁ = 0.0669, wR ₂ = 0.1019
Largest diff. peak/hole / e Å ⁻³	0.42/-0.47

Table 3.5 Crystal data and structure refinement for **1**(X = *m*-Cl).

Empirical formula	C ₁₅ H ₁₂ ClNO ₃
Formula weight	289.71
Temperature/K	100(2)
Crystal system	monoclinic
Space group	I2/a
a/Å	17.4699(12)
b/Å	6.8917(5)
c/Å	22.137(2)
α/°	90
β/°	103.5700(16)
γ/°	90
Volume/Å ³	2590.8(3)
Z	8
ρ _{calc} /g/cm ³	1.485
μ/mm ⁻¹	0.301
F(000)	1200.0
Crystal size/mm ³	0.28 × 0.22 × 0.06
Radiation	MoKα (λ = 0.71073)
2θ range for data collection/°	4.798 to 55.446
Index ranges	-22 ≤ h ≤ 22, -9 ≤ k ≤ 9, -28 ≤ l ≤ 28
Reflections collected	49286
Independent reflections	3036 [R _{int} = 0.0385, R _{sigma} = 0.0153]
Data/restraints/parameters	3036/64/272
Goodness-of-fit on F ²	1.301
Final R indexes [I ≥ 2σ (I)]	R ₁ = 0.0524, wR ₂ = 0.1264
Final R indexes [all data]	R ₁ = 0.0557, wR ₂ = 0.1277
Largest diff. peak/hole / e Å ⁻³	0.35/-0.29

Table 3.6 Crystal data and structure refinement for **2**(X = *p*-NO₂).

Empirical formula	C ₁₆ H ₁₄ N ₂ O ₅
Formula weight	314.29
Temperature/K	100(2)
Crystal system	triclinic
Space group	P-1
a/Å	7.7842(5)
b/Å	9.7899(6)
c/Å	10.0423(6)
α/°	81.677(2)
β/°	82.193(2)
γ/°	67.584(2)
Volume/Å ³	697.29(8)
Z	2
ρ _{calc} /g/cm ³	1.497
μ/mm ⁻¹	0.113
F(000)	328.0
Crystal size/mm ³	0.54 × 0.44 × 0.36
Radiation	MoKα (λ = 0.71073)
2θ range for data collection/°	4.524 to 60.384
Index ranges	-11 ≤ h ≤ 11, -13 ≤ k ≤ 13, -14 ≤ l ≤ 14
Reflections collected	31746
Independent reflections	4121 [R _{int} = 0.0480, R _{sigma} = 0.0333]
Data/restraints/parameters	4121/0/210
Goodness-of-fit on F ²	1.029
Final R indexes [I ≥ 2σ (I)]	R ₁ = 0.0440, wR ₂ = 0.1003
Final R indexes [all data]	R ₁ = 0.0645, wR ₂ = 0.1111
Largest diff. peak/hole / e Å ⁻³	0.38/-0.31

Table 3.7 Crystal data and structure refinement for **2**(X = *p*-Cl).

Empirical formula	C ₁₆ H ₁₄ ClNO ₃
Formula weight	303.73
Temperature/K	100(2)
Crystal system	orthorhombic
Space group	P2 ₁ 2 ₁ 2 ₁
a/Å	9.8726(5)
b/Å	10.9075(5)
c/Å	12.7229(6)
α/°	90
β/°	90
γ/°	90
Volume/Å ³	1370.07(11)
Z	4
ρ _{calc} /g/cm ³	1.473
μ/mm ⁻¹	0.288
F(000)	632.0
Crystal size/mm ³	0.48 × 0.42 × 0.3
Radiation	MoKα (λ = 0.71073)
2θ range for data collection/°	4.92 to 60.168
Index ranges	-13 ≤ h ≤ 13, -15 ≤ k ≤ 15, -17 ≤ l ≤ 17
Reflections collected	49019
Independent reflections	4021 [R _{int} = 0.0391, R _{sigma} = 0.0199]
Data/restraints/parameters	4021/0/192
Goodness-of-fit on F ²	1.029
Final R indexes [I ≥ 2σ (I)]	R ₁ = 0.0272, wR ₂ = 0.0636
Final R indexes [all data]	R ₁ = 0.0309, wR ₂ = 0.0655
Largest diff. peak/hole / e Å ⁻³	0.26/-0.20
Flack parameter	0.013(13)

Table 3.8 Crystal data and structure refinement for **2**(X = *p*-CN).

Empirical formula	C ₁₇ H ₁₄ N ₂ O ₃
Formula weight	294.30
Temperature/K	100(2)
Crystal system	orthorhombic
Space group	Pna2 ₁
a/Å	25.6129(11)
b/Å	7.2650(3)
c/Å	7.5367(3)
α/°	90
β/°	90
γ/°	90
Volume/Å ³	1402.41(10)
Z	4
ρ _{calc} /g/cm ³	1.394
μ/mm ⁻¹	0.097
F(000)	616.0
Crystal size/mm ³	0.36 × 0.2 × 0.1
Radiation	MoKα (λ = 0.71073)
2θ range for data collection/°	5.828 to 60.164
Index ranges	-36 ≤ h ≤ 36, -10 ≤ k ≤ 10, -10 ≤ l ≤ 10
Reflections collected	73700
Independent reflections	4118 [R _{int} = 0.0300, R _{sigma} = 0.0125]
Data/restraints/parameters	4118/1/201
Goodness-of-fit on F ²	1.032
Final R indexes [I ≥ 2σ (I)]	R ₁ = 0.0278, wR ₂ = 0.0735
Final R indexes [all data]	R ₁ = 0.0298, wR ₂ = 0.0748
Largest diff. peak/hole / e Å ⁻³	0.28/-0.17
Flack parameter	0.11(13)

3.4.7 ROTATIONAL BARRIER CALCULATIONS

Following instructions from a benchmark study on determining the accurate level of theory for rotational barriers, we optimized the ground state and transition state for our rotors using a triple zeta basis set (def2-TZVP) with multiple density functionals and corrected for thermodynamic contributions. Geometries the ground (GS) and transition (TS) states were optimized at B3LYP-D3(BJ)/def2-TZVP level of theory using Turbomole suite of programs (version 6.5).¹⁰⁹⁻¹¹¹ The m4 grid was used; convergence criteria were 10^{-8} Hartree and 10^{-5} atomic units as the maximum norm of the cartesian gradient.¹¹² Vibrational analysis was also carried out at B3LYP-D3(BJ)/def2-TZVP level with a vibrational scaling factor of 0.965 and the experimentally determined coalescence temperatures. Single-point calculations were carried out on the B3LYP-D3(BJ)-optimized geometries at B2GP-PLYP-D3(BJ)/def2-TZVP level of theory (using ultrafine grid) using Gaussian 09 package (Figure 3.59 and Table 3.9 and 3.10).¹¹³⁻¹¹⁵ The XYZ coordinates for the ground and transition state structures of **1** and **2** are in Tables 3.13-3.15.

To eliminate error in GS energy, the calculated GS energies for the *syn*- and *anti*-conformers were averaged. Systematic errors imposed by the averaging should be cancelled out in the difference of the rotational barriers because both the phenol and anisole rotors have the ground states averaged. The hydrogen bond stability in the GS and TS phenol rotors was assessed by comparing the calculated energies for the hydrogen bonding (HB) versus non-hydrogen-bonding (nHB) configurations (Figure 3.60). The non-hydrogen bonding configuration was constructed by freezing the C₍₆₎-C₍₁₎-O-H dihedral angle to 0° (with C₍₂₎ being the connection point to the imide moiety) and then re-optimizing the GS structures at the B3LYP-D3(BJ)/def2-TZVP level within this constraint.

Table 3.9 Calculated (ΔG^\ddagger calc., kcal/mol)_a and experimental (ΔG^\ddagger exp., kcal/mol)_b rotational barrier energies for rotors **1** and **2** as well as the error (kcal/mol)_c for the calculations reported as the difference between the calculated and experimental values.

Compound label	substituent	ΔG^\ddagger calc. (kcal/mol)	ΔG^\ddagger exp. (kcal/mol)	Temperature (°C)	Error (kcal/mol)
1	H	10.08	10.89	-55	-0.82
1	<i>m</i> -Cl	9.54	10.08	-65	-0.53
1	<i>m</i> -NO ₂	9.51	9.99	-62	-0.49
1	<i>p</i> -Cl	9.84	10.39	-60	-0.54
1	<i>p</i> -CN	9.15	9.96	-65	-0.81
1	<i>p</i> -NO ₂	8.99	9.73	-67	-0.75
1	<i>p</i> -t-Amyl	10.13	10.91	-55	-0.78
2	H	20.13	20.77	113	-0.64
2	<i>m</i> -Cl	19.60	20.15	95	-0.55
2	<i>m</i> -NO ₂	18.83	19.58	86	-0.75
2	<i>p</i> -Cl	19.60	20.11	98	-0.51
2	<i>p</i> -CN	19.41	20.36	103	-0.94
2	<i>p</i> -NO ₂	19.17	19.35	82	-0.19
2	<i>p</i> -t-Amyl	19.70	20.35	105	-0.65

^aB2GP-PLYP-D3(BJ)/def2-TZVP; ^b via coalescence temperature; ^c ΔG^\ddagger calc. - ΔG^\ddagger exp.

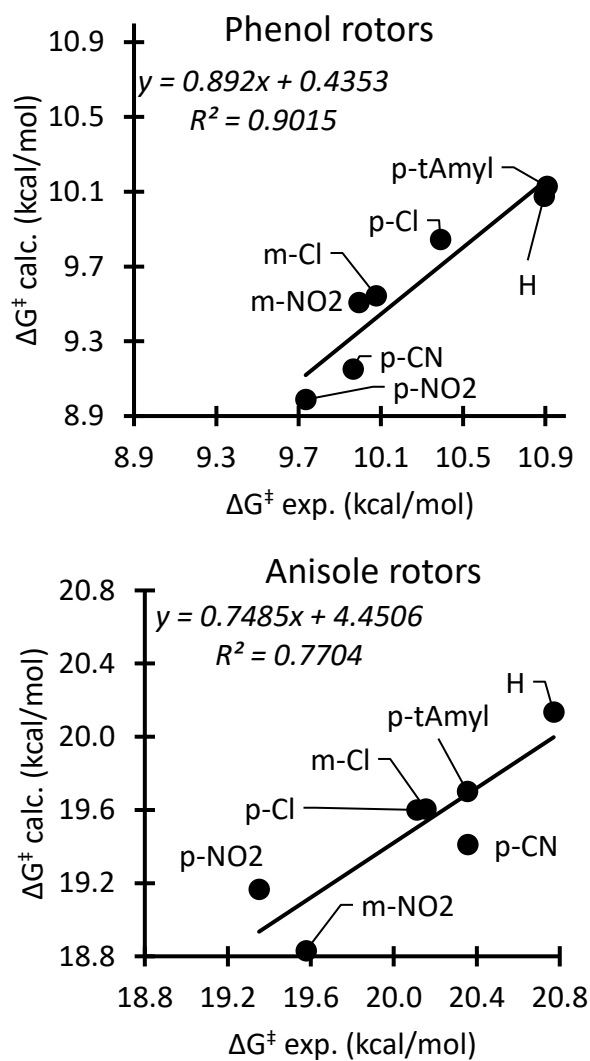


Figure 3.59 Correlation of the calculated ($\Delta G^\ddagger_{\text{calc.}}$) and experimental ($\Delta G^\ddagger_{\text{exp.}}$) rotational barriers for the phenol (left) and anisole (right) rotors. Structures were calculated at the B2GP-PLYP-D3(BJ)/def2-TZVP level of theory with thermodynamic corrections.

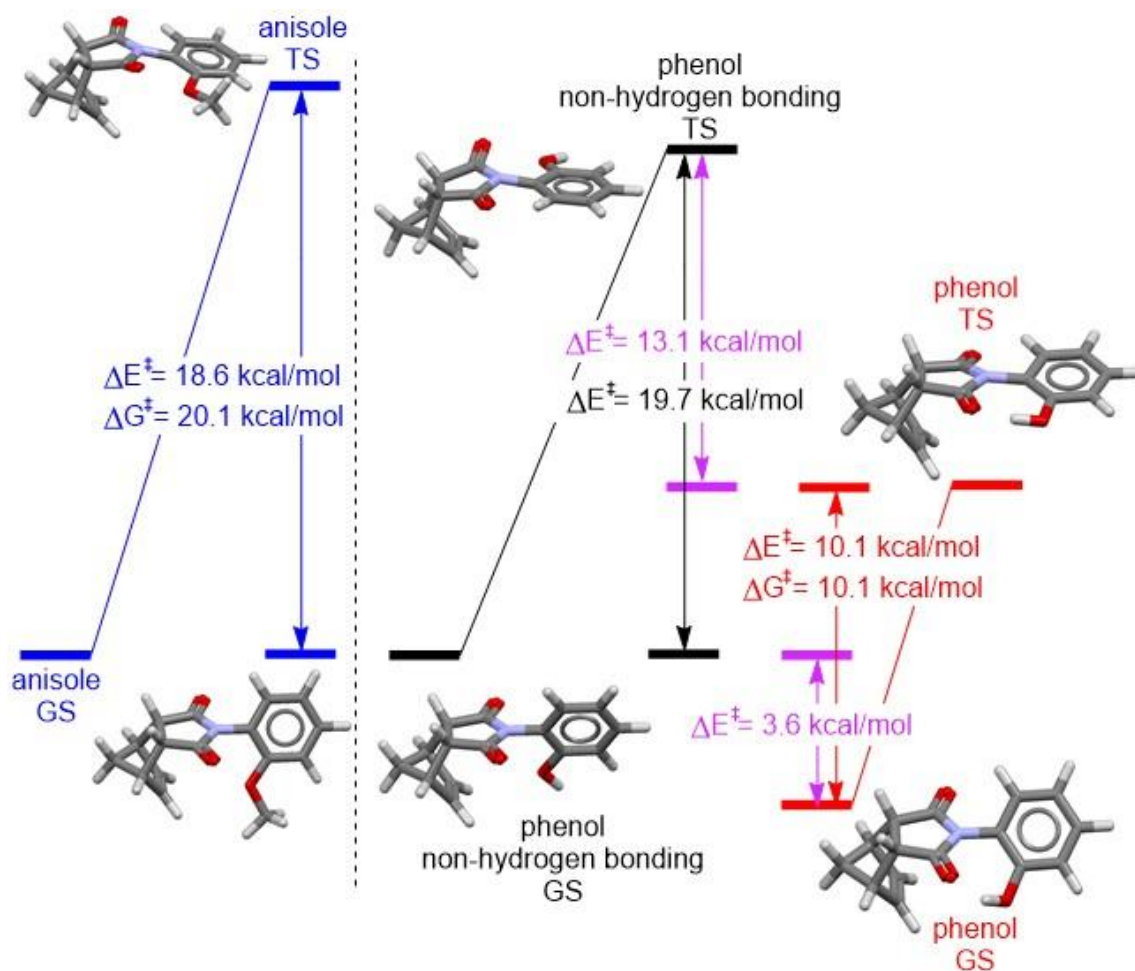


Figure 3.60 Calculated rotational barriers for the unsubstituted phenol **1** and anisole **2** rotors with (ΔG^\ddagger) and without (ΔE^\ddagger) thermodynamic corrections.

Table 3.10 Statistical values for the error of the calculated (B2GP-PLYP-D3(BJ)/def2-TZVP) rotational barriers for the phenol and anisole rotors.

Rotors	average error	standard error
Phenol rotors 1	-0.67	0.14
Anisole rotors 2	-0.60	0.22
All rotors 1 and 2	-0.64	0.18

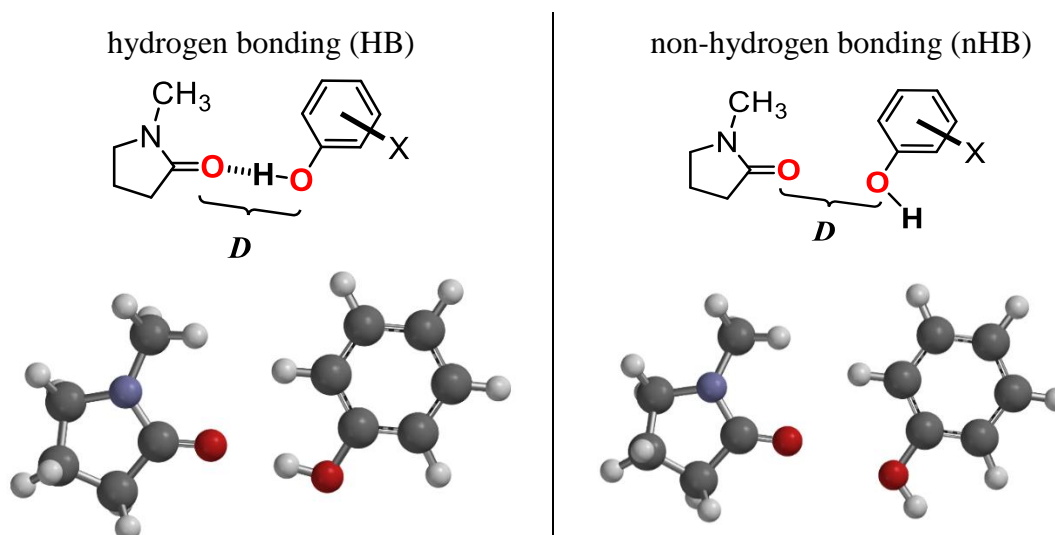


Figure 3.61 Two configurations of the bimolecular complex of NMP and phenol (X=H) used for SAPT analysis: hydrogen bonding (HB, left) and non-hydrogen bonding (nHB, right).

3.4.8 SYMMETRY ADAPTED PERTURBATION THEORY CALCULATIONS

The origins of the amplified catalyzing effect (ACE) of the transition state hydrogen bond in the phenol rotors **1** were investigated symmetry adapted perturbation theory (SAPT(CCSD)/cc-pVTZ). SAPT calculations can deconstruct interaction energy of an intermolecular complex into four fundamental energy terms: electrostatics (E_{elst}), exchange-repulsion (E_{exch}), induction/polarization (E_{ind}) and London dispersion (E_{disp}). The SAPT calculations were carried out on a simple bimolecular complex comprised of NMP and phenol in *two* distinct configurations of the NMP-phenol complex, i.e., hydrogen bonding (**HB**) and non-hydrogen bonding (**nHB**) (Figure 3.61) using the Q-Chem⁸⁴ software package.

To mimic the transition state in the rotors, the NMP amide (-NCH₃-CO-CH₂-) motif and phenol were kept coplanar to each other by a dihedral constraint of 0° between the residing planes. The ∠OHO was locked at 180° for the configuration with a hydrogen bond (Figure 3.61, left). The O-to-O distances (**D**) was systematically altered from 3.00 to 2.00 Å (over 11 steps of 0.1 Å intervals) to generate a potential energy profile using the M06-2X/6-31G* level of theory. The complex without a hydrogen bond (Figure 3.61, right) was made by freezing all the atoms in the complex with a hydrogen bond at each discrete **D** except the phenolic hydrogen, which had a dihedral angle constrained to 0° with the carbon ortho to the hydroxyl group. The geometry of the complex without a hydrogen bond was then optimized at the M06-2X/6-31G* level of theory for each discrete **D** with constraints on all the frozen atoms except the phenolic hydrogen.

The component terms (E_{elst} , E_{exch} , E_{ind} , and E_{disp}) for the NMP-phenol **HB** and **nHB** configurations (Figure 3.61) at 11 discrete O-to-O distances (**D**) between 2.0 and 3.0 Å

were obtained and tabulated in Table 3.11. The ACE's were characterized as the difference ($\Delta E = E^{\text{HB}} - E^{\text{nHB}}$) in the calculated total and component energy terms between the NMP-phenol **HB** and **nHB** configurations. The XYZ coordinates of the NMP-phenol complex in both configurations at 11 different O-to-O distances are listed in Table 3.16-3.23.

Table 3.11 SAPT total (E_{total} , kcal/mol) and component energies (E_{elst} , E_{exch} , E_{ind} , and E_{disp} , kcal/mol) for the NMP-phenol complex in two configurations (Figure 3.61) at 11 different O-to-O distances (D) as well as the differences in energy ($\Delta E = E^{\text{HB}} - E^{\text{nHB}}$) between the two configurations.

E^{HB} for the configuration with hydrogen bond					
D (Å)	$E_{\text{elst}}^{\text{HB}}$	$E_{\text{exch}}^{\text{HB}}$	$E_{\text{ind}}^{\text{HB}}$	$E_{\text{disp}}^{\text{HB}}$	$E_{\text{total}}^{\text{HB}}$
3.0	-8.75	4.42	-1.28	-3.19	-8.80
2.9	-10.05	6.51	-1.56	-3.78	-8.87
2.8	-11.68	9.55	-1.93	-4.50	-8.56
2.7	-13.73	13.94	-2.47	-5.39	-7.65
2.6	-16.33	20.24	-3.26	-6.52	-5.87
2.5	-19.65	29.17	-4.51	-7.94	-2.93
2.4	-23.90	41.73	-6.58	-9.82	1.43
2.3	-29.29	59.18	-10.16	-12.08	7.65
2.2	-35.99	83.08	-16.47	-15.09	15.54
2.1	-43.94	115.26	-27.60	-18.97	24.75
2.0	-52.44	157.62	-47.13	-24.00	34.04
E^{nHB} for the configuration without hydrogen bond					
D (Å)	$E_{\text{elst}}^{\text{nHB}}$	$E_{\text{exch}}^{\text{nHB}}$	$E_{\text{ind}}^{\text{nHB}}$	$E_{\text{disp}}^{\text{nHB}}$	$E_{\text{total}}^{\text{nHB}}$
3.0	1.95	1.64	-0.58	-2.30	0.72
2.9	1.99	2.36	-0.66	-2.66	1.04
2.8	1.98	3.41	-0.76	-3.09	1.54
2.7	1.86	4.93	-0.88	-3.59	2.31
2.6	1.58	7.14	-1.03	-4.20	3.48
2.5	1.04	10.35	-1.23	-4.94	5.22
2.4	-0.12	14.98	-1.50	-5.85	7.51
2.3	-1.40	22.29	-1.89	-6.96	12.05
2.2	-3.80	31.01	-2.51	-8.33	16.37
2.1	-7.51	44.22	-3.55	-10.06	23.11
2.0	-13.11	62.63	-5.36	-12.23	31.93
$\Delta E = E^{\text{HB}} - E^{\text{nHB}}$					
D (Å)	ΔE_{elst}	ΔE_{exch}	ΔE_{ind}	ΔE_{disp}	ΔE_{total}
3.0	-10.70	2.77	-0.70	-0.89	-9.51
2.9	-12.04	4.14	-0.89	-1.11	-9.91
2.8	-13.65	6.14	-1.17	-1.41	-10.10
2.7	-15.58	9.01	-1.58	-1.80	-9.96
2.6	-17.91	13.09	-2.23	-2.31	-9.35
2.5	-20.70	18.82	-3.28	-3.00	-8.15
2.4	-23.78	26.75	-5.09	-3.97	-6.09
2.3	-27.89	36.88	-8.28	-5.12	-4.41
2.2	-32.19	52.07	-13.96	-6.75	-0.83
2.1	-36.43	71.04	-24.05	-8.92	1.63
2.0	-39.33	94.99	-41.77	-11.77	2.12

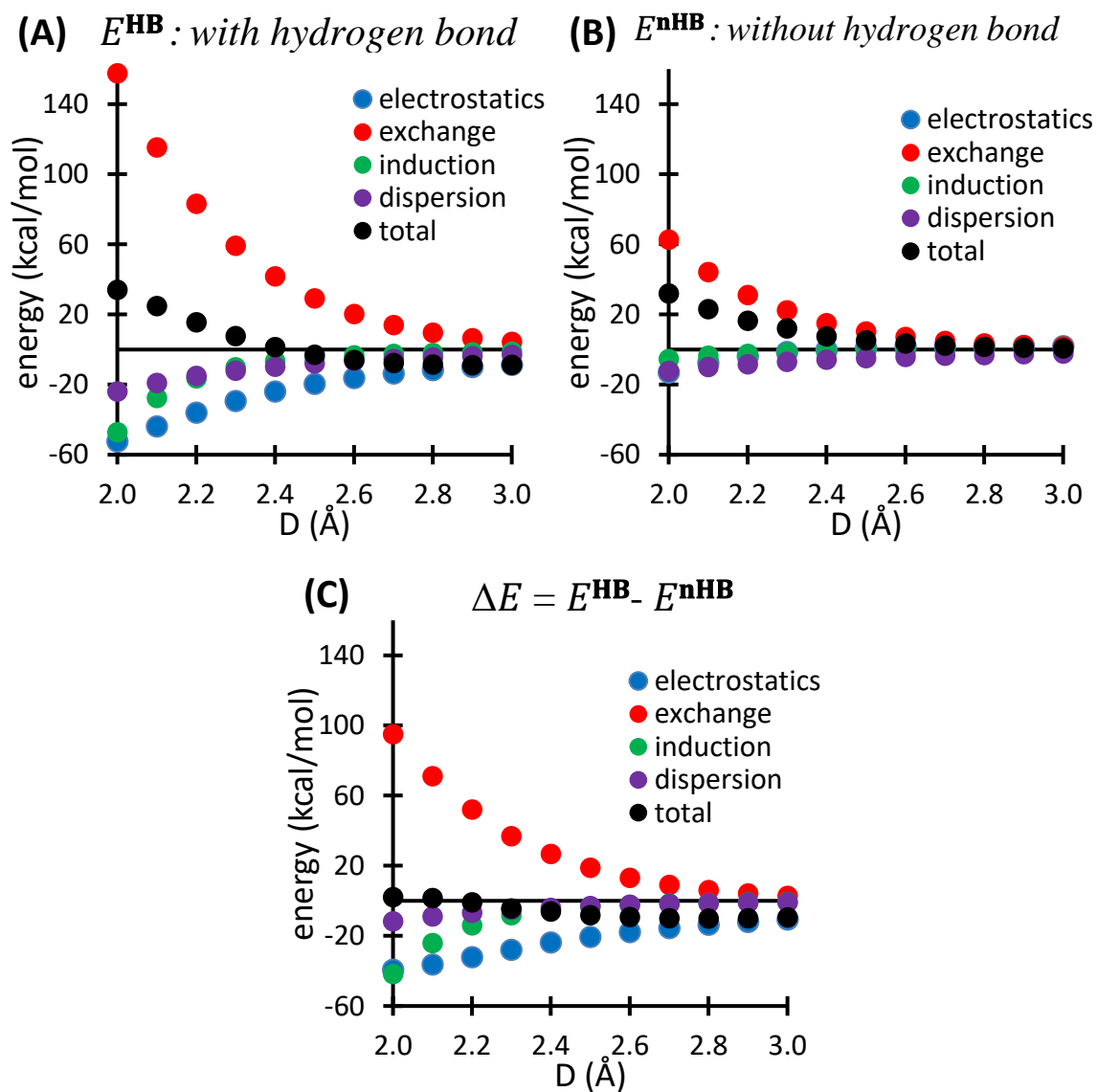


Figure 3.62 SAPT energies for the NMP-phenol complex between 2.0 and 3.0 Å in the configurations with (A) and without (B) hydrogen bond as well as the corresponding energy difference (C).

The relative insensitivity of the ACE's in substituted phenol rotors against electrostatic alterations was examined via a series of similar SAPT calculations on bimolecular complexes comprised of NMP and substituted phenols (X = H, *p*-NO₂, *m*-NO₂, *p*-CN, *p*-Cl, and *m*-Cl). In this study, the O-to-O distance (*D*) at 2.5 Å is the only distance used to mimic the TS of the phenol and control rotors. The geometric constraints described previously for the unsubstituted phenol were applied on the NMP-substituted phenol complexes in the configurations with and without (Figure 3.61) hydrogen bond. The geometric optimizations and SAPT calculations were carried out at the same levels of theory as described above. The component terms (E_{elst} , E_{exch} , E_{ind} , and E_{disp}) for the six bimolecular complexes of NMP and substituted phenols with and without hydrogen bond were obtained and tabulated in Table 3.12.

The hydrogen bond ACE's were characterized similarly as above. The ACE for each hydrogen bond was based on the difference ($\Delta E = E^{\text{HB}} - E^{\text{nHB}}$) in the calculated total (ΔE_{total}) and component energy terms (ΔE_{elst} , ΔE_{exch} , ΔE_{ind} , and ΔE_{disp}) between the configurations of with and without hydrogen bond for the six bimolecular complexes (X = H, *p*-NO₂, *m*-NO₂, *p*-CN, *p*-Cl, and *m*-Cl). These energy differences were plotted against the measured association energies (ΔG_{Ka}) to explore the origins of the relatively constant ACE's observed in substituted phenol rotors (Figure 3.63). The electrostatic term (ΔE_{elst}) of the hydrogen bond ACE was relatively constant despite the presence of EWG substituents, resulting a flat trend line in the correlation plot against the measured association energy (Figure 3.63A). However, moderate changes were observed in the exchange (ΔE_{exch}) and induction (ΔE_{ind}) terms as well as the total energy (ΔE_{total}) of the hydrogen bond ACE's upon introducing EWG substituents. Nevertheless, these changes

were significantly less in comparison to the observed changes in association energy for the host-guest complex of NMP and substituted phenols in solution.

Table 3.12 SAPT total (E_{total} , kcal/mol) and component energies (E_{elst} , E_{exch} , E_{ind} , and E_{disp} , kcal/mol) for the NMP-phenol complex in two configurations (Figure 3.61) at 2.5 Å as well as the differences in energy ($E^{\Delta} = E^{\text{HB}} - E^{\text{nHB}}$) between the two configurations.

E^{HB} for the configuration with hydrogen bond						
Fundamental energy	H	p-NO ₂	m-NO ₂	p-Cl	m-Cl	p-CN
$E_{\text{elst}}^{\text{HB}}$	-19.65	-21.72	-21.32	-20.43	-20.32	-21.31
$E_{\text{exch}}^{\text{HB}}$	29.17	28.54	28.68	28.93	28.89	28.69
$E_{\text{indu}}^{\text{HB}}$	-4.51	-5.13	-5.02	-4.73	-4.71	-5.01
$E_{\text{disp}}^{\text{HB}}$	-7.94	-7.84	-7.85	-7.91	-7.91	-7.87
$E_{\text{total}}^{\text{HB}}$	-2.93	-6.16	-5.51	-4.15	-4.05	-5.49
E^{nHB} for the configuration without hydrogen bond						
	H	p-NO ₂	m-NO ₂	p-Cl	m-Cl	p-CN
$E_{\text{elst}}^{\text{nHB}}$	1.04	-1.02	-0.65	0.26	0.36	-0.61
$E_{\text{exch}}^{\text{nHB}}$	10.35	10.17	10.23	10.25	10.31	10.21
$E_{\text{indu}}^{\text{nHB}}$	-1.23	-1.23	-1.26	-1.23	-1.23	-1.23
$E_{\text{disp}}^{\text{nHB}}$	-4.94	-4.91	-4.90	-4.94	-4.95	-4.92
$E_{\text{total}}^{\text{nHB}}$	5.22	3.00	3.42	4.33	4.49	3.44
$\Delta E = E^{\text{HB}} - E^{\text{nHB}}$						
	H	p-NO ₂	m-NO ₂	p-Cl	m-Cl	p-CN
$\Delta E_{\text{elst.}}$	-20.70	-20.70	-20.67	-20.69	-20.68	-20.69
$\Delta E_{\text{exch.}}$	18.82	18.38	18.44	18.68	18.58	18.48
$\Delta E_{\text{ind.}}$	-3.28	-3.90	-3.76	-3.50	-3.49	-3.77
$\Delta E_{\text{disp.}}$	-3.00	-2.93	-2.94	-2.97	-2.96	-2.95
ΔE_{total}	-8.15	-9.16	-8.93	-8.48	-8.54	-8.93

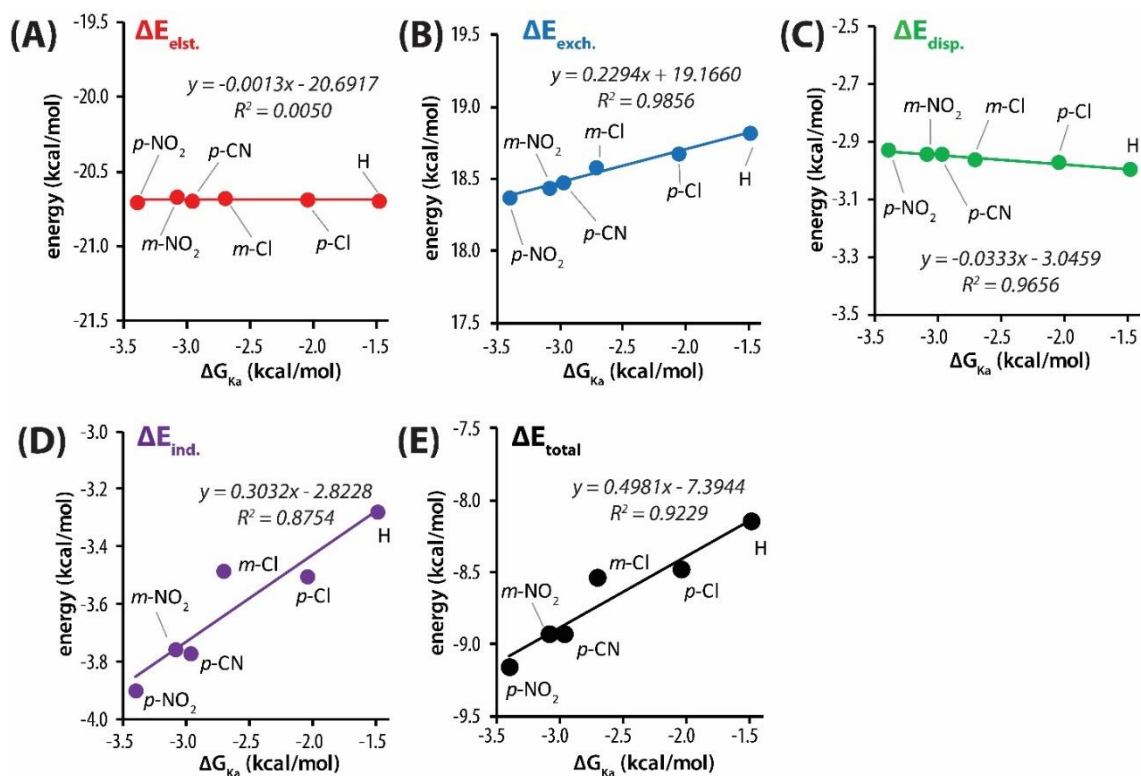


Figure 3.63 Correlations of the calculated hydrogen bond ACE total (ΔE_{total} , kcal/mol) and component energy terms (ΔE_{elst} , ΔE_{exch} , ΔE_{ind} , and ΔE_{disp} kcal/mol) with the experimentally measured association energies (ΔG_{Ka} , kcal/mol) in the bimolecular complexes of NMP and substituted phenols. The calculated total and component energies were tabulated in Table 3.12, and the experimentally measured association energies were tabulated in Table 3.2.

Table 3.13 XYZ coordinates for the GS and TS structures of anisole rotor 2

H 0.694200 -2.215100 3.956500 C 0.510500 -1.160600 3.739700 C 1.423500 -0.591800 2.630900 C 0.721900 0.723600 2.350200 C -0.585300 0.534700 2.534200 C -0.788700 -0.913000 2.941700 H 0.555000 -0.577900 4.659300 H 2.491300 -0.543500 2.822700 H 1.204600 1.598500 1.941900 H -1.384000 1.226000 2.308800 H -1.734400 -1.157400 3.416200 C -0.473900 -1.788500 1.674800 H -0.750600 -2.827400 1.853100 C 1.037400 -1.571800 1.463800 H 1.628200 -2.485200 1.527000 C 1.171100 -0.996100 0.071000 C -1.130200 -1.314000 0.396600 N -0.116900 -0.887700 -0.471200 O 2.184300 -0.683700 -0.499000 O -2.307600 -1.290200 0.143700 C -0.372500 -0.331700 -1.754700 C -0.847100 0.749000 -4.259500 C -0.846800 -1.133200 -2.778200 C -0.145800 1.035000 -1.970100 C -0.375600 1.566600 -3.237600 C -1.091800 -0.597900 -4.037100 H -1.022500 -2.181400 -2.577500 H -0.197300 2.613600 -3.431600 H -1.464000 -1.228800 -4.832600 H -1.024900 1.178500 -5.237100 O 0.273800 1.750700 -0.900300 C 0.619800 3.111900 -1.090500 H 1.424100 3.215800 -1.823700 H 0.963900 3.470300 -0.123300 H -0.244100 3.702700 -1.408200	H 0.545500 -1.695200 4.203500 C 1.051000 -0.775300 3.901800 C 1.918500 -0.937800 2.633700 C 2.195900 0.518900 2.308500 C 1.125200 1.227000 2.672300 C 0.107300 0.259900 3.250000 H 1.609100 -0.364300 4.742400 H 2.779900 -1.596700 2.684600 H 3.064700 0.872300 1.772300 H 0.939800 2.275700 2.491200 H -0.679100 0.691400 3.861800 C -0.427300 -0.606800 2.053500 H -1.272600 -1.216000 2.372000 C 0.809200 -1.425000 1.632900 H 0.674200 -2.503300 1.711400 C 1.055700 -1.065200 0.184200 C -0.821800 0.184700 0.826200 N 0.069500 -0.150100 -0.201400 O 1.940600 -1.466100 -0.528200 O -1.715900 0.984400 0.726700 C -0.008800 0.415100 -1.502600 C -0.193700 1.528800 -4.029000 C 0.971300 1.283300 -1.949800 C -1.091900 0.078200 -2.326000 C -1.182700 0.653200 -3.592000 C 0.887500 1.843600 -3.219000 H 1.798500 1.514500 -1.292800 H -2.012400 0.417900 -4.241500 H 1.656100 2.520600 -3.565700 H -0.275800 1.963900 -5.016800 O -1.976400 -0.812100 -1.817500 C -3.154000 -1.091900 -2.556600 H -3.734200 -0.181900 -2.730500 H -3.733000 -1.779600 -1.945300 H -2.920200 -1.566000 -3.514200	H 4.600500 0.452000 0.194900 C 3.963200 -0.433100 0.248200 C 2.821000 -0.308600 1.281300 C 1.971900 -1.501100 0.889300 C 2.080400 -1.660500 -0.431000 C 2.999400 -0.572900 -0.950300 H 4.572200 -1.323200 0.401500 H 3.086200 -0.222800 2.330900 H 1.311500 -2.033100 1.558900 H 1.525400 -2.347500 -1.053400 H 3.425200 -0.723400 -1.937800 C 2.230700 0.801100 -0.801500 H 2.769900 1.590800 -1.321300 C 2.125600 0.986600 0.705600 H 2.626800 1.873200 1.088400 C 0.651000 1.108800 0.995000 C 0.809700 0.762600 -1.290700 N -0.076100 0.685500 -0.178500 O 0.216400 1.555800 2.016300 O 0.504900 0.799300 -2.457600 C -1.445900 0.231300 -0.324000 C -4.065200 -0.742100 -0.810600 C -1.824400 -0.328800 -1.550800 C -2.428100 0.233800 0.702300 C -3.717800 -0.229500 0.427500 C -3.102300 -0.806600 -1.799500 H -1.108300 -0.369500 -2.348000 H -4.457000 -0.203000 1.212800 H -3.329300 -1.217700 -2.773900 H -5.073800 -1.093500 -0.985500 O -2.092100 0.648300 1.938100 C -3.069400 0.731900 2.955400 H -3.886100 1.403700 2.674700 H -2.549100 1.136700 3.820200 H -3.479700 -0.251900 3.204000

Table 3.14 XYZ coordinates for the GS and TS structure of phenol rotor **1** with hydrogen bond

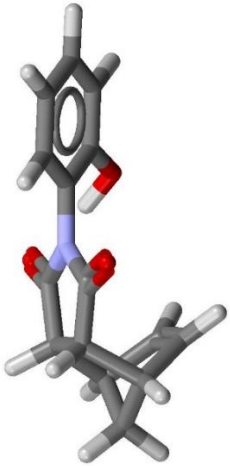
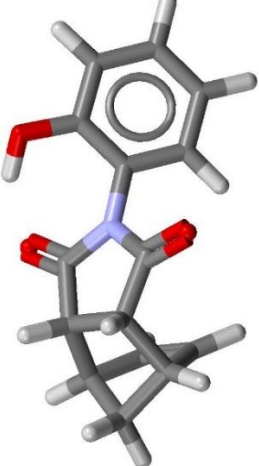
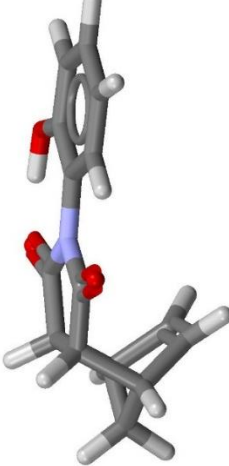
		
H -0.044600 -3.904900 -1.875500	H -0.397300 -5.329400 -0.583000	H 0.007800 -3.963800 -1.850000
C 0.276700 -3.667100 -0.859200	C -0.112200 -5.066600 0.437700	C 0.350800 -3.681100 -0.852500
C 1.335700 -2.544800 -0.794100	C 0.910000 -3.910700 0.513700	C 1.356700 -2.509000 -0.854600
C 1.318100 -2.239200 0.692900	C 0.842100 -3.585000 1.994400	C 1.375300 -2.164000 0.622400
C 0.072800 -2.431100 1.131100	C -0.408200 -3.810200 2.402200	C 0.154800 -2.399200 1.108300
C -0.770900 -2.868800 -0.052200	C -1.205700 -4.288700 1.202700	C -0.705600 -2.907300 -0.032900
H 0.596400 -4.574200 -0.348100	H 0.220900 -5.955500 0.971900	H 0.730000 -4.556600 -0.327200
H 2.306700 -2.729900 -1.242900	H 1.898700 -4.073000 0.095700	H 2.319100 -2.657300 -1.334200
H 2.147400 -1.823800 1.246500	H 1.647600 -3.143500 2.563200	H 2.207500 -1.704500 1.135700
H -0.317000 -2.206300 2.113100	H -0.829800 -3.592900 3.372800	H -0.210900 -2.170000 2.098600
H -1.717200 -3.350000 0.175200	H -2.143000 -4.795000 1.411600	H -1.623100 -3.420100 0.238200
C -0.912000 -1.618700 -0.996400	C -1.357500 -3.057100 0.234700	C -0.930000 -1.695500 -1.016100
H -1.637900 -1.816300 -1.784600	H -2.056700 -3.286800 -0.568200	H -1.677200 -1.951000 -1.765900
C 0.522900 -1.397900 -1.503300	C 0.082600 -2.803900 -0.240100	C 0.458300 -1.426100 -1.568700
H 0.631300 -1.466600 -2.585300	H 0.221200 -2.896700 -1.316600	H 0.546300 -1.516400 -2.650400
C 0.889100 -0.008500 -1.054400	C 0.391300 -1.390800 0.177500	C 0.769400 -0.013100 -1.176100
C -1.286500 -0.338100 -0.289700	C -1.784700 -1.777400 0.912800	C -1.342500 -0.416200 -0.342500
N -0.187800 0.554200 -0.387700	N -0.698000 -0.868500 0.857600	N -0.267500 0.541700 -0.420100
O 1.968200 0.533000 -1.209000	O 1.424100 -0.786800 -0.044000	O 1.816400 0.515700 -1.505500
O -2.318300 -0.094500 0.273900	O -2.844600 -1.549100 1.429000	O -2.417800 -0.263300 0.171800
C -0.206500 1.860100 0.195800	C -0.730900 0.411600 1.495500	C -0.305400 1.858900 0.232400
C -0.396800 4.345000 1.429200	C -0.969200 2.882300 2.747700	C -0.603100 4.328000 1.595700
C -1.319400 2.670500 -0.019500	C -1.219600 0.497000 2.797800	C -1.459700 2.181400 0.967800
C 0.839700 2.310400 1.015100	C -0.324500 1.572800 0.822000	C 0.731400 2.833900 0.199200
C 0.723900 3.556800 1.629000	C -0.457900 2.803600 1.463400	C 0.540500 4.042500 0.885200
C -1.419600 3.908500 0.592500	C -1.340700 1.725000 3.425700	C -1.616000 3.380700 1.636600
H -2.115700 2.310300 -0.653800	H -1.524100 -0.406600 3.304100	H -2.260800 1.472000 1.012700
H 1.540600 3.884400 2.258100	H -0.142500 3.687300 0.925200	H 1.357800 4.748500 0.825500
H -2.291700 4.524600 0.421100	H -1.727000 1.777800 4.434500	H -2.531600 3.562800 2.182600
H -0.467400 5.308300 1.917700	H -1.066600 3.848200 3.226600	H -0.701600 5.275900 2.109100
O 1.951300 1.573900 1.269800	O 0.162700 1.560600 -0.444600	O 1.921800 2.761000 -0.414400
H 2.230900 1.149400 0.434400	H 0.770600 0.799100 -0.528000	H 2.008900 1.911100 -0.910800

Table 3.15 XYZ coordinates for the GS and TS structure of phenol rotor **1** without hydrogen bond

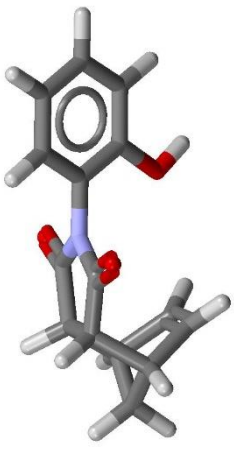
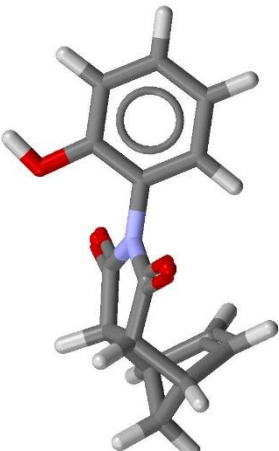
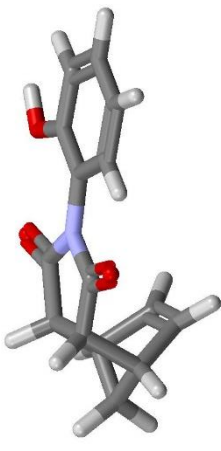
											
H	4.429200	0.836400	-0.484600	H	-0.888800	-4.359800	-0.791300	H	-1.677100	4.947600	-6.177500
C	3.968700	-0.014200	0.022500	C	-0.053600	-4.026300	-0.171700	C	-1.750500	3.914400	-5.831500
C	2.899200	0.393000	1.060200	C	0.841800	-2.972900	-0.861600	C	-0.477400	3.411000	-5.116200
C	2.248800	-0.952200	1.323200	C	1.662400	-2.497800	0.324200	C	-1.001600	2.128400	-4.498800
C	2.290600	-1.652200	0.188800	C	0.883600	-2.557600	1.406000	C	-2.283000	2.325800	-4.182500
C	2.966700	-0.789700	-0.860800	C	-0.475700	-3.072900	0.968500	C	-2.643300	3.743900	-4.582400
H	4.739500	-0.657700	0.445400	H	0.510200	-4.886600	0.187500	H	-2.051900	3.266900	-6.653700
H	3.220100	0.957800	1.930400	H	1.395800	-3.273100	-1.745900	H	0.440800	3.337600	-5.690400
H	1.727100	-1.212600	2.231700	H	2.656400	-2.080600	0.253600	H	-0.394300	1.266100	-4.264800
H	1.815400	-2.601400	-0.011100	H	1.113100	-2.201600	2.400000	H	-2.933200	1.657100	-3.637500
H	3.348900	-1.300200	-1.739700	H	-1.121200	-3.463800	1.749200	H	-3.700800	3.972500	-4.670800
C	1.969800	0.379500	-1.194100	C	-1.140000	-1.936200	0.110700	C	-1.871500	4.709200	-3.603600
H	2.323100	0.947300	-2.054600	H	-2.179200	-2.182000	-0.105800	H	-2.219500	5.733100	-3.730800
C	1.928300	1.191200	0.115800	C	-0.239800	-1.867700	-1.138800	C	-0.413200	4.484600	-3.961700
H	2.267700	2.221100	0.009100	H	-0.763500	-2.072000	-2.072100	H	0.117200	5.373000	-4.301400
C	0.477300	1.194000	0.543000	C	0.295800	-0.453500	-1.171300	C	0.229400	3.992700	-2.699700
C	0.542400	-0.057200	-1.441700	C	-1.080000	-0.555500	0.726400	C	-1.983000	4.340500	-2.150200
N	-0.246900	0.454800	-0.403600	N	-0.251200	0.233800	-0.079200	N	-0.708400	3.866600	-1.670600
O	-0.003400	1.727900	1.508400	O	1.072200	0.019600	-1.959600	O	1.422200	3.748900	-2.654300
O	0.128600	-0.727100	-2.353100	O	-1.622700	-0.178600	1.733600	O	-3.004300	4.441000	-1.524900
C	-1.642000	0.207700	-0.290700	C	0.044800	1.595000	0.199100	C	-0.499600	3.326700	-0.318800
C	-4.368600	-0.260000	-0.060700	C	0.628900	4.257000	0.712300	C	-0.351300	2.308500	2.324100
C	-2.528200	0.779300	-1.191900	C	0.824300	1.938500	1.293000	C	-1.615500	3.277000	0.535300
C	-2.119000	-0.620800	0.727600	C	-0.462000	2.588400	-0.641000	C	0.731400	2.833900	0.199200
C	-3.488900	-0.839700	0.842800	C	-0.155300	3.921300	-0.383000	C	0.759800	2.342200	1.512700
C	-3.892400	0.547300	-1.086600	C	1.117800	3.269100	1.558700	C	-1.555800	2.782700	1.824500
H	-2.132500	1.406900	-1.978900	H	1.195000	1.149000	1.932300	H	-2.557600	3.641300	0.179200
H	-3.861300	-1.473200	1.640400	H	-0.538800	4.693900	-1.040200	H	1.720000	1.982500	1.856900
H	-4.575600	0.996000	-1.794500	H	1.724800	3.530800	2.414300	H	-2.453900	2.775200	2.427000
H	-5.430500	-0.443500	0.039500	H	0.856200	5.297800	0.903100	H	-0.277400	1.918200	3.331000
O	-1.211700	-1.187300	1.567200	O	-1.245500	2.196800	-1.680900	O	1.921800	2.761000	-0.414400
H	-1.671600	-1.733300	2.214300	H	-1.533200	2.970000	-2.178500	H	2.602000	2.368700	0.185400

Table 3.16 XYZ coordinates for NMP-phenol complex with a hydrogen bond at D = 2.0 Å (left), D = 2.1 Å (middle) and D = 2.2 (right)

C	-2.925187	1.666576	0.664758	C	-2.958647	1.683265	0.664756	C	-2.992360	1.699382	0.664759
H	-3.051441	1.676828	-0.425183	H	-3.084884	1.694877	-0.425173	H	-3.118572	1.712305	-0.425158
C	-1.762255	2.574389	1.048332	C	-1.787159	2.579992	1.048376	C	-1.812702	2.585318	1.048415
H	-1.646690	3.403127	0.345873	H	-1.663825	3.407708	0.346034	H	-1.681870	3.411976	0.346183
C	-0.569087	1.649635	0.997023	C	-0.602785	1.644014	0.996831	C	-0.636928	1.638572	0.996638
C	-2.470926	0.293722	1.117578	C	-2.517341	0.306111	1.117330	C	-2.563612	0.318190	1.117098
N	-1.044427	0.346526	0.929937	N	-1.090421	0.345464	0.929584	N	-1.136407	0.344538	0.929241
O	0.598166	2.000901	1.058326	O	0.567739	1.984227	1.058094	O	0.536658	1.968073	1.057856
C	5.356258	0.070336	0.902502	C	5.396388	0.054364	0.902526	C	5.436904	0.038951	0.902545
C	3.335517	1.967545	1.018898	C	3.393670	1.970563	1.019373	C	3.451777	1.973340	1.019832
C	5.685838	1.431683	0.966394	C	5.738820	1.412527	0.966600	C	5.791729	1.393921	0.966789
C	4.015045	-0.341775	0.896678	C	4.051341	-0.345056	0.896745	C	4.088265	-0.348169	0.896815
C	3.000196	0.616124	0.955564	C	3.045592	0.622379	0.955859	C	3.091397	0.628401	0.956151
C	4.664291	2.381321	1.024679	C	4.726295	2.371765	1.025111	C	4.788010	2.362357	1.025521
H	6.720771	1.766301	0.971569	H	6.776868	1.737352	0.971744	H	6.832700	1.709252	0.971896
C	3.746713	-1.394857	0.846888	H	3.773067	-1.395548	0.846815	H	3.800406	-1.396069	0.846755
H	1.960334	0.297147	0.950486	H	2.002761	0.313242	0.950815	H	2.045787	0.328800	0.951146
H	4.901141	3.441048	1.074424	H	4.973150	3.429199	1.075000	H	5.044515	3.417485	1.075544
C	-0.208932	-0.810533	1.147248	C	-0.265878	-0.819470	1.146651	C	-0.322519	-0.827908	1.146073
H	-0.248635	-1.079846	2.206450	H	-0.308041	-1.088559	2.205815	H	-0.367053	-1.096756	2.205201
H	0.826404	-0.587101	0.875706	H	0.771502	-0.605788	0.875061	H	0.716747	-0.623668	0.874430
H	-0.578668	-1.638996	0.537702	H	-0.643472	-1.644310	0.537008	H	-0.707678	-1.649176	0.536341
H	-1.871113	2.952892	2.069240	H	-1.892357	2.959349	2.069351	H	-1.914350	2.965471	2.069453
H	-3.872936	1.972689	1.116193	H	-3.903426	1.998249	1.116313	H	-3.934187	2.022914	1.116438
H	-2.679500	0.130458	2.180374	H	-2.727365	0.144662	2.180117	H	-2.775017	0.158510	2.179878
H	-2.909650	-0.510614	0.520836	H	-2.963691	-0.493953	0.520500	H	-3.017297	-0.477678	0.520187
O	2.369896	2.928600	1.076906	O	2.437177	2.940688	1.077605	O	2.504187	2.952151	1.078283
H	1.504867	2.475682	1.067835	H	1.567906	2.495965	1.068533	H	1.630891	2.515386	1.069217
H	6.154011	-0.679807	0.856781	H	6.187015	-0.703276	0.856627	H	6.220576	-0.725870	0.856472

Table 3.17 XYZ coordinates for NMP-phenol complex with a hydrogen bond at D = 2.3 Å (left), D = 2.4 Å (middle) and D = 2.5 (right)

C	-3.026323	1.714948	0.664767	C	-3.060534	1.729984	0.664780	C	-3.094987	1.744510	0.664796
H	-3.152504	1.729136	-0.425138	H	-3.186678	1.745393	-0.425113	H	-3.221089	1.761097	-0.425084
C	-1.838860	2.590382	1.048448	C	-1.865609	2.595199	1.048477	C	-1.892927	2.599781	1.048502
H	-1.700792	3.415951	0.346320	H	-1.720556	3.419652	0.346446	H	-1.741130	3.423096	0.346562
C	-0.671494	1.633301	0.996444	C	-0.706460	1.628194	0.996251	C	-0.741807	1.623245	0.996058
C	-2.609748	0.329962	1.116880	C	-2.655760	0.341433	1.116676	C	-2.701655	0.352607	1.116484
N	-1.182382	0.343737	0.928910	N	-1.228344	0.343047	0.928590	N	-1.274289	0.342459	0.928280
O	0.504961	1.952420	1.057612	O	0.472681	1.937251	1.057363	O	0.439851	1.922548	1.057111
C	5.477797	0.024076	0.902561	C	5.519059	0.009719	0.902573	C	5.560679	-0.004141	0.902581
C	3.509834	1.975898	1.020278	C	3.567838	1.978254	1.020709	C	3.625788	1.980422	1.021126
C	5.844575	1.375852	0.966963	C	5.897368	1.358306	0.967122	C	5.950115	1.341269	0.967267
C	4.125794	-0.351122	0.896888	C	4.163901	-0.353924	0.896962	C	4.202564	-0.356582	0.897038
C	3.137590	0.634201	0.956440	C	3.184149	0.639791	0.956726	C	3.231056	0.645182	0.957008
C	4.849450	2.353102	1.025911	C	4.910626	2.344008	1.026281	C	4.971550	2.335076	1.026632
H	6.888290	1.681981	0.972028	H	6.943659	1.655514	0.972140	H	6.998824	1.629826	0.972236
H	3.828691	-1.396434	0.846707	H	3.857882	-1.396654	0.846668	H	3.887942	-1.396743	0.846640
H	2.089375	0.343844	0.951480	H	2.133494	0.358393	0.951814	H	2.178113	0.372469	0.952148
H	5.115263	3.405918	1.076058	H	5.185421	3.394510	1.076544	H	5.255014	3.383267	1.077004
C	-0.378858	-0.835879	1.145513	C	-0.434901	-0.843414	1.144971	C	-0.490652	-0.850539	1.144447
H	-0.425678	-1.104470	2.204608	H	-0.483926	-1.111735	2.204035	H	-0.541803	-1.118580	2.203480
H	0.662149	-0.640784	0.873813	H	0.607711	-0.657176	0.873211	H	0.553440	-0.672882	0.872622
H	-0.771301	-1.653630	0.535699	H	-0.834360	-1.657704	0.535082	H	-0.896871	-1.661427	0.534489
H	-1.937065	2.971276	2.069547	H	-1.960476	2.976783	2.069634	H	-1.984556	2.982006	2.069715
H	-3.965221	2.046719	1.116568	H	-3.996529	2.069698	1.116701	H	-4.028107	2.091884	1.116838
H	-2.822469	0.172007	2.179655	H	-2.869735	0.185159	2.179448	H	-2.916825	0.197972	2.179255
H	-3.070490	-0.461787	0.519897	H	-3.123292	-0.446275	0.519627	H	-3.175724	-0.431138	0.519376
O	2.570926	2.963028	1.078941	O	2.637396	2.973354	1.079579	O	2.703599	2.983164	1.080199
H	1.693808	2.533990	1.069886	H	1.756647	2.551821	1.070541	H	1.819398	2.568918	1.071181
H	6.254683	-0.747627	0.856318	H	6.289325	-0.768582	0.856164	H	6.324489	-0.788769	0.856011

Table 3.18 XYZ coordinates for NMP-phenol complex with a hydrogen bond at D = 2.6 Å (left), D = 2.7 Å (middle) and D = 2.8 (right)

C	-3.129679	1.758546	0.664816	C	-3.164604	1.772111	0.664839	C	-3.199759	1.785223	0.664865
H	-3.255735	1.776270	-0.425052	H	-3.290611	1.790933	-0.425016	H	-3.325713	1.805107	-0.424977
C	-1.920793	2.604141	1.048523	C	-1.949186	2.608291	1.048540	C	-1.978084	2.612241	1.048554
H	-1.762483	3.426302	0.346668	H	-1.784582	3.429283	0.346766	H	-1.807400	3.432055	0.346855
C	-0.777515	1.618447	0.995866	C	-0.813566	1.613794	0.995674	C	-0.849944	1.609279	0.995484
C	-2.747441	0.363491	1.116305	C	-2.793125	0.374091	1.116138	C	-2.838715	0.384413	1.115981
N	-1.320217	0.341964	0.927979	N	-1.366126	0.341552	0.927689	N	-1.412016	0.341215	0.927408
O	0.406501	1.908294	1.056855	O	0.372660	1.894471	1.056596	O	0.338355	1.881064	1.056336
C	5.602648	-0.017523	0.902586	C	5.644956	-0.030446	0.902589	C	5.687594	-0.042929	0.902589
C	3.683682	1.982420	1.021531	C	3.741519	1.984259	1.021922	C	3.799299	1.985952	1.022301
C	6.002825	1.324725	0.967400	C	6.055503	1.308661	0.967521	C	6.108157	1.293061	0.967631
C	4.241761	-0.359103	0.897116	C	4.281468	-0.361494	0.897194	C	4.321667	-0.363762	0.897274
C	3.278291	0.650383	0.957286	C	3.325836	0.655403	0.957561	C	3.373677	0.660252	0.957831
C	5.032235	2.326311	1.026965	C	5.092691	2.317713	1.027282	C	5.152929	2.309285	1.027583
H	7.053806	1.604895	0.972315	H	7.108620	1.580697	0.972379	H	7.163280	1.557208	0.972430
H	3.918835	-1.396712	0.846620	H	3.950526	-1.396569	0.846607	H	3.982983	-1.396326	0.846603
H	2.223202	0.386090	0.952483	H	2.268736	0.399276	0.952816	H	2.314689	0.412044	0.953149
H	5.324067	3.372198	1.077438	H	5.392604	3.361307	1.077849	H	5.460648	3.350599	1.078238
C	-0.546117	-0.857283	1.143939	C	-0.601303	-0.863668	1.143447	C	-0.656215	-0.869718	1.142970
H	-0.599320	-1.125033	2.202945	H	-0.656486	-1.131120	2.202427	H	-0.713310	-1.136865	2.201926
H	0.499338	-0.687939	0.872048	H	0.445408	-0.702381	0.871487	H	0.391650	-0.716240	0.870939
H	-0.958852	-1.664827	0.533918	H	-1.020319	-1.667927	0.533369	H	-1.081291	-1.670753	0.532841
H	-2.009281	2.986964	2.069789	H	-2.034626	2.991669	2.069857	H	-2.060567	2.996137	2.069919
H	-4.059957	2.113309	1.116978	H	-4.092074	2.134003	1.117120	H	-4.124457	2.153997	1.117264
H	-2.963751	0.210452	2.179076	H	-3.010523	0.222607	2.178909	H	-3.057152	0.234445	2.178754
H	-3.227805	-0.416371	0.519143	H	-3.279554	-0.401966	0.518928	H	-3.330989	-0.387917	0.518728
O	2.769538	2.992489	1.080800	O	2.835216	3.001358	1.081383	O	2.900638	3.009800	1.081950
H	1.882055	2.585321	1.071807	H	1.944611	2.601065	1.072420	H	2.007062	2.616183	1.073018
H	6.360162	-0.808222	0.855858	H	6.396330	-0.826972	0.855707	H	6.432982	-0.845051	0.855557

Table 3.19 XYZ coordinates for NMP-phenol complex with a hydrogen bond at D = 2.9 Å (left) and D = 3.0 (right)

C	-3.235138	1.797900	0.664894	C	-3.270735	1.810161	0.664925
H	-3.361036	1.818810	-0.424936	H	-3.396575	1.832062	-0.424892
C	-2.007469	2.616004	1.048565	C	-2.037322	2.619587	1.048573
H	-1.830907	3.434632	0.346936	H	-1.855076	3.437026	0.347009
C	-0.886632	1.604897	0.995296	C	-0.923614	1.600643	0.995109
C	-2.884217	0.394464	1.115834	C	-2.929638	0.404251	1.115697
N	-1.457885	0.340947	0.927136	N	-1.503732	0.340742	0.926872
O	0.303611	1.868057	1.056075	O	0.268451	1.855435	1.055813
C	5.730552	-0.054988	0.902586	C	5.773822	-0.066643	0.902581
C	3.857021	1.987511	1.022669	C	3.914685	1.988947	1.023025
C	6.160793	1.277912	0.967732	C	6.213414	1.263198	0.967822
C	4.362336	-0.365914	0.897354	C	4.403456	-0.367955	0.897434
C	3.421797	0.664937	0.958098	C	3.470182	0.669467	0.958360
C	5.212959	2.301025	1.027869	C	5.272791	2.292934	1.028141
H	7.217803	1.534404	0.972468	H	7.272199	1.512263	0.972494
H	4.016174	-1.395991	0.846605	H	4.050067	-1.395572	0.846613
H	2.361037	0.424411	0.953479	H	2.407760	0.436394	0.953807
H	5.528221	3.340077	1.078606	H	5.595343	3.329742	1.078954
C	-0.710862	-0.875454	1.142509	C	-0.765249	-0.880895	1.142062
H	-0.769802	-1.142290	2.201441	H	-0.825971	-1.147416	2.200973
H	0.338065	-0.729545	0.870405	H	0.284654	-0.742327	0.869883
H	-1.141782	-1.673323	0.532333	H	-1.201811	-1.675659	0.531844
H	-2.087082	3.000381	2.069977	H	-2.114149	3.004413	2.070029
H	-4.157101	2.173319	1.117409	H	-4.190002	2.191998	1.117555
H	-3.103646	0.245972	2.178610	H	-3.150014	0.257197	2.178477
H	-3.382126	-0.374216	0.518543	H	-3.432980	-0.360855	0.518372
O	2.965809	3.017839	1.082499	O	3.030733	3.025499	1.083032
H	2.069403	2.630709	1.073602	H	2.131631	2.644673	1.074173
H	6.470104	-0.862486	0.855408	H	6.507683	-0.879308	0.855261

Table 3.20 XYZ coordinates for NMP-phenol complex without a hydrogen bond at D = 2.0 Å (left), D = 2.1 Å (middle) and D = 2.2 (right)

C	-2.968730	1.620656	0.663104	C	-3.002659	1.637761	0.663098	C	-3.036821	1.654284	0.663099
H	-3.094984	1.630908	-0.426837	H	-3.128896	1.649372	-0.426831	H	-3.163033	1.667208	-0.426818
C	-1.805797	2.528469	1.046677	C	-1.831172	2.534487	1.046718	C	-1.857163	2.540220	1.046755
H	-1.690233	3.357206	0.344218	H	-1.707837	3.362204	0.344377	H	-1.726332	3.366879	0.344523
C	-0.612629	1.603715	0.995368	C	-0.646798	1.598510	0.995173	C	-0.681390	1.593474	0.994977
C	-2.514469	0.247802	1.115924	C	-2.561354	0.260607	1.115672	C	-2.608073	0.273092	1.115437
N	-1.087970	0.300605	0.928283	N	-1.134434	0.299959	0.927926	N	-1.180869	0.299441	0.927581
O	0.554623	1.954981	1.056671	O	0.523726	1.938723	1.056437	O	0.492197	1.922975	1.056196
C	5.312715	0.024415	0.900847	C	5.352375	0.008859	0.900868	C	5.392442	-0.006147	0.900885
C	3.291974	1.921625	1.017243	C	3.349657	1.925058	1.017715	C	3.407315	1.928243	1.018172
C	5.642295	1.385763	0.964740	C	5.694807	1.367023	0.964943	C	5.747267	1.348824	0.965129
C	3.971503	-0.387695	0.895023	C	4.007328	-0.390560	0.895088	C	4.043804	-0.393267	0.895155
C	2.956654	0.570203	0.953910	C	3.001579	0.576874	0.954201	C	3.046935	0.583303	0.954491
C	4.620749	2.335401	1.023024	C	4.682283	2.326261	1.023454	C	4.743549	2.317259	1.023861
H	6.677228	1.720381	0.969914	H	6.732855	1.691847	0.970086	H	6.788239	1.664155	0.970236
C	3.703170	-1.440777	0.845233	H	3.729054	-1.441053	0.845158	H	3.755945	-1.441167	0.845095
H	1.916791	0.251227	0.948831	H	1.958749	0.267738	0.949157	H	2.001325	0.283703	0.949486
H	4.857598	3.395128	1.072770	H	4.929137	3.383695	1.073342	H	5.000053	3.372387	1.073884
C	-0.252475	-0.856453	1.145594	C	-0.309891	-0.864975	1.144994	C	-0.366980	-0.873006	1.144413
H	-0.292178	-1.125767	2.204796	H	-0.352054	-1.134064	2.204157	H	-0.411514	-1.141853	2.203541
H	0.782862	-0.633021	0.874052	H	0.727489	-0.651292	0.873403	H	0.672286	-0.668766	0.872770
H	-0.622211	-1.684917	0.536048	H	-0.687485	-1.689814	0.535350	H	-0.752139	-1.694274	0.534680
H	-1.914655	2.906971	2.067585	H	-1.936369	2.913844	2.067693	H	-1.958811	2.920373	2.067793
H	-3.916479	1.926768	1.114538	H	-3.947438	1.952744	1.114655	H	-3.978648	1.977816	1.114778
H	-2.723043	0.084538	2.178719	H	-2.771378	0.099157	2.178459	H	-2.819479	0.113412	2.178218
H	-2.953193	-0.556535	0.519182	H	-3.007704	-0.539457	0.518842	H	-3.061758	-0.522775	0.518527
O	2.326353	2.882679	1.075251	O	2.393164	2.895184	1.075947	O	2.459725	2.907053	1.076622
H	2.724063	3.761451	1.114167	H	2.800263	3.770090	1.114949	H	2.875814	3.778120	1.115703
H	6.110469	-0.725728	0.855126	H	6.143002	-0.748780	0.854969	H	6.176114	-0.770968	0.854812

Table 3.21 XYZ coordinates for NMP-phenol complex without a hydrogen bond at D = 2.3 Å (left), D = 2.4 Å (middle) and D = 2.5 (right)

C	-3.071213	1.670248	0.663105	C	-3.105834	1.685673	0.663116	C	-3.140678	1.700578	0.663131
H	-3.197395	1.684436	-0.426800	H	-3.231978	1.701082	-0.426777	H	-3.266781	1.717165	-0.426750
C	-1.883750	2.545682	1.046786	C	-1.910909	2.550888	1.046813	C	-1.938619	2.555849	1.046837
H	-1.745682	3.371251	0.344658	H	-1.765856	3.375341	0.344782	H	-1.786822	3.379164	0.344897
C	-0.716384	1.588601	0.994782	C	-0.751760	1.583883	0.994587	C	-0.787498	1.579313	0.994392
C	-2.654639	0.285262	1.115217	C	-2.701060	0.297121	1.115012	C	-2.747346	0.308675	1.114819
N	-1.227273	0.299037	0.927248	N	-1.273644	0.298736	0.926926	N	-1.319981	0.298527	0.926614
O	0.460071	1.907720	1.055950	O	0.427381	1.891294	1.055699	O	0.394159	1.878616	1.055445
C	5.432907	-0.020624	0.900898	C	5.473759	-0.034593	0.900909	C	5.514987	-0.048073	0.900916
C	3.464944	1.931198	1.018615	C	3.522538	1.933942	1.019045	C	3.580096	1.936490	1.019461
C	5.799685	1.331152	0.965300	C	5.852068	1.313995	0.965458	C	5.904423	1.297337	0.965602
C	4.080903	-0.395822	0.895226	C	4.118601	-0.398235	0.895298	C	4.156873	-0.400514	0.895373
C	3.092700	0.589501	0.954778	C	3.138849	0.595480	0.955062	C	3.185364	0.601250	0.955342
C	4.804560	2.308402	1.024249	C	4.865326	2.299696	1.024617	C	4.925859	2.291144	1.024967
H	6.843400	1.637281	0.970365	H	6.898359	1.611202	0.970476	H	6.953133	1.585894	0.970570
H	3.783801	-1.441134	0.845044	H	3.812582	-1.440966	0.845004	H	3.842250	-1.440675	0.844974
H	2.044485	0.299144	0.949817	H	2.088194	0.314082	0.950150	H	2.132421	0.328537	0.950483
H	5.070373	3.361218	1.074396	H	5.140121	3.350198	1.074880	H	5.209322	3.339335	1.075338
C	-0.423748	-0.880579	1.143851	C	-0.480201	-0.887725	1.143307	C	-0.536343	-0.894471	1.142781
H	-0.470569	-1.149170	2.202946	H	-0.529226	-1.156046	2.202371	H	-0.587495	-1.162512	2.201815
H	0.617258	-0.685484	0.872151	H	0.562411	-0.701487	0.871547	H	0.507748	-0.716814	0.870957
H	-0.816192	-1.698330	0.534037	H	-0.879660	-1.702016	0.533418	H	-0.942563	-1.705359	0.532824
H	-1.981955	2.926576	2.067885	H	-2.005776	2.932471	2.067970	H	-2.030248	2.938074	2.068049
H	-4.010112	2.002019	1.114905	H	-4.041829	2.025387	1.115037	H	-4.073799	2.047952	1.115173
H	-2.867360	0.127307	2.177993	H	-2.915035	0.140848	2.177784	H	-2.962516	0.154040	2.177590
H	-3.115380	-0.506487	0.518234	H	-3.168592	-0.490586	0.517963	H	-3.221416	-0.475070	0.517711
O	2.526036	2.918328	1.077278	O	2.592096	2.929043	1.077915	O	2.657907	2.939232	1.078533
H	2.950736	3.785590	1.116431	H	3.025047	3.792542	1.117133	H	3.098768	3.799016	1.117810
H	6.209793	-0.792327	0.854655	H	6.244025	-0.812893	0.854500	H	6.278797	-0.832701	0.854345

Table 3.22 XYZ coordinates for NMP-phenol complex without a hydrogen bond at D = 2.6 Å (left), D = 2.7 Å (middle) and D = 2.8 (right)

C	-3.175745	1.714984	0.663149	C	-3.211029	1.728910	0.663172	C	-3.246527	1.742375	0.663198
H	-3.301802	1.732709	-0.426718	H	-3.337036	1.747733	-0.426683	H	-3.372481	1.762259	-0.426645
C	-1.966860	2.560579	1.046857	C	-1.995611	2.565091	1.046873	C	-2.024853	2.569394	1.046887
H	-1.808549	3.382740	0.345002	H	-1.831007	3.386083	0.345099	H	-1.854168	3.389208	0.345187
C	-0.823581	1.574885	0.994199	C	-0.859991	1.570593	0.994007	C	-0.896712	1.566431	0.993817
C	-2.793507	0.319930	1.114639	C	-2.839550	0.330891	1.114471	C	-2.885484	0.341565	1.114314
N	-1.366284	0.298402	0.926313	N	-1.412552	0.298352	0.926022	N	-1.458785	0.298368	0.925740
O	0.360435	1.864732	1.055188	O	0.326235	1.851271	1.054929	O	0.291586	1.838216	1.054669
C	5.556581	-0.061085	0.900920	C	5.598530	-0.073646	0.900922	C	5.640825	-0.085776	0.900921
C	3.637616	1.938858	1.019864	C	3.695094	1.941058	1.020255	C	3.752530	1.943105	1.020634
C	5.956758	1.281164	0.965734	C	6.009078	1.265461	0.965854	C	6.061389	1.250214	0.965964
C	4.195694	-0.402664	0.895450	C	4.235043	-0.404694	0.895527	C	4.274898	-0.406609	0.895606
C	3.232224	0.606821	0.955620	C	3.279411	0.612203	0.955894	C	3.326908	0.617404	0.956164
C	4.986169	2.282749	1.025299	C	5.046266	2.274513	1.025615	C	5.106160	2.266437	1.025916
H	7.007740	1.561334	0.970649	H	7.062194	1.537497	0.970712	H	7.116512	1.514360	0.970762
H	3.872769	-1.440273	0.844953	H	3.904101	-1.439770	0.844941	H	3.936214	-1.439174	0.844935
H	2.177135	0.342528	0.950817	H	2.222311	0.356076	0.951149	H	2.267920	0.369196	0.951481
H	5.278000	3.328636	1.075772	H	5.346179	3.318107	1.076182	H	5.413879	3.307752	1.076571
C	-0.592184	-0.900844	1.142272	C	-0.647728	-0.906868	1.141780	C	-0.702984	-0.912565	1.141303
H	-0.645387	-1.168594	2.201278	H	-0.702911	-1.174320	2.200760	H	-0.760078	-1.179712	2.200258
H	0.453272	-0.731501	0.870381	H	0.398982	-0.745581	0.869820	H	0.344881	-0.759087	0.869272
H	-1.004918	-1.708389	0.532252	H	-1.066745	-1.711128	0.531702	H	-1.128059	-1.713600	0.531174
H	-2.055348	2.943402	2.068123	H	-2.081051	2.948469	2.068190	H	-2.107336	2.953290	2.068252
H	-4.106024	2.069747	1.115312	H	-4.138499	2.090803	1.115453	H	-4.171225	2.111150	1.115596
H	-3.009817	0.166891	2.177409	H	-3.056948	0.179407	2.177242	H	-3.103920	0.191597	2.177087
H	-3.273872	-0.459933	0.517477	H	-3.325979	-0.445166	0.517261	H	-3.377757	-0.430764	0.517061
O	2.723471	2.948927	1.079134	O	2.788791	2.958158	1.079716	O	2.853869	2.966952	1.080282
H	3.171918	3.805047	1.118464	H	3.244518	3.810669	1.119095	H	3.316587	3.815912	1.119704
H	6.314095	-0.851784	0.854192	H	6.349905	-0.870172	0.854040	H	6.386213	-0.887898	0.853890

Table 3.23 XYZ coordinates for NMP-phenol complex without a hydrogen bond at D = 2.9 Å (left) and D = 3.0 (right)

C	-3.282236	1.755397	0.663226	C	-3.318149	1.767993	0.663258
H	-3.408134	1.776307	-0.426603	H	-3.443989	1.789894	-0.426559
C	-2.054567	2.573500	1.046897	C	-2.084736	2.577420	1.046905
H	-1.878005	3.392128	0.345268	H	-1.902490	3.394858	0.345342
C	-0.933729	1.562394	0.993628	C	-0.971028	1.558475	0.993441
C	-2.931315	0.351960	1.114167	C	-2.977052	0.362083	1.114030
N	-1.504983	0.298444	0.925468	N	-1.551146	0.298574	0.925205
O	0.256513	1.825553	1.054408	O	0.221037	1.813267	1.054146
C	5.683455	-0.097492	0.900919	C	5.726409	-0.108810	0.900914
C	3.809923	1.945008	1.021001	C	3.867272	1.946779	1.021357
C	6.113695	1.235408	0.966064	C	6.166000	1.221030	0.966155
C	4.315238	-0.408417	0.895686	C	4.356042	-0.410122	0.895767
C	3.374699	0.622434	0.956430	C	3.422769	0.627299	0.956692
C	5.165861	2.258522	1.026202	C	5.225377	2.250766	1.026474
H	7.170705	1.491900	0.970800	H	7.224785	1.470095	0.970827
H	3.969076	-1.438494	0.844937	H	4.002653	-1.437739	0.844946
H	2.313940	0.381907	0.951812	H	2.360346	0.394226	0.952140
H	5.481123	3.297573	1.076938	H	5.547930	3.287574	1.077286
C	-0.757960	-0.917957	1.140841	C	-0.812662	-0.923063	1.140394
H	-0.816900	-1.184793	2.199774	H	-0.873385	-1.189584	2.199306
H	0.290967	-0.772049	0.868737	H	0.237240	-0.784494	0.868216
H	-1.188880	-1.715827	0.530666	H	-1.249225	-1.717827	0.530176
H	-2.134180	2.957878	2.068309	H	-2.161562	2.962245	2.068362
H	-4.204199	2.130816	1.115741	H	-4.237416	2.149830	1.115888
H	-3.150744	0.203469	2.176943	H	-3.197428	0.215030	2.176810
H	-3.429223	-0.416719	0.516876	H	-3.480394	-0.403023	0.516705
O	2.918711	2.975335	1.080832	O	2.983319	2.983331	1.081365
H	3.388145	3.820804	1.120292	H	3.459210	3.825370	1.120860
H	6.423006	-0.904990	0.853741	H	6.460269	-0.921475	0.853594

CHAPTER 4 $\pi\cdots\pi_{(AR)}$ INTERACTIONS ARE BEST DESCRIBED AS
ELECTROSTATIC INTERACTIONS

4.1 ABSTRACT

A series of 6 molecular rotors were synthesized to investigate the ability of $n \cdots \pi_{(ar)}$ interaction to stabilize transition states (TSs) of bond rotation. Steric contributions to the rotational barrier were isolated using control rotors, which could not form the $n \cdots \pi_{(ar)}$ interactions. The TS stabilization of up to ~ 4 kcal/mol was consistent with the formation of a strong $n \cdots \pi_{(ar)}$ interaction between the imide carbonyl oxygens and the *ortho* R-group in the planar TS. Rotors with a $n \rightarrow \pi^*$ interaction in the TS were used as a reference to determine if the $n \cdots \pi_{(ar)}$ acts similarly. Computational studies effectively modeled the TS stabilization and geometry, and NBO analysis suggests the stabilizing nature of $n \cdots \pi_{(ar)}$ interactions in stabilizing the TS are governed by electrostatics.

4.2 MAIN TEXT

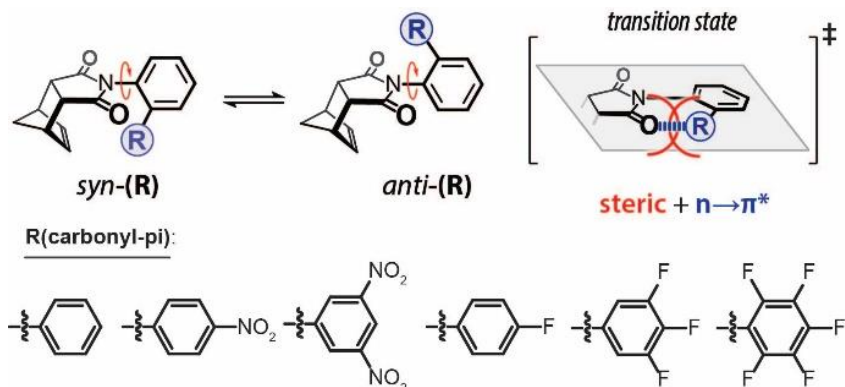
The $n \cdots \pi_{(ar)}$ interaction is a non-covalent interaction between a lone pair and the π -face of an aromatic ring.^{116–118} The $n \cdots \pi_{(ar)}$ interaction has been cited as a contributor to protein stability, small molecule catalysts, and molecular conformations.^{119–122} However, there are limited experimental studies quantifying the $n \cdots \pi_{(ar)}$ interaction strength.^{88,123} Therefore, the goal of this work is to systematically measure TS stabilizing effects of the $n \cdots \pi_{(ar)}$ interaction between the oxygen of a carbonyl and a substituted aromatic ring using an *N*-phenylimide molecular rotor to address three questions: (1) Is the $n \cdots \pi_{(ar)}$ interaction a stabilizing TS interaction? (2) How much stabilization can the $n \cdots \pi_{(ar)}$ interaction provide? (3) What is the fundamental nature of the $n \cdots \pi_{(ar)}$ interaction?

Stabilizing TS $n \cdots \pi_{(ar)}$ interactions can modulate the rate of rotation and lower the rotational barriers of our molecular rotors providing the opportunity to study this interaction. The *N*-phenylimide molecular rotor (Figure 4.1) has been successfully used to

measure the kinetic effects of non-covalent interactions such as intermolecular and intramolecular hydrogen bonding, metal coordination, and $n \rightarrow \pi^*$ interactions.^{15,72,73,77} The *N*-phenylimide rotor forms distinct *syn*- and *anti*-conformations, which slowly interconvert due to restricted rotation about the C-N single bond (Figure 4.1). The R-group at the *ortho*-position of the *N*-phenyl rotor is held in close proximity to the imide carbonyl oxygen in the planar transition state of the bond rotation, usually within the VDW radii. Thus, the magnitude of the non-covalent TS interactions can be assessed by measuring, changes in the rate of rotation of the molecular rotor.

In a previous study, we measured the ability of $C=O \cdots C=O$ ($n \rightarrow \pi^*$) interactions that stabilize the TSs via charge-transfer, and we were curious if charge-transfer was also governing the $C=O \cdots Ph$ ($n \cdots \pi_{(ar)}$) interaction. The $n \cdots \pi_{(ar)}$ interaction has been described as both electrostatic and charge transfer interactions. Electrostatic interactions are attractive and repulsive interactions formed between partial charges on the two interacting groups. Charge-transfer interactions are attractive interactions formed from the overlap and mixing of orbitals. Differentiating electrostatic and charge-transfer interactions can be difficult as both can involve oppositely charged groups or surfaces. For example, electrostatic potential (ESP) maps have been used to predict whether electrostatic and charge-transfer interactions can occur (see section 1.4.1.4 of this dissertation for a description of how ESP maps are calculated).^{13,124} Electron deficient regions on ESP maps have been referred to as π^* and σ^* holes which can interact with electron rich lone pairs. However, using ESP maps to identify charge-transfer interactions does not provide direct evidence for causation. Specifically, the hypothesis that all electron deficient regions (π^* and σ^* holes) of an ESP map will participate in a charge-transfer interactions with a lone pair has not been validated.

Methods for characterizing and identifying $n \rightarrow \pi^*$ charge-transfer driven interaction have been extensively discussed by Raines and coworkers.¹² For example, a characteristic indicator for the formation of charge-transfer interactions are geometrical changes in the acceptor group due to the partial covalent bonding in the $n \rightarrow \pi^*$ interactions.



Scheme 4.1 Isomerization process for the molecular rotors used in this study.

The rotational barriers were measured using exchange spectroscopy (EXSY).^{78,92} All rotors were studied at temperatures in the slow exchange regime (0 – 90 °C) where the *syn*- and *anti*-conformers gave distinct sets of peaks. Eyring plots measured the enthalpy and entropy of the rotational barriers, and free energy ($\Delta G^\ddagger_{\text{exp}}$) of rotation was calculated for 25 °C for all rotors (Table 4.2). The measured $\Delta G^\ddagger_{\text{exp}}$ values ranged from 17.4 kcal/mol (R = Ph-F₅) to 21.5 kcal/mol (R = Ph).

The TS $n \cdots \pi_{(\text{ar})}$ interaction was initially assessed for rotors with substituted phenyl groups with varying numbers of EWG's on the phenyl substituents. Rotors with an increasing number of fluorinated substituents (Ph-F₁, Ph-F₃ and Ph-F₅) had successively lower rotational barriers. Rotors with an increasing number of nitro substituents also had lower rotational barriers.

Table 4.1 Properties of the $n \cdots \pi_{(ar)}$ rotors.

Rotor	ΔG^\ddagger exp (kcal/mol)	ΔG^\ddagger calc (kcal/mol)	distance (Å)	Θ (degree)	σ^m	center ESP (kcal/mol)
H	21.5	20.6	2.571	7.52	0.00	-20.9
F ₁	20.8	20.8	2.572	7.08	0.34	-13.3
F ₃	19.8	19.8	2.553	6.83	1.02	2.0
F ₅	17.4	16.9	2.564	5.82	1.70	15.8
NO ₂	19.4	19.4	2.526	8.03	0.71	-2.4
(NO ₂) ₂	18.13	17.84	2.536	6.66	1.42	14.5

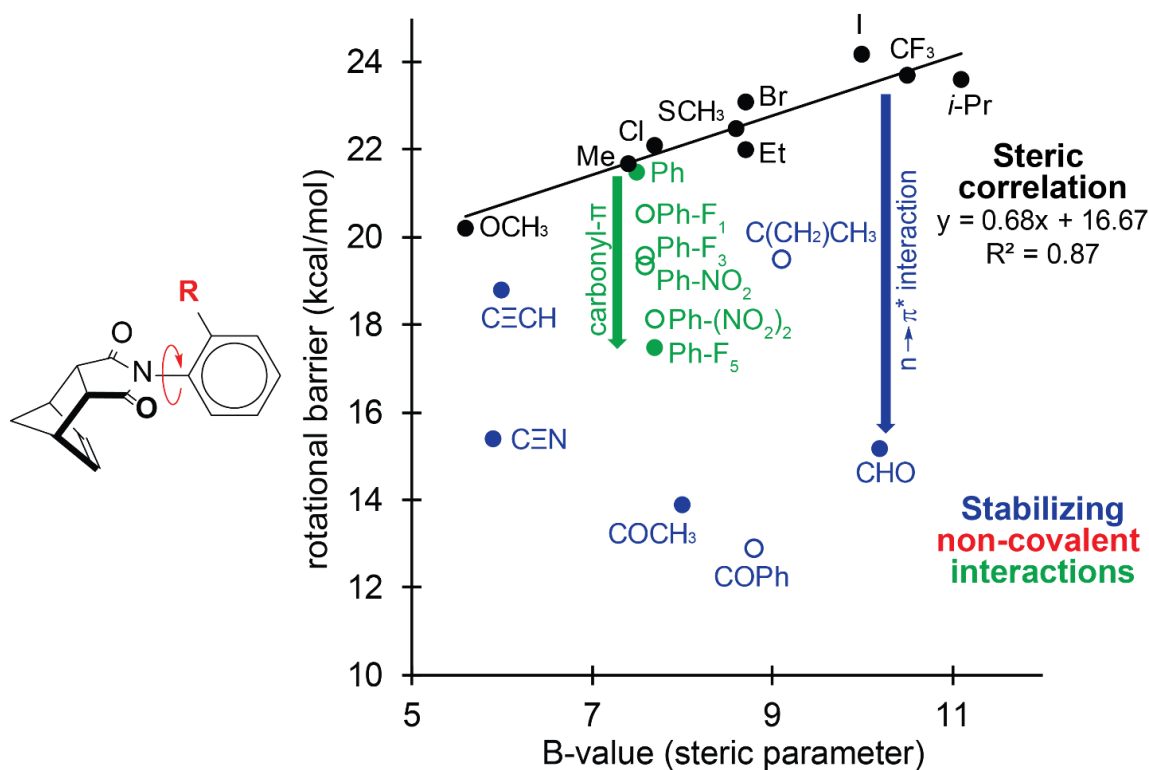


Figure 4.1 Correlation plot of the experimentally measured rotational barriers for $n \rightarrow \pi^*$ rotors and $n \cdots \pi_{(ar)}$ rotors versus the steric B-values of the R groups. The steric trendline is drawn through the rotors that have ortho R groups without a π^* orbital (black circles) and thus lack $n \rightarrow \pi^*$ interactions. The blue circles correspond to the rotors that form $n \rightarrow \pi^*$ interactions and the green circles correspond to the rotors that form $n \cdots \pi_{(ar)}$ interactions.

In a previous study,¹⁵ we established that the rotational barriers of most *N*-phenylimide molecular rotors were well correlated with Mazzanti's steric parameter^{16–20} (B-value). Rotors which had rotational barriers that deviated from the steric correlation line most likely formed additional stabilizing interaction in the TS. For example, this was how rotors which formed stabilizing TS $n \rightarrow \pi^*$ interactions (Figure 4.1, blue circles) were identified, and the interaction energies were measured. If we add the $n \cdots \pi_{(ar)}$ rotors to this plot, we can likewise test whether they also form stabilizing TS NCIs and quantify the TS stabilization (Figure 4.1, green circles). Interestingly, the unsubstituted phenyl rotor was very close to the steric trend line ($\Delta\Delta G_{exp}^\ddagger = -0.3$ kcal/mol) suggesting that the unsubstituted phenyl rotor does not form any additional TS NCIs. However, the $n \cdots \pi_{(ar)}$ interaction becomes stabilizing after electron withdrawing groups were added to the phenyl arm. The absence of a stabilizing interaction between the unsubstituted phenyl ring and the imide carbonyl was unexpected, as multiple literature sources claim that the $n \cdots \pi_{(ar)}$ interaction was stabilizing regardless of the nature of the aromatic surface.^{119,123,125}

The TS stabilization for the substituted $n \cdots \pi_{(ar)}$ rotors was correlated with various electrostatic parameters. Specifically, the TS stabilization (as measured by the difference between the $n \cdots \pi_{(ar)}$ rotors barrier heights and the steric trendline) was plotted against the ESP values for the center of the substituted phenyl rings, as well as against the sum of the Hammett sigma meta values for the substituents. The strong linear correlation of the phenyl rotational barrier with these electrostatic parameters, provides evidence that the $n \cdots \pi_{(ar)}$ interactions in the rotors had a strong electrostatic component. The same trend was observed in a separate study of the $n \cdots \pi_{(ar)}$ interaction.⁸⁸ The correlation between the ESP

values of rotors that form $n \rightarrow \pi^*$ interactions are provided in Figure 4.2 for comparison (Figure 4.2A, blue circles).¹⁵

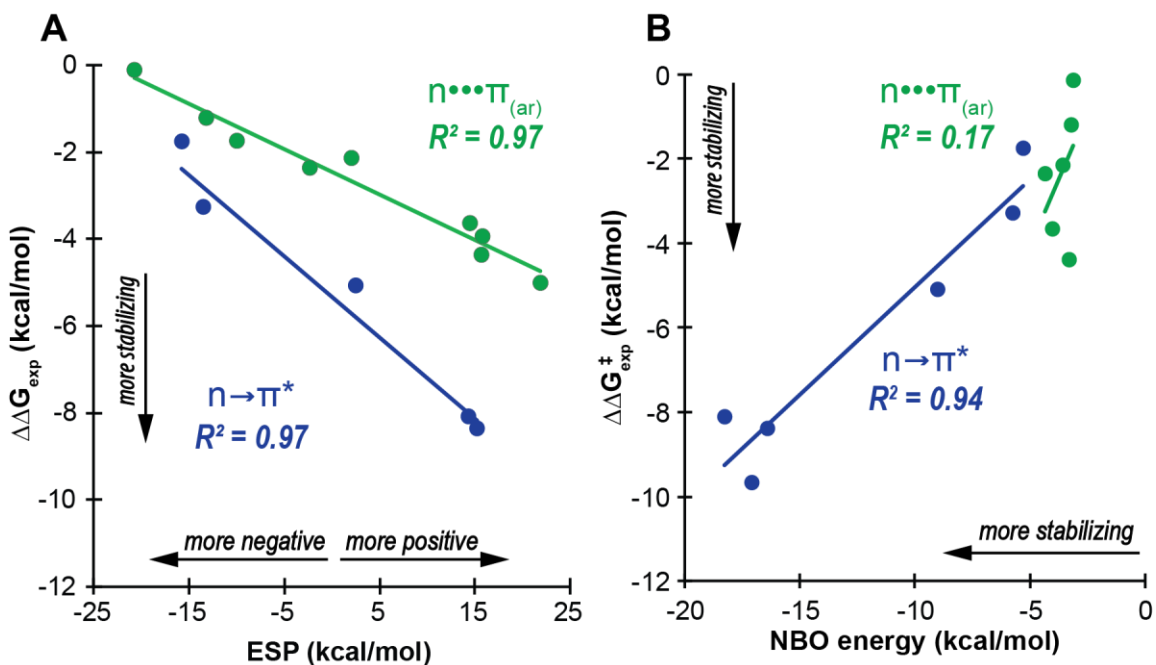


Figure 4.2 Correlation plot of the measured TS stabilization ($\Delta\Delta G_{\text{exp}}^{\ddagger}$) and the calculated ESP parameters (ESP) for the $n \cdots \pi_{(\text{ar})}$ and $n \rightarrow \pi^*$ rotors. (B) Correlation plot of the measured TS stabilization ($\Delta\Delta G_{\text{exp}}^{\ddagger}$) and the calculated NBO energy for the $n \cdots \pi_{(\text{ar})}$ and $n \rightarrow \pi^*$ rotors.

Computational studies were conducted to corroborate the experimental results, and to model TS structures, which could be utilized in perturbative calculations that breakdown the interacting into fundamental energies. First the rotational barriers for $n \cdots \pi_{(\text{ar})}$ rotors were calculated at the B3LYP-D3/6-311G* level of theory, the GS and TS structures were verified by frequency analysis, with thermodynamic corrections.

The calculations of the rotational barrier for the *N*-phenylimide molecular rotor were benchmarked in previous chapters at the B3LYP-D3/6-311G* level of theory. The calculated rotational barriers were determined by taking the difference in Gibb's free energy between the calculated TS and GS structures. The energies of the two GS's of the

rotors were averaged because their energy difference was below the accuracy for DFT functionals. The averaged GS energies were then subtracted from the TS energy to yield the calculated rotational barrier. Utilizing this method, the calculations were able to reproduce the experimental rotational barriers with an accuracy of ± 1.3 kcal/mol, suggesting that the TS and GS geometries were also accurate. The calculations also overestimated the rotational barriers by 0.9 kcal/mol on average.

For the intramolecular $n \cdots \pi_{(ar)}$ TS interactions, there was no structural evidence of a charge-transfer interaction. One indicator of a charge-transfer interaction is structural alteration of the acceptor groups like pyramidalization and bond elongation. There was no evidence of geometric changes in the acceptor groups in the TSs. Furthermore, in all six rotors, the $O \cdots C$ distance between the imide carbonyl and the first carbon of the aromatic ring was very constant despite the variations in the TS stabilization energies (2.55 ± 0.02 Å). The C-C bond lengths in the *ortho*-phenyl group were the same in the GSs and TSs (1.396 ± 0.003 Å). There was also no apparent change in pyramidalization of the first carbon of the aromatic ring ($6.99 \pm 0.7^\circ$) (as measured by Θ in Figure 2.3).

Natural bond orbital (NBO) calculations were used to quantify the stabilization from mixing two orbitals. The NBO analysis was performed to estimate the stabilization from the $n \cdots \pi_{(ar)}$ interaction gained from charge-transfer. NBO calculations were performed on the TS geometries of the rotors. The charge-transfer interaction energies (NBO energy) between the lone pair of the imide oxygen and the π^* of the *ipso*-carbon of the acceptor phenyl group were small and showed little variation in comparison to the wide range of TS stabilization energies. The analysis shows that there was very little stabilization gained by mixing the orbitals of the interacting groups for the $n \cdots \pi_{(ar)}$ interaction.

In order to test whether the $n \rightarrow \pi^*$ and $n \cdots \pi_{(ar)}$ interactions were comprised of similar fundamental interactions, their correlation to two parameters, electrostatic potential and natural bond order, and geometrical alterations were assessed. The TS stabilization ($\Delta\Delta G_{\text{exp.}}^\ddagger$) for both the $n \rightarrow \pi^*$ and $n \cdots \pi_{(ar)}$ interactions have strong correlations with the ESP parameter. The $n \rightarrow \pi^*$ interactions were correlated well with the NBO energies, but the $n \cdots \pi_{(ar)}$ interactions appear to be independent of the NBO energies. There were dramatic geometrical alterations in the TS of the $n \rightarrow \pi^*$ rotors. However, there was no significant geometrical alteration of the TS acceptor carbons for the $n \cdots \pi_{(ar)}$ interactions. From the above information, it is apparent that the $n \cdots \pi_{(ar)}$ interaction has little or no contribution from charge-transfer and is primarily driven by electrostatics

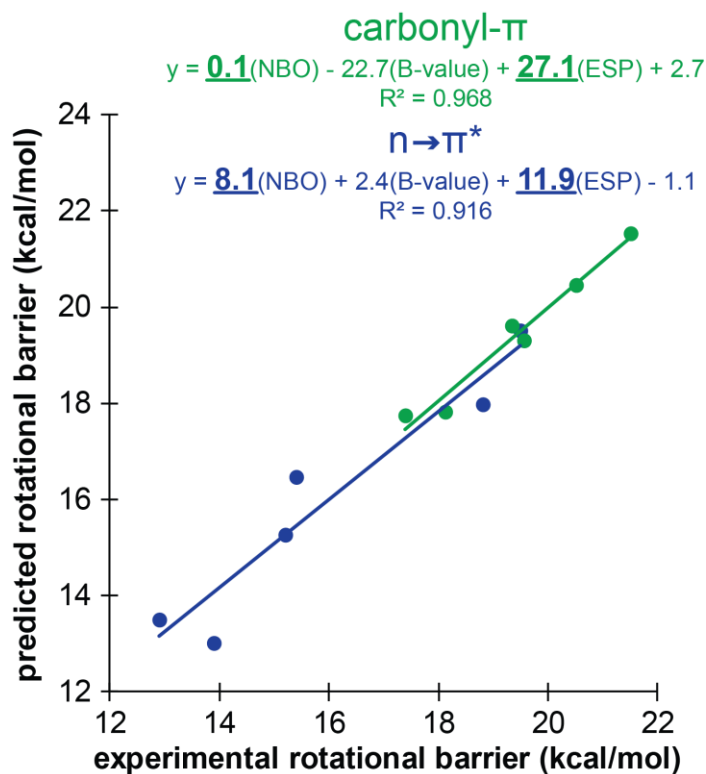


Figure 4.3 Linear free energy plot for the $n \cdots \pi_{(ar)}$ and $n \rightarrow \pi^*$ rotors.

Using three parameters (NBO, B-value, and ESP) an additive LFER model can be constructed to predict the barriers for both the $n \rightarrow \pi^*$ and $n \cdots \pi_{(ar)}$ rotors. By normalizing the parameters from 0 to 1, the coefficients of the LFER model can be utilized to determine the importance of each parameter to the rotational barrier. As expected, the $n \cdots \pi_{(ar)}$ interaction is best explained by the ESP parameter which had the largest coefficient (27.1). The coefficient for the B-value parameter is -22.7 in the $n \cdots \pi_{(ar)}$ model to balance the ESP parameter; removing the B-value parameter from the $n \cdots \pi_{(ar)}$ model has a negligible impact on the correlation. This is due to a small range of B-values for the rotors containing the $n \cdots \pi_{(ar)}$ interaction (B-values = 7.7-7.5 kcal/mol). Meanwhile the $n \rightarrow \pi^*$ interaction is equally explained by both ESP and NBO parameters which had coefficients of 11.9 and 8.1 respectively.

4.3 CONCLUSION

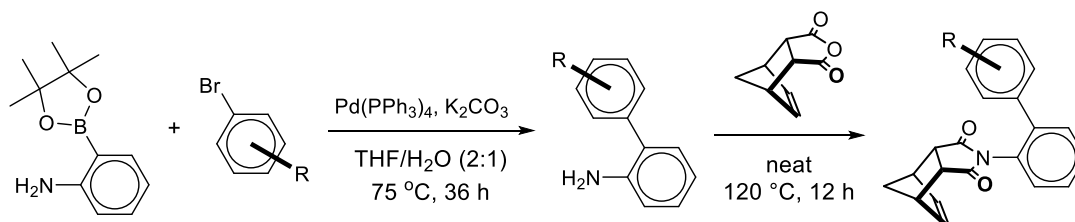
The *N*-phenylimide molecular rotor was successfully employed to measure the kinetic and TS stabilizing effects of the $n \cdots \pi_{(ar)}$ interaction. A clear trend was observed. When more electron withdrawing groups were added onto the phenyl arm, the barrier decreased. The maximum experimentally observed TS stabilization was ~5 kcal/mol. This TS effect is twice the $n \cdots \pi_{(ar)}$ interaction strength observed in thermodynamically stable structures and complexes.⁸⁸ The nature of the $n \cdots \pi_{(ar)}$ interaction was compared with the previously studied $n \rightarrow \pi^*$ interactions using the same *N*-phenylimide molecular rotor framework. The $n \rightarrow \pi^*$ interaction had a significant contribution from both charge-transfer and electrostatics. In contrast, the $n \cdots \pi_{(ar)}$ interaction is governed mostly by electrostatic interaction and not by charge-transfer. No geometrical changes were observed for the interacting groups nor were the barriers correlated with the NBO energies for the $n \cdots \pi_{(ar)}$

interaction. This study also demonstrates that ESP maps can identify places where charge-transfer could occur on a molecule, but ESP maps alone do not accurately predict the formation of charge-transfer interactions. To accurately identify charge-transfer interactions ESP maps need to be used with NBO analysis.

4.3 SUPPLEMENTAL INFORMATION

4.3.1 GENERAL EXPERIMENTAL INFORMATION

NMR spectra were recorded on a Bruker 400 and 500 MHz spectrometer. Chemical shifts are reported in ppm (δ) referenced to solvent residue. All spectra given for characterization purposes were taken at room temperature. All chemicals and solvents were purchased from commercial suppliers and used as received. Flash chromatography was performed using silica gel from Sorbent Technologies (60 Å, 200 – 400 mesh).



Scheme 4.2 General route for synthesizing molecular rotors.

4.3.2 SYNTHESIS

All of the rotors were prepared via a thermal condensation between an ortho substituted aniline and a bicyclic anhydride (Scheme 4.2).⁸⁷ Rotors **12** was reported previously, the synthesis and characterization will not be detailed here. The rest of the rotors are newly reported compounds and fully characterized.

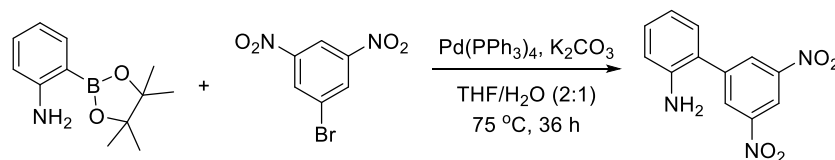


Figure 4.4 General route for the synthesis of the ortho-phenyl substituted anilines

2-Aminophenylboronic acid pinacol (0.100 mg, 0.46 mmol), 1-bromo-3,5-dinitrobenzene (0.338 mg, 1.37 mmol), Tetrakis(triphenylphosphine)palladium(0) (0.026 mg, 0.02 mmol), and potassium carbonate (0.315 mg, 2.28 mmol) were added to a round bottom flask, which was then connected to a Schlenk line connected water jacketed condenser. The round bottom flask was purged 3x with N₂ gas. Deionized H₂O (which was bubbled with N₂ gas) was mixed with THF in a 2:1 mixture and 10 mL of the THF:H₂O mixture was then added to the purged round bottom flask. The round bottom was then heated at 75 °C for 36 hours. After letting the vial cool to room temperature, the crude material was purified by column chromatography to give aniline 11.



Figure 4.5 Synthesis of rotor (Ph-F)

cis-5-Norbornene-*endo*-2,3-dicarboxylic anhydride (100 mg, 0.61 mmol) and 4'-fluoro-[1,1'-biphenyl]-2-amine (125 mg, 0.67 mmol) were added to a 20-dram vial with a magnetic stir bar. The vial was then capped and heated to 120 °C in a silicon oil bath for 12 hours while stirring. After letting the vial cool to room temperature, the crude material was purified by column chromatography to give the desired product as a white powder (187 mg, 92%). ¹H NMR (400 MHz, tetrachloroethane-d₂) δ 7.47-6.90 (m, 8H *syn* and *anti*), 6.18 (s, 2H *anti*), 5.27 (s, 2H *syn*), 3.32 (m, 4H *syn* and *anti*), 1.67-1.39 (m, 2H *syn* and *anti*). ¹³C NMR (100 MHz, tetrachloroethane-d₂) δ 177.18, 176.78, 163.62, 161.17, 140.24, 134.70, 134.47, 130.95, 130.14, 130.06, 130.00, 129.93, 128.94, 128.78, 115.52, 115.31, 114.87, 114.66, 52.82, 52.47, 46.79, 45.71, 45.45, 44.86. ¹⁹F NMR (376 MHz, tetrachloroethane-d₂), 113.88 (s, 1F *anti*), 114.22 (s, 1F *syn*).

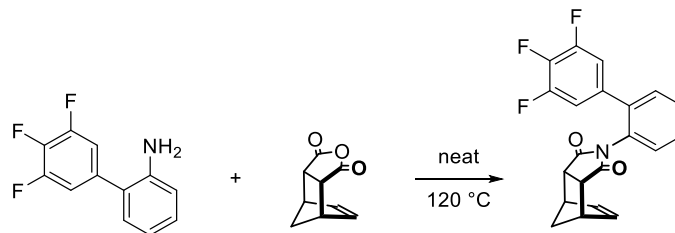


Figure 4.6 Synthesis of rotor (Ph-F₃)

cis-5-Norbornene-*endo*-2,3-dicarboxylic anhydride (100 mg, 0.61 mmol) and 3',4',5'-trifluoro-[1,1'-biphenyl]-2-amine (150 mg, 0.67 mmol) were added to a 20-dram vial with a magnetic stir bar. The vial was then capped and heated to 120 °C in a silicon oil bath for 12 hours while stirring. After letting the vial cool to room temperature, the crude material was purified by column chromatography to give the desired product as a white powder (205 mg, 91%). ¹H NMR (400 MHz, chloroform-d) δ 7.42-7.18 (m, 3H *syn* and *anti*), 7.01-6.91 (m, 1H *syn* and *anti*), 6.83-6.74 (m, 2H *syn* and *anti*), 6.21 (s, 2H *anti*), 5.53 (s, 2H *syn*), 3.37-3.17 (m, 4H *syn* and *anti*), 1.70-1.62 (m, 1H *syn* and *anti*), 1.49-1.45 (m, 1H *syn* and *anti*). ¹³C NMR (100 MHz, chloroform-d) δ 176.88, 176.55, 152.12, 152.06, 149.67, 149.63, 149.53, 134.66, 134.45, 130.44, 129.83, 129.50, 128.82, 113.99, 113.94, 113.78, 112.84, 112.78, 112.68, 112.62, 53.05, 52.36, 46.87, 45.68, 45.41, 44.80. ¹⁹F NMR (376 MHz, chloroform-d) -133.98 (d, 2F, *J*=20 Hz, *anti*), -133.98 (d, 2F, *J*=20 Hz, *syn*), -161.44 (t, 1F, *J*=20 Hz, *anti*), -161.90 (d, 1F, *J*=20 Hz, *syn*).

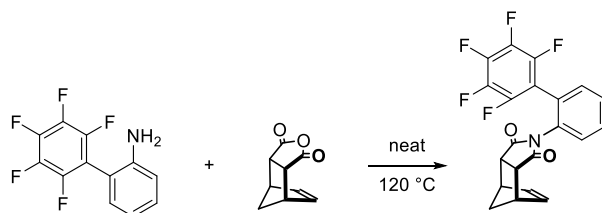


Figure 4.7 Synthesis of rotor (Ph-F₅)

cis-5-Norbornene-*endo*-2,3-dicarboxylic anhydride (100 mg, 0.61 mmol) and 2',3',4',5',6'-pentafluoro-[1,1'-biphenyl]-2-amine (174 mg, 0.67 mmol) were added to a 20-dram vial with a magnetic stir bar. The vial was then capped and heated to 120 °C in a silicon oil bath for 12 hours while stirring. After letting the vial cool to room temperature, the crude material was purified by column chromatography to give the desired product as a white powder (212 mg, 86%). ¹H NMR (400 MHz, chloroform-*d*) δ 7.61-7.53 (m, 2H *syn* and *anti*), 7.44-7.35 (m, 1H *syn* and *anti*), 7.27-7.18 (m, 1H, *syn* and *anti*), 6.27 (s, 2H, *anti*), 5.73 (s, 2H, *syn*), 3.47-3.30 (m, 4H *syn* and *anti*), 1.79-1.75 (m, 1H *syn* and *anti*), 1.58-1.57 (m, 1H *syn* and *anti*). ¹³C NMR (100 MHz, chloroform-*d*) δ 175.90, 175.60, 134.66, 134.24, 131.87, 131.33, 130.77, 130.56, 129.33, 129.27, 129.03, 128.49, 53.17, 52.29, 46.64, 45.66, 45.44, 44.91. ¹⁹F NMR (376 MHz, chloroform-*d*) δ -138.30 (dd, 2H, *J*=20, 8 Hz *syn*), -140.70 (dd, 2H, *J*=20, 8 Hz *anti*), 153.87 (t, 1H, *J*=20 Hz *anti*), 154.79 (t, 1H, *J*=20 Hz *syn*), 161.39 (td, 2H *J*=20, 8 Hz *anti*), 161.92 (td, 2H, *J*=20, 8 Hz *syn*).

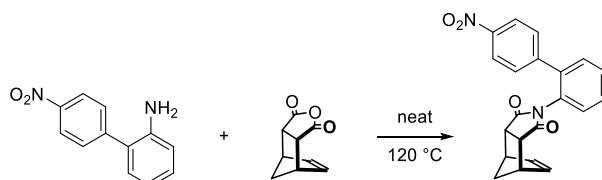


Figure 4.8 Synthesis of rotor (Ph-NO₂)

cis-5-Norbornene-*endo*-2,3-dicarboxylic anhydride (100 mg, 0.61 mmol) and 4'-nitro-[1,1'-biphenyl]-2-amine (144 mg, 0.67 mmol) were added to a 20-dram vial with a magnetic stir bar. The vial was then capped and heated to 120 °C in a silicon oil bath for 12 hours while stirring. After letting the vial cool to room temperature, the crude material was purified by column chromatography to give the desired product as a white powder (204 mg, 93%). ¹H NMR (400 MHz, chloroform-*d*) δ 8.17-8.13 (m, 2H *syn* and *anti*), 7.52-

7.30 (m, 5H *syn* and *anti*), 6.98-6.96 (m, 1H *syn* and *anti*), 6.18 (s, 2H *anti*), 5.22 (s, 2H *syn*), 3.33-3.12 (m, 4H *syn* and *anti*), 1.67-1.42 (m, 2H *syn* and *anti*). ¹³C NMR (100 MHz, chloroform-d) δ 176.71, 176.07, 148.49, 142.12, 136.00, 134.70, 134.47, 130.87, 130.75, 130.57, 130.29, 129.89, 129.85, 129.68, 129.27, 128.51, 117.82, 52.97, 52.40, 46.74, 45.67, 45.52, 44.75.

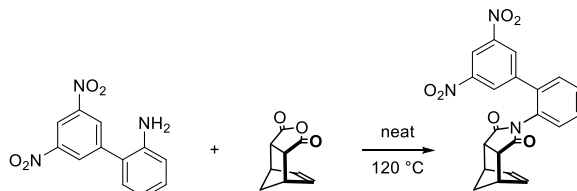


Figure 4.9 Synthesis of rotator (Ph-(NO₂)₂)

cis-5-Norbornene-*endo*-2,3-dicarboxylic anhydride (100 mg, 0.61 mmol) and 3',5'-dinitro-[1,1'-biphenyl]-2-amine (174 mg, 0.67 mmol) were added to a 20-dram vial with a magnetic stir bar. The vial was then capped and heated to 120 °C in a silicon oil bath for 12 hours while stirring. After letting the vial cool to room temperature, the crude material was purified by column chromatography to give the desired product as a white powder (207 mg, 84%). ¹H NMR (400 MHz, chloroform-d) δ 9.00 (t, *J*=2 Hz 1H *syn*), 8.93 (t, *J*=2 Hz *anti*), 8.39 (d, *J*=2 Hz *anti*), 8.34 (d, *J*=2 Hz *syn*), 7.52-7.42 (m, 3H *syn* and *anti*), 7.25-7.13 (m, 1H *syn* and *anti*), 6.22 (s, 2H *anti*), 5.29 (s, 2H *syn*), 3.42-3.16 (m, 4H *syn* and *anti*), 1.71-1.43 (m, 2H *syn* and *anti*). ¹³C NMR (100 MHz, chloroform-d) δ 177.03, 176.61, 147.33, 145.32, 138.88, 134.73, 134.66, 130.68, 130.55, 130.13, 129.92, 129.77, 129.45, 129.01, 123.75, 123.11, 100.00, 52.50, 46.83, 45.71, 45.57, 44.90.

3.4.3 ^1H , ^{13}C , AND ^{19}F NMR SPECTRA

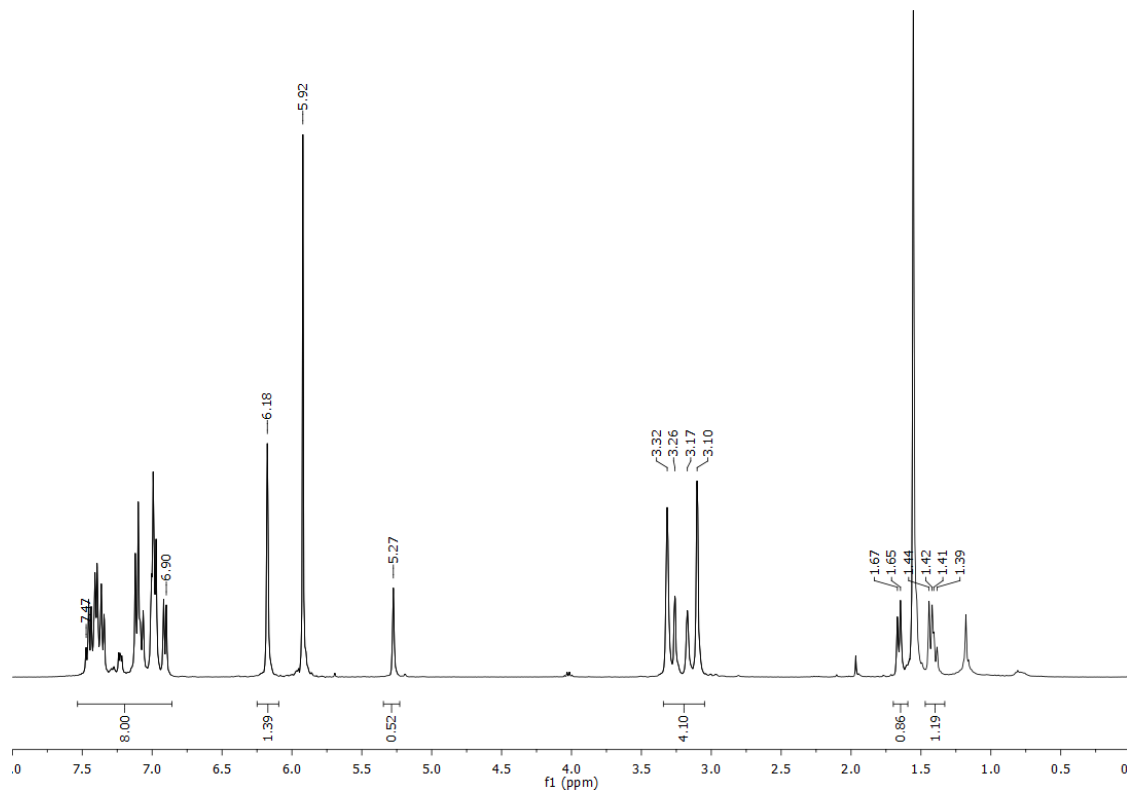


Figure 4.10 ^1H NMR spectra of rotor 13 (400 MHz, chloroform-d)

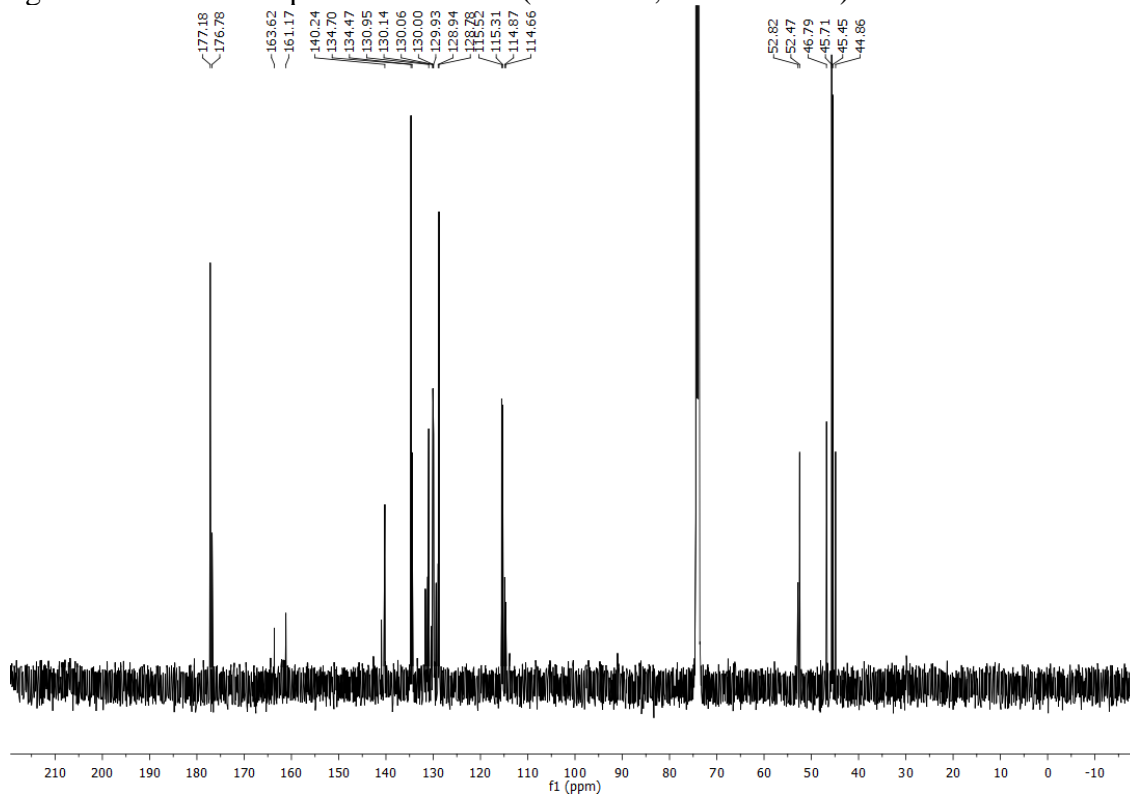


Figure 4.11 ^{13}C NMR spectra of rotor (Ph-H) (400 MHz, chloroform-d)

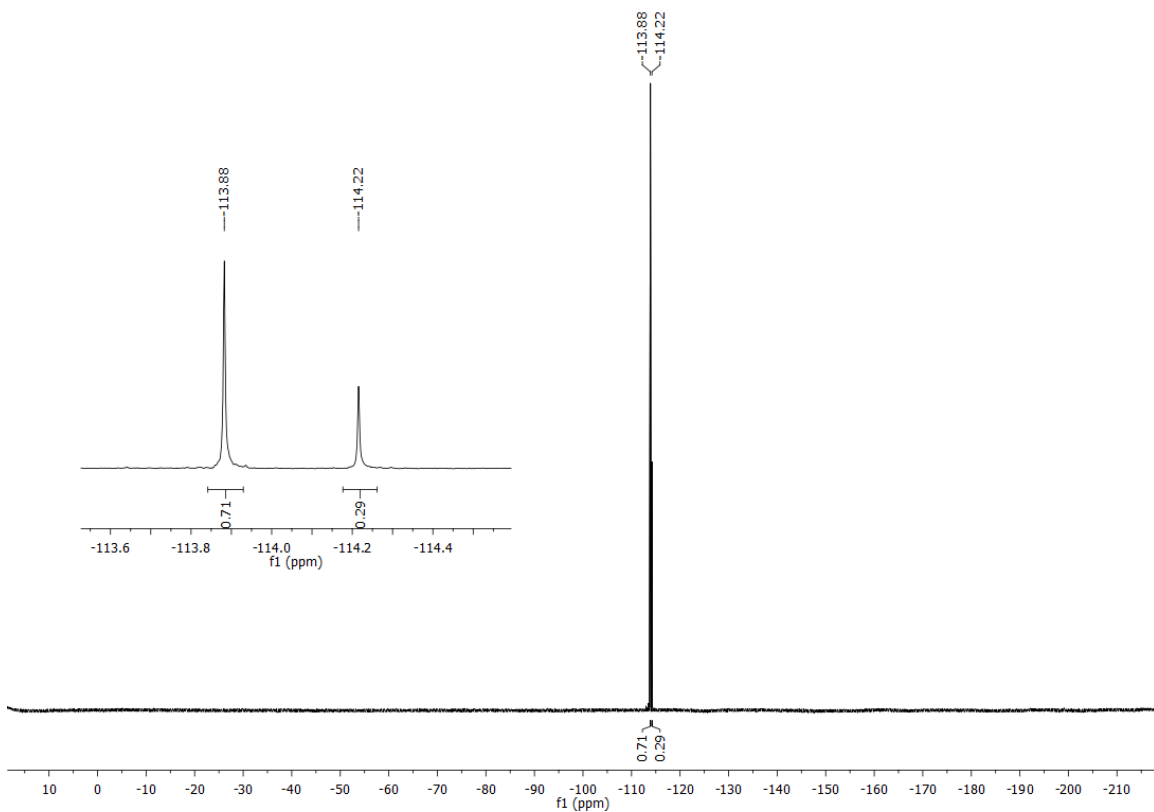


Figure 4.12 ^{19}F NMR spectra of rotor (Ph-H) (400 MHz, chloroform-d)

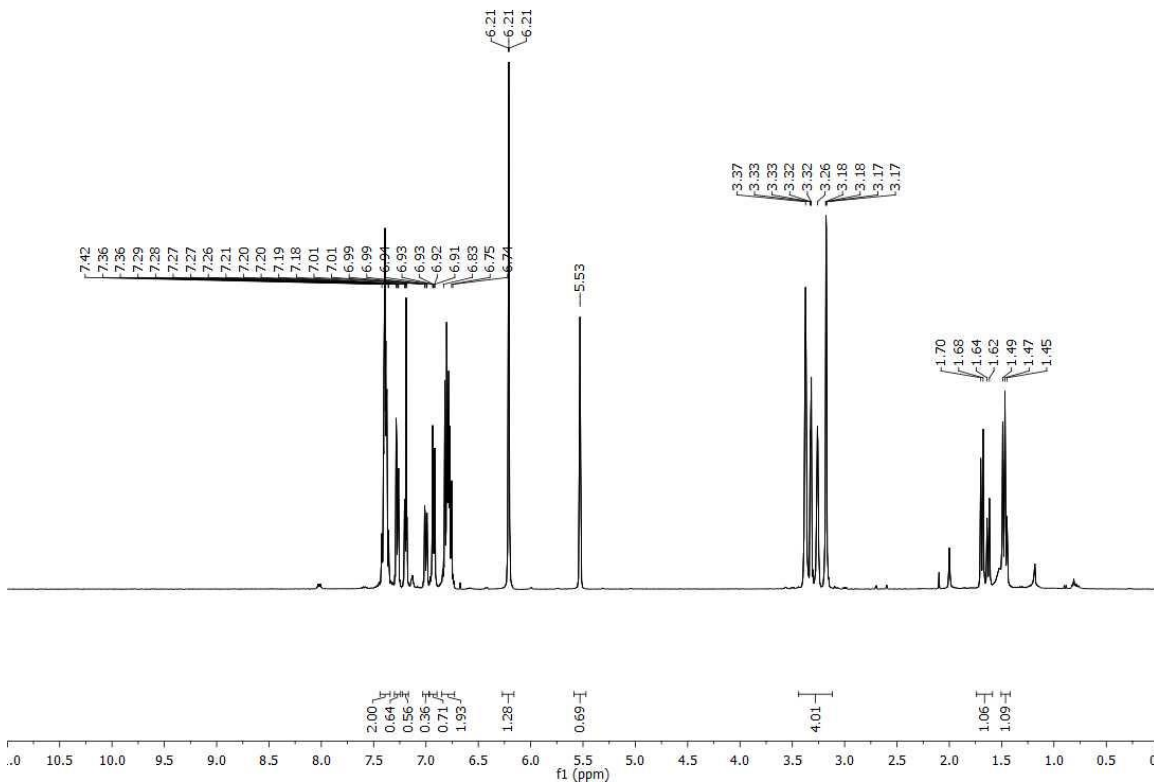


Figure 4.13 ^1H NMR spectra of rotor (Ph-p-F) (400 MHz, chloroform-d)

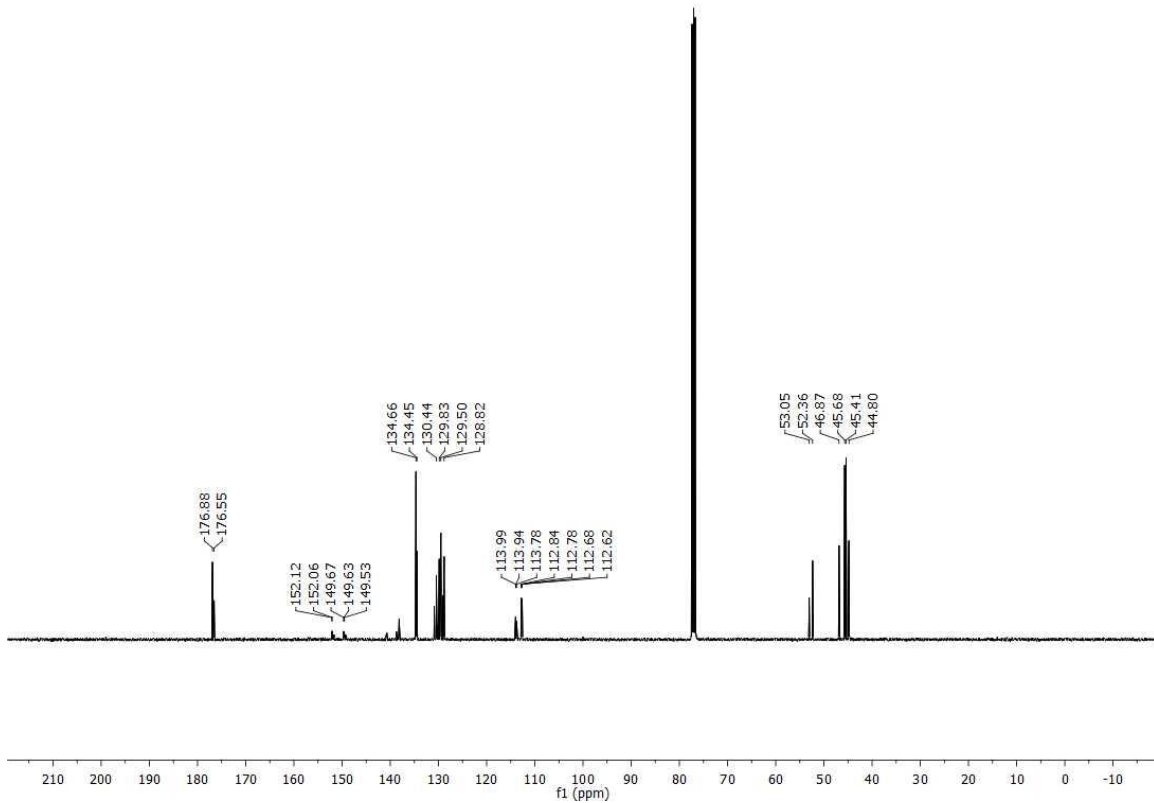


Figure 4.14 ^{13}C NMR spectra of rotor (Ph-*p*-F) (400 MHz, chloroform-d)

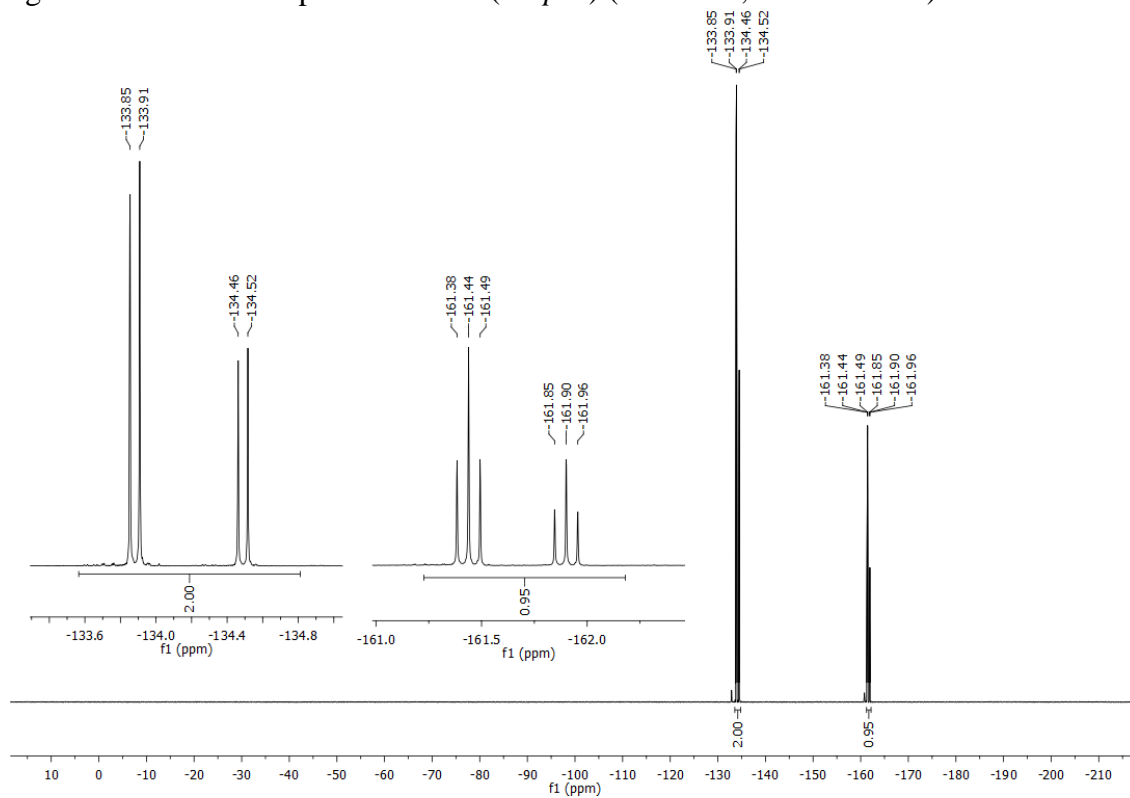


Figure 4.15 ^{19}F NMR spectra of rotor (Ph-*m,m,p*- F_3) (400 MHz, chloroform-d)

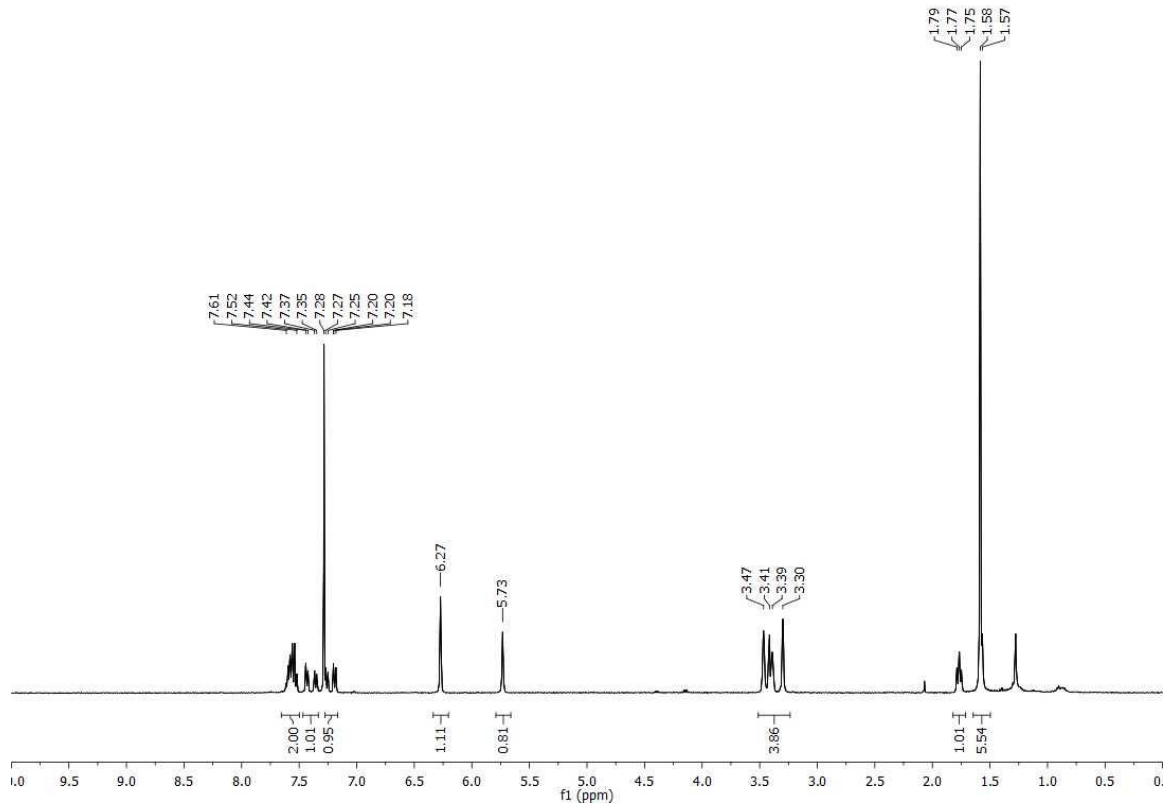


Figure 4.16 ^1H NMR spectra of rotor ($\text{Ph-}m,m,p\text{-F}_3$) (400 MHz, chloroform-d)

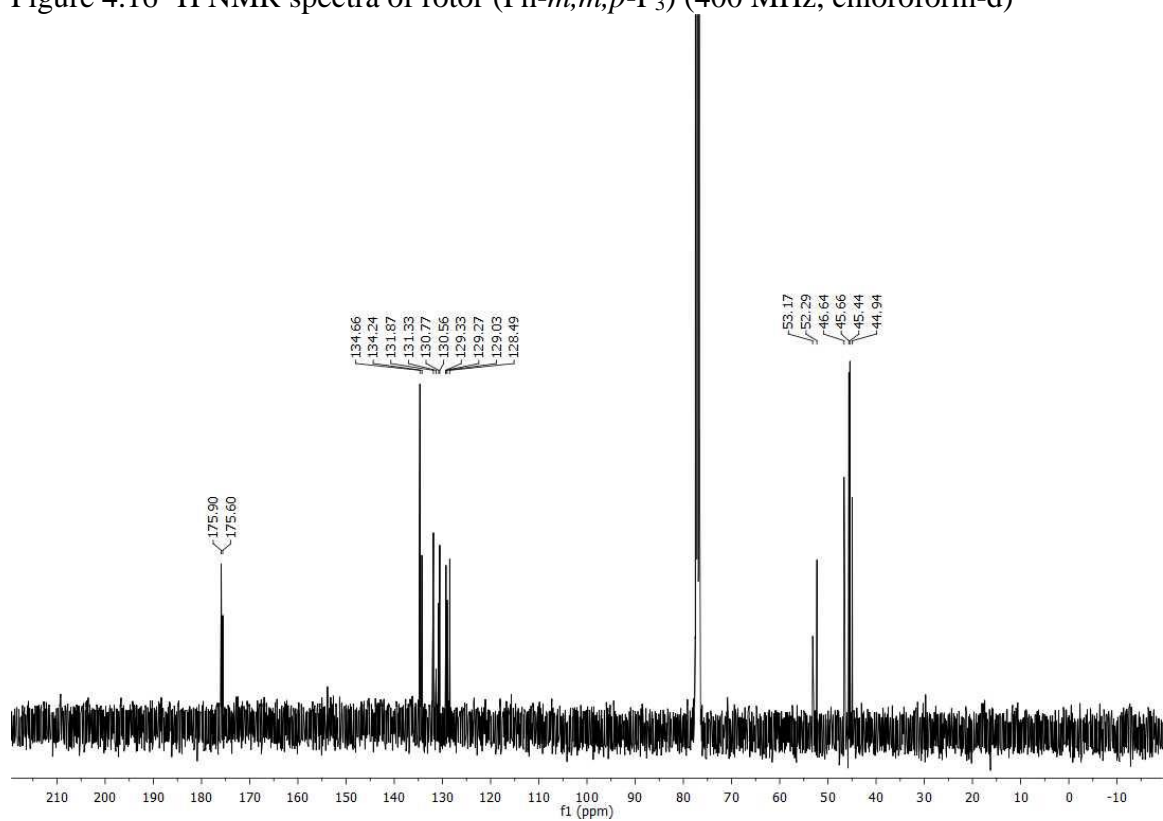


Figure 4.17 ^{13}C NMR spectra of rotor (Ph-F_5) (400 MHz, chloroform-d)

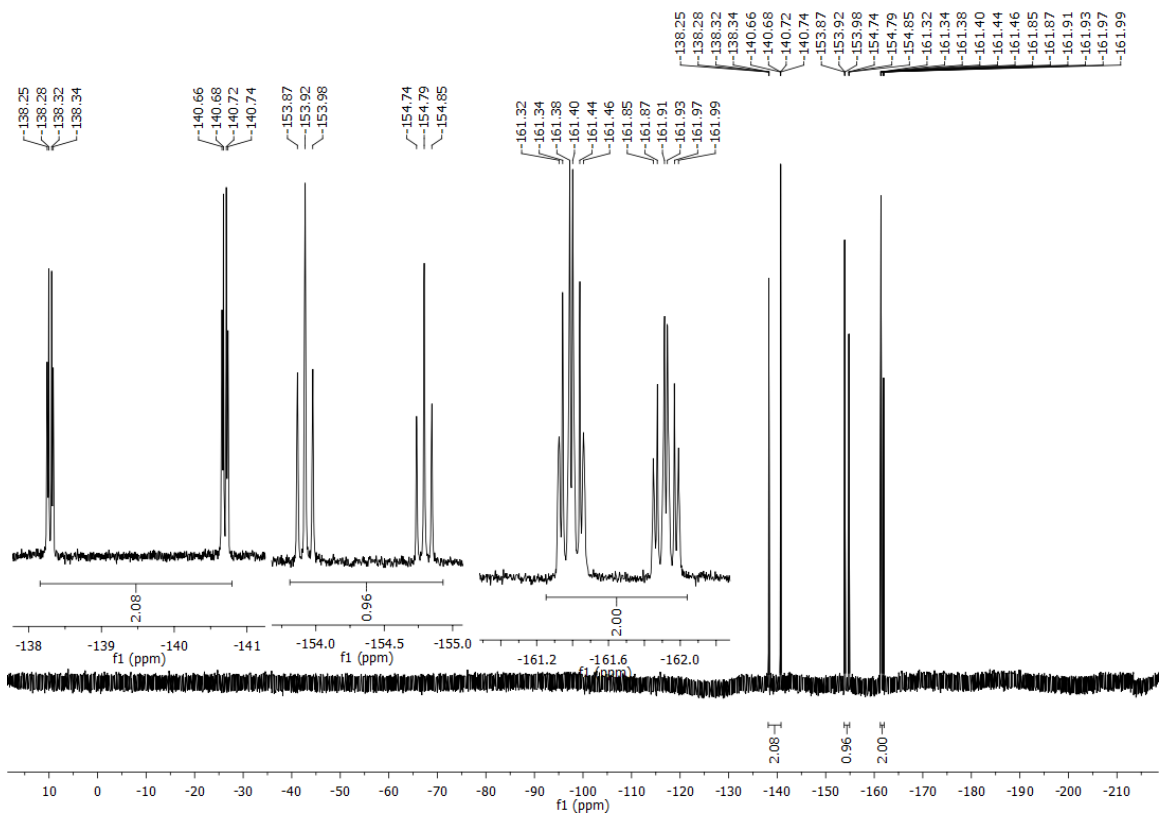


Figure 4.18 ^{19}F NMR spectra of rotor (Ph- F_5) (400 MHz, chloroform-d)

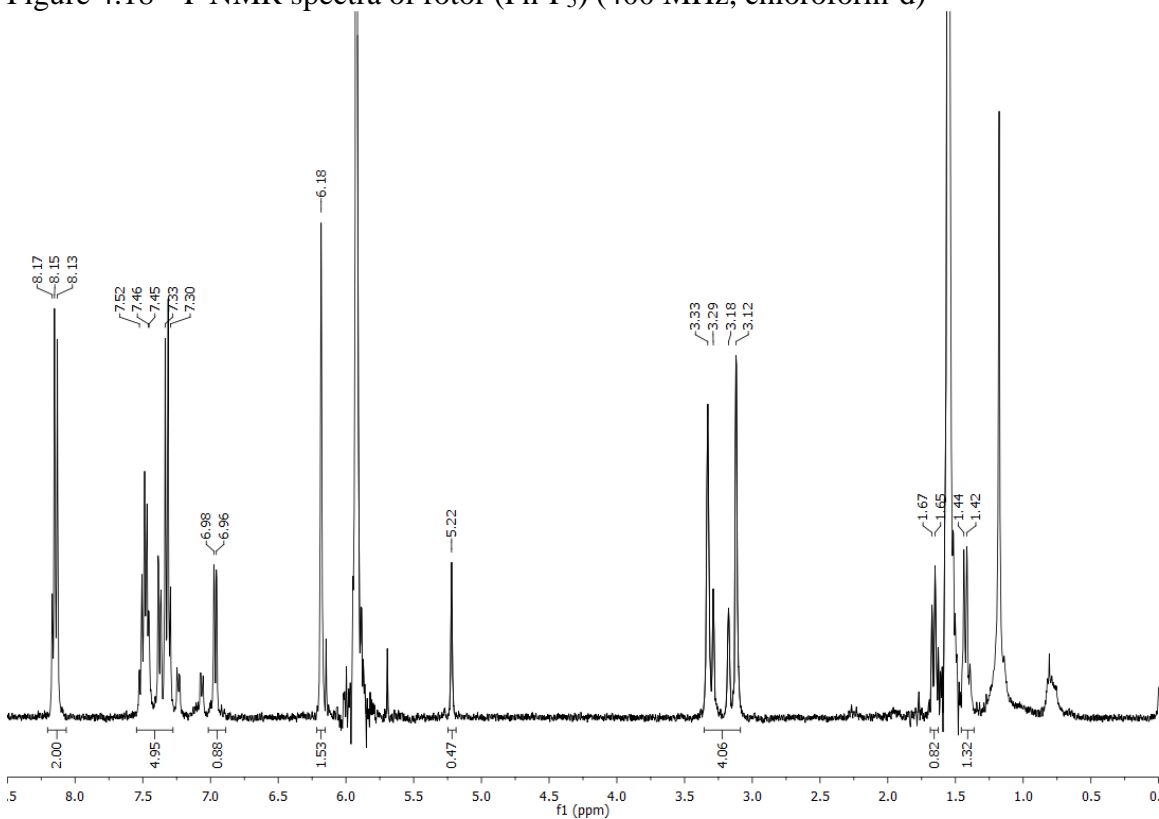


Figure 4.19 ^1H NMR spectra of rotor (Ph-*p*- NO_2) (400 MHz, chloroform-d)

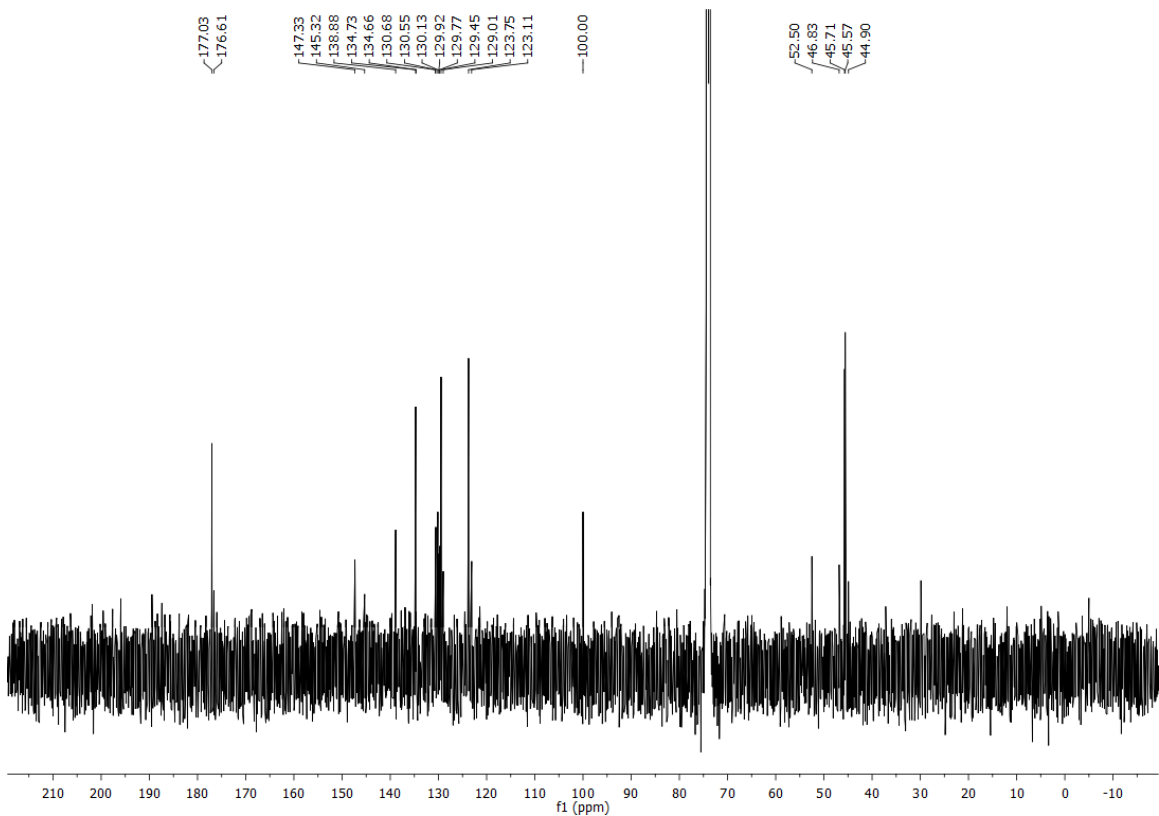


Figure 4.20 ^{13}C NMR spectra of rotor (Ph-p-NO_2) (400 MHz, chloroform-d)

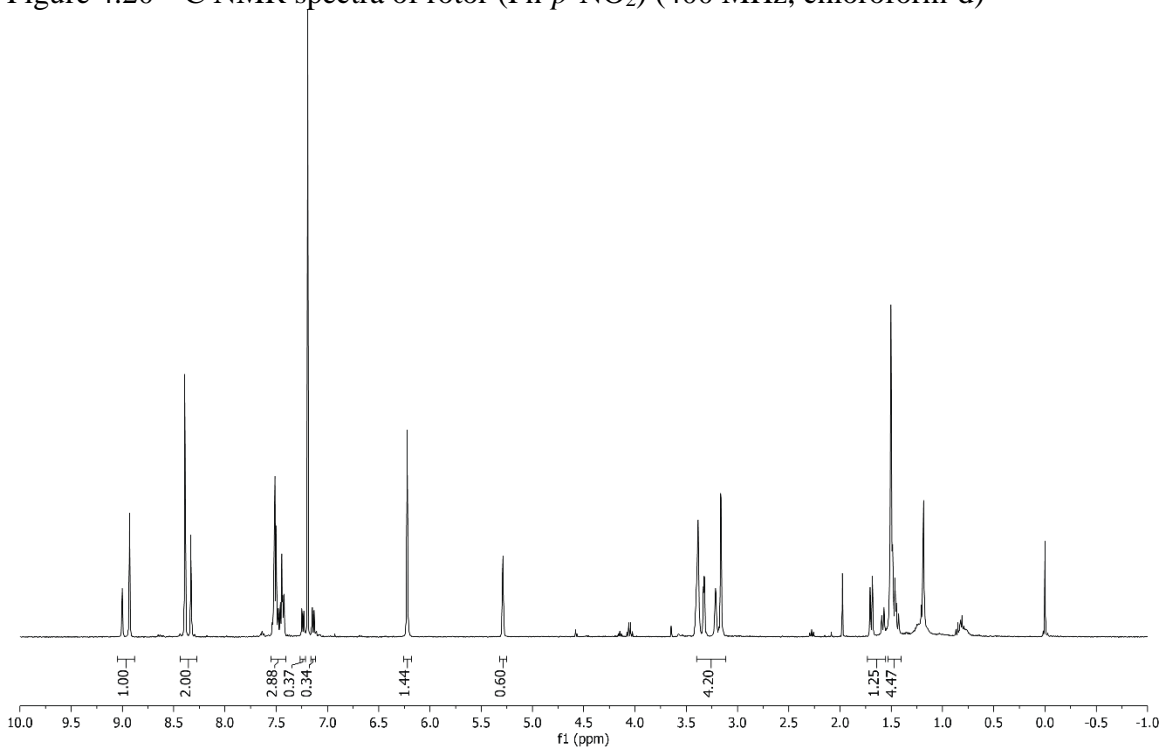


Figure 4.21 ^1H NMR spectra of rotor ($\text{Ph-m,m-(NO}_2)_2$) (400 MHz, chloroform-d)

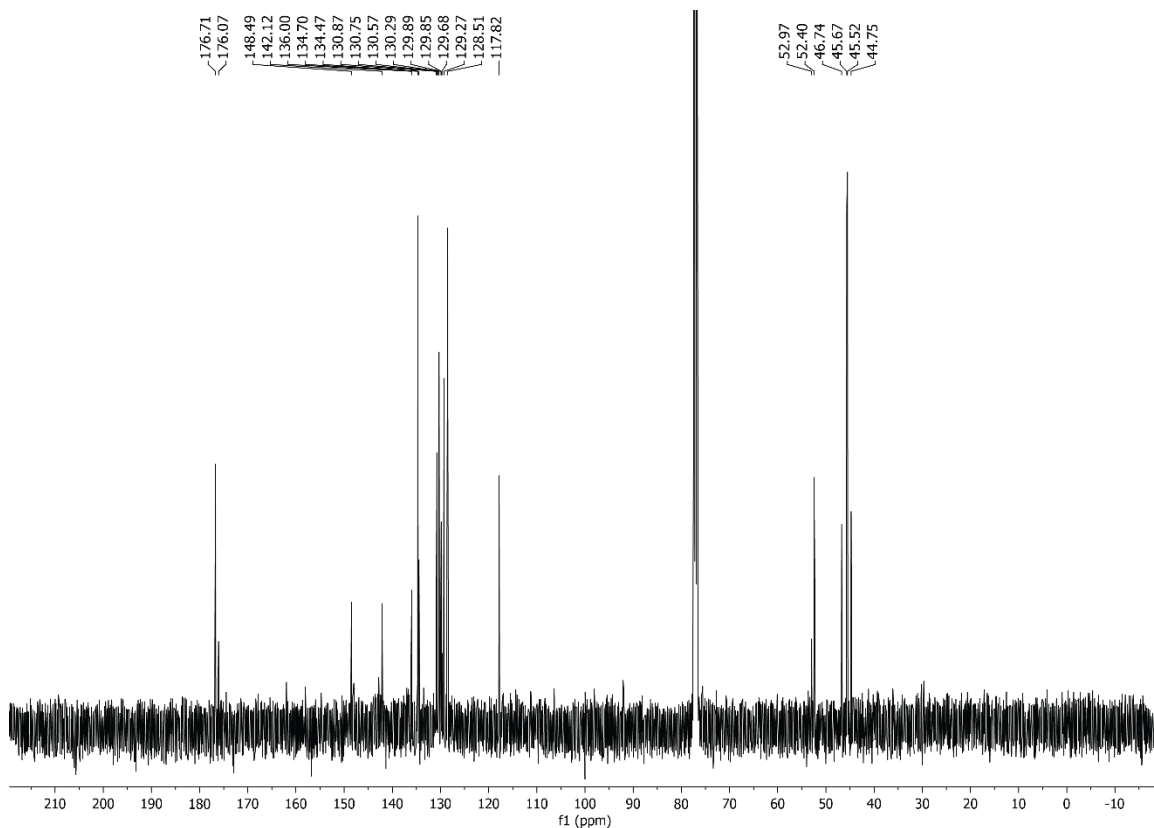


Figure 4.22 ^{13}C NMR spectra of rotor ($\text{Ph-}m,m\text{-(NO}_2)_2$) (400 MHz, chloroform-d)

4.3.4 EXPERIMENTAL DETERMINATION OF THE ROTATIONAL BARRIERS

The rotational barriers of the rotors (Table 4.2) were determined via exchange spectroscopy (EXSY) NMR experiments. EXSY NMR is observable by running nuclear overhauser effect spectroscopy (NOESY) NMR experiments. In the spectra obtained from the NOESY experiments, out of phase signals off the diagonal of the 2D spectra originate from the nuclear overhauser effect, while in phase signals off the diagonal originate from exchange dynamics.⁷⁸ Integration of the signals were performed using topspin software, and rate constants were obtained using the EXSYCalc software.

The rotational barrier for each rotor were extrapolated to room temperature for consistency. The TS enthalpy (ΔH^\ddagger) and entropy (ΔS^\ddagger) for rotor were obtained from the

Eyring plots (Figure 4.18) following Equation 4.1. The rotation barriers were determined by plugging the enthalpy and entropy along with a temperature into Equation 4.2.

Due to the large difference in temperature ranges needed to determine each rotational barrier two different solvents with similar chemical properties but different melting/boiling temperatures were chosen. Dichloromethane-d₂ (melting point = -95, boiling point = 40 °C) was an appropriate choice as a solvent for the rotors which required a temperature range below 25 °C. Meanwhile, tetrachloroethane-d₂ (melting point = -45, boiling point = 145 °C) was an appropriate choice as a solvent for the rotors which required a temperature range above 25 °C.

$$\ln\left(\frac{k_{ex}}{T}\right) = \frac{-\Delta H^\ddagger}{R} \cdot \frac{1}{T} + \ln\left(\frac{k_B}{h}\right) + \frac{-\Delta S^\ddagger}{R} \dots\dots\dots \text{Equation 4.1}$$

$$\Delta G^\ddagger = \Delta H^\ddagger - T\Delta S^\ddagger \dots\dots\dots \text{Equation 4.2}$$

Table 4.2 Experimental rotational barriers for the rotors in chapter 4 via EXSY NMR

Rotor	rotational barrier (kcal/mol)						
	<i>syn</i> → <i>anti</i>			<i>anti</i> → <i>syn</i>			<i>average</i>
Rotor	ΔG^\ddagger^a	ΔH^\ddagger	$T\Delta S^\ddagger^a$	ΔG^\ddagger^a	ΔH^\ddagger	$T\Delta S^\ddagger^a$	ΔG^\ddagger^a
H	21.25	22.84	1.57	21.70	23.18	1.47	21.48
F ₁	20.08	20.70	0.62	20.94	22.92	1.99	20.51
F ₃	19.33	20.15	0.82	19.76	20.48	0.73	19.54
F ₅	17.31	18.64	1.33	17.50	18.21	0.71	17.41
NO ₂	18.99	21.05	2.06	19.69	21.64	1.95	19.34
(NO ₂) ₂	17.88	17.53	-0.35	18.38	17.75	-0.62	18.13

^a at 298.15 K.

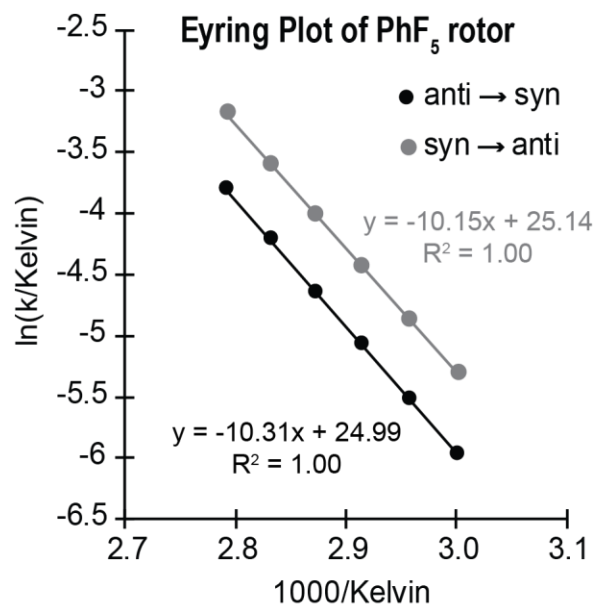


Figure 4.23 Eyring plot for the Ph-F₅ rotor

4.3.5 ROTATIONAL BARRIER CALCULATIONS

Following instructions from a benchmark study on determining the accurate level of theory for rotational barriers, we optimized the ground state (GS) and transition state (TS) for our rotors using B3LYP-D3(0)/6-311G* and corrected for thermodynamic contributions. All calculations were performed using Spartan '18. Convergence criteria were 10^{-4} Hartree and 10^{-4} atomic units as the maximum norm of the cartesian gradient. Vibrational analysis was also carried out at B3LYP-D3(0)/6-311G* and at 25 °C. The XYZ coordinates for the GS and TS structures are in tables 4.3 – 4.7. To eliminate error in GS energy, the calculated GS energies for the *syn*- and *anti*- conformers were averaged. The calculations overestimated the barriers on average by 0.9 kcal/mol with a standard deviation of ± 1.3 kcal/mol. Overall, the root mean square deviation was 1.50 kcal/mol.

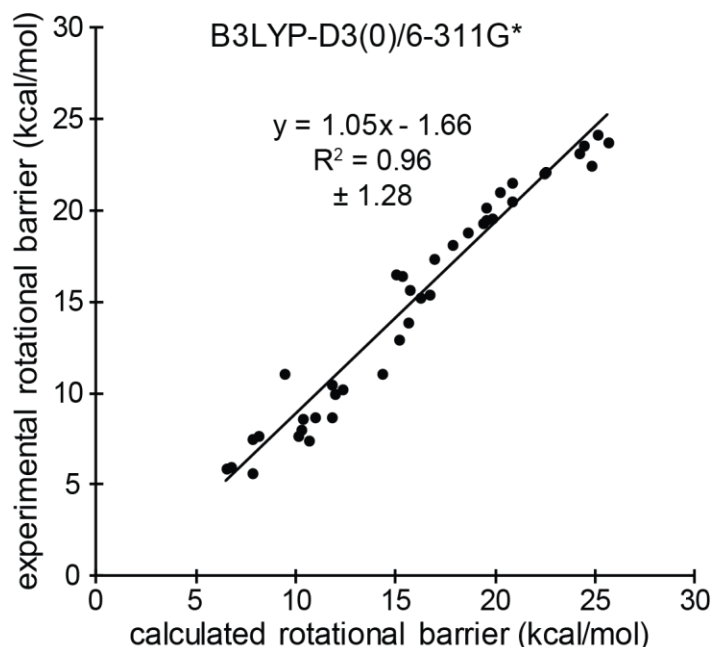


Figure 4.24 Correlation of the calculated ($\Delta G_{\text{calc}}^{\ddagger}$) and experimental ($\Delta G_{\text{exp}}^{\ddagger}$) rotational barriers used in this dissertation. Structures were calculated at the B3LYP-D3(0)/6-311G* level of theory with thermodynamic corrections.

Table 4.3 XYZ coordinates of the GS and TS structures of Ph-F₁

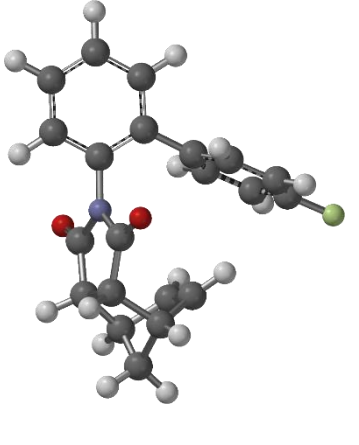
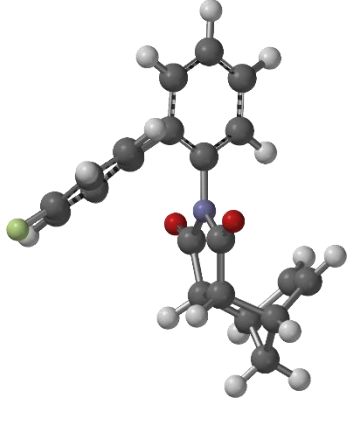
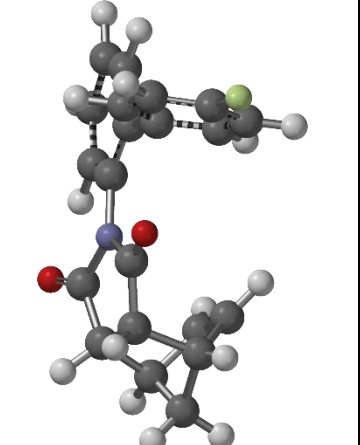
		
H 1.823549 -1.658324 -5.081935	H -5.305197 1.085285 0.130265	H 1.224689 -0.528517 -5.170643
C 1.732086 -1.270732 -4.072491	C -4.224819 0.984254 0.133830	C 1.185954 -0.417921 -4.092142
C 1.476966 -0.290085 -1.485950	C -1.463321 0.707517 0.132388	C 1.063944 -0.196359 -1.259145
C 0.515471 -1.361929 -3.404464	C -3.614979 0.060740 -0.708298	C 0.195889 -1.046372 -3.356432
C 2.825145 -0.673968 -3.449148	C -3.449413 1.784603 0.970224	C 2.099026 0.372699 -3.411167
C 2.696725 -0.190116 -2.152701	C -2.066827 1.637724 0.974344	C 2.035260 0.475608 -2.030466
C 0.361796 -0.862635 -2.106663	C -2.223649 -0.085033 -0.737528	C 0.077933 -0.945340 -1.958297
H -0.342198 -1.811109 -3.894524	H -4.216898 -0.546711 -1.376388	H -0.558213 -1.632493 -3.869936
H 3.774339 -0.591525 -3.967598	H -3.919803 2.511317 1.623769	H 2.875315 0.913043 -3.942983
H 3.538981 0.265693 -1.644756	H -1.444789 2.229972 1.635528	H 2.780465 1.073183 -1.539893
N 1.399669 0.178604 -0.138605	N -0.051345 0.518198 0.216285	N 1.150114 -0.014805 0.181089
C 1.435483 1.538316 0.212644	C 0.890293 1.482079 -0.167953	C 2.263244 0.601378 0.835576
C 1.433518 1.619138 1.728278	C 2.260845 0.958505 0.214400	C 1.886329 0.918568 2.259937
C 1.333223 0.155207 2.216129	C 2.014459 -0.442406 0.815450	C 0.528738 0.259666 2.477521
C 1.309975 -0.690345 0.960260	C 0.514286 -0.640422 0.775964	C 0.208568 -0.427504 1.173419
H 2.340840 2.130903 2.056164	H 2.905769 0.960289 -0.665737	H 2.677508 0.571295 2.925209
O 1.454381 2.449428 -0.575936	O 0.622436 2.532885 -0.695929	O 3.343853 0.850157 0.361315
O 1.224779 -1.890268 0.880348	O -0.114119 -1.590262 1.167273	O -0.688995 -1.210819 1.030513
C -0.002835 0.145981 3.048230	C 2.597911 -0.313833 2.275313	C -0.420737 1.477657 2.826378
H -0.105844 -0.721861 3.696911	H 2.778549 -1.272408 2.757518	H -1.358634 1.173066 3.286422
H 2.171545 -0.163410 2.839175	H 2.502818 -1.253972 0.273267	H 0.501011 -0.479404 3.278811
C 0.156948 2.294778 2.357263	C 2.946861 1.741572 1.398492	C 1.592378 2.455482 2.513491
H 0.203646 3.381830 2.377347	H 3.446151 2.655406 1.082678	H 2.492411 3.042257 2.685939
C 0.114243 1.541494 3.708745	C 3.813017 0.598637 1.979909	C 0.573813 2.311786 3.670377
H 1.020844 1.666370 4.309981	H 4.516722 0.171503 1.258558	H 0.967846 1.774503 4.538747
H -0.760626 1.799154 4.308683	H 4.348723 0.894187 2.884028	H 0.159131 3.270195 3.988371
C -1.043531 1.672693 1.662576	C 1.908221 1.879868 2.503251	C 0.670281 2.929097 1.400664
H -1.617934 2.146983 0.877718	H 1.362406 2.789108 2.723789	H 0.982845 3.526148 0.552948
C -1.133420 0.401365 2.064379	C 1.700569 0.664224 3.020191	C -0.519375 2.347244 1.585463
H -1.789868 -0.361522 1.667958	H 0.947282 0.376829 3.743179	H -1.373581 2.374489 0.920048
C -0.980944 -0.918247 -1.458744	C -1.591773 -1.040650 -1.682507	C -1.172242 -1.607675 -1.464436
C -3.541868 -1.036726 -0.396639	C -0.446278 -2.813649 -3.486145	C -3.563346 -2.844483 -0.791818
C -1.449795 -2.096684 -0.870741	C -0.667260 -0.591621 -2.633607	C -1.232614 -2.992671 -1.298393
C -1.816145 0.202811 -1.488317	C -1.924816 -2.399203 -1.655216	C -2.345968 -0.861528 -1.331120
C -3.103757 0.151104 -0.961159	C -1.355830 -3.293617 -2.556599	C -3.547428 -1.472640 -0.985372
C -2.734184 -2.162320 -0.334860	C -0.090029 -1.474532 -3.541526	C -2.425428 -3.619040 -0.950536
F -4.790589 -1.096043 0.119682	F 0.109316 -3.676793 -4.367000	F -4.728605 -3.448111 -0.454177
H -1.455340 1.122477 -1.935764	H -0.415396 0.462671 -2.675432	H -0.332803 -3.585619 -1.421476
H -0.796449 -2.958604 -0.814522	H -2.617591 -2.762567 -0.904545	H -2.319293 0.211135 -1.492270
H -3.765257 1.009271 -0.982774	H -1.598314 -4.349934 -2.542426	H -2.484968 -4.691384 -0.802663
H -3.113566 -3.067147 0.125823	H 0.615809 -1.139763 -4.293056	H -4.464313 -0.905974 -0.868875

Table 4.4 XYZ coordinates of the GS and TS structures of Ph-F₃

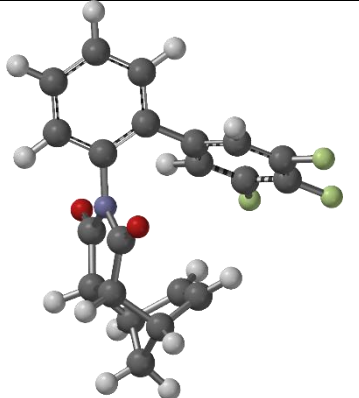
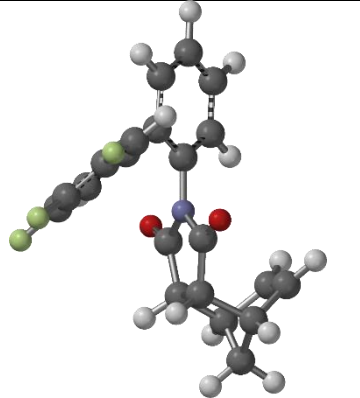
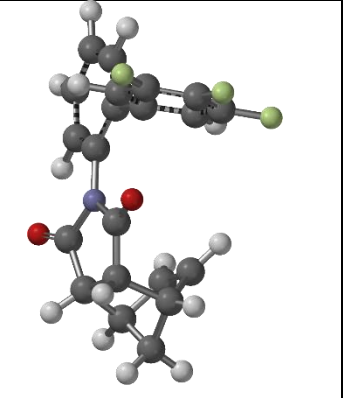
		
H 1.982412 -1.939299 -4.964477	H -5.306802 1.146162 0.053246	H 1.222676 -0.511604 -5.183523
C 1.840469 -1.476228 -3.993636	C -4.226656 1.045855 0.065362	C 1.187634 -0.406997 -4.104477
C 1.455520 -0.297315 -1.504701	C -1.458347 0.773501 0.079924	C 1.072478 -0.195056 -1.268397
C 0.586626 -1.500934 -3.393372	C -3.613524 0.081716 -0.725894	C 0.189388 -1.024671 -3.371000
C 2.906505 -0.850368 -3.352762	C -3.451619 1.886663 0.860797	C 2.116504 0.361317 -3.419532
C 2.712249 -0.269097 -2.104880	C -2.069505 1.742918 0.873095	C 2.056390 0.459766 -2.038223
C 0.369563 -0.902657 -2.147309	C -2.221528 -0.063057 -0.748324	C 0.079644 -0.929479 -1.972567
H -0.250313 -1.969796 -3.900414	H -4.213709 -0.558927 -1.363634	H -0.572599 -1.598880 -3.886327
H 3.885795 -0.822876 -3.818002	H -3.921671 2.646433 1.475683	H 2.902847 0.888620 -3.949404
H 3.535329 0.199403 -1.577115	H -1.452278 2.378074 1.496189	H 2.813286 1.040277 -1.545167
N 1.331745 0.235762 -0.182514	N -0.042685 0.619491 0.159260	N 1.153523 -0.014383 0.171415
C 1.138012 1.593396 0.115805	C 0.858365 1.675347 -0.062448	C 2.264413 0.603260 0.832540
C 1.269446 1.752776 1.621026	C 2.246872 1.168702 0.262383	C 1.882285 0.912788 2.256779
C 1.447823 0.318595 2.169272	C 2.068815 -0.315755 0.648710	C 0.521809 0.257026 2.465447
C 1.427594 -0.586775 0.956265	C 0.575995 -0.566542 0.599519	C 0.203148 -0.419393 1.156579
H 2.123981 2.403634 1.821177	H 2.899988 1.332521 -0.596177	H 2.669725 0.559116 2.923070
O 0.905851 2.447736 -0.703499	O 0.544609 2.779594 -0.429930	O 3.344525 0.857138 0.361199
O 1.486439 -1.788769 0.925149	O -0.009132 -1.574379 0.902250	O -0.705182 -1.189457 1.002845
C 0.243280 0.162620 3.164106	C 2.674385 -0.389431 2.102600	C -0.425579 1.476193 2.817730
H 0.351374 -0.675456 3.849865	H 2.918885 -1.400111 2.422941	H -1.365985 1.171947 3.272645
H 2.393616 0.165830 2.694576	H 2.576112 -1.013143 -0.020514	H 0.488377 -0.487079 3.261840
C -0.004349 2.272768 2.382602	C 2.887718 1.795959 1.560940	C 1.591999 2.449140 2.517448
H -0.117189 3.354844 2.358599	H 3.326889 2.777783 1.395226	H 2.493167 3.032074 2.696450
C 0.236077 1.594806 3.756692	C 3.829000 0.629236 1.948714	C 0.568924 2.302060 3.669852
H 1.183464 1.879409 4.225791	H 4.544196 0.367099 1.162784	H 0.957895 1.758674 4.536615
H -0.584435 1.759576 4.457142	H 4.361992 0.808512 2.884541	H 0.156138 3.259918 3.991652
C -1.183736 1.454464 1.883691	H 1.854810 1.692187 2.673468	C 0.675435 2.931544 1.403708
H -1.936836 1.820433 1.199968	H 1.259854 2.520039 3.039291	H 0.992348 3.534762 0.562002
C -1.033020 0.205601 2.336235	C 1.733855 0.401172 3.000512	C -0.516943 2.352951 1.581259
H -1.631270 -0.661174 2.084636	H 1.015241 -0.041922 3.678444	H -1.370665 2.390524 0.915718
C -0.996302 -0.902922 -1.563396	C -1.606682 -1.071556 -1.647181	C -1.166954 -1.594287 -1.475710
C -3.595058 -0.894685 -0.528340	C -0.471160 -2.977066 -3.356434	C -3.560322 -2.848308 -0.755574
C -1.634436 -2.108566 -1.256828	C -0.630832 -0.693447 -2.575183	C -1.208782 -2.977985 -1.305007
C -1.664762 0.306579 -1.356803	C -2.012579 -2.407549 -1.583357	C -2.338376 -0.846916 -1.341614
C -2.949957 0.293949 -0.846199	C -1.446082 -3.340178 -2.433977	C -3.513090 -1.476478 -0.969721
C -2.922445 -2.091902 -0.748083	C -0.075738 -1.645600 -3.412933	C -2.395943 -3.585077 -0.934899
F -3.596890 1.452510 -0.615834	F -1.823642 -4.627772 -2.376510	F -4.643157 -0.763158 -0.811915
F -4.834851 -0.888612 -0.023846	F 0.071157 -3.887693 -4.174500	F -4.704540 -3.449412 -0.398655
F -3.548794 -3.241109 -0.445883	F 0.857861 -1.291161 -4.313190	F -2.445886 -4.915604 -0.745344
H -1.192524 1.254461 -1.583764	H -0.313214 0.337163 -2.672506	H -0.322827 -3.589493 -1.421243
H -1.136001 -3.060611 -1.390940	H -2.739214 -2.740837 -0.853188	H -2.347730 0.224620 -1.498495

Table 4.5 XYZ coordinates of the GS and TS structures of Ph-F₅

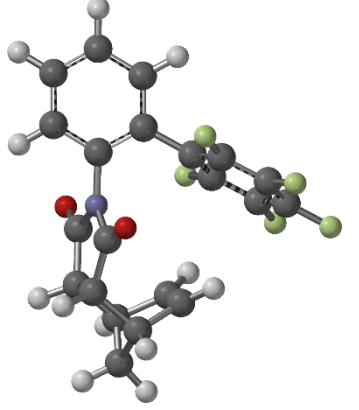
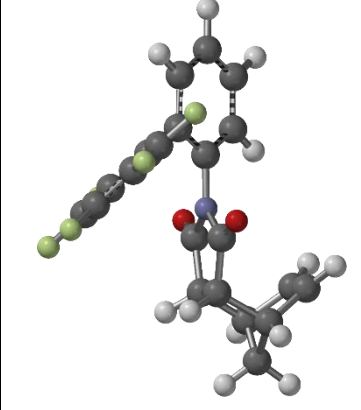
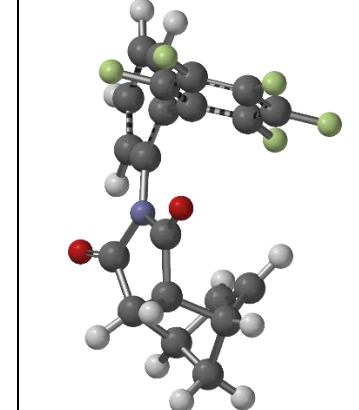
		
H 1.916855 -1.720156 -5.053005	H -4.362942 1.091617 2.219664	H 1.249044 -0.463884 -5.154444
C 1.785305 -1.309667 -4.057676	C -3.284787 1.042709 2.112062	C 1.197380 -0.372396 -4.075538
C 1.433273 -0.274656 -1.496178	C -0.517374 0.920500 1.814026	C 1.055347 -0.200609 -1.246605
C 0.565105 -1.449530 -3.408756	C -2.649857 1.825477 1.156337	C 0.211001 -1.024367 -3.361487
C 2.829884 -0.634067 -3.431374	C -2.533341 0.198931 2.926292	C 2.088811 0.420313 -3.373038
C 2.655268 -0.125353 -2.150304	C -1.153794 0.135496 2.773764	C 2.014547 0.502569 -1.993348
C 0.365567 -0.920463 -2.130033	C -1.260928 1.788398 0.999694	C 0.095767 -0.944875 -1.967371
H -0.256127 -1.959817 -3.899936	H -3.231787 2.481816 0.519378	H -0.533850 -1.611316 -3.888806
H 3.782102 -0.511327 -3.935839	H -3.020674 -0.416891 3.674463	H 2.859034 0.983051 -3.889284
H 3.462888 0.390950 -1.646132	H -0.558882 -0.518916 3.397195	H 2.742732 1.111414 -1.488576
N 1.314392 0.206232 -0.158618	N 0.895781 0.819514 1.669083	N 1.125608 -0.051907 0.193610
C 1.531803 1.552690 0.202289	C 1.782951 0.946283 2.759572	C 2.248237 0.525107 0.860840
C 1.462534 1.634736 1.712977	C 3.185641 0.734677 2.235584	C 1.852123 0.886540 2.268573
C 1.263144 0.183626 2.203847	C 3.030716 0.465377 0.723560	C 0.477467 0.261878 2.468180
C 1.101139 -0.644510 0.943223	C 1.538408 0.477112 0.464898	C 0.155531 -0.414390 1.161676
H 2.384146 2.098497 2.070471	H 3.787631 1.613873 2.472036	H 2.620090 0.534883 2.958695
O 1.752895 2.443037 -0.575903	O 1.447926 1.154499 3.896330	O 3.343479 0.705280 0.399689
O 0.838220 -1.817343 0.861204	O 0.975336 0.226856 -0.571287	O -0.775672 -1.156319 1.006127
C -0.019858 0.275646 3.110439	C 3.706127 -0.944308 0.533242	C -0.446877 1.496239 2.772245
H -0.135140 -0.560294 3.797407	H 3.966913 -1.168826 -0.498985	H -1.399052 1.225094 3.224204
H 2.112254 -0.208766 2.767786	H 3.508688 1.215347 0.089920	H 0.421101 -0.473154 3.272109
C 0.220829 2.384994 2.325491	C 3.892663 -0.573284 2.757103	C 1.584793 2.424067 2.470062
H 0.314198 3.468816 2.298472	H 4.323514 -0.467167 3.750652	H 2.489737 3.002565 2.646120
C 0.190336 1.687448 3.709365	C 4.852670 -0.817195 1.565964	C 0.543231 2.335912 3.603640
H 1.122511 1.791604 4.274239	H 5.527870 0.022000 1.370893	H 0.912186 1.818176 4.494840
H -0.648916 2.010840 4.327696	H 5.431746 -1.736649 1.670204	H 0.138910 3.311482 3.878591
C -1.034545 1.795061 1.698490	C 2.917410 -1.724924 2.558296	C 0.696568 2.875825 1.323823
H -1.621377 2.271412 0.924816	H 2.343398 -2.188479 3.351032	H 1.033434 3.443391 0.464229
C -1.182263 0.554118 2.173655	C 2.811790 -1.949301 1.244440	C -0.506397 2.325229 1.501422
H -1.912162 -0.184656 1.870637	H 2.130324 -2.625936 0.744201	H -1.342819 2.341558 0.812460
C -0.977594 -1.022770 -1.508716	C -0.620110 2.638667 -0.031041	C -1.142620 -1.616257 -1.477524
C -3.553804 -1.203133 -0.397589	C 0.653229 4.160635 -2.024609	C -3.531747 -2.849376 -0.725454
C -1.556782 -2.257519 -1.217989	C 0.387881 3.548127 0.281118	C -1.234661 -2.992824 -1.381208
C -1.732368 0.114978 -1.234112	C -0.976403 2.522235 -1.375214	C -2.283331 -0.874048 -1.214282
C -3.004337 0.039040 -0.685058	C -0.356037 3.268676 -2.366850	C -3.469417 -1.468510 -0.833472
C -2.829122 -2.358078 -0.669579	C 1.029032 4.299847 -0.694555	C -2.412631 -3.615612 -1.000753
F -1.229419 1.331414 -1.488526	F -1.924373 1.654009 -1.746346	F -2.219767 0.466172 -1.255386
F -3.689078 1.155618 -0.404257	F -0.712593 3.127848 -3.647316	F -4.546259 -0.728686 -0.554934
F -4.771335 -1.288093 0.144147	F 1.259319 4.881753 -2.970684	F -4.670981 -3.438040 -0.359374
F -3.361515 -3.553738 -0.396664	F 1.997978 5.160365 -0.359816	F -2.476124 -4.945779 -0.902541
F -0.888906 -3.386820 -1.470410	F 0.778944 3.709233 1.555701	F -0.163953 -3.754395 -1.637708

Table 4.6 XYZ coordinates of the GS and TS structures of Ph-NO₂

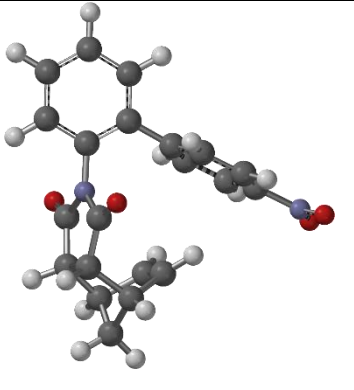
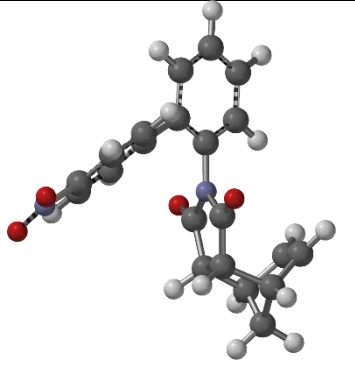
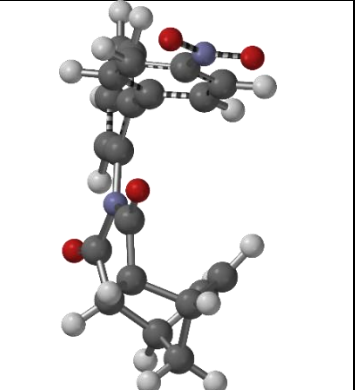
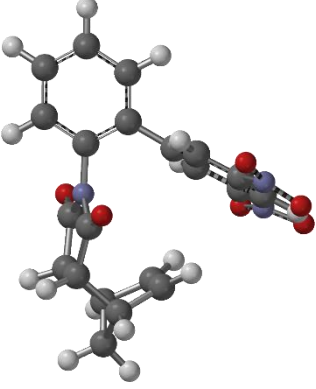
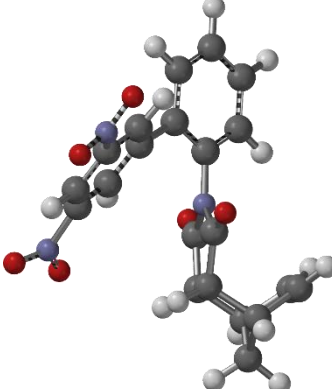
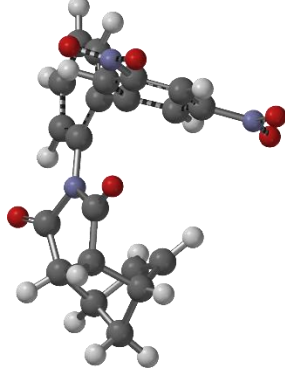
		
H 2.079457 -1.603831 -5.102468 C 1.984468 -1.210544 -4.095772 C 1.723041 -0.215622 -1.513333 C 0.772466 -1.320993 -3.422466 C 3.067882 -0.587895 -3.480948 C 2.937466 -0.098412 -2.186701 C 0.618182 -0.812360 -2.128860 H -0.078449 -1.789523 -3.906055 H 4.012974 -0.491300 -4.004187 H 3.774340 0.373979 -1.685394 N 1.641432 0.248509 -0.165554 C 1.693429 1.606842 0.194187 C 1.689071 1.677829 1.709742 C 1.580009 0.211707 2.189832 C 1.540087 -0.625751 0.929428 H 2.598372 2.183140 2.041837 O 1.724180 2.520549 -0.590453 O 1.432386 -1.823132 0.840281 C 0.249256 0.207415 3.030528 H 0.144757 -0.661138 3.677773 H 2.420418 -0.117623 2.804302 C 0.416353 2.356994 2.343057 C 0.467221 3.443697 2.364907 C 0.375544 1.601028 3.693203 H 1.284851 1.720682 4.291175 H -0.495788 1.861155 4.296916 C -0.789947 1.741848 1.651988 H -1.369485 2.225013 0.876256 C -0.885062 0.470683 2.053136 H -1.551455 -0.287999 1.665168 C -0.721481 -0.880300 -1.478723 C -3.274664 -1.017072 -0.408251 C -1.187831 -2.074068 -0.918130 C -1.550990 0.247044 -1.477735 C -2.834324 0.185772 -0.949352 C -2.466827 -2.149058 -0.378961 H -1.187511 1.174438 -1.905549 H -0.535126 -2.937130 -0.887069 H -3.491326 1.044926 -0.949702 H -2.843874 -3.062493 0.060946 N -4.639343 -1.093156 0.160893 O -4.993691 -2.159744 0.645575 O -5.330467 -0.084107 0.114533	H 0.309404 -5.312547 1.293799 C 0.311653 -4.232239 1.194539 C 0.308322 -1.467035 0.924079 C -0.495327 -3.625061 0.238853 C 1.113028 -3.453384 2.026575 C 1.117832 -2.070440 1.882793 C -0.525465 -2.233240 0.098596 H -1.135637 -4.229267 -0.395505 H 1.741087 -3.921941 2.776414 H 1.753743 -1.448245 2.501379 N 0.392321 -0.055449 0.740699 C 0.042191 0.881228 1.725633 C 0.435478 2.251498 1.211707 C 1.011909 2.013696 -0.201382 C 0.943111 0.518224 -0.419797 H -0.433685 2.910587 1.235217 O -0.467447 0.605505 2.782760 O 1.305851 -0.104582 -1.384622 C 2.484064 2.568851 -0.085921 H 2.955532 2.752945 -1.049088 H 0.467829 2.523389 -0.998404 C 1.642937 2.907497 1.986045 H 1.348248 3.400640 2.910113 C 2.223311 3.777332 0.845459 H 1.509361 4.499911 0.437736 H 3.141095 4.292522 1.134837 C 2.731366 1.848196 2.095770 H 2.958128 1.290077 2.995932 C 3.226552 1.646129 0.870142 H 3.933349 0.885197 0.563315 C -1.441331 -1.607246 -0.886492 C -3.190220 -0.468490 -2.715307 C -2.391584 -0.664829 -0.469167 C -1.385733 -1.964347 -2.239143 C -2.258672 -1.400633 -3.159809 C -3.270053 -0.091438 -1.378456 H -2.454273 -0.400171 0.580390 H -0.633316 -2.668986 -2.573576 H -2.222473 -1.661280 -4.209013 H -4.016865 0.627741 -1.069857 N -4.123012 0.137511 -3.689591 O -4.904833 0.984618 -3.276206 O -4.057776 -0.242445 -4.851446	H 1.440594 -0.391709 -5.168819 C 1.414211 -0.271641 -4.091154 C 1.317389 -0.015852 -1.258596 C 0.417738 -0.873856 -3.342404 C 2.354049 0.498299 -3.423711 C 2.302997 0.617478 -2.043595 C 0.317251 -0.758718 -1.944238 H -0.348562 -1.452776 -3.846040 H 3.141561 1.010798 -3.966098 H 3.066330 1.199415 -1.562270 N 1.406026 0.186274 0.177614 C 2.510798 0.823464 0.830538 C 2.141815 1.106826 2.264153 C 0.786834 0.441063 2.477185 C 0.457773 -0.215879 1.161649 H 2.938310 0.745035 2.915288 O 3.577128 1.111727 0.347991 O -0.462958 -0.970063 0.998096 C -0.162634 1.650348 2.856852 H -1.097431 1.334956 3.315655 H 0.764924 -0.315286 3.262508 C 1.848081 2.636749 2.553179 H 2.748143 3.220996 2.733161 C 0.836238 2.467313 3.712246 H 1.235225 1.912083 4.566890 H 0.422522 3.418149 4.053094 C 0.919685 3.131200 1.454497 H 1.227007 3.748035 0.619156 C -0.268467 2.544546 1.633941 H -1.128334 2.588542 0.976776 C -0.930371 -1.421575 -1.443024 C -3.315073 -2.675834 -0.783095 C -0.973359 -2.806712 -1.254802 C -2.116772 -0.685198 -1.348651 C -3.311299 -1.303049 -1.009224 C -2.159140 -3.439192 -0.911297 H -0.064225 -3.388365 -1.356842 H -2.098533 0.383325 -1.532431 H -2.204472 -4.506830 -0.743035 H -4.234211 -0.745565 -0.920624 N -4.579375 -3.341350 -0.415313 O -4.551593 -4.549823 -0.215114 O -5.585820 -2.647350 -0.330092

Table 4.7 XYZ coordinates of the GS and TS structures of Ph-(NO₂)₂

		
H 2.233421 -1.611966 -5.025677	H -5.382952 -0.303068 1.410384	H 1.599608 -0.282779 -5.121940
C 2.108069 -1.196626 -4.031558	C -4.302559 -0.334556 1.320612	C 1.548700 -0.161804 -4.045530
C 1.771544 -0.146194 -1.475352	C -1.527537 -0.403544 1.076073	C 1.404896 0.084479 -1.213952
C 0.892257 -1.336158 -3.372333	C -3.663300 0.465301 0.381054	C 0.565324 -0.804209 -3.312583
C 3.155687 -0.514152 -3.417784	C -3.552042 -1.169982 2.143927	C 2.435630 0.658542 -3.365260
C 2.989589 0.000476 -2.137614	C -2.168257 -1.206530 2.016605	C 2.362246 0.773695 -1.985645
C 0.699654 -0.797018 -2.096012	C -2.270257 0.456849 0.247987	C 0.440845 -0.686801 -1.917695
H 0.066079 -1.845793 -3.857354	H -4.247055 1.126546 -0.250870	H -0.173953 -1.406919 -3.828838
H 4.103943 -0.393306 -3.929927	H -4.042195 -1.798943 2.879019	H 3.200390 1.213430 -3.898075
H 3.803267 0.512553 -1.638039	H -1.572966 -1.859007 2.642555	H 3.089783 1.394487 -1.496798
N 1.664667 0.320236 -0.131191	N -0.109067 -0.486998 0.955559	N 1.484964 0.260007 0.222900
C 1.831872 1.668769 0.241920	C 0.763240 -0.289146 2.046858	C 2.607228 0.864094 0.884697
C 1.827957 1.726243 1.756043	C 2.175056 -0.482443 1.543983	C 2.226053 1.172193 2.308239
C 1.635357 0.266562 2.227991	C 2.043364 -0.801259 0.038755	C 0.870459 0.505081 2.521360
C 1.489852 -0.550535 0.960488	C 0.554751 -0.850406 -0.233367	C 0.541257 -0.149939 1.205380
H 2.766825 2.175032 2.087357	H 2.750025 0.420975 1.754494	H 3.018014 0.826512 2.973134
O 1.951720 2.579464 -0.536509	O 0.404639 -0.021702 3.164866	O 3.686142 1.101148 0.405741
O 1.262695 -1.730104 0.861628	O 0.001595 -1.141179 -1.263504	O -0.377237 -0.909660 1.041671
C 0.345196 0.343749 3.125408	C 2.775256 -2.188216 -0.106125	C -0.083019 1.714236 2.896129
H 0.217182 -0.512439 3.784700	H 3.059194 -2.429927 -1.128259	H -1.013491 1.398760 3.363385
H 2.479371 -0.126852 2.798445	H 2.495411 -0.044080 -0.605542	H 0.849367 -0.250988 3.306854
C 0.607849 2.475007 2.411040	C 2.917077 -1.752308 2.109639	C 1.921597 2.705847 2.571664
H 0.715848 3.557561 2.419279	H 3.331387 -1.605050 3.104941	H 2.819142 3.297436 2.740146
C 0.570702 1.733035 3.769792	C 3.900681 -1.991869 0.937263	C 0.915869 2.544923 3.737568
H 1.504156 1.807631 4.337049	H 4.548487 -1.134410 0.729540	H 1.321833 2.002336 4.597033
H -0.264505 2.045528 4.398965	H 4.511046 -2.886487 1.074289	H 0.498793 3.497637 4.068416
C -0.653020 1.922410 1.763872	C 1.986012 -2.942913 1.928962	C 0.984877 3.182638 1.471891
H -1.237546 2.441670 1.015224	H 1.419195 -3.407570 2.726398	H 1.283546 3.795209 0.630249
C -0.809535 0.664382 2.190439	C 1.907342 -3.206246 0.620240	C -0.200935 2.595285 1.664866
H -1.542104 -0.058527 1.855700	H 1.259690 -3.921852 0.129358	H -1.068505 2.632918 1.017219
C -0.644717 -0.893104 -1.468880	C -1.623918 1.316746 -0.771369	C -0.808788 -1.342621 -1.419723
C -3.253307 -1.077601 -0.406325	C -0.325663 2.853935 -2.762453	C -3.239845 -2.569789 -0.677998
C -1.181385 -2.135547 -1.122982	C -0.503288 2.088859 -0.458159	C -0.885508 -2.727223 -1.279781
C -1.410550 0.257780 -1.270991	C -2.099160 1.330038 -2.086317	C -1.964218 -0.578284 -1.246547
C -2.695354 0.143497 -0.751234	C -1.457660 2.103871 -3.043932	C -3.145389 -1.199049 -0.865858
C -2.468109 -2.203430 -0.602947	C 0.134610 2.812913 -1.455625	C -2.090854 -3.309820 -0.905402
H -1.023240 1.232980 -1.532975	H -0.110671 2.116841 0.547627	H -0.018173 -3.353607 -1.436230
H -0.604179 -3.041960 -1.240340	H -2.943233 0.720810 -2.379494	H -1.947550 0.494007 -1.383014
H -4.251926 -1.149489 -0.001586	H 0.178129 3.429338 -3.524938	H -4.165511 -3.038598 -0.379796
N -3.032627 -3.529503 -0.243353	N 1.384812 3.528815 -1.119761	N -2.156807 -4.783513 -0.742590
O -2.373712 -4.516821 -0.531487	O 1.786683 4.369294 -1.907781	O -1.146871 -5.423799 -0.999113
O -4.120428 -3.543781 0.313384	O 1.945989 3.211134 -0.077050	O -3.215771 -5.263277 -0.365910
N -3.505804 1.366967 -0.550457	N -1.978479 2.101538 -4.435220	N -4.352478 -0.369161 -0.639034
O -2.957402 2.444087 -0.749572	O -1.350700 2.734969 -5.270042	O -4.233874 0.843251 -0.758533
O -4.665311 1.225287 -0.196246	O -3.002712 1.470916 -4.651179	O -5.387789 -0.946313 -0.342696

4.3.6 ELECTROSTATIC POTENTIAL MAP CALCULATIONS

Electrostatic potential maps were calculated for the substituents of the molecular rotors with a methyl group replaced for the rest of the rotor (Figure 4.25). The ESP maps located in Figure 4.25 show the positive and negative regions around the molecules. Regions in yellow, orange, and red have a partial negative charge, with the red regions being the most negative and yellow the least. Regions in green, cyan, and blue have a partial positive charge, with the blue regions being the most positive and green the least. The values for the aromatic groups were selected for the center of the rings, while the values for the carbonyl, acetylene, and cyanide groups were obtained by selecting the first carbon attached to the phenyl rotor. The ESP maps were calculated at the B3LYP-D3/6-311G* level of theory.

4.3.7 NATURAL BOND ORBITAL CALCULATIONS

Natural bond order (NBO) calculations were carried out using Q-Chem version 5.0 which incorporates the NBO version 5.0 program. Geometry optimizations were performed using Spartan'18 at the B3LYP-D3/6-311G* level of theory and ground state conformations were confirmed by 0 negative IR frequencies. Coordinates (Tables 4.3 – 4.7) were subsequently imported to Q-Chem for NBO analysis. NBO calculations were performed as a single point calculation, at the ω B97M-V/6-311G* level of theory on the imported geometries. The calculations were performed on the optimized TS structures of the rotors to examine the possible contribution of an orbital-orbital $n \rightarrow \pi^*$ interaction. The $n \rightarrow \pi^*$ interaction energy from the imide carbonyl oxygen lone pair (n) and the anti-bonding orbital on the R-group (π^*) are reported in table.

Table 4.8 ESP parameters calculated at the B3LYP-D3/6-311G* level of theory

Rotor substituent	ESP (kcal/mol)
Ph	-20.9
Ph-F1	-13.3
Ph-F3	2.0
Ph-F5	15.8
Ph-NO ₂	-2.4
(NO ₂) ₂	14.5
Py	-10.0
Py-F4	22.0
Uracil	15.9
CHO	15.18
COCH ₃	14.34
COPh	6.57
C(CH ₂)CH ₃	-13.60
CCH	-15.80
CN	2.49

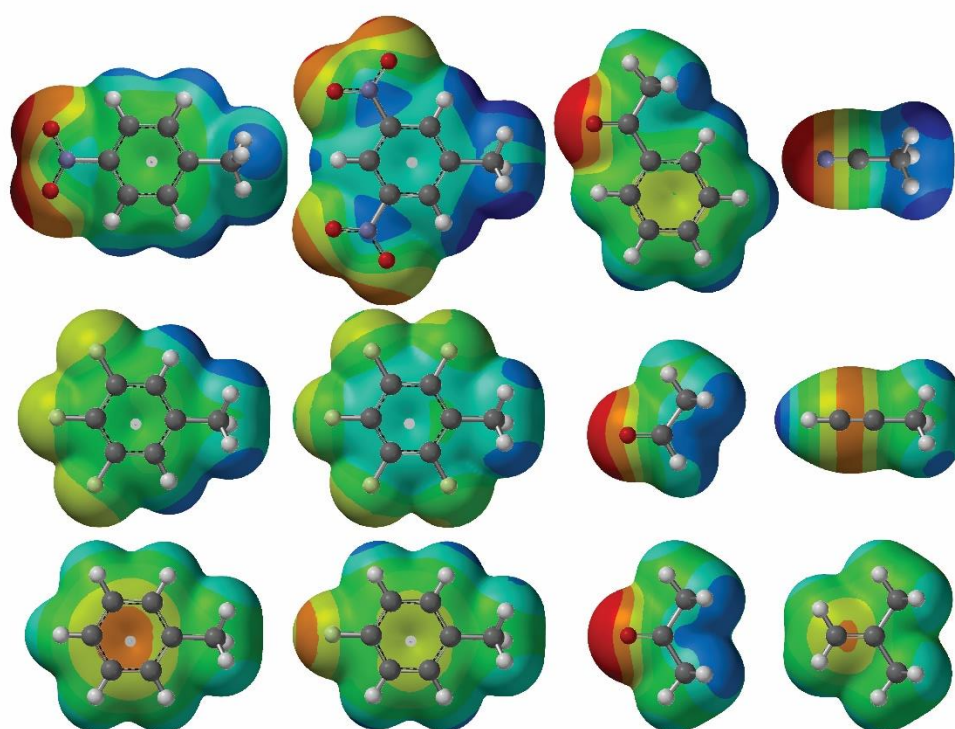


Figure 4.25 ESP maps for the R-groups used in this study.

Table 4.9 NBO energy from the $n \rightarrow \pi^*$ orbital-orbital interaction

Rotor substituent	NBO energy (kcal/mol)
Ph	-3.1
Ph-F1	-3.2
Ph-F3	-3.6
Ph-F5	-3.3
Ph-NO ₂	-4.4
(NO ₂) ₂	-4.1
CHO	-16.4
COCH ₃	-18.3
COPh	-17.1
C(CH ₂)CH ₃	-5.7
CCH	-5.3
CN	-9.0

CHAPTER 5 FUTURE WORK

5.1 OUTLOOK

There are many different directions that future research on molecular rotors can be proceeded. Three specific directions were explored in which the *N*-phenylimide rotors were utilized to answer interesting questions; (1) Is there enhanced repulsion in lone pair – lone pair interactions? (2) What is the most accurate level of theory to calculate rotational barriers? (3) Can the rotational barriers be modeled using empirical parameters?

5.2 LONE PAIR – LONE PAIR REPULSION

There are many theories which describe lone pairs. One of the most common is the valence shell electron pair repulsion (VSEPR) model.¹²⁶ VSEPR theory is commonly taught to in undergraduate classes and is useful to predict geometrical arrangements of atoms. VSEPR predicts the orientation of lone pairs off an oxygen of water, but this model assumes that lone pairs take up more physical space and has greater steric size than bonded atoms. We now know that the VSEPR model is correct for the wrong reasons. Molecular orbital theory and hybridization can also predict the locations of lone pairs based on orbital orientation rather than a space filling model. There are many studies on interactions involving a lone pair such as Chapters 2, 3, and 4 in this dissertation, but there are very few studies of lone pair – lone pair interactions. The goal of this section is to answer the question: does the lone pair – lone pair interaction involve extra destabilization?

The rotational barriers were measured using exchange spectroscopy (EXSY).^{78,92} All rotors were studied in the slow exchange regime (0 – 90 °C) where the *syn*- and *anti*-conformers gave distinct sets of peaks. Eyring plots provided the enthalpy and entropy of the rotational barriers, and free energy ($\Delta G_{\text{exp}}^{\ddagger}$) of rotation was recalculated at 25 °C for all

rotors (Table 2.1). The measured $\Delta G^{\ddagger}_{\text{exp}}$ values ranged from 20.2 (R = OCH₃) to 24.2 (R = D).

The rotational barrier of the rotors in this study is primarily governed by steric hindrance. There are two types of rotors, one where the first atom of the R-group has a lone pair (lone pair series) and another where the first atoms does not have a lone pair (alkyl series). By correlating the rotational barriers to the B-value (steric) parameter, two separate trend lines were identified (Figure 5.1). The rotors which have a lone pair on the first atom (Figure 5.1, black circles) have slightly higher rotational barriers with than the rotors which do not have lone pairs on the first atom (Figure 5.1, black circles).

The difference between these two lines is essentially negligible. For example, the difference between the two lines is 0.9 kcal/mol when the B-value is 10 kcal/mol. Thus, the lone pair – lone pair interaction does not appear to have any apparent extra repulsive interactions. The reason for the small difference between these two lines is most likely due to electrostatic attraction in the alkyl series and electrostatic repulsion in the lone pair series.

5.3 ACCURACY IN CALCULATING ROTATIONAL BARRIERS

There are many different functional and basis set pairs that could be used to calculate rotational barriers. Thankfully, there are general functionals which perform adequately for most purposes. For example, the B3LYP functional is accurate for many different applications and works well with both a small basis sets like 6-31G* and a small grid size like SG-1 (50,194). However, the M06-2X functional is also accurate for many different applications but works best with a large basis sets like aug-cc-pVTZ and large grid size like SG-3 (99,590).

When deciding which functional and basis set pair to use for benchmarking, the available computing needs to be considered. For example, if only a few functionals can be used in a benchmark, then general functionals should be tested rather than specific ones. Doing so will at least provide an adequately accurate series of calculations.

The B3LYP-D3(0)/6-311G* level of theory was found to be adequately for the geometry optimization conducted in this dissertation. A few different combinations of functional and basis set pairs were also calculated to test for accuracy (Table 5.1). The B3LYP-D3(0)/6-311G* functional and basis set pair was the most accurate pair. However, the provided benchmark is limited in scope. If more computational resources are available larger basis sets like the 6-311++G(2df,2pd) and aug-cc-VTZ could be tested, along with double hybrid functionals like the ω B97M(2).

5.4 EMPIRICAL MODEL OF ROTATIONAL BARRIERS

The primary origin of the rotational barriers in this dissertation is steric hindrance. Thus, a simple empirical steric model can be created which can encompass multiple systems to predict rotational barrier energies. The empirical system is based on the combination of the overlap of substituents in the planar TS and the electrostatic interactions between the substituents.

The empirical model used by Sternhell²¹ was expanded to 3 additional molecular rotors (Figure 5.2). The size of each substituent was optimized to provide the best fit, and the electrostatic charge for each substituent is from the MMFF charge for the overlapping atom. Similar substituents were examined for each system, which enabled a more accurate estimate of the steric radii relative to the original study. The overlap of the substituents in the TS is based on the molecular mechanic optimized GS structures. The GS structure was

rotated to approximate their overlap in the TS. The optimized radii are found in Table 5.2. The correlation plot of the combination or individual rotors along with their independent correlations can be found in Figure 5.3.

This empirical model can be used to make quick approximations of rotational barriers, or even predict if a molecule will have atropisomers. The root mean square deviation of this model is 0.76 kcal/mol which is more accurate than the DFT benchmark on the same rotors. The versatility of this model should be further increased by adding in more molecular rotors with similar overlapping substituents in their TSs.

Table 5.1 Statistical analysis for the calculated rotational barriers in this dissertation.

Basis set	B3LYP	B3LYP-D3(0)	B97	ω B97M-V
6-31G*	1.26	1.15	1.38	
6-311G*	2.08	1.10		1.30
def2-TZVP		1.53		

All values are root mean square deviations.

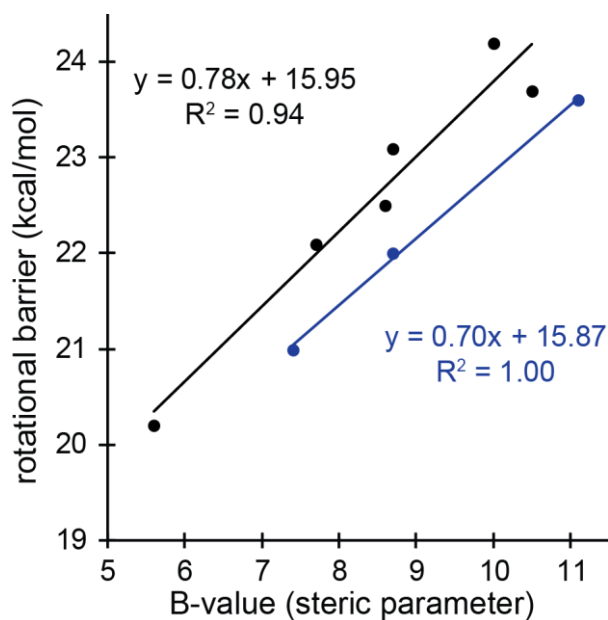
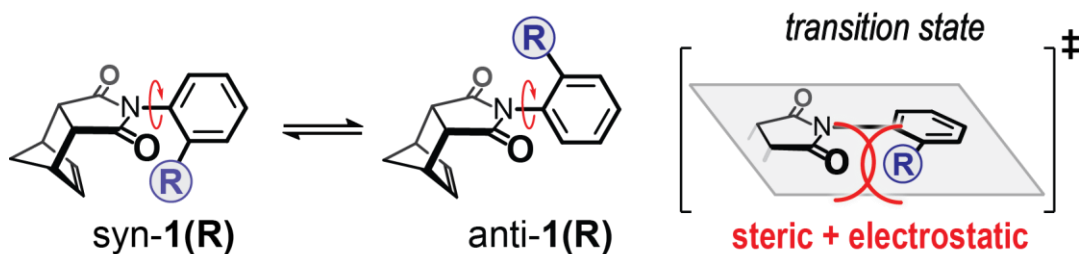
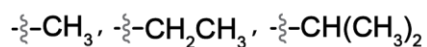


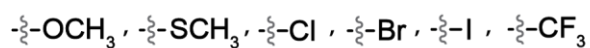
Figure 5.1 Steric correlation plot



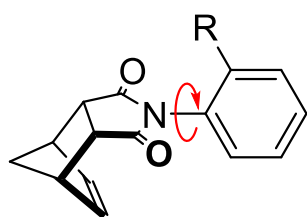
R (alkyl):



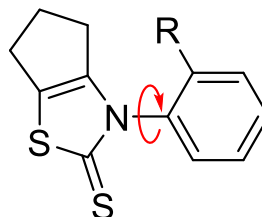
R (lone pair):



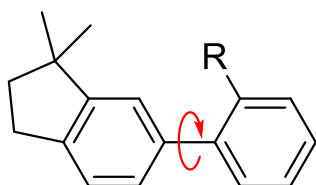
Scheme 5.1 rotational barrier for the steric substituents



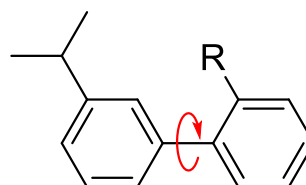
Imide



Thiazole-2-thione



Biphenyl



Biphenyl

Figure 5.2 Four different molecular rotors used to study substituents effective radii.^{15-21,94}

Table 5.2 Effective radii of the substituents

Substituent	Sternhell	this work	Substituent	Sternhell	this work
NH ₂	1.79	2.17	Ph-F ₂		2.25
NHCH ₃	1.91	2.36	Ph-F ₃		2.41
NHPh		1.78	Ph-F ₄		1.62
NHCOCH ₃	1.58	1.84	Ph-F ₅		1.87
N(CH ₃) ₂	1.61	2.05	CH=CH ₂		2.19
N ⁺ (CH ₃) ₃	2.27	3.74	C≡CH		1.89
NO ₂	1.61	2.12	C≡N	1.51	1.80
OH	1.53	1.84	CHO		2.47
OCH ₃	1.52	1.85	COOH		2.21
OCH ₂ F		2.28	COOCH ₃	1.62	2.13
OCHF ₂		2.16	COCH ₃	1.56	2.09
OCF ₃		1.75	(CO)C(CH ₃) ₃		2.10
OPh		1.91	SH	1.8	2.03
OCH ₂ OCH ₃		1.96	SCH ₃	1.82	2.34
CH ₃	1.8	2.29	SCF ₃		2.48
CH ₂ F		1.37	SPh		2.31
CHF ₂		1.94	F	1.47	1.58
CF ₃	2.2	2.68	Cl	1.73	2.17
CH ₂ CH ₃		2.35	Br	1.86	2.47
CH(CH ₃) ₂	2.2	2.66	I	1.97	2.65
C(CH ₃) ₃		3.42	C=O		1.92
CH ₂ Ph		2.45	H	1.2	0.86
Ph	1.62	2.14	C=S		2.74
Ph-F ₁		2.37	C-CH ₂		2.81

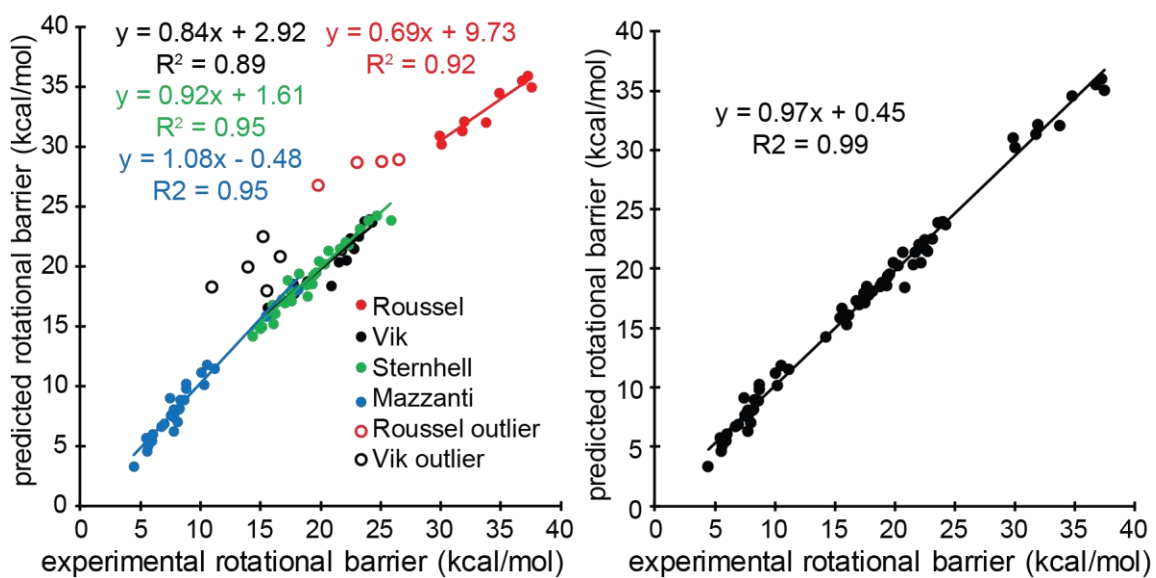


Figure 5.3 (Left) correlation plot of the individual rotors to the predicted rotational barrier with some outliers. (Right) combination of the individual rotors correlated to the predicted rotational barrier.

REFERENCES

- (1) Hobza, P.; Muller-Dethlefs, K. *Non-Covalent Interactions*; 2009.
- (2) Jacob N. Israelachvili. *Intermolecular and Surface Forces*, 3rd ed.; Elsevier, 2011.
- (3) Mati, I. K.; Cockroft, S. L. Molecular Balances for Quantifying Non-Covalent Interactions. *Chem. Soc. Rev.* **2010**, *39* (11), 4195–4205.
- (4) Neel, A. J.; Hilton, M. J.; Sigman, M. S.; Toste, F. D. Exploiting Non-Covalent π Interactions for Catalyst Design. *Nature* **2017**, *543* (7647), 637–646.
- (5) Raynal, M.; Ballester, P.; Vidal-Ferran, A.; Leeuwen, P. W. N. M. van. Supramolecular Catalysis. Part 1: Non-Covalent Interactions as a Tool for Building and Modifying Homogeneous Catalysts. *Chem. Soc. Rev.* **2014**, *43* (5), 1660–1733.
- (6) Zondlo, N. J. Non-Covalent Interactions: Fold Globally, Bond Locally. *Nat. Chem. Biol.* **2010**, *6* (8), 567–568.
- (7) Orlandi, M.; Coelho, J. A. S.; Hilton, M. J.; Toste, F. D.; Sigman, M. S. Parametrization of Non-Covalent Interactions for Transition State Interrogation Applied to Asymmetric Catalysis. *J. Am. Chem. Soc.* **2017**, *139* (20), 6803–6806.
- (8) Noyori, R. Asymmetric Catalysis: Science and Opportunities (Nobel Lecture). *Angew. Chem. Int. Ed.* **2002**, *41* (12), 2008–2022.
- (9) Wheeler, S. E.; Seguin, T. J.; Guan, Y.; Doney, A. C. Noncovalent Interactions in Organocatalysis and the Prospect of Computational Catalyst Design. *Acc. Chem. Res.* **2016**, *49* (5), 1061–1069.
- (10) Reid, J. P.; Sigman, M. S. Comparing Quantitative Prediction Methods for the Discovery of Small-Molecule Chiral Catalysts. *Nat. Rev. Chem.* **2018**, *2* (10), 290.
- (11) Knowles, R. R.; Jacobsen, E. N. Attractive Noncovalent Interactions in Asymmetric Catalysis: Links between Enzymes and Small Molecule Catalysts. *Proc. Natl. Acad. Sci.* **2010**, *107* (48), 20678–20685.
- (12) Newberry, R. W.; Raines, R. T. The $N \rightarrow \pi^*$ Interaction. *Acc. Chem. Res.* **2017**, *50* (8), 1838–1846.
- (13) Hunter, C. A. Quantifying Intermolecular Interactions: Guidelines for the Molecular Recognition Toolbox. *Angew. Chem. Int. Ed.* **2004**, *43* (40), 5310–5324.
- (14) Mardirossian, N.; Head-Gordon, M. Thirty Years of Density Functional Theory in Computational Chemistry: An Overview and Extensive Assessment of 200 Density Functionals. *Mol. Phys.* **2017**, *115* (19), 2315–2372.
- (15) Vik, E. C.; Li, P.; Pellechia, P. J.; Shimizu, K. D. Transition-State Stabilization by $N \rightarrow \pi^*$ Interactions Measured Using Molecular Rotors. *J. Am. Chem. Soc.* **2019**, *141* (42), 16579–16583.
- (16) Lunazzi, L.; Mancinelli, M.; Mazzanti, A.; Lepri, S.; Ruzziconi, R.; Schlosser, M. Rotational Barriers of Biphenyls Having Heavy Heteroatoms as Ortho-Substituents: Experimental and Theoretical Determination of Steric Effects. *Org. Biomol. Chem.* **2012**, *10* (9), 1847–1855.

- (17) Mazzanti, A.; Lunazzi, L.; Ruzziconi, R.; Spizzichino, S.; Schlosser, M. The Torsional Barriers of 2-Hydroxy- and 2-Fluorobiphenyl: Small but Measurable. *Chem. - Eur. J.* **2010**, *16* (30), 9186–9192.
- (18) Ruzziconi, R.; Spizzichino, S.; Mazzanti, A.; Lunazzi, L.; Schlosser, M. The Biphenyl-Monitored Effective Size of Unsaturated Functional or Fluorinated Ortho Substituents. *Org. Biomol. Chem.* **2010**, *8* (19), 4463–4471.
- (19) Ruzziconi, R.; Spizzichino, S.; Lunazzi, L.; Mazzanti, A.; Schlosser, M. B Values as a Sensitive Measure of Steric Effects. *Chem. – Eur. J.* **2009**, *15* (11), 2645–2652.
- (20) Mazzanti, A.; Lunazzi, L.; Minzoni, M.; Anderson, J. E. Rotation in Biphenyls with a Single Ortho-Substituent. *J. Org. Chem.* **2006**, *71* (15), 5474–5481.
- (21) Bott, G.; Field, L. D.; Sternhell, S. Steric Effects. A Study of a Rationally Designed System. *J. Am. Chem. Soc.* **1980**, *102* (17), 5618–5626.
- (22) Taft, R. W. Linear Free Energy Relationships from Rates of Esterification and Hydrolysis of Aliphatic and Ortho-Substituted Benzoate Esters. *J. Am. Chem. Soc.* **1952**, *74* (11), 2729–2732.
- (23) Taft, R. W. Linear Steric Energy Relationships. *J. Am. Chem. Soc.* **1953**, *75* (18), 4538–4539.
- (24) Charton, M. The Upsilon Steric Parameter — Definition and Determination. In *Steric Effects in Drug Design*; Austel, V., Balaban, A. T., Bonchev, D., Charton, M., Fujita, T., Iwamura, H., Mekenyan, O., Motoc, I., Eds.; Topics in Current Chemistry; Springer: Berlin, Heidelberg, 1983; pp 57–91.
- (25) Charton, M. Steric Effects. I. Esterification and Acid-Catalyzed Hydrolysis of Esters. *J. Am. Chem. Soc.* **1975**, *97* (6), 1552–1556.
- (26) Charton, M. Nature of the Ortho Effect. II. Composition of the Taft Steric Parameters. *J. Am. Chem. Soc.* **1969**, *91* (3), 615–618.
- (27) Gallo, R. Treatment of Steric Effects. In *Progress in Physical Organic Chemistry*; John Wiley & Sons, Ltd, 2007; pp 115–163.
- (28) Pauling, L.; Corey, R. B. Atomic Coordinates and Structure Factors for Two Helical Configurations of Polypeptide Chains. *Proc. Natl. Acad. Sci.* **1951**, *37* (5), 235–240.
- (29) Brethomé, A. V.; Fletcher, S. P.; Paton, R. S. Conformational Effects on Physical-Organic Descriptors: The Case of Sterimol Steric Parameters. *ACS Catal.* **2019**, *9* (3), 2313–2323.
- (30) Hirsch, J. A. Table of Conformational Energies—1967. In *Topics in Stereochemistry*; John Wiley & Sons, Ltd, 2007; pp 199–222.
- (31) Jensen, F. R.; Bushweller, C. H. Conformational Preferences in Cyclohexanes and Cyclohexenes. In *Advances in Alicyclic Chemistry*; Hart, H., Karabatsos, G. J., Eds.; Elsevier, 1971; Vol. 3, pp 139–194.
- (32) Ernest L. Eliel; Samuel H. Wilen. *Stereochemistry of Organic Compounds*; Wiley, 1993.
- (33) Ernest L. Eliel; Samuel H. Wilen; Michael P. Doyle. *Basic Organic Stereochemistry*; Wiley, 2001.
- (34) Hohenstein, E. G.; Sherrill, C. D. Wavefunction Methods for Noncovalent Interactions. *Wiley Interdiscip. Rev. Comput. Mol. Sci.* **2012**, *2* (2), 304–326.
- (35) Szalewicz, K. Symmetry-Adapted Perturbation Theory of Intermolecular Forces. *Wiley Interdiscip. Rev. Comput. Mol. Sci.* **2012**, *2* (2), 254–272.

- (36) Weinhold, F. Natural Bond Orbital Analysis: A Critical Overview of Relationships to Alternative Bonding Perspectives. *J. Comput. Chem.* **2012**, *33* (30), 2363–2379.
- (37) Jorgensen, W. L. The Many Roles of Computation in Drug Discovery. *Science* **2004**, *303* (5665), 1813–1818.
- (38) Yilmazer, N. D.; Korth, M. Comparison of Molecular Mechanics, Semi-Empirical Quantum Mechanical, and Density Functional Theory Methods for Scoring Protein–Ligand Interactions. *J. Phys. Chem. B* **2013**, *117* (27), 8075–8084.
- (39) Hartree, D. R. The Wave Mechanics of an Atom with a Non-Coulomb Central Field. Part II. Some Results and Discussion. *Math. Proc. Camb. Philos. Soc.* **1928**, *24* (1), 111–132.
- (40) Slater, J. C. The Self Consistent Field and the Structure of Atoms. *Phys. Rev.* **1928**, *32* (3), 339–348.
- (41) Jensen, F. Atomic Orbital Basis Sets. *Wiley Interdiscip. Rev. Comput. Mol. Sci.* **2013**, *3* (3), 273–295.
- (42) Klein, R. A.; Zottola, M. A. Pople versus Dunning Basis-Sets for Group IA Metal Hydrides and Some Other Second Row Hydrides: The Case against a De Facto Standard. *Chem. Phys. Lett.* **2006**, *419* (1), 254–258.
- (43) Pritchard, B. P.; Altarawy, D.; Didier, B.; Gibson, T. D.; Windus, T. L. New Basis Set Exchange: An Open, Up-to-Date Resource for the Molecular Sciences Community. *J. Chem. Inf. Model.* **2019**.
- (44) Riley, K. E.; Op't Holt, B. T.; Merz, K. M. Critical Assessment of the Performance of Density Functional Methods for Several Atomic and Molecular Properties. *J. Chem. Theory Comput.* **2007**, *3* (2), 407–433.
- (45) Burgi, H. B.; Dunitz, J. D.; Shefter, Eli. Geometrical Reaction Coordinates. II. Nucleophilic Addition to a Carbonyl Group. *J. Am. Chem. Soc.* **1973**, *95* (15), 5065–5067.
- (46) Burgi, H. B.; Dunitz, J. D.; Shefter, E. Chemical Reaction Paths. IV. Aspects of O···C = O Interactions in Crystals. *Acta Crystallogr. B* **1974**, *30* (6), 1517–1527.
- (47) Burgi, H. B.; Dunitz, J. D.; Lehn, J. M.; Wipff, G. Stereochemistry of Reaction Paths at Carbonyl Centres. *Tetrahedron* **1974**, *30* (12), 1563–1572.
- (48) Bartlett, G. J.; Choudhary, A.; Raines, R. T.; Woolfson, D. N. N→ π^* Interactions in Proteins. *Nat. Chem. Biol.* **2010**, *6* (8), 615–620.
- (49) Shoulders, M. D.; Raines, R. T. Collagen Structure and Stability. *Annu. Rev. Biochem.* **2009**, *78* (1), 929–958.
- (50) Hodges, J. A.; Raines, R. T. Energetics of an n → Π^* Interaction That Impacts Protein Structure. *Org. Lett.* **2006**, *8* (21), 4695–4697.
- (51) Choudhary, A.; Gandla, D.; Krow, G. R.; Raines, R. T. Nature of Amide Carbonyl–Carbonyl Interactions in Proteins. *J. Am. Chem. Soc.* **2009**, *131* (21), 7244–7246.
- (52) Wilhelm, P.; Lewandowski, B.; Trapp, N.; Wennemers, H. A Crystal Structure of an Oligoproline PPII-Helix, at Last. *J. Am. Chem. Soc.* **2014**, *136* (45), 15829–15832.
- (53) Choudhary, A.; Kamer, K. J.; Raines, R. T. A Conserved Interaction with the Chromophore of Fluorescent Proteins. *Protein Sci.* **2012**, *21* (2), 171–177.
- (54) Chyan, W.; Kilgore, H. R.; Gold, B.; Raines, R. T. Electronic and Steric Optimization of Fluorogenic Probes for Biomolecular Imaging. *J. Org. Chem.* **2017**, *82* (8), 4297–4304.

- (55) Breton, G. W.; Crasto, C. J. Substituted 2-(Dimethylamino)Biphenyl-2'-Carboxaldehydes as Substrates for Studying $N \rightarrow \pi^*$ Interactions and as a Promising Framework for Tracing the Bürgi–Dunitz Trajectory. *J. Org. Chem.* **2015**, *80* (15), 7375–7384.
- (56) Newberry, R. W.; VanVeller, B.; Guzei, I. A.; Raines, R. T. $N \rightarrow \pi^*$ Interactions of Amides and Thioamides: Implications for Protein Stability. *J. Am. Chem. Soc.* **2013**, *135* (21), 7843–7846.
- (57) Kilgore, H. R.; Raines, R. T. $N \rightarrow \pi^*$ Interactions Modulate the Properties of Cysteine Residues and Disulfide Bonds in Proteins. *J. Am. Chem. Soc.* **2018**, *140* (50), 17606–17611.
- (58) Jakobsche, C. E.; Choudhary, A.; Miller, S. J.; Raines, R. T. $N \rightarrow \pi^*$ Interaction and $n(\pi)$ Pauli Repulsion Are Antagonistic for Protein Stability. *J. Am. Chem. Soc.* **2010**, *132* (19), 6651–6653.
- (59) Blanco, S.; López, J. C.; Mata, S.; Alonso, J. L. Conformations of γ -Aminobutyric Acid (GABA): The Role of the $N \rightarrow \pi^*$ Interaction. *Angew. Chem. Int. Ed.* **2010**, *49* (48), 9187–9192.
- (60) Paulini, R.; Müller, K.; Diederich, F. Orthogonal Multipolar Interactions in Structural Chemistry and Biology. *Angew. Chem. Int. Ed.* **2005**, *44* (12), 1788–1805.
- (61) Liu, P.; Yang, X.; Birman, V. B.; Houk, K. N. Origin of Enantioselectivity in Benzotetramisole-Catalyzed Dynamic Kinetic Resolution of Azlactones. *Org. Lett.* **2012**, *14* (13), 3288–3291.
- (62) Pollock, S. B.; Kent, S. B. H. An Investigation into the Origin of the Dramatically Reduced Reactivity of Peptide-Prolyl-Thioesters in Native Chemical Ligation. *Chem. Commun.* **2011**, *47* (8), 2342–2344.
- (63) Lajkiewicz, N. J.; Roche, S. P.; Gerard, B.; Porco, J. A. Enantioselective Photocycloaddition of 3-Hydroxyflavones: Total Syntheses and Absolute Configuration Assignments of (+)-Ponapensin and (+)-Elliptifoline. *J. Am. Chem. Soc.* **2012**, *134* (31), 13108–13113.
- (64) Windsor, I. W.; Gold, B.; Raines, R. T. An $N \rightarrow \pi^*$ Interaction in the Bound Substrate of Aspartic Proteases Replicates the Oxyanion Hole. *ACS Catal.* **2018**, *9* (2), 1464–1471.
- (65) Choudhary, A.; Kamer, K. J.; Powner, M. W.; Sutherland, J. D.; Raines, R. T. A Stereoelectronic Effect in Prebiotic Nucleotide Synthesis. *ACS Chem. Biol.* **2010**, *5* (7), 655–657.
- (66) Persch, E.; Dumele, O.; Diederich, F. Molecular Recognition in Chemical and Biological Systems. *Angew. Chem. Int. Ed.* **2015**, *54* (11), 3290–3327.
- (67) Biedermann, F.; Schneider, H.-J. Experimental Binding Energies in Supramolecular Complexes. *Chem. Rev.* **2016**, *116* (9), 5216–5300.
- (68) Uyeda, C.; Jacobsen, E. N. Transition-State Charge Stabilization through Multiple Non-Covalent Interactions in the Guanidinium-Catalyzed Enantioselective Claisen Rearrangement. *J. Am. Chem. Soc.* **2011**, *133* (13), 5062–5075.
- (69) Harper, K. C.; Sigman, M. S. Three-Dimensional Correlation of Steric and Electronic Free Energy Relationships Guides Asymmetric Propargylation. *Science* **2011**, *333* (6051), 1875–1878.

- (70) Badjić, J. D.; Nelson, A.; Cantrill, S. J.; Turnbull, W. B.; Stoddart, J. F. Multivalency and Cooperativity in Supramolecular Chemistry. *Acc. Chem. Res.* **2005**, *38* (9), 723–732.
- (71) Cheong, P. H.-Y.; Legault, C. Y.; Um, J. M.; Çelebi-Ölçüm, N.; Houk, K. N. Quantum Mechanical Investigations of Organocatalysis: Mechanisms, Reactivities, and Selectivities. *Chem. Rev.* **2011**, *111* (8), 5042–5137.
- (72) Rushton, G. T.; Vik, E. C.; Burns, W. G.; Rasberry, R. D.; Shimizu, K. D. Guest Control of a Hydrogen Bond-Catalysed Molecular Rotor. *Chem. Commun.* **2017**, 53 (92), 12469–12472.
- (73) Roussel, C.; Vanthuyne, N.; Bouchekara, M.; Djafri, A.; Elguero, J.; Alkorta, I. Atropisomerism in the 2-Arylimino-N-(2-Hydroxyphenyl)Thiazoline Series: Influence of Hydrogen Bonding on the Racemization Process. *J. Org. Chem.* **2008**, *73* (2), 403–411.
- (74) Dial, B. E.; Pellechia, P. J.; Smith, M. D.; Shimizu, K. D. Proton Grease: An Acid Accelerated Molecular Rotor. *J. Am. Chem. Soc.* **2012**, *134* (8), 3675–3678.
- (75) Dial, B. E.; Rasberry, R. D.; Bullock, B. N.; Smith, M. D.; Pellechia, P. J.; Profeta, S.; Shimizu, K. D. Guest-Accelerated Molecular Rotor. *Org. Lett.* **2011**, *13* (2), 244–247.
- (76) Han, S.; Wu, Y.; Duan, R.; Jiang, H.; Wang, Y. Fluoride-Controlled Molecular Brake Systems. *Asian J. Org. Chem.* **2019**, *8* (1), 83–87.
- (77) Wu, Y.; Wang, G.; Li, Q.; Xiang, J.; Jiang, H.; Wang, Y. A Multistage Rotational Speed Changing Molecular Rotor Regulated by PH and Metal Cations. *Nat. Commun.* **2018**, *9* (1), 1953.
- (78) Kirill Nikitin; Ryan O’Gara. Mechanisms and Beyond: Elucidation of Fluxional Dynamics by Exchange NMR Spectroscopy. *Chem. – Eur. J.* **2019**, *25* (18), 4551–4589.
- (79) Ian R. Kleckner; Mark P. Foster. An Introduction to NMR-Based Approaches for Measuring Protein Dynamics. *Biochimica et Biophysica Acta (BBA) - Proteins and Proteomics* **1814** (8), 942–968.
- (80) Kishikawa, K.; Yoshizaki, K.; Kohmoto, S.; Yamamoto, M.; Yamaguchi, K.; Yamada, K. Control of the Rotational Barrier and Spatial Disposition of TheN-(2'-Methylphenyl) Group in Succinimides Bysubstituent and Solvent Effects. *J. Chem. Soc. Perkin 1* **1997**, No. 8, 1233–1240.
- (81) Galabov, B.; Ilieva, S.; Koleva, G.; Allen, W. D.; Iii, H. F. S.; Schleyer, P. von R. Structure–Reactivity Relationships for Aromatic Molecules: Electrostatic Potentials at Nuclei and Electrophile Affinity Indices. *Wiley Interdiscip. Rev. Comput. Mol. Sci.* **2013**, *3* (1), 37–55.
- (82) Newberry, R. W.; Bartlett, G. J.; VanVeller, B.; Woolfson, D. N.; Raines, R. T. Signatures of N→π* Interactions in Proteins. *Protein Sci.* **2014**, *23* (3), 284–288.
- (83) Choudhary, A.; Raines, R. T. Signature of N→π* Interactions in α-Helices. *Protein Sci.* **2011**, *20* (6), 1077–1081.
- (84) Shao, Y.; Gan, Z.; Epifanovsky, E.; Gilbert, A. T. B.; Wormit, M.; Kussmann, J.; Lange, A. W.; Behn, A.; Deng, J.; Feng, X.; et al. Advances in Molecular Quantum Chemistry Contained in the Q-Chem 4 Program Package. *Mol. Phys.* **2015**, *113* (2), 184–215.

- (85) Zimmnicka, M. M. Conformational Features of Thioamide-Containing Dipeptoids and Peptoid–Peptide Hybrids—Computational and Experimental Approaches. *J. Phys. Chem. A* **2018**, *122* (39), 7819–7831.
- (86) Zavitsas, A. A. The Relation between Bond Lengths and Dissociation Energies of Carbon–Carbon Bonds. *J. Phys. Chem. A* **2003**, *107* (6), 897–898.
- (87) Carroll, W. R.; Zhao, C.; Smith, M. D.; Pellechia, P. J.; Shimizu, K. D. A Molecular Balance for Measuring Aliphatic CH– π Interactions. *Org. Lett.* **2011**, *13* (16), 4320–4323.
- (88) Li, P.; Vik, E. C.; Maier, J. M.; Karki, I.; Strickland, S. M. S.; Umana, J. M.; Smith, M. D.; Pellechia, P. J.; Shimizu, K. D. Electrostatically Driven CO– π Aromatic Interactions. *J. Am. Chem. Soc.* **2019**, *141* (32), 12513–12517.
- (89) Masson, E. Torsional Barriers of Substituted Biphenyls Calculated Using Density Functional Theory: A Benchmarking Study. *Org. Biomol. Chem.* **2013**, *11* (17), 2859–2871.
- (90) Pascoe, D. J.; Ling, K. B.; Cockroft, S. L. The Origin of Chalcogen-Bonding Interactions. *J. Am. Chem. Soc.* **2017**, *139* (42), 15160–15167.
- (91) Koebel, M. R.; Cooper, A.; Schmadeke, G.; Jeon, S.; Narayan, M.; Sirimulla, S. S. \cdots O and S \cdots N Sulfur Bonding Interactions in Protein–Ligand Complexes: Empirical Considerations and Scoring Function. *J. Chem. Inf. Model.* **2016**, *56* (12), 2298–2309.
- (92) Ciogli, A.; Kumar, S. V.; Mancinelli, M.; Mazzanti, A.; Perumal, S.; Severi, C.; Villani, C. Atropisomerism in 3-Arylthiazolidine-2-Thiones. A Combined Dynamic NMR and Dynamic HPLC Study. *Org. Biomol. Chem.* **2016**, *14* (47), 11137–11147.
- (93) Cabot, R.; Hunter, C. A.; Varley, L. M. Hydrogen Bonding Properties of Non-Polar Solvents. *Org. Biomol. Chem.* **2010**, *8* (6), 1455–1462.
- (94) Belot, V.; Farran, D.; Jean, M.; Albalat, M.; Vanthuyne, N.; Roussel, C. Steric Scale of Common Substituents from Rotational Barriers of N-(o-Substituted Aryl)Thiazoline-2-Thione Atropisomers. *J. Org. Chem.* **2017**, *82* (19), 10188–10200.
- (95) Cook, J. L.; Hunter, C. A.; Low, C. M. R.; Perez-Velasco, A.; Vinter, J. G. Solvent Effects on Hydrogen Bonding. *Angew. Chem. Int. Ed.* **2007**, *46* (20), 3706–3709.
- (96) Wang, B.; Jiang, W.; Dai, X.; Gao, Y.; Wang, Z.; Zhang, R.-Q. Molecular Orbital Analysis of the Hydrogen Bonded Water Dimer. *Sci. Rep.* **2016**, *6*, 22099.
- (97) Warshel, A.; Sharma, P. K.; Kato, M.; Xiang, Y.; Liu, H.; Olsson, M. H. M. Electrostatic Basis for Enzyme Catalysis. *Chem. Rev.* **2006**, *106* (8), 3210–3235.
- (98) Thordarson, P. Determining Association Constants from Titration Experiments in Supramolecular Chemistry. *Chem. Soc. Rev.* **2011**, *40* (3), 1305–1323.
- (99) APEX3 Version 2016.5-0 and SAINT+ Version 8.37A; APEX3 Version 2016.5-0 and SAINT+ Version 8.37A; Bruker AXS, Inc.: Madison, W.I., U.S.A., 2016.
- (100) Krause, L.; Herbst-Irmer, R.; Sheldrick, G. M.; Stalke, D. Comparison of Silver and Molybdenum Microfocus X-Ray Sources for Single-Crystal Structure Determination. *J. Appl. Crystallogr.* **2015**, *48* (1), 3–10.
- (101) Sheldrick, G. M. Crystal Structure Refinement with SHELXL. *Acta Crystallogr. Sect. C Struct. Chem.* **2015**, *71* (1), 3–8.
- (102) Sheldrick, G. M. A Short History of SHELX. *Acta Crystallogr. A* **2008**, *64* (1), 112–122.

- (103) Dolomanov, O. V.; Bourhis, L. J.; Gildea, R. J.; Howard, J. a. K.; Puschmann, H. OLEX2: A Complete Structure Solution, Refinement and Analysis Program. *J. Appl. Crystallogr.* **2009**, *42* (2), 339–341.
- (104) Sheldrick, G. M. SHELXT – Integrated Space-Group and Crystal-Structure Determination. *Acta Crystallogr. Sect. Found. Adv.* **2015**, *71* (1), 3–8.
- (105) Le Page, Y. Computer Derivation of the Symmetry Elements Implied in a Structure Description. *J. Appl. Crystallogr.* **1987**, *20* (3), 264–269.
- (106) Spek, A. L. LEPAGE – an MS-DOS Program for the Determination of the Metrical Symmetry of a Translation Lattice. *J. Appl. Crystallogr.* **1988**, *21* (5), 578–579.
- (107) Spek, A. L. PLATON, An Integrated Tool for the Analysis of the Results of a Single Crystal Structure Determination. *Acta Crystallogr. A* **1990**, *46* (s1), 34–34.
- (108) Spek, A. L. Structure Validation in Chemical Crystallography. *Acta Crystallogr. D Biol. Crystallogr.* **2009**, *65* (2), 148–155.
- (109) Ahlrichs, R.; Bär, M.; Häser, M.; Horn, H.; Kölmel, C. Electronic Structure Calculations on Workstation Computers: The Program System Turbomole. *Chem. Phys. Lett.* **1989**, *162* (3), 165–169.
- (110) Sierka, M.; Hogekamp, A.; Ahlrichs, R. Fast Evaluation of the Coulomb Potential for Electron Densities Using Multipole Accelerated Resolution of Identity Approximation. *J. Chem. Phys.* **2003**, *118* (20), 9136–9148.
- (111) Deglmann, P.; May, K.; Furche, F.; Ahlrichs, R. Nuclear Second Analytical Derivative Calculations Using Auxiliary Basis Set Expansions. *Chem. Phys. Lett.* **2004**, *384* (1), 103–107.
- (112) Eichkorn, K.; Weigend, F.; Treutler, O.; Ahlrichs, R. Auxiliary Basis Sets for Main Row Atoms and Transition Metals and Their Use to Approximate Coulomb Potentials. *Theor. Chem. Acc.* **1997**, *97* (1–4), 119–124.
- (113) M. J. Frisch; G. W. Trucks; H. B. Schlegel; G. E. Scuseria; M. A. Robb; J. R. Cheeseman; G. Scalmani; V. Barone; G. A. Petersson. *Gaussian 09, Revision A.02*; Gaussian 09, Revision A.02; Gaussian, Inc.: Wallingford, C.T., U.S.A., 2009.
- (114) Karton, A.; Tarnopolsky, A.; Lamère, J.-F.; Schatz, G. C.; Martin, J. M. L. Highly Accurate First-Principles Benchmark Data Sets for the Parametrization and Validation of Density Functional and Other Approximate Methods. Derivation of a Robust, Generally Applicable, Double-Hybrid Functional for Thermochemistry and Thermochemical Kinetics. *J. Phys. Chem. A* **2008**, *112* (50), 12868–12886.
- (115) Kozuch, S.; Gruzman, D.; Martin, J. M. L. DSD-BLYP: A General Purpose Double Hybrid Density Functional Including Spin Component Scaling and Dispersion Correction. *J. Phys. Chem. C* **2010**, *114* (48), 20801–20808.
- (116) Egli, M.; Sarkhel, S. Lone Pair–Aromatic Interactions: To Stabilize or Not to Stabilize. *Acc. Chem. Res.* **2007**, *40* (3), 197–205.
- (117) K. Singh, S.; Das, A. The $n \rightarrow \pi^*$ Interaction: A Rapidly Emerging Non-Covalent Interaction. *Phys. Chem. Chem. Phys.* **2015**, *17* (15), 9596–9612.
- (118) Mooibroek, T. J.; Gamez, P.; Reedijk, J. Lone Pair– π Interactions: A New Supramolecular Bond? *CrystEngComm* **2008**, *10* (11), 1501–1515.
- (119) Gorske, B. C.; Bastian, B. L.; Geske, G. D.; Blackwell, H. E. Local and Tunable $N \rightarrow \pi^*$ Interactions Regulate Amide Isomerism in the Peptoid Backbone. *J. Am. Chem. Soc.* **2007**, *129* (29), 8928–8929.

- (120) Jin, J.; He, B.; Zhang, X.; Lin, H.; Wang, Y. SIRT2 Reverses 4-Oxononanoyl Lysine Modification on Histones. *J. Am. Chem. Soc.* **2016**, *138* (38), 12304–12307.
- (121) Rennie, M. L.; Doolan, A. M.; Raston, C. L.; Crowley, P. B. Protein Dimerization on a Phosphonated Calix[6]Arene Disc. *Angew. Chem. Int. Ed.* **2017**, *56* (20), 5517–5521.
- (122) Gimenez, D.; Zhou, G.; Hurley, M. F. D.; Aguilar, J. A.; Voelz, V. A.; Cobb, S. L. Fluorinated Aromatic Monomers as Building Blocks To Control α -Peptoid Conformation and Structure. *J. Am. Chem. Soc.* **2019**, *141* (8), 3430–3434.
- (123) Singh, S. K.; Mishra, K. K.; Sharma, N.; Das, A. Direct Spectroscopic Evidence for an $N \rightarrow \pi^*$ Interaction. *Angew. Chem. Int. Ed.* **2016**, *55* (27), 7801–7805.
- (124) Wang, H.; Wang, W.; Jin, W. J. σ -Hole Bond vs π -Hole Bond: A Comparison Based on Halogen Bond. *Chem. Rev.* **2016**, *116* (9), 5072–5104.
- (125) Stringer, J. R.; Crapster, J. A.; Guzei, I. A.; Blackwell, H. E. Construction of Peptoids with All Trans-Amide Backbones and Peptoid Reverse Turns via the Tactical Incorporation of N-Aryl Side Chains Capable of Hydrogen Bonding. *J. Org. Chem.* **2010**, *75* (18), 6068–6078.
- (126) Gillespie, R. J.; Nyholm, R. S. Inorganic Stereochemistry. *Q. Rev. Chem. Soc.* **1957**, *11* (4), 339–380.
- (127) Hansch, Corwin.; Leo, A.; Taft, R. W. A Survey of Hammett Substituent Constants and Resonance and Field Parameters. *Chem. Rev.* **1991**, *91* (2), 165–195.

APPENDIX A EMPIRICAL PARAMETERS

This appendix lists out empirical parameters for common substituents off an aromatic ring. These parameters can be utilized to explain non-covalent interactions governed by exchange and electrostatics.

Table A.1 Empirical parameters used to model steric hindrance for common substituents.

R	A	B	E _s	ν	S.S.	C.R.	B ₁	B ₅	L
CH ₃	1.70	7.4	0.00	0.52	19.3	33.7	1.52	2.04	2.87
CH ₂ CH ₃	1.75	8.7	-0.07				1.52	3.17	4.11
CH(CH ₃) ₂	2.15	1.1	-0.47	0.76	22.2	36.7	1.90	3.17	4.11
C(CH ₃) ₃	>4.5	15.4	-1.54				2.60	3.17	4.11
C≡CH	0.41	6.0					1.60	1.60	4.66
C≡N	0.17	5.9		0.40	15.8		1.60	1.60	4.23
Ph	3.0	7.5	-2.55		17.6	31.7	1.71	3.11	6.28
Ph-F ₅		7.7					1.60		
CH=CH ₂	1.35	8.2					1.60	3.09	4.29
CHO	0.80	10.2					1.60	2.36	3.53
COCH ₃	1.17	8.0					1.60	3.13	4.06
COPh							1.60		
COOH	1.35*	7.7					1.60	2.66	3.91
COOCH ₃	1.27	7.7			17.5		1.64	3.36	4.73
OH	0.87*	5.4		0.32	16.1	23.0	1.35	1.93	2.74
OCH ₃	0.60	5.6	1.11	0.36	16.0	25.0	1.35	3.07	3.98
OCF ₃		5.5					1.35	3.61	4.57
OPh							1.35		
OCH ₂ OCH ₃		5.7		0.63			1.35		
SH	0.17				19.4		1.70		
SCH ₃	0.70	8.6		0.64	19.5		1.70		
SCF ₃							1.70		
SPh	0.80	8.3					1.70		
NH ₂	1.45*	8.1		0.35	19.3	29.9	1.35	1.97	2.78
NHCH ₃	1.00*				20.2		1.35	3.08	3.53
NHPh							1.35	5.95	4.53
NHCOCH ₃					17.0		1.35	3.61	5.09
N(CH ₃) ₂	2.10	6.9		0.43	17.5	30.0	1.35	3.08	3.53
N(Ph) ₂							1.35		
N ⁺ (CH ₃) ₃		18.1			22.5				
NO ₂	1.05	7.6	-1.07		17.4		1.35	2.44	3.44
F	0.15	4.4		0.27	14.2		1.35	1.35	2.65
Cl	0.43	7.7	0.09	0.55	18.8		1.80	1.80	3.52
Br	0.38	8.7	-0.06	0.65	19.8		1.95	1.95	3.82
I	0.43	10.0	-0.29	0.78	20.6		2.15	2.15	4.23
CF ₃	2.10	10.5	-1.16	0.90	22.0	37.5	1.99	2.61	3.30

* Solvent dependent, (A) A-value cyclohexane isomerization,³⁰⁻³³ (B) B-value parameter by Mazzanti,¹⁶⁻²⁰ (E_s) Taft steric parameter,^{22,23,27} (ν) Charton steric parameter,²⁴ (S.S.) Biphenyl rotational barriers,²¹ (C.R.) N-arylthiazoline-2-thione rotational barriers,⁹⁴ (B₁, B₅, L) Sterimol parameters.²⁹

Table A.2 Empirical parameters used to model electrostatics for common substituents.

R	σ_m	σ_p	F	R
CH ₃	-0.07	-0.17	0.01	-0.18
CH ₂ CH ₃	-0.07	-0.15	0.00	-0.15
CH(CH ₃) ₂	-0.04	-0.15	0.04	-0.19
C(CH ₃) ₃	-0.10	-0.20	-0.02	-0.18
CCH	0.21	0.23	0.22	0.01
CN	0.56	0.66	0.51	0.15
Ph	0.06	-0.01	0.12	-0.13
Ph-F ₅	0.26	0.27	0.27	0.00
CHCH ₂	0.06	-0.04	0.13	-0.17
CHO	0.35	0.42	0.33	0.09
COCH ₃	0.38	0.50	0.33	0.17
COPh	0.34	0.43	0.31	0.12
COOH	0.37	0.45	0.34	0.11
COOCH ₃	0.37	0.45	0.34	0.11
OH	0.12	-0.37	0.33	-0.70
OCH ₃	0.12	-0.27	0.29	-0.56
OCF ₃	0.38	0.35	0.39	-0.04
OPh	0.25	-0.03	0.37	-0.40
SH	0.25	0.15	0.30	-0.15
SCH ₃	0.15	0.00	0.23	-0.23
SCF ₃	0.40	0.50	0.36	0.14
SPh	0.23	0.07	0.30	-0.23
NH ₂	-0.16	-0.66	0.08	-0.74
NHCH ₃	-0.21	-0.70	0.03	-0.73
NHPh	-0.02	-0.56	0.22	-0.78
NHCOCH ₃	0.21	0.00	0.31	-0.31
N(CH ₃) ₂	-0.16	-0.83	0.15	-0.98
N(Ph) ₂	0.00	-0.22	0.12	-0.34
NO ₂	0.71	0.78	0.65	0.13
F	0.34	0.06	0.45	-0.39
Cl	0.37	0.23	0.42	-0.29
Br	0.39	0.23	0.45	-0.22
I	0.35	0.18	0.42	-0.24
CF ₃	0.43	0.54	0.38	0.16

All values are from a single source.¹²⁷

APPENDIX B COPYRIGHT CLEARANCE

Copyright Clearance for Chapter 2



RightsLink®



Transition-State Stabilization by $n \rightarrow \pi^*$ Interactions Measured Using Molecular Rotors

Author: Erik C. Vik, Ping Li, Perry J. Pellechia, et al

Publication: Journal of the American Chemical Society

Publisher: American Chemical Society

Date: Oct 1, 2019

Copyright © 2019, American Chemical Society

PERMISSION/LICENSE IS GRANTED FOR YOUR ORDER AT NO CHARGE

This type of permission/license, instead of the standard Terms & Conditions, is sent to you because no fee is being charged for your order. Please note the following:

- Permission is granted for your request in both print and electronic formats, and translations.
- If figures and/or tables were requested, they may be adapted or used in part.
- Please print this page for your records and send a copy of it to your publisher/graduate school.
- Appropriate credit for the requested material should be given as follows: "Reprinted (adapted) with permission from (COMPLETE REFERENCE CITATION). Copyright (YEAR) American Chemical Society." Insert appropriate information in place of the capitalized words.
- One-time permission is granted only for the use specified in your request. No additional uses are granted (such as derivative works or other editions). For any other uses, please submit a new request.